Synthesis of Linear and Radial Higher-Order Catenanes, and Functional Aspect of a [2]Catenane

By

MANA BHANJAN PODH

Enrolment No: CHEM11201604020

National Institute of Science Education and Research(NISER), Bhubaneshwar, Odisha-752050

A thesis submitted to the

Board of Studies in Chemical Sciences

In partial fulfillment of requirements

for the Degree of

DOCTOR OF PHILOSOPHY

of

HOMI BHABHA NATIONAL INSTITUTE

September, 2025

Homi Bhabha National Institute[1]

Recommendations of the Viva Voce Committee

As members of the Viva Voce Committee, we certify that we have read the dissertation prepared by **Mana Bhanjan Podh** entitled **"Synthesis of Linear and Radial Higher-Order Catenanes, and Functional Aspect of a [2]Catenane"** and recommend that it may be accepted as fulfilling the thesis requirement for the award of Degree of Doctor of Philosophy.

Chairman	Prof. A. Srinivasan	13/04/2026
Guide	Dr. Chandra Shekhar Purohit	13/04/2026
Examiner	Prof. Mrityunjay D. Pandey	13/04/2026
Member 1	Prof. Jogendra Nath Behera	13/04/2026
Member 2	Dr. Nagendra K Sharma	13/04/2026
Member 3	Dr. Akhilesh Kumar Singh	13/04/2026

Final approval and acceptance of this thesis is contingent upon the candidate's submission of the final copies of the thesis to HBNI.

We hereby certify that we have read this thesis prepared under our direction and recommend that it may be accepted as fulfilling the thesis requirement.

Date: 13/04/2026
Place: NISER, Bhubaneswar

Dr. Chandra Shekhar Purohit
Guide

[1]This page is to be included only for final submission after successful completion of viva voce.

STATEMENT BY AUTHOR

This dissertation has been submitted in partial fulfillment of requirements for an advanced degree at Homi Bhabha National Institute (HBNI) and is deposited in the Library to be made available to borrowers under rules of the HBNI.

Brief quotations from this dissertation are allowable without special permission, provided that accurate acknowledgement of source is made. Requests for permission for extended quotation from or reproduction of this manuscript in whole or in part may be granted by the Competent Authority of HBNI when in his or her judgment the proposed use of the material is in the interests of scholarship. In all other instances, however, permission must be obtained from the author.

Mana Bhanjan Podh

MANA BHANJAN PODH

Name & Signature of the student

DECLARATION

I, hereby declare that the investigation presented in the thesis has been carried out by me. The work is original and has not been submitted earlier as a whole or in part for a degree / diploma at this or any other Institution / University.

Mana Bhanjan Podh

MANA BHANJAN PODH

Name & Signature of the student

CERTIFICATION ON ACADEMIC INTEGRITY

Undertaking by the Student:

1. I **MANA BHANJAN PODH** (name of the student), HBNI Enrolment No. **CHEM11201604020** hereby undertake that the Thesis, titled "**Synthesis of Linear and Radial Higher-Order Catenanes, and Functional Aspect of a [2]Catenane**" Is prepared by me and is the original work undertaken by me...

2. I also hereby undertake that this document has been duly checked through a plagiarism detection tool and the document is found to be plagiarism free as per the guidelines of the Institute/UGC.

3. I am aware and undertake that if plagiarism is detected in my thesis at any stage in the future, suitable penalty will be imposed as applicable as per the guidelines of the Institute/UGC.

Mana Bhanjan Podh
13.04.2026

Signature of the Student with date

Endorsed by the Thesis Supervisor:

I certify that the thesis written by the Researcher is plagiarism free as mentioned above by the student.

13/04/26

Signature of the Thesis Supervisor with date

Name: **Dr. Chandra Shekhar Purohit**
Designation: Associate Professor
Department/ Centre : School of chemical sciences
Name of the CI/ OCC : NISER, Bhubaneswar

List of Publications arising from the thesis

Journal (#Pertaining to thesis ‡Authors contributed equally)

1. # **M. B. Podh** ‡, R. Ratha ‡, C. S. Purohit, "Template Assisted One-Pot Synthesis of [2], Linear [3], and Radial [4]Catenane via Click Reaction." *Chem. Asian J.* **2024**, *19*, e202400031
2. # **M. B. Podh** ‡, R. Ratha ‡, C. S. Purohit, "Template Assisted Synthesis of Linear [5]Catenane by Post-Functionalization of Templated [2]Catenane and Using Click Reaction." *Chem. Asian J.* **2024**, *19*, e202400351
3. # R. Ratha ‡, **M. B. Podh** ‡, P. Ghosh, T. K. Majhi, and C. S. Purohit, "Metal Ion-Responsive Dynamics in a Homo [2]Catenane: Circumrotation and Pirouetting." *ChemistrySelect* **2025**. *10*, e04348.
4. S. Prusty, **M. B. Podh**, C. S. Purohit, A Molecular Figure of Eight: Synthesis and Characterization. *ChemistrySelect* **2018**, *3*, 9690-9693

Conferences

1. Template Assisted Synthesis of Linear [5]Catenane by Post Functionalization of Templated [2]Catenane and Using Click Reaction at National Bioorganic Chemistry Conference(**NBCC-2018**), held at NISER, Bhubaneswar from 22th-24th December, 2018 **(In-person poster)**
2. Template Assisted One-Pot Synthesis of [2], Linear [3], and Radial [4]Catenane via Click Reaction at 1st KIIT-CRSI seminar on Modern trend in chemical sciences, held at KIIT, Bhubaneswar on 5th September, 2023 **(In-person poster)**
3. Template Assisted Synthesis of Linear [5]Catenane by Post Functionalization of Templated [2]Catenane and Using Click Reaction at International conference on Emerging Smart

Materials in Applied chemistry **(ESMAC-2023)**, held at KIIT, Bhubaneswar from 18th-20th November, 2023 **(In-person oral)**

Mana Bhanjan Podh

MANA BHANJAN PODH

Name & Signature of the student

Dedicated

to

Nation and Parents

ACKNOWLEDGEMENTS

I express my profound gratitude to my supervisor, Dr. Chandra Shekhar Purohit, for his invaluable guidance, steadfast support, and the intellectual freedom he continually encouraged during my PhD journey. I remain deeply indebted to him for his confidence in my abilities and for granting me the privilege of conducting this research under his distinguished mentorship.

I extend my sincere gratitude to Prof. H. N. Ghosh, Director of NISER, and Prof. Sudhakar Panda, former Director of NISER, for granting access to the essential laboratory facilities. I also acknowledge with deep appreciation the financial assistance provided by DAE and CSIR.

I wish to express my sincere gratitude to my Doctoral Committee members, Prof. A. Srinivasan, Prof. J. N. Behera, Dr. N. K. Sharma, Dr. A. K. Singh (IIT Bhubaneswar), and Dr. C. S. Purohit, for their constructive guidance and encouragement throughout my research. I am also thankful to the faculty members who taught me during my coursework, and to the School of Chemical Sciences faculty for their generous support and assistance.

I thank Dr. Arun Kumar and Dr. Priyanka Pandey for providing laboratory chemicals, and Mr. Prakash Behera, Mr. Amit, Mr. Sanjaya Mishra, Mr. Deepak Behera, Mr. Anil, and Ms. Roshalin, for their assistance in recording Mass, NMR, and X-ray data. I am also grateful to all non-academic staff of the School of Chemical Sciences and the Institute for their support.

I wish to express my sincere appreciation to my lab members, Dr. Ratha Bhai, Sanjanya, Priyanka, Subhra Jyoti, Suraj, Paresh, and Tanmaya, for their unwavering support, encouragement, and collaborative spirit throughout the course of my research.

I sincerely thank my co-authors, Dr. Radha Krishna Ratha, Dr. Priyanka Ghosh, and Tanmaya, for their significant contributions, assistance with experiments, and valuable discussions that have greatly enriched this work.

Above all, I am deeply grateful to my parents, grandmother, Rinku, and Pinku for their unconditional love, care, and unwavering support throughout this challenging yet fulfilling journey. Their constant encouragement and belief in my abilities have been my greatest source of strength, helping me persevere through difficult times.

Mana Bhanjan Podh

MANA BHANJAN PODH

CONTENTS

SYNOPSIS

(This thesis has been organized into four chapter)

Catenanes are a fascinating class of mechanically interlocked molecules composed of two or more macrocyclic rings that are linked together like the links of a chain, without covalent bonds holding the rings together. This topology imparts unique properties that are fundamentally different from those of traditional covalently bonded molecules. Although catenanes are initially synthesizes in the early 1960s, but their practical synthesis remained limited due to low efficiency and poor selectivity. A breakthrough came with the development of template-directed synthetic strategies, which rely on non-covalent interactions—such as metal coordination, hydrogen bonding, and π–π stacking—to guide and assemble the components in a controlled manner. These methods not only improved the yield and purity of catenanes but also enabled the design of complex and functional interlocked architectures.

The mechanical bond in catenanes allows for controlled relative motion between the interlocked rings, giving rise to dynamic behaviours such as shuttling, pirouetting, and circumrotation. These motions can be triggered by external stimuli such as pH, light, redox conditions, or metal-ion exchange, making catenanes highly attractive for the construction of molecular switches, motors, and responsive materials. Moreover, the possibility of incorporating multiple functional groups and binding sites within the rings has expanded their application potential in fields like molecular electronics, drug delivery, and smart materials.

Recent advances have shifted attention toward the synthesis of higher-order catenanes, including linear [n]catenanes and catenated polymers, which offer even greater conformational freedom and the potential for flexible, mechanically resilient materials. However, the synthesis of such systems remains challenging, often yielding complex product mixtures and requiring intricate design and functionalization strategies. Despite these hurdles, ongoing progress in

templating approaches and click chemistry has opened promising routes for the controlled assembly of well-defined, multiring catenane structures, paving the way for their integration into next-generation functional materials.

Chapter 1 outlines the historical background of catenane synthesis, beginning with the nomenclature used to describe these mechanically interlocked molecules [**Figure 1**].

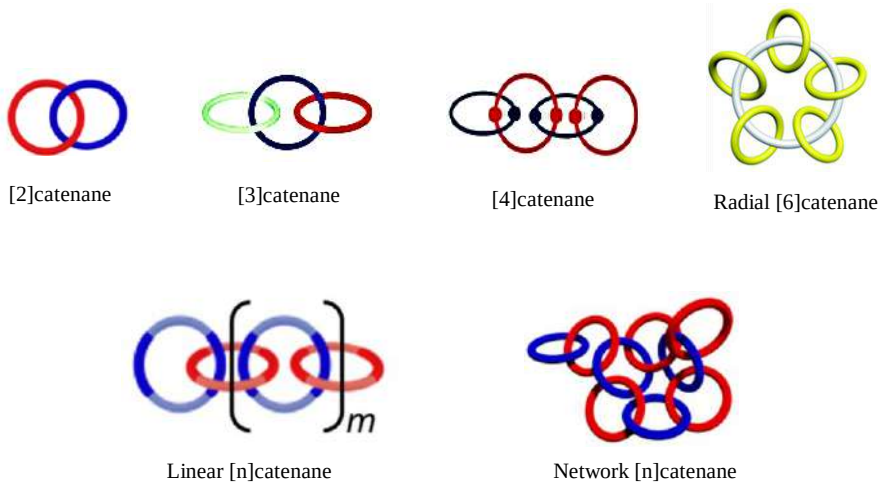

Figure 1. Nomenclature of various catenane based on number of interlocked rings.

It traces the evolution of various synthetic strategies developed over time, with particular emphasis on template-directed methods involving metal coordination, hydrogen bonding, and/or π–π stacking interactions [Figure 2]. The chapter also provides a brief overview of selected applications of catenanes, highlighting their potential use in smart materials.

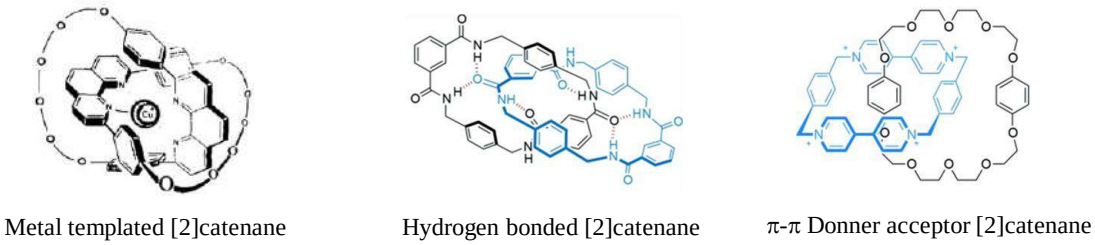

Figure 2. Various template-directed catenane synthesis such as metal coordination, hydrogen bonding, π-π donner acceptor.

Polymers composed entirely of mechanically interlocked rings—such as linear [n]catenanes—are considered promising candidates for functional materials due to their potentially enhanced flexibility, arising from increased conformational freedom. However, the synthesis of such polymers remains a significant challenge, as current methodologies often yield complex mixtures rather than well-defined high-molecular-weight products. Consequently, research efforts have shifted toward the controlled synthesis of low-molecular-weight catenated oligomers.

The design and synthesis of higher-order catenanes present considerable challenges due to the need for precise molecular organization and the necessity to overcome competing intramolecular and intermolecular interactions. Chapter-2 deals with of a one-pot synthetic strategy was employed to successfully construct [2]catenane, linear [3]catenane, and radial [4]catenane through sequential ring-closing reactions facilitated by copper-catalyzed azide–alkyne cycloaddition (click chemistry). This modular approach yielded three distinct and isolable products, corresponding to systems formed via two, four, and six click reactions between appropriately functionalized coupling partners **[Figure 3]**. The isolated yields decreased progressively with increasing molecular complexity—40% for [2]catenane, 12% for linear [3]catenane, and 4% for radial [4]catenane.[**Figure 5**] Such distribution of product is likely due to factors such as the bite angle and conformational flexibility of the reacting components. Subsequent demetallation of the cobalt(III)-templated complexes afforded the corresponding fully organic catenanes. Further, mass spectrometric analysis also suggested the formation of a higher-order species consisting of five interlocked rings coordinated with four Co(III) ions, although this complex could not be isolated in pure form. All these catenanes were purified using column chromatography and fully characterized by ^{1}H NMR, ^{13}C NMR, and ESI-MS spectroscopy. Notably, the presence of uncoordinated binding sites in these structures offers scope for further post-functionalization, making them suitable precursors for the

synthesis of even more complex, higher-order catenanes.

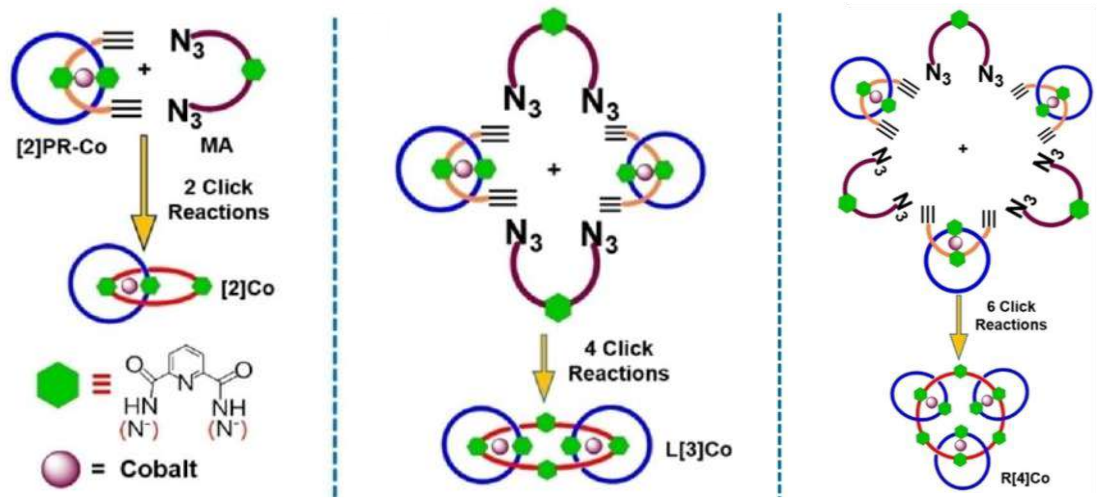

Figure 3. Schematic representation for the formation of various catenane through two, four, six click reaction respectively.

Chapter 3 details the synthesis of a linear [5]catenane via post-functionalization of a Co(III)-templated [2]catenane, which was specifically designed to contain a free pyridine-diamide moiety. This uncoordinated site was subsequently metalated with Co(III) to generate two distinct [3]pseudorotaxanes—one bearing terminal azide groups and the other bearing terminal alkyne groups. These intermediates were then coupled using a copper-catalyzed azide–alkyne cycloaddition ("click" reaction), resulting in the formation of a linear [5]catenane in 40% yield **[Figure 4]**. Subsequent demetallation afforded the metal-free linear [5]catenane. In addition to the target compound, linear [3]- and [2]catenanes were also observed as side products. This approach demonstrates the utility of the anionic, non-labile pyridine-diamide motif as a robust templating center, with potential for further functionalization toward the synthesis of higher-order, mechanically interlocked architectures.

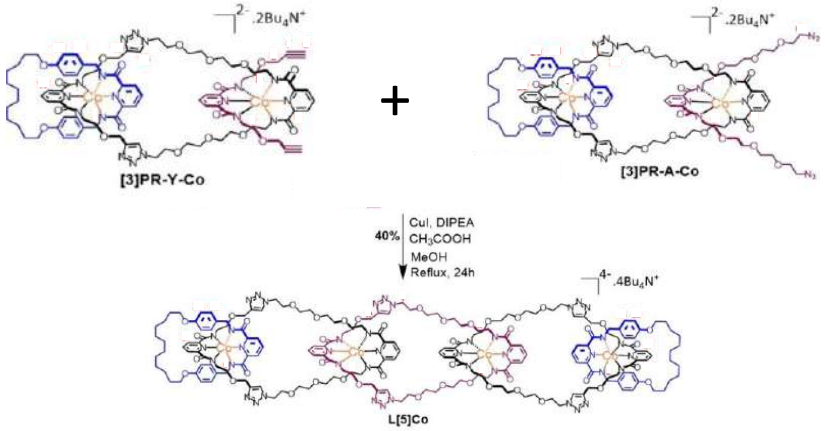

Figure 4. Reaction scheme for the synthesis of Co-templated [5]catenane from the alkyne and azide [3]pseudorotaxane

Chapter 4 presents the reversible interconversion between two homo-[2]catenanes, each containing four templating centers, achieved through a sequence of metalation, demetallation, and re-metalation steps. A cartonic representation of this process is depicted in **[figure 5]**. Each ring incorporates a bidentate diphenyl-phenanthroline and a tridentate pyridine-diamide metal-binding site. The coordination sites are strategically designed to exhibit orthogonal complexation behavior with specific metal ions, enabling controlled relative motion between the interlocked rings. The chosen metal ions, Cu(I) and Co(III), differ in geometry—tetrahedral for Cu(I) and octahedral for Co(III)—resulting in conformationally distinct yet stable complexes. Switching from Cu(I) to Co(III) induces a pronounced co-conformational change, accompanied by pirouetting and circumrotation motions of the interlocked rings. These structural transformations are tracked using distinct ^{1}H NMR signals, color changes in solution, and further supported by ^{13}C NMR, mass spectrometry, UV-visible spectroscopy, and variable-temperature NMR studies. Notably, the presence of two unoccupied templating sites, even after complexation with one metal, makes this system a promising platform for the one-pot synthesis of higher-order even-numbered homo-catenanes.

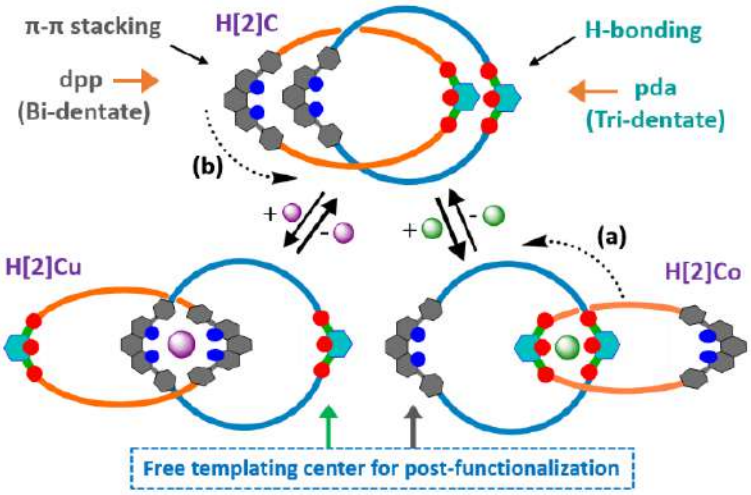

Figure 5. Schematic representation of interconversion between Cu-metal templated homo [2]catenane and Co-metal templated homo[2]catenane through organic homo [2]catenane

List of Schemes

List of Figures

List of Abbreviations

1.	**MIMs**	**Mechanically interlocked molecules**
2.	**DNA**	**Deoxyribonucleic acid**
3.	**PT**	**Passive metal template**
4.	**$CBPQT^{4+}$**	**Cyclobis (paraquat-p-phenylene)**
5.	**ORR**	**Oxygen reduction reactions**
6.	**3D**	**Three dimension**
7.	**MC**	**Macrocycle**
8.	**MY**	**Bis-alkyne functionalized ligand**
9.	**^{1}H NMR**	**Proton nuclear magnetic resonance**
10.	**^{13}C NMR**	**Carbon-13 nuclear magnetic resonance**
11.	**HRMS**	**High Resolution Mass Spectrometry**
12.	**HBr**	**Hydrobromic acid**
13.	**Boc anhydride**	**Di-tert-butyl dicarbonate**
14.	**CH_3CN**	**Acetonitrile**
15.	**TFA**	**Trifluoroacetic acid**
16.	**DCM**	**Dichloromethane**
17.	**RT**	**Room temperture**
18.	**°C**	**Degree Celsius(temperature)**
19.	**NaOH**	**Sodium Hydroxide**
20.	**Et_3N**	**Triethylamine**
21.	**TsCl**	**p-Toluenesulfonyl chloride**
22.	**DMAP**	**4-Dimethylaminopyridin**
23.	**NaN_3**	**Sodium azide**
24.	**KCN**	**Potassium cyanide**

25.	**DMF**	**N,N-Dimethylformamide**
26.	**PPh_3**	**Triphenylphosphine**
27.	**NaH**	**Sodium hydride**
28.	**THF**	**Tetrahydrofuran**
29.	**H_2O**	**Water**
30.	**[2]Co-C or [2]Co**	**Cobalt(III)-metalated [2]Catenane**
31.	**L[3]Co**	**Cobalt(III)-metalated [3]Catenane**
32.	**R[4]Co**	**Cobalt(III)-metalated Radial [4]Catenane**
33.	**m/z**	**Molecular mass/charge**
34.	**[2]**	**[2]Catenane**
35.	**L[3]**	**[3]Catenane**
36.	**R[4]**	**Radial [4]Catenane**
37.	**CD_3OD**	**Deuterated methanol**
38.	**$CDCl_3$**	**Deuterated Chloroform**
39.	**DMSO-d_6**	**Dimethyl Sulfoxide-d_6**
40.	**[2]PR–Co**	**Bis(alkyne) functionalized pseudorotaxane**
41.	**$Co(OAc)_2.4H_2O$**	**Cobalt(II) acetate tetrahydrate**
42.	**$Pd(OAc)_2$**	**Palladium(II) acetate**
43.	**$PdCl_2(CH_3CN)_2$**	**Bis(acetonitrile)palladium dichloride**
44.	**BuNOAc**	**Tetrabutylammonium acetate**
45.	**MeOH**	**Methanol**
46.	**EtOAc**	**Ethyl acetate**
47.	**CuI**	**Copper(I) iodide**
48.	**Zn**	**Zinc**
49.	**AcOH or CH_3COOH**	**Acetic acid**
50.	**DIPEA**	**N,N-Diisopropylethylamine**
51.	**v/v**	**Volume-volume percentage**
52.	**UV light**	**Ultraviolet light**
53.	**ESI^+**	**Electrospray ionization, positive ion mode**
54.	**ESI^-**	**Electrospray ionization, negative ion mode**
55.	**ppm**	**Parts per million**
56.	**VT NMR**	**Variable temperature nuclear magnetic resonance**
57.	**MS-MS experiment**	**Tandem mass spectrometry**
58.	**CuAAC**	**Copper catalysed azide-alkyne cycloaddition**
59.	**$SoCl_2$**	**Thionyl chloride**
60.	**K_2CO_3**	**Potassium carbonate**

61.	**MHz**	**Megahertz**
62.	**Hz**	**Hertz**
63.	**ESI MS**	**Electrospray ionization mass spectrometry**
64.	**g**	**Gram**
65.	**mL**	**Milliliter**
66.	**Rb flask**	**Round bottom flask**
67.	**mmol**	**Millimole**
68.	**N**	**Normality**
69.	**s**	**Singlet**
70.	**d**	**Doublet**
71.	**t**	**Triplet**
72.	**q**	**Quartet**
73.	**m**	**Multiplet**
74.	**dd**	**Doublet of doublet**
75.	**$NaHCO_3$**	**Sodium bicarbonate**
76.	**H**	**Hydrogen**
77.	**br**	**Broad**
78.	δ	**Chemical shift**
79.	**N_2**	**Nitrogen gas**
80.	**Na_2SO_4**	**Sodium bicarbonate**
81.	*J*	**Coupling constant**
82.	**pH**	**Potential of Hydrogen**
83.	**TLC**	**Thin-Layer Chromatography**
84.	**Na_4EDTA**	**Tetrasodium ethylenediaminetetraacetate**
85.	**DI Water**	**Deionized water**
86.	**MeOH-d4**	**Deuterated Methanol**
87.	**[2]Co-dimer or [2]Co-C**	**Co(III)-template [2]catenane**
88.	**[3]PR-Y-Co**	**Bis(alkyne) functionalized [3]pseudorotaxane**
89.	**L[5]Co**	**Co(III)-template linear [5]catenane**
90.	**R_f**	**Retention factor**
91.	**L[2]Co-D or [2]Co-D**	**Dimer of Co(III)-template linear[2]catenane**
92.	**[3]PR-A-Co**	**Bis(azide) functionalized [3]pseudorotaxane**
93.	**L[5]**	**Fully organic linear [5]catenane**
94.	**SiO_2**	**Silicon dioxide**
95.	**CPL**	**Circularly polarized luminescence**
96.	**pda**	**Pyridine-diamine**

97.	**dpp**	**Diphenyl-phenanthroline**
98.	**H[2]C**	**Homo [2]catenane**
99.	**H[2]Cu**	**Cu(I)-mediated Homo [2]catenate**
100.	**H[2]Co**	**Co(III)-mediated Homo [2]catenate**
101.	**$NH_2CH_2CH_2NH_2$**	**Ethylene Diamine**
102.	**2D-COSY**	**Two dimensional correlation spectroscopy**
103.	**FWHM**	**Full width at half maximum**
104.	**nm**	**nanometer**
105.	**λ_{max}**	**The wavelength of maximum light absorption for a specific substance in a UV-Vis spectrum**
106.	**λ_{em}**	**The wavelength of the electromagnetic radiation emitted by an atom or molecule when it transitions from a higher energy state to a lower one**
107.	**MLCT**	**Metal-to-ligand charge transfer**
108.	**UV Visible light**	**Ultraviolet and visible light**
109.	**Li**	**Lithium**
110.	**MnO2**	**Manganese dioxide**
111.	**MALDI-TOF MS**	**Matrix-assisted laser desorption/ionization time of flight mass spectrometry**
112.	**Temp.**	**Temperature**

Chapter-1: Classification and different strategies to synthesis catenane, and its functional aspect

Chapter 2: Template Assisted One-Pot Synthesis of [2], Linear [3], and Radial [4]Catenane via Click Reaction

Chapter 3: Template Assisted Synthesis of Linear [5]Catenane by Post-Functionalization of Templated [2]Catenane and Using Click Reaction

Chapter 4: Metal Ion-Responsive Dynamics in a Homo [2]Catenane: Circumrotation and Pirouetting

Chapter 1: Classification and different strategies to synthesis catenane, and its functional aspect

1.1. What are catenanes?

The term *catenane* was introduced by Emanuel Wasserman in 1960 to describe molecules composed of interlocked rings that are mechanically linked but lack covalent bonding between the components.[1] The name catenane is derived from the Latin word catena, meaning chain. These compounds are macrocycles interlocked into chain-like or shackle-like structures. (**Figure 1.1a**). Catenanes can be classified as linear, radial, or cyclic, based on the arrangement of their interlocked ring. In catenanes, the number of interlocked rings is indicated in square brackets before the name. Thus, linear [6]catenane represents a catenane with six interlocked rings linked together in a sequential linear fashion. Topology dictates macrocycle arrangement: linear catenanes form sequential interlocks, radial ones cluster around a central core, and complex types exhibit multidirectional interlocking. A necklace-like arrangement, with one large ring encircling smaller ones, defines a radial catenane, whereas a closed-loop interlock defines a cyclic catenane, reflecting centralized versus continuous topology. **Figure-1.1** represents various catenanes with six rings. The simplest catenane is a [2]catenane comprising two interlocked rings. Although catenane synthesis was first reported in the 1960s, it remains challenging, and the construction of higher-order catenanes is still in its infancy. Thus far, only single report of a linear polycatenane has been documented in literature.[2] This field gained momentum by the Nobel Prize in 2016 for molecular machine to Jean-Pierre Sauvage, Sir J. Fraser Stoddart and Bernard L. Feringa for the design and synthesis of molecular machines.

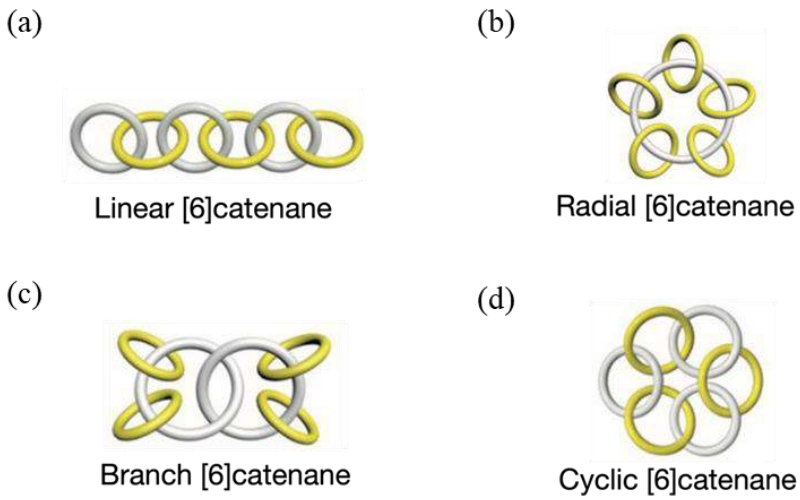

Figure 1.1. Schematic representation of different types of catenanes based on the spatial arrangement and orientation of interlocked macrocycles (a) Linear [6]catenane, (b) Radial [6]catenane, (c) Branched [6]catenane, and (d) Cyclic [6]catenane.

1.2. Classification of catenane:

While a simple classification is outlined above, a more detailed description is needed, as catenanes can be categorized in several ways. As noted earlier, the classification of catenane is primarily based on the number of interlocked rings, arrangement and orientation, structural composition, leading to the following categories:

1.2.1. [2]catenane- It comprises two interlocked rings, also called hopf link since this is the simplest form of catenane.(**Figure 1.2**)

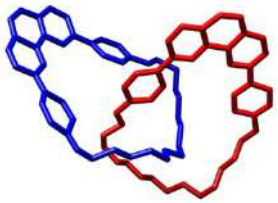

Figure 1.2. The first [2]catenane synthesized by Sauvage's group using a template-directed approach.[3]

1.2.2. Linear [n]Catenane – A linear catenane is a topology where rings are interlocked in a chain, each linked only to its immediate neighbors. A [5]catenane with five interlocked rings arranged like the Olympic rings is called an Olympiadane. (**Figure 1.3)**

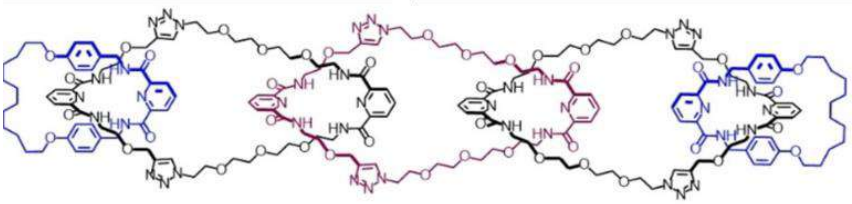

Figure 1.3. A linear [5]catenane, reported from the work of this thesis.[4]

1.2.3. Radial Catenane – In a radial catenane, or "molecular necklace," all rings interlock via a central ring, whose cleavage disassembles the structure; unlike linear or cyclic catenanes, which have no single point of failure. (**Figure 1.4)**

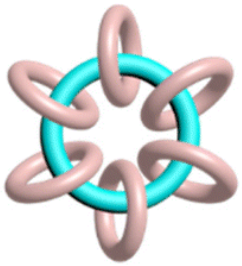

Figure 1.4. Cartoon representation of a radial [7]catenane.

1.2.4. Cyclic [n]Catenane – Cyclic catenanes form closed loops, with each ring linked to two neighbors, rendering all rings equivalent and unlike linear catenanes, which have terminal rings, or radial catenanes, which rely on a central hub for structural integrity. A cartoon representation is shown in **figure 1d**.

1.2.5. Branched [n]Catenane – A more complex topology in which some rings are interlocked with multiple others, resulting in a branched or tree-like structure. (**Figure 1c)** Some other names are also used in literatures.

1.2.6. Homo-catenane – A catenane in which all interlocked rings share the same chemical composition and structure. For example, a [2]catenane consisting of two identical macrocyclic rings. (**Figure 1.5**)

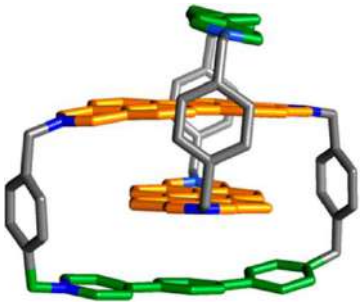

Figure 1.5. A homo-catenane synthesized through π-π donor-acceptor interaction, reported by Stoddart.[5]

1.2.7. Hetero-catenane – A hetero-catenane comprises interlocked rings that differ in composition, size, or functional groups, in contrast to homo-catenanes with identical rings. For example, a [2]catenane composed of one crown ether ring and one cyclophane ring may be called a Hetero catenane.(**Figure 1.6**)

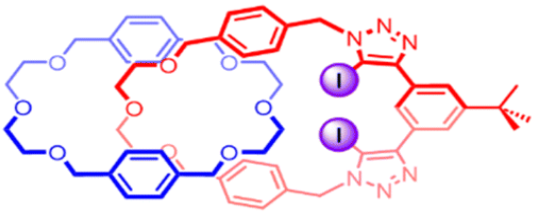

Figure 1.6. A hereto-catenane synthesized through halogen bonding, reported by Paul D Beer.[6]

1.2.8. Metallated-catenane (Metalla-catenane) – In a metallated catenane, metal ions typically coordinate with ligands within or between the rings, often directing the self-assembly of the catenane and helping to stabilize the interlocked architecture. (**Figure 1.7**)

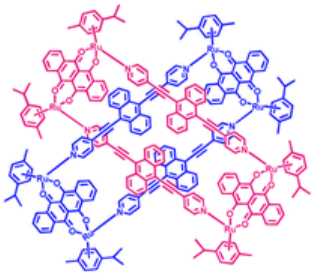

Figure 1.7. Ruthenium(II)-based metalla[2]catenane reported by Chi and co-workers.[7]

1.2.9. Polymeric Catenane – A polymeric catenane is a supramolecular or covalent polymer composed of repeating catenane units or structures where two or more rings are mechanically interlocked. This structure can exhibit unique mechanical properties, like elasticity, sliding motion, or stimuli-responsiveness, due to the mobility of the interlocked rings. They can be liner or radial or mixed ones. (**Figure 1.8**)

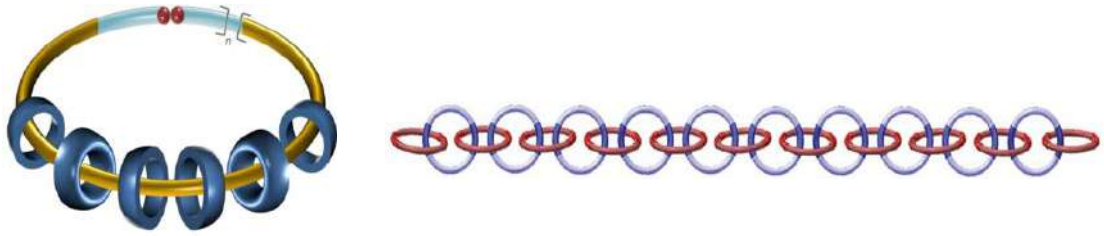

Figure 1.8. Cartoon representation of (a) radial[8] and (b) linear polycatenanes.[2]

Catenanes can also be classified by their functional properties, such as stimuli-responsive or pH-sensitive types. Stimuli-responsive catenanes undergo reversible conformational changes in response to external triggers like pH, light, or redox conditions. These dynamic systems are crucial for molecular machines, switches, and other nanoscale devices in supramolecular chemistry and nanotechnology.

1.3. Historic prospective and synthetic methods:

1.3.1. The statistical approach:

The first successful isolation and characterization of catenanes was serendipitously achieved by Wasserman and coworkers during the synthesis of a large-chain macrocycle via acyloin condensation (Scheme 1.1). By using the macrocycle as a solvent in xylene, they improved the yield to ~1%. This approach relies entirely on the accidental threading of a macrocycle by a macrocycle precursor, which is then closed to form a catenane, and is therefore termed the statistical method.[1]

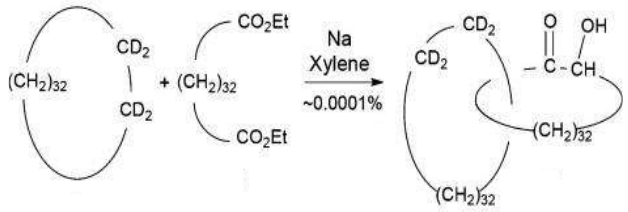

Scheme 1.1. Wassermann (1960) reported the statistical formation of a [2]catenane.

1.3.2. Covalent template-directed strategy:

Due to the low yield, statistical methods could not be well studied. Wasserman and Frisch suggested the use of molecular scaffolds and directed synthesis to improve the yield of interlocked molecules[9]. Consequently, Lüttringhaus and Schill devised a covalent template-directed strategy to construct catenanes in appreciable quantities in 1964.[10] In this approach, a pre-catenane is formed with macrocycles held by a temporary covalent bond; cleaving it releases one ring to yield the catenane. Unlike the statistical method, this directed synthesis offers higher efficiency and greater structural control. (**Figure 1.9**).

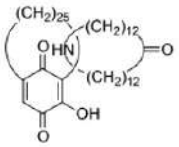

Figure 1.9. Covalent-directed synthesis of a [2]catenane reported by Lüttringhaus and Schill.

Although this method involves multiple synthetic steps and yields are low, it offers a route to interlocked structures that do not rely chance of threading during the synthesis. In recent years, various template such as ester,[11] and azo template are used to synthesis of catenane. All these covalent template methods suffer with multi-step synthesis with low yields.

1.3.3. The metal directed template method:

In 1983, Sauvage developed a metal-ion template-directed method for catenane synthesis, achieving a yield of approximately 40%. They used Cu^{I} cation, which binds two phenanthroline

ligands orthogonally due to its tetrahedral geometry, to synthesize a Cu^{I}-[2]catenane via single or double[12] ring closing strategy with Williamson ether synthesis. Compared to statistical or covalent-template methods, this metal-ion templating offers significantly higher yields and precise control over ring orientation. The copper template was removed to obtain the metal-free catenane (**Scheme 1.2**). Cu[I] templating is often combined with ring-closing methods like Glaser coupling,[13] and Grubbs metathesis for macrocyclization.[14]

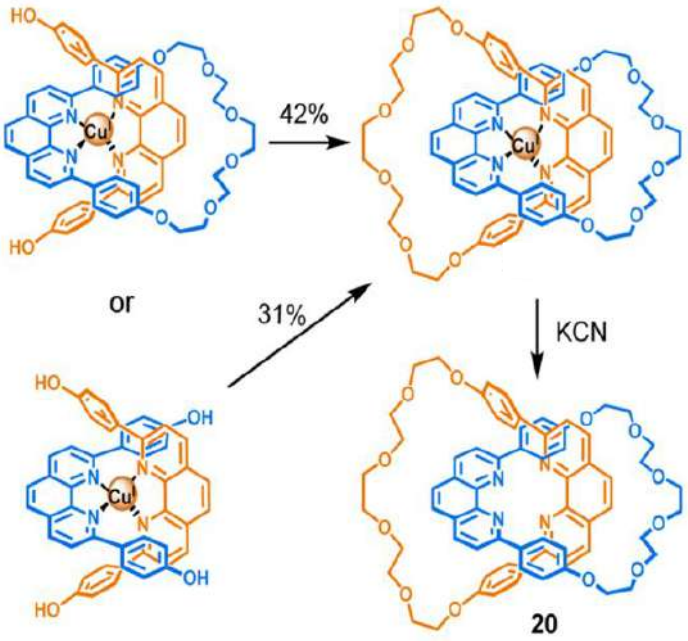

Scheme 1.2. Sauvage's Cu(I)-templated synthesis of [2]catenanes via single and double macro-cyclization.

The stability of the phenanthroline–Cu(I) complex is crucial for successful catenane synthesis, providing an effective template. With a very high formation constant (10^{13} M^{-2} in aqueous solution), the complex remains intact under reaction conditions, holding the phenanthroline ligands in a defined orientation and facilitating ring closure. The templating Cu^{+} ion can then be quantitatively removed with KCN, yielding the metal-free catenane.

This approach led to the development of the passive metal template (PT) method, where preorganization is dictated by the metal ion's preferred geometry, and ring closure forms the

mechanical bonds. Synthetic efficiency depends on both the metal's complexation strength and the effectiveness of the ring-closing reaction.

Pd(II), with a square-planar geometry, offers a contrasting coordination environment to the tetrahedral Cu(I) template, allowing formation of interlocked structures with a tridentate and monodentate ligand. Prof. Leigh's group used a tridentate pyridine-2,6-dicarboxamide and a monodentate 2,6-dimethylene-oxypyridine derivative to form a Pd(II)-templated pseudorotaxane, which underwent ring-closing metathesis (RCM) via alkene-functionalized ligands to yield the [2]catenane in 78% yield.

Compared to Cu(I)-templated synthesis, the Pd(II)-PT method provides higher yields, greater structural precision, and broader flexibility in ligand design, highlighting the advantages of square-planar templating in constructing complex interlocked architectures.[15](**Scheme 1.3**)

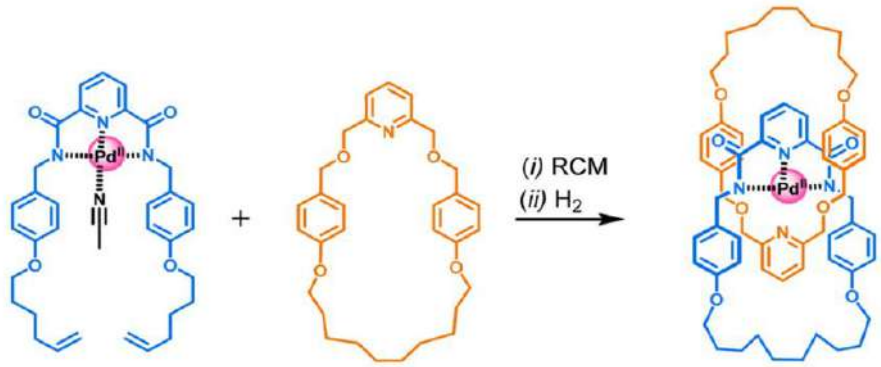

Scheme 1.3. [2]Catenane synthesis via Pd(II)-templated strategy using Grubbs ring-closing metathesis.

Nitschke et al. reported use of a Pd(II)-templated self-assembly strategy using aldehyde and amine. In this strategy, the Pd(II)-ion facilitates the condensation reaction and serves as a template to form a schiff base complex, enabling the synthesis of a [2]catenane.[16] (**Scheme 1.4**).Subsequently, various other geometries such as penta-coordinated Zn^{2+}[17], Ru, Rh complexes, were also employed as templates.

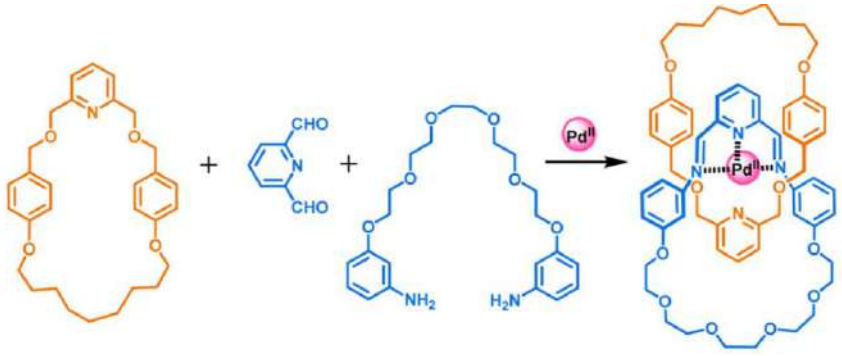

Scheme 1.4. [2]Catenane synthesis via Pd(II)-templated schiff base formation.

The six-coordinate octahedral coordination geometry of transition metals was equally adapted for the PT methodology, providing considerably facile and productive access to a series of [2]catenanes. Many metal ions that can adopt octahedral coordination such as Mn^{2+}, Fe^{2+}, Ni^{2+}, Cu^{2+}, Zn^{2+}, Cd^{2+}, Hg^{2+}, were utilized as template for [2]catenanes synthesis.[18] The ring closing were done by Grubb's catalyst. (**Scheme 1.5**)

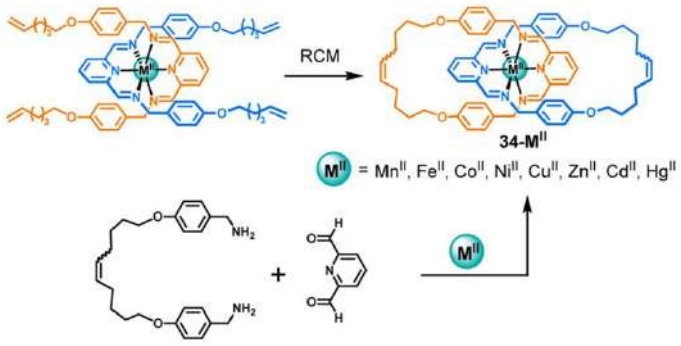

Scheme 1.5. Reaction scheme for the synthesis of an orthogonal, octahedral transition metal-templated [2]catenane.

Leigh and co-workers employed Co(III) as a template in combination with pyridine amide ligands. The complex was generated from Co(II) as the starting material, which was oxidized to Co(III) upon exposure to air. This complex was highly stable and inert to various reaction conditions owing to non-labile nature of the Co(III)-center.[19] Due to the high stability of the complex, demetallation was achieved using Zn/acetic acid, affording the metal-free catenane in 65% yield.(**Figure 1.10**)

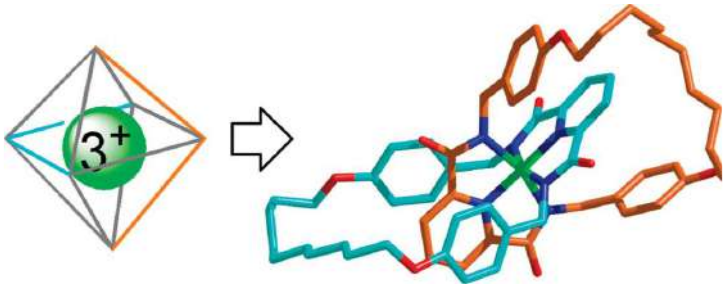

Figure 1.10: X-ray crystal structure of a non-labile Co(III)-templated [2]catenane.

Even the linear geometry of Au(I) has been exploited for the synthesis of catenanes, using appropriately substituted pyridine derivatives. (**Scheme 1.6**)

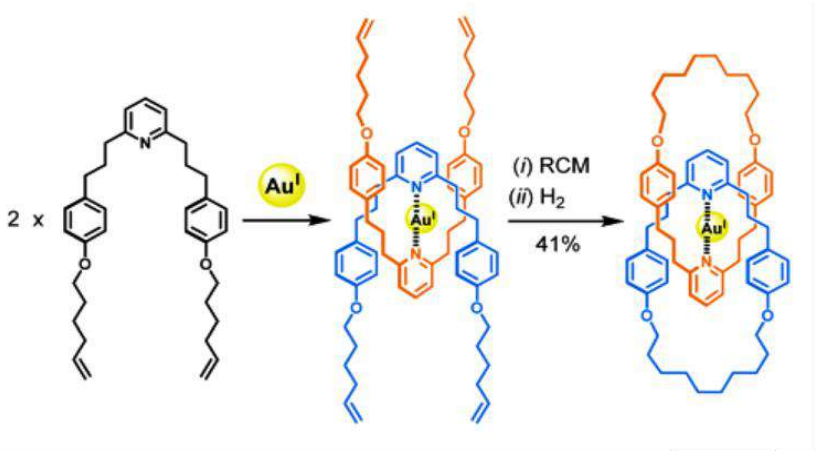

Scheme 1.6. Linear Au(I)-templated [2]catenane synthesis via Grubbs ring-closing metathesis.

1.3.4. The anion directed synthesis:

Apart from metal-ion templates, anions such as chloride, sulfate, and nitrate have also been employed as templates. The chloride ion, in particular, fits well into a suitable tetrahedral binding site. This fact is exploited by Beer's group to synthesis of [2]catenane (45%) as the major and a [3]catenane (5%) as minor product.[20] Chloride ion was used to create a tetrahedral environment through hydrogen bonding with the amide hydrogen atoms of pyridinium and phenyl units, leading to the formation of a pre-catenane complex. The Grubbs catalyst was then employed to close the intermediate, yielding catenanes. (**Scheme 1.7**)

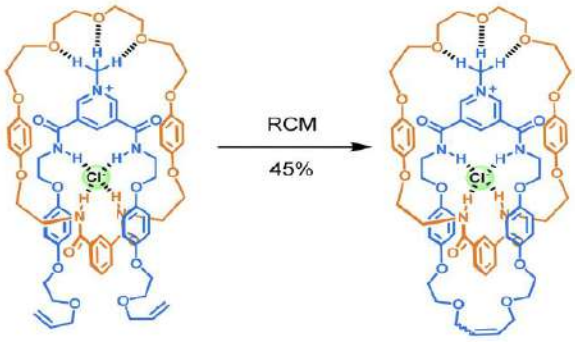

Scheme 1.7. Chloride-templated [2]catenane synthesis via Grubbs ring-closing metathesis.

The tetrahedral sulfate anion has also been used as a template for catenane synthesis. As a dianion, it promotes hydrogen bonding with amide protons of two monocationic precursors, enabling 80% yield of a bis-pyridinium nicotinamide [2]catenane. The final ring closure was achieved through a 'double-clipping' RCM strategy.[21] (**Figure 1.11**)

Figure 1.11. Sulfate-anion-templated homo [2]catenane synthesized via Grubbs ring-closing metathesis reported by Paul D. Beer.

1.3.5. Donor-acceptor catenanes with π–π interaction:

Numerous examples demonstrate the use of supramolecular forces, such as donor–acceptor interactions, to preorganize molecules for ring closure in catenane synthesis. In 1987, Stoddart and co-workers uncovered that cyclobis (paraquat-p-phenylene) $CBPQT^{4+}$ and bispara-phenylene-34-crown-10 derivative forms donor-acceptor complexes in acetonitrile solution and in solid state. Using this interaction, they synthesized a [2]catenane in 70% yield. (**Scheme 1.8**)

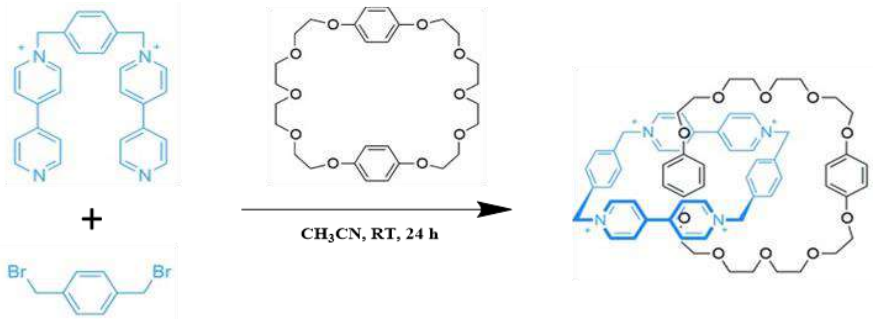

Scheme 1.8. Reaction scheme for the synthesis [2]catenane through π-π donor acceptor interaction reported by stoddart.

In a similar line, Sanders and co-workers have developed neutral donor-acceptor ligand systems for the synthesis of catenanes (**Scheme 1.9**). These precursor molecules are having better solubility in organic solvents than cationic viologen-based macrocycles used by Stoddart. They used phthalimide derivative as electron deficient component and a naphthalene derivative as electron rich counterpart, which self-assembled through π–π stacking interaction. The phthalimide derivative was functionalized with terminal alkynes, while two naphthalene derivatives were incorporated into a crown ether–based macrocycle. Following self-assembly, intermolecular oxidative coupling (analogous to the Glaser coupling of terminal alkynes) afforded the [2]catenane.[22]

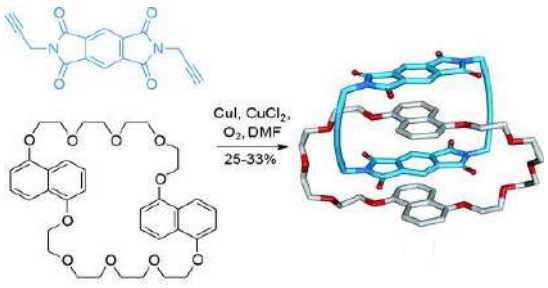

Scheme 1.9. Sanders' synthesis of a [2]catenane through π–π donor–acceptor interactions and oxidative alkyne coupling.

1.3.6. Hydrogen bonding as the driving force:

Hydrogen bonding, alone or with other non-covalent interactions, directs the assembly of mechanically interlocked molecules such as catenanes. The synthesis of the first system was

serendipitous. Hunter and Purvis wanted to investigate the cyclic diamide (**Figure 1.12**) as a receptor for p-benzoquinone[23], with amide protons donating hydrogen bonds to quinone oxygens.

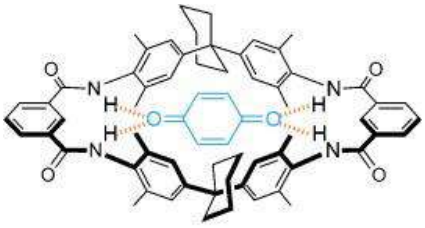

Figure 1.12. Hunter's cyclic diamide macrocycles which act as benzoquinone receptor.

To improve macrocyclization efficiency, they synthesized a catenane via a two-step procedure.[24] (**Scheme 1.10**).

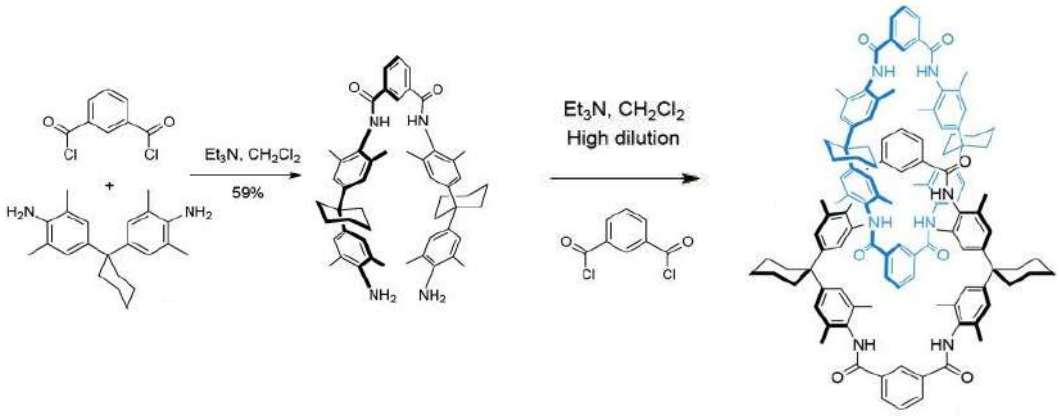

Scheme 1.10. Reaction scheme for the synthesis of Hunter's benzylic amide based [2]catenane.

Leigh's group serendipitously discovered a benzylic amide [2]catenane while making a macrocyclic CO_2 receptor.[25] This [2]catenane was prepared in a single-pot, eight-component condensation of dibenzylamine and isophthaloyl dichloride, yielding 20% (Scheme 1.11). The method efficiently produces a [2]catenane from commercial reagents, with in-situ templating stabilized by hydrogen bonding and π–π stacking. The insolubility of the product in the reaction medium allows it to be isolated easily by simple filtration.

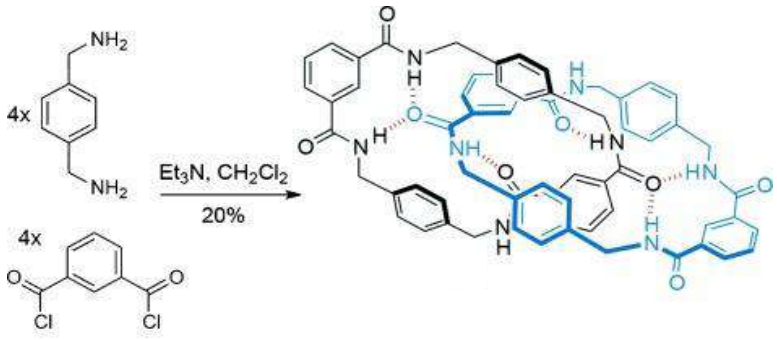

Scheme 1.11. Reaction scheme for the synthesis of a benzylic amide-based [2]catenane.

Various interaction such as halogen bonding, hydrophobic effects and metallacycle formation are also used for catenane synthesis. As the aim of the thesis is to synthesize higher ordered catenae, [n]catenane with n>2, are discussed in the respective chapters.

1.4. Applications of catenanes:

Mechanically interlocked molecules (MIMs), such as catenanes, comprise macrocycles linked by mechanical bonds that allow relative motion and co-conformational flexibility. Their unique topology and dynamics make them valuable for molecular machines, switches, catalysts, sensors, and stimuli-responsive materials. Due to thesis scope, only a few notable examples are discussed.

1.4.1. Catenanes as switches:

The rings of a [2]catenane exhibit continuous relative motion, and controlling this motion is crucial for molecular nanomachines. Sauvage's group was the first to show that external stimuli can regulate ring movement.[26] They exploited the distinct coordination preferences of Cu(I) and Cu(II): Cu(I) favors a tetrahedral geometry, whereas Cu(II) typically adopts square-pyramidal or octahedral geometries. Sauvage's group designed a [2]catenane with one ring bearing a phenanthroline metal-binding site and the other containing both phenanthroline and terpyridine units. Altering the copper oxidation state chemically or electrochemically changes

its coordination geometry, driving the ring to switch between two distinct conformations. (**Scheme 1.12**)

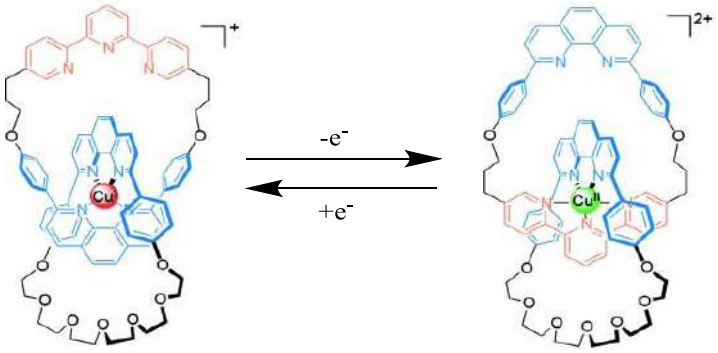

Scheme 1.12. Sauvage's oxidation-state-controlled switching of Cu-metalated hetero [2]catenanes.

Sauvage and co-workers have also demonstrated similar ring switching in a [2]catenane by altering the pH.[27] They exploited the proton-binding ability of phenanthroline units to achieve this function. Upon protonation, the phenanthroline units dimerize, while in the absence of a proton, lone-pair repulsion keeps them apart. In the study, protonation was induced with trifluoroacetic acid, and deprotonation was achieved using pyridine (**Scheme 1.13**)

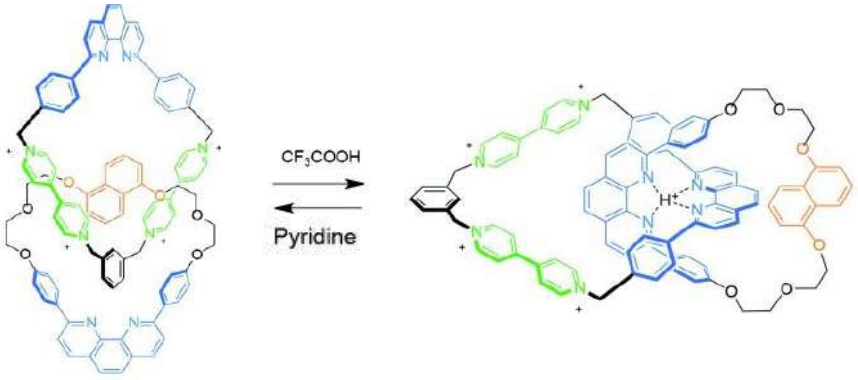

Scheme 1.13. Sauvage's pH-induced switching of a [2]catenane between two distinct co-conformational states.

A three stage switch is demonstrated by Leigh's group.[28] The coordination of anions and solvents plays a crucial role in this study. When $Pd(OAc)_2$ is used as salt, the acetate ion does

not coordinate (and the amide protons deprotonated and absent), allowing the two pyridine units to form the rings of the [2]catenane in a distinct conformation.

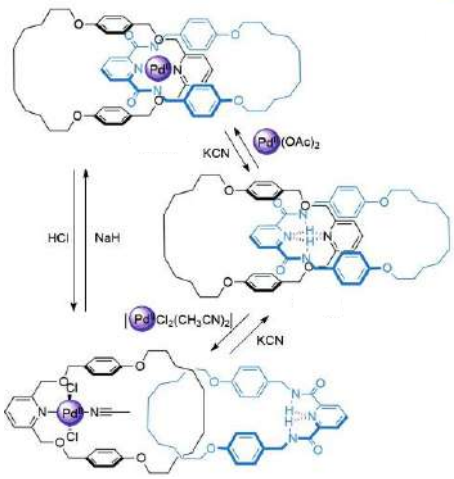

Scheme 1.14. Variable Pd^{2+} coordination modes enable the [2]catenane to switch among three distinct states. However, the observable molecular switching occurs primarily between two different co-conformational states.

Upon demetallation, hydrogen bonding between amide protons and pyridine nitrogens favors a new conformation. With $PdCl_2(CH_3CN)_2$, Pd^{2+} coordinates only to the pyridine unit, stabilized by two chlorides and one acetonitrile and leaving the pyridine diamide uncoordinated, inducing a half-turn in the [2]catenane's relative orientation in solution and solid state. The system can also be switched via protonation and deprotonation using HCl and NaH. (**Scheme 1.14**)

Nondirectional switching among three sites or stations in a [2]catenane can be achieved using photochemical energy.[29] Three sites, referred to as stations and labeled A, B, and C in **Figure 1.13**, are incorporated into a macrocyclic ring. Each site has binding affinity for the smaller benzylic amide macrocycle, though the strengths of these interactions differ. The binding affinities of stations A and B can be drastically reduced through photoinduced isomerization to the maleamide (Z) form using UV light at 350 nm. This photoisomerization occurs at different wavelengths due to the varying distances of the benzophenone group from stations A and B.

Initially, when the larger macrocycle is in the (E,E) state, the relative binding affinities of the stations for the smaller macrocycle are A > B > C.

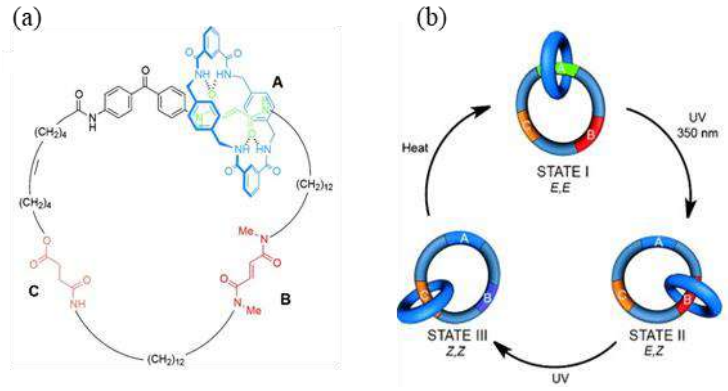

Figure 1.13. (a) The chemical structure of the [2]catenane enables molecular switching (b) A [2]catenane exhibiting molecular switching among three distinct states by modulating the binding affinities of the benzylic macrocycles.

Upon isomerization of station A to the Z form, the order changes to B > C > A, and when both stations A and B are converted to the Z form, the affinities become C > A ≈ B. Thus, the small macrocycle moves sequentially through the stations as the stations are isomerized by UV light. (**Figure 1.13**)

Switching in other catenanes, has been accomplished using anion binding[30] and photo-chemical stimuli(**Scheme 1.15**).[31]

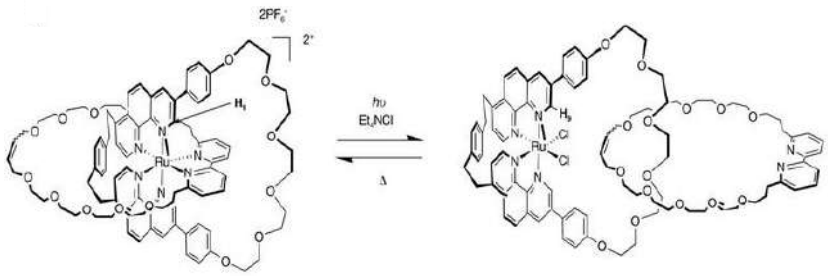

Scheme 1.15. A [2]catenane in which one macrocycle undergoes a half rotation upon exposure to light.

This mechanical bonding allows the interlocked components to move relative to one another, leading to large-amplitude co-conformational changes.[32] The unique topology and dynamic

behavior of these molecules open the door to a wide range of advanced applications in molecular machines[33](**Figure 1.14**), switches,[34] catalyst,[35] sensors,[36] and responsive materials.[37]

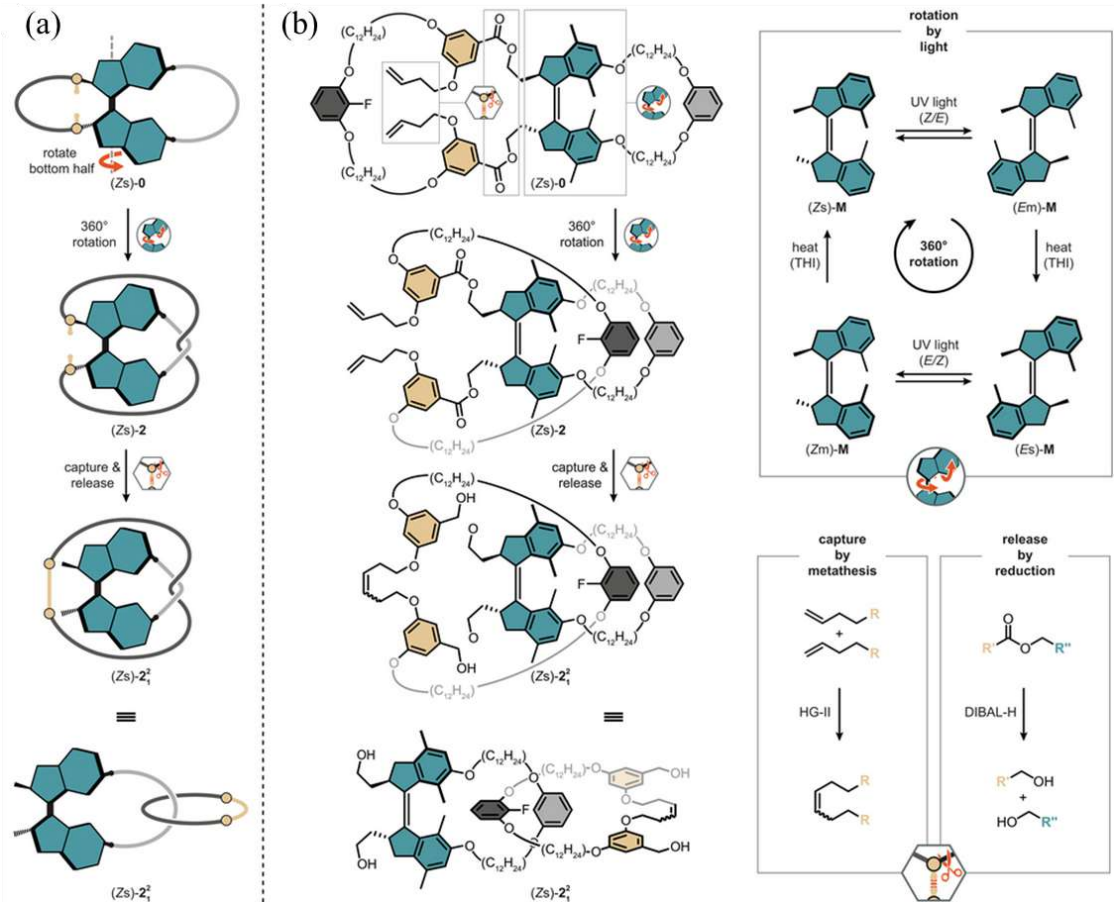

Figure 1.14. (a) Schematic representation of the molecular machine synthesis of a [2]catenane. (b) Reaction scheme illustrating the 360° rotation of the machine unit, including ring-closing metathesis and ester cleavage via reduction.

Catenanes serve as versatile platforms for catalysis, as their interlocked structures can encapsulate catalytic centers, providing a controlled microenvironment that can enhance reactivity and selectivity.[38]Additionally, their dynamic nature enables the design of stimuli-responsive catalysts, in which external triggers can switch the catalytic activity on or off, offering control over reaction processes[35] Catenanes have been employed in various catalytic

processes, including catalysis[39], click reaction catalysts,[35] electrocatalysis[40](**Figure 1.15**), photocatalysis[41].

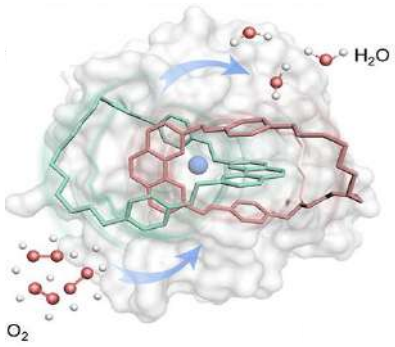

Figure 1.15. The mechanical interlocking in [2]catenanes enhances their electrocatalytic activity for oxygen reduction reactions (ORR).

The interlocked architecture of catenanes creates defined cavities and channels, making them suitable for selective ion binding and transport. This property is exploited in the design of ion sensors and transport systems, where catenanes can selectively recognize and transport specific ions across membranes or within materials[42]. Their ability to undergo conformational changes upon ion binding further enhances their utility in stimuli-responsive sensing applications. Catenanes find applications in ion transport, guest encapsulation[43] (**Scheme 1.16**), sensors and selective binding[6].

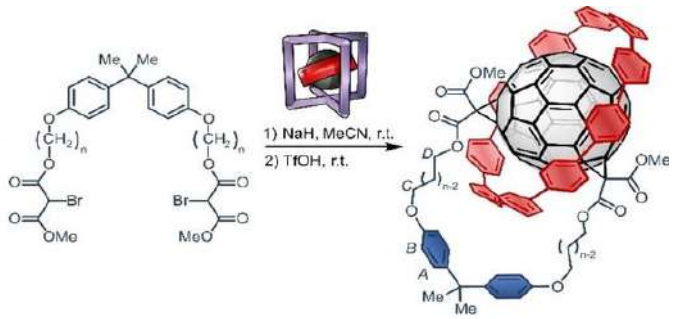

Scheme 1.16. Reaction scheme for the synthesis of [2]catenanes capable of encapsulating C_{60}.

The unique structural features and dynamic properties of catenanes play a crucial role in the development of molecular machines and switches. The mechanically interlocked rings of

catenanes can undergo controlled relative movements, enabling the construction of molecular devices that switch states in response to external stimuli such as light, pH, or redox conditions[29]. As a result of switching, Catenanes find applications in data storage[44](**Figure 1.16**), molecular electronics,[45] and responsive materials.

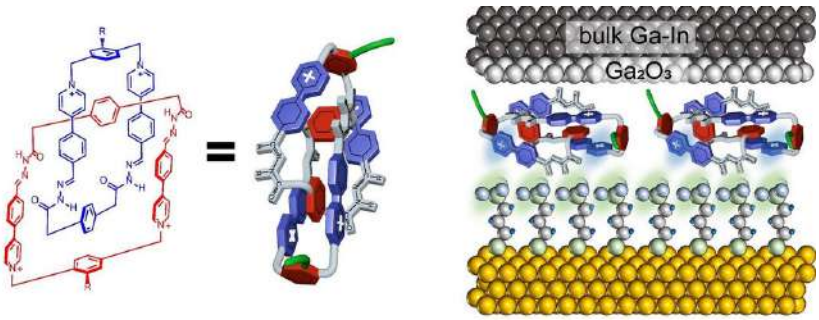

Figure 1.16. Molecular and schematic representation of a [2]catenane functioning as a non-volatile memory device.

Chiral catenanes exhibit optical activity and can emit circularly polarized light(CPL), making them valuable in chiral optoelectronics. Their unique structures allow precise tuning of light-emitting properties, which is beneficial in developing advanced photonic devices and sensors that rely on CPL. These characteristics enable their use in Chiral Optoelectronics[46], Circularly Polarized Luminescence (CPL) Devices[47](**Figure 1.17**), Tunable Light Emission[34]. The ability to control the emission of circularly polarized light has important implications in chiral sensing, bioimaging, and 3D display technologies.

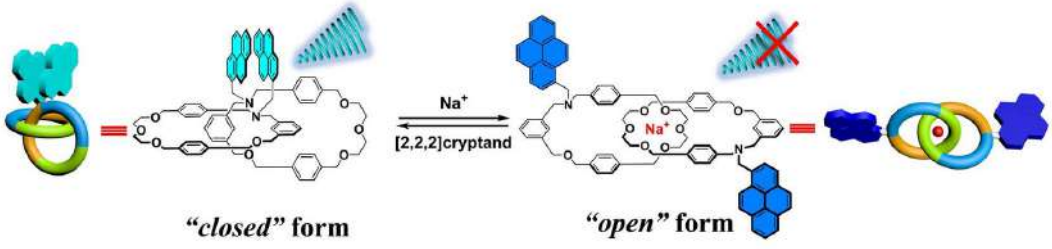

Figure 1.17. [2]Catenane exhibiting circularly polarized luminescence (CPL) properties.

Catenanes can undergo mechanical movements in response to external forces, a property harnessed in mechanochemical switching applications. The application of mechanical stress

can induce conformational changes in catenanes, resulting in alterations of their physical or chemical properties. This behavior is explored in the development of materials that respond to mechanical stimuli, such as stress-responsive polymers[48](**Figure 1.18**) and smart materials[49].

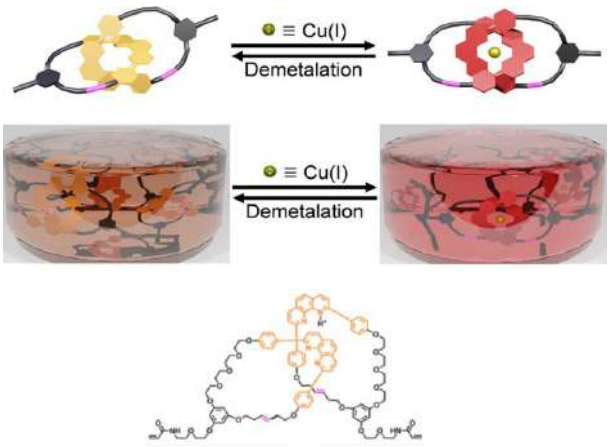

Figure 1.18. Metalation-demetalation processes can modulate the mechanical properties of catenane-crosslinked gels.

1.5. Reference:

[1] E. Wasserman, *J. Am. Chem. Soc.* **1960**, *82*, 4433-4434.

[2] Q. Wu, P. M. Rauscher, X. Lang, R. J. Wojtecki, J. J. de Pablo, M. J. A. Hore, S. J. Rowan, *Science* **2017**, *358*, 1434-1439.

[3] M. Cesario, C. O. Dietrich-Buchecker, J. Guilhem, C. Pascard, J. P. Sauvage, *J. Chem. Soc., Chem. Commun.* **1985**, 244-247.

[4] M. B. Podh, R. Ratha, C. S. Purohit, *Chem. Asian J.* **2024**, *19*, e202400351.

[5] X. Gong, J. Zhou, K. J. Hartlieb, C. Miller, P. Li, O. K. Farha, J. T. Hupp, R. M. Young, M. R. Wasielewski, J. F. Stoddart, *J. Am. Chem. Soc.* **2018**, *140*, 6540-6544.

[6] H. M. Tay, A. Docker, C. Hua, P. D. Beer, *Chem. Sci.* **2024**, *15*, 13074-13081.

[7] H. Lee, P. Elumalai, N. Singh, H. Kim, S. U. Lee, K.-W. Chi, *J. Am. Chem. Soc.* **2015**, *137*, 4674-4677.

[8] T. Higashi, K. Morita, X. Song, J. Zhu, A. Tamura, N. Yui, K. Motoyama, H. Arima, J. Li, *Commun. Chem.* **2019**, *2*, 78.

[9] H. L. Frisch, E. Wasserman, *J. Am. Chem. Soc.* **1961**, *83*, 3789-3795.

[10] G. Schill, A. Lüttringhaus, *Angew. Chem. Int. Ed.* **1964**, *3*, 546-547.

[11] a) S. Duda, A. Godt, *Eur. J. Org. Chem.* **2003**, *2003*, 3412-3420; b) C. Schweez, S. Höger, *Chem. Eur. J.* **2018**, *24*, 12006-12009; c) S. Pilon, S. Ingemann Jørgensen, J. H. van Maarseveen, *Chem. Eur. J.* **2021**, *27*, 2310-2314; d) Y. Segawa, M. Kuwayama, Y. Hijikata, M. Fushimi, T. Nishihara, J. Pirillo, J. Shirasaki, N. Kubota, K. Itami, *Science* **2019**, *365*, 272-276.

[12] C. O. Dietrich-Buchecker, J. P. Sauvage, J. P. Kintzinger, *Tetra. Lett.* **1983**, *24*, 5095-5098.

[13] a) C. O. Dietrich-Buchecker, A. Khemiss, J. P. Sauvage, *J. Chem. Soc., Chem. Commun.* **1986**, 1376-1378; b) J.-M. Kern, J.-P. Sauvage, J.-L. Weidmann, *Tetrahedron* **1996**, *52*, 10921-10934.

[14] B. Mohr, J.-P. Sauvage, R. H. Grubbs, M. Weck, *Angew. Chem. Int. Ed.* **1997**, *36*, 1308-1310.

[15] A. M. Fuller, D. A. Leigh, P. J. Lusby, A. M. Slawin, D. B. Walker, *J. Am. Chem. Soc.* **2005**, *127*, 12612-12619.

[16] C. Browne, T. K. Ronson, J. R. Nitschke, *Angew. Chem. Int. Ed.* **2014**, *53*, 10701-10705.

[17] a) C. Hamann, J.-M. Kern, J.-P. Sauvage, *Inorg. Chem.* **2003**, *42*, 1877-1883; b) T. Prakasam, M. Lusi, E. Nauha, J.-C. Olsen, M. Sy, C. Platas-Iglesias, L. J. Charbonnière, A. Trabolsi, *Chem. Commun.* **2015**, *51*, 5840-5843.

[18] D. A. Leigh, P. J. Lusby, S. J. Teat, A. J. Wilson, J. K. Y. Wong, *Angew. Chem. Int. Ed.* **2001**, *40*, 1538-1543.

[19] D. A. Leigh, P. J. Lusby, R. T. McBurney, A. Morelli, A. M. Z. Slawin, A. R. Thomson, D. B. Walker, *J. Am. Chem. Soc.* **2009**, *131*, 3762-3771.

[20] M. R. Sambrook, P. D. Beer, J. A. Wisner, R. L. Paul, A. R. Cowley, *J. Am. Chem. Soc.* **2004**, *126*, 15364-15365.

[21] B. Huang, S. M. Santos, V. Felix, P. D. Beer, *Chem. Commun.* **2008**, 4610-4612.

[22] D. G. Hamilton, J. K. M. Sanders, J. E. Davies, W. Clegg, S. J. Teat, *Chem. Commun.* **1997**, 897-898.

[23] C. A. Hunter, D. H. Purvis, *Angew. Chem. Int. Ed.* **1992**, *31*, 792-795.

[24] a) C. A. Hunter, *J. Am. Chem. Soc.* **1992**, *114*, 5303-5311; b) H. Adams, F. J. Carver, C. A. Hunter, *J. Chem. Soc., Chem. Commun.* **1995**, 809-810.

[25] A. G. Johnston, D. A. Leigh, R. J. Pritchard, M. D. Deegan, *Angew. Chem. Int. Ed.* **1995**, *34*, 1209-1212.

[26] a) A. Livoreil, C. O. Dietrich-Buchecker, J.-P. Sauvage, *J. Am. Chem. Soc.* **1994**, *116*, 9399-9400; b) F. Baumann, A. Livoreil, W. Kaim, J.-P. Sauvage, *Chem. Commun.* **1997**, 35-36; c) A. Livoreil, J.-P. Sauvage, N. Armaroli, V. Balzani, L. Flamigni, B. Ventura, *J. Am. Chem. Soc.* **1997**, *119*, 12114-12124.

[27] D. B. Amabilino, C. O. Dietrich-Buchecker, A. Livoreil, L. Pérez-García, J.-P. Sauvage, J. F. Stoddart, *J. Am. Chem. Soc.* **1996**, *118*, 3905-3913.

[28] D. A. Leigh, P. J. Lusby, A. M. Z. Slawin, D. B. Walker, *Chem. Commun.* **2005**, 4919-4921.

[29] D. A. Leigh, J. K. Y. Wong, F. Dehez, F. Zerbetto, *Nature* **2003**, *424*, 174-179.

[30] a) A. Andrievsky, F. Ahuis, J. L. Sessler, F. Vögtle, D. Gudat, M. Moini, *J. Am. Chem. Soc.* **1998**, *120*, 9712-9713; b) K.-Y. Ng, V. Felix, S. M. Santos, N. H. Rees, P. D. Beer, *Chem. Commun.* **2008**, 1281-1283; c) N. H. Evans, C. J. Serpell, P. D. Beer, *Chem. Eur. J.* **2011**, *17*, 7734-7738.

[31] P. Mobian, J.-M. Kern, J.-P. Sauvage, *Angew. Chem. Int. Ed.* **2004**, *43*, 2392-2395.

[32] Y. Yao, Y. C. Tse, S. K.-M. Lai, Y. Shi, K.-H. Low, H. Y. Au-Yeung, *Nat. Commun.* **2024**, *15*, 1952.

[33] T. Wachsmuth, R. Kluifhooft, M. Müller, L. Zeiß, M. Kathan, *Science* **2025**, *389*, 526-531.

[34] S. Yang, C.-X. Zhao, S. Crespi, X. Li, Q. Zhang, Z.-Y. Zhang, J. Mei, H. Tian, D.-H. Qu, *Chem.* **2021**, *7*, 1544-1556.

[35] A. Bessaguet, Q. Blancart-Remaury, P. Poinot, I. Opalinski, S. Papot, *Angew. Chem. Int. Ed.* **2023**, *62*, e202216787.

[36] K. M. Bąk, B. Trzaskowski, M. J. Chmielewski, *Chem. Sci.* **2024**, *15*, 1796-1809.

[37] H. Xing, Z. Li, W. Wang, P. Liu, J. Liu, Y. Song, L. Wu Zi, W. Zhang, F. Huang, *CCS Chem.* **2020**, *2*, 513-523.

[38] R. Mitra, H. Zhu, S. Grimme, J. Niemeyer, *Angew. Chem. Int. Ed.* **2017**, *56*, 11456-11459.

[39] L. Zhu, J. Li, J. Yang, H. Y. Au-Yeung, *Chem. Sci.* **2020**, *11*, 13008-13014.

[40] X. Mo, Y. Deng, S. K.-M. Lai, X. Gao, H.-L. Yu, K.-H. Low, Z. Guo, H.-L. Wu, H. Y. Au-Yeung, E. C. M. Tse, *J. Am. Chem. Soc.* **2023**, *145*, 6087-6099.

[41] Y. Jiao, L. Đorđević, H. Mao, R. M. Young, T. Jaynes, H. Chen, Y. Qiu, K. Cai, L. Zhang, X.-Y. Chen, Y. Feng, M. R. Wasielewski, S. I. Stupp, J. F. Stoddart, *J. Am. Chem. Soc.* **2021**, *143*, 8000-8010.

[42] H. Min Tay, T. G. Johnson, A. Docker, M. J. Langton, P. D. Beer, *Angew. Chem. Int. Ed.* **2023**, *62*, e202312745.

[43] F. M. Steudel, E. Ubasart, L. Leanza, M. Pujals, T. Parella, G. M. Pavan, X. Ribas, M. von Delius, *Angew. Chem. Int. Ed.* **2023**, *62*, e202309393.

[44] Y. Xie, C.-Y. Wang, N. Chen, Z. Cao, G. Wu, B. Yin, Y. Li, *Angew. Chem. Int. Ed.* **2023**, *62*, e202309605.

[45] Y.-H. Kim, S. S. Jang, Y. H. Jang, W. A. Goddard, *Phys. Rev. Lett.* **2005**, *94*, 156801.

[46] Y. Wang, W.-L. Zhao, Z. Gao, C. Qu, X. Li, Y. Jiang, L. Hu, X.-Q. Wang, M. Li, W. Wang, C.-F. Chen, H.-B. Yang, *Angew. Chem. Int. Ed.* **2025**, *64*, e202417458.

[47] Y. Wang, J. Gong, X. Wang, W.-J. Li, X.-Q. Wang, X. He, W. Wang, H.-B. Yang, *Angew. Chem. Int. Ed.* **2022**, *61*, e202210542.

[48] M. A. Nosiglia, N. D. Colley, M. K. Danielson, M. S. Palmquist, A. O. Delawder, S. L. Tran, G. H. Harlan, J. C. Barnes, *J. Am. Chem. Soc.* **2022**, *144*, 9990-9996.

[49] M. Zhang, G. De Bo, *J. Am. Chem. Soc.* **2020**, *142*, 5029-5033.

Chapter 2: Template Assisted One-Pot Synthesis of [2], Linear [3], and Radial [4]Catenane via Click Reaction

2.1. Abstract:

Design and synthesis of higher order catenane are unexpectedly complex and involve precise cooperation among the precursors overcoming competing and opposing interactions. We achieved synthesis of [2], linear [3], radial [4]catenane in a one-pot reaction by consecutive ring closing through click reactions. This synthesis gave three isolable products due to two, four, and six-click reactions between suitable coupling partners. Yields of the isolate templated-catenane decrease from lower to higher-ordered catenane (40%, 12%, and 4%), probably due to the bite angle as well as the flexibility of the reacting partners.

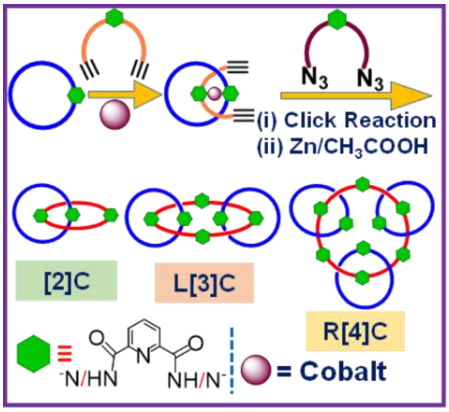

Removal of templating cobalt(III) ion leads to the formation of fully organic [2], linear [3], and radial [4]catenane. These synthesized catenanes were purified by column chromatography and characterized by ^{1}H-NMR, ^{13}C-NMR, and ESI-MS spectroscopy. The synthesized catenanes have free binding sites suitable for post-functionalization and may be used for the synthesis of higher-ordered catenane.

2.2. Introduction:

In recent years, synthesis of supramolecular topologies/architectures comprising mechanically interlocked molecules (MIMs) and investigations into their properties have gained significant attention.[1] Study of MIMs are essential to understand biologically important knotted structures those are found in DNA, proteins, and polymers, playing a vital role in their functions.[2] These structures also have a wide range of applications as molecular machines such as a molecular motor,[3] molecular pump,[4] ion transport system,[5] and photoswitch.[6] Among MIMs, catenanes are a class of interlocked molecules and are fascinating due to their molecular topologies. In recent times, many applications, such as in catalysis, [7] photo-catalysis, [8] as electro catalyst, [9] a catalyst for click reaction, [10] memory device, [11] and guest molecule encapsulation, [12] etc. have surfaced for this class of molecules. Also, structurally modified catenanes show optical activity and chirality. [13] Common strategies for catenane synthesis include self-assembly, π-π stacking, hydrogen bond, halogen bond, metal templated, and covalent bonding. [14] Among these methods, use of a template is the most common one. The template brings the precursor units to suitable orientation for effective ring closing; therefore, higher yields can be realized.[15] Despite development of various synthetic methods, higher (≥ 4) catenanes are still difficult to achieve, and only two reports of poly[n]catenane synthesis exists in literature so far; one solely organic poly[n]catenane using Zn^{2+} template with double bond metathesis for ring closing,[16] and other one is a recent report of infinite twisted metalla-poly[n]catenane linked due to Ag^{+}.[17] The major difficulty is the lower yield in the ring-closing step(s).[18] Thus, click chemistry is conceived as one of the methods for the ring-closing step[19] and subsequently employed for the synthesis of [2], radial [4], and branched [8]catenanes.[20] Another reaction for ring closing is the Grubbs ring closing metathesis.[21] In the synthesis of complex molecular architectures such as square knot, and granny knot, both these reactions have been used.[22] Although the use of click reaction for the

synthesis of catenanes and rotaxanes is well explored,[20d] only a few reports exist for the synthesis of higher (n > 3) catenanes.[20a–c] These reports are restricted to a limited number of topological structures and need to be explored further in terms of a wide range of available templates and other useful tectons.[19e,20b,c]

Among higher-ordered catenanes, radial [n]-catenane, also known as molecular necklace (when n > 3), are catenanes with a cyclic backbone containing (n-1) catenated peripheral rings.[23] Different strategies are adapted for the construction of these peripherally interlocked structures that include: head to tail cyclization of a pseudo-polyrotaxane[24]/ polyrotaxane,[25] using macrocycles having multiple recognition sites as the template,[26] utilizing metal coordination for macro-cylisation of [2]pseudorotaxane monomer[27] and covalent bonding.[28]

Sauvage group reported the synthesis of [n]catenane and radial-[n]catenane using Cu(I) as a template and Glaser coupling as a ring-closing step.[15a,23] Similar to this report, the click reaction with suitable substrate can combine in various ratios to give many products that may include linear or radial catenane(s) but have never been investigated.

Thus, we designed suitable pre-organized coupling partners for click reaction(s) that would either cyclize to [2], [3] linear, or higher radial catenanes and study the possible outcome of this one-pot reaction. Although there are few reports, we choose Co(III) as our template due to its non-labile nature in the amide complexes. Thus, the templated assembly, once synthesized, is quite stable under various reaction conditions and can be used further.[29] In this chapter, we report a one-pot synthesis and characterization of [2], linear [3], radial [4] and radial [5] pre-catenate complex using a cobalt(III)-template for threading and click reaction as the ring closing method. The synthesized templated catenanes are formed hierarchically with different polarities and can be observed and separated using chromatographic methods.

2.3. Result and discussion:

2.3.1. Design of ligand MA, MC, and MY:

As planned, we synthesized a macrocycle **MC** (**Scheme 2.1**) from 2,6-pyridinedicarbonyl dichloride and a long-chain diamine.

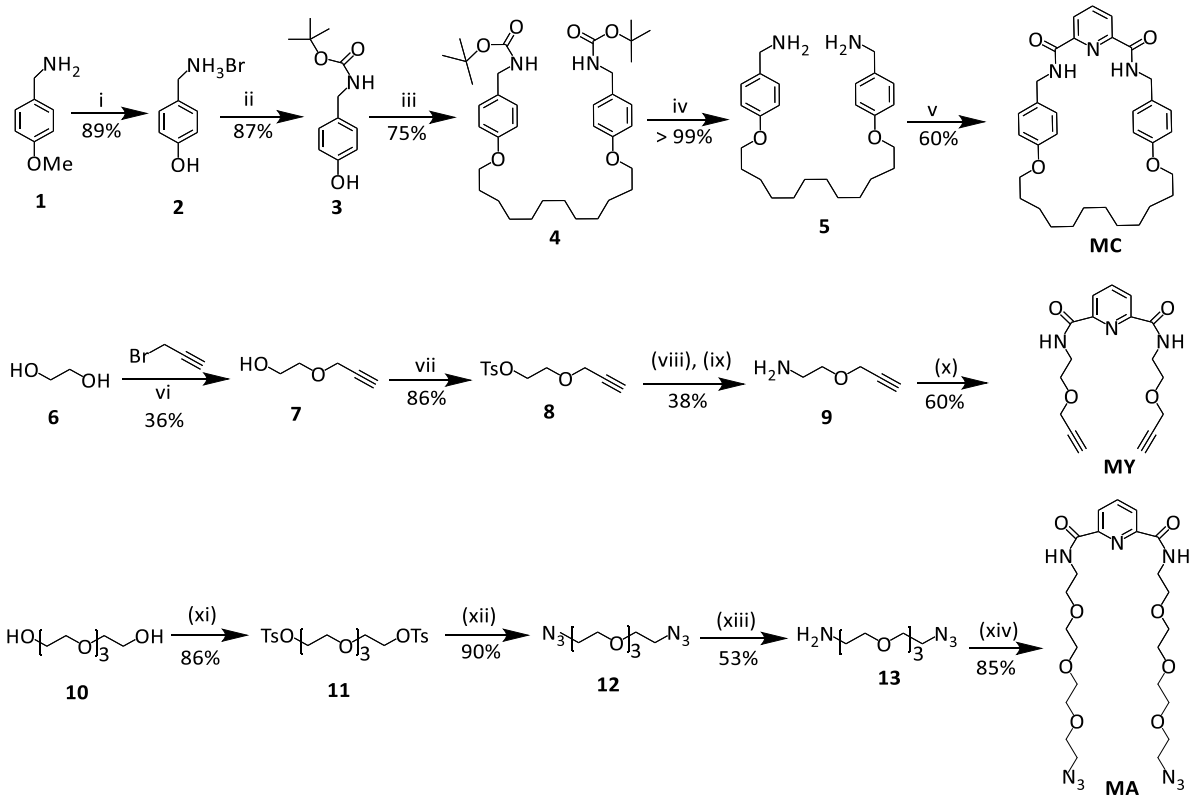

Scheme 2.1. Regents and condition for synthesis of monomers and macrocycle: (i) 48% HBr, reflux, 12 h (ii) Boc anhydride, MeOH, RT, 24 h (iii) 1,12-dibromododecane, CH_3CN, reflux, 18 h (iv) TFA, DCM, RT, 3 h, NaOH (v) pyridine-2,6-dicarbonyl dichloride, Et_3N, DCM (high dilution), RT, 18 h (vi) NaOH, 45 ˚C (vii) TsCl, Et_3N, 0.05 eq. DMAP, DCM, RT, 3 h (viii) NaN_3, DMF, 55 ˚C, 12 h (ix) PPh_3, THF, H_2O, RT, 12 h (x) pyridine-2,6-dicarbonyl dichloride, Et_3N, DCM, RT, 18 h (xi) TsCl, Et_3N, 0.05 eq. DMAP, DCM, RT, 3 h (xii) NaN_3, EtOH, 90 ˚C, 36 h (xiii) PPh_3, THF, H_2O, 24 h (xiv) pyridine-2,6-dicarbonyl dichloride, Et_3N, DCM, RT, 18 h.

The reaction was carried out in DCM at room temperature under high dilute condition for getting the maximum yield (55%). It was characterized with ^{1}H-NMR, ^{13}C-NMR, and HRMS (m/z for [**MC** +H]$^{+}$ 544.3180, found: 544.3212) (Full data are given in **section 2.6.2**). **MC** would be threaded with the help of cobalt ion, providing orthogonal interactions with the threading unit. The long chain non-interfering twelve-member alkyl chain for **MC** was selected to provide space for the threading unit to come in and to enhance the solubility of the macrocycle in common organic solvent.

The threading unit (**MY**), having two terminal alkyne groups (for ring closing click reaction), is synthesized from 2,6-pyridinedicarbonyl dichloride and a monoamine with alkyne terminal in DCM at RT (**Scheme 2.1**). **MY** could be synthesized in 73% yield, characterized with ^{1}H-NMR, ^{13}C NMR, and HRMS (m/z for [**MY**+H]$^{+}$ 330.1446, found: 330.1472)(Full data are given in **section 2.6.2**). We deliberately used a short chain (–CH_2–CH_2–O–CH_2–) linker between –NH and the alkyne group for this unit to provide less flexibility and have a proper bite angle for the ring-closing step. Thus, the cobalt ion will be coordinated with two pyridine and four amide nitrogen atoms from **MC** and **MY**.

The coupling partner for click reaction **MA** has two terminal azide groups was synthesized from 2,6-pyridinedicarbonyl dichloride and another monoamine with azide terminal in DCM at RT (**Scheme 2.1**). The monoamine compound **11** was synthesized via selective reduction of the diazide using PPh_3 in 53% yield; the reduced yield is attributed to the concurrent formation of the diamine derivative in a considerable amount. Here, we put a long spacer (tetra-ethylene glycol units) to make it flexible, to avoid steric crowding during the ring-closing, and to enhance the solubility of the product. Also, crown ether moiety could respond to stimuli due to Na^{+} and K^{+} ions and could enhance its functionality. The choice of the pyridine diamide unit in **MA** is to provide another site for metal complexation that will enable the synthesis of various higher-order catenanes. **MA** was obtained in 90% yield and characterized by ^{1}H-NMR, ^{13}C NMR, and HRMS (m/z for [**MA**+ Na]$^{+}$ 590.2688, found: 590.2660, (Full data are given in **section 2.6.2**).

As depicted in the cartoon representation in **Figure 2.1**, the ligands **MA** and **MY** are designed to have a geometry with a proper bite angle as their linkers are 2,6-functionalized at pyridine diamide (**Scheme 2.2**). Thus, consecutive click reactions in radial fashion between di-azide and di-alkyne reacting partners leads to a ring-closing reaction that results formation of macrocycle without any alkyne and/or azide terminus along with other products. Hence, **[2]Co** is a result of two click reactions, and **L[3]Co** is the result of four click reactions and is a linear catenane. But six click reactions forms a macrocycle, called radial **R[4]Co** catenane by definition.

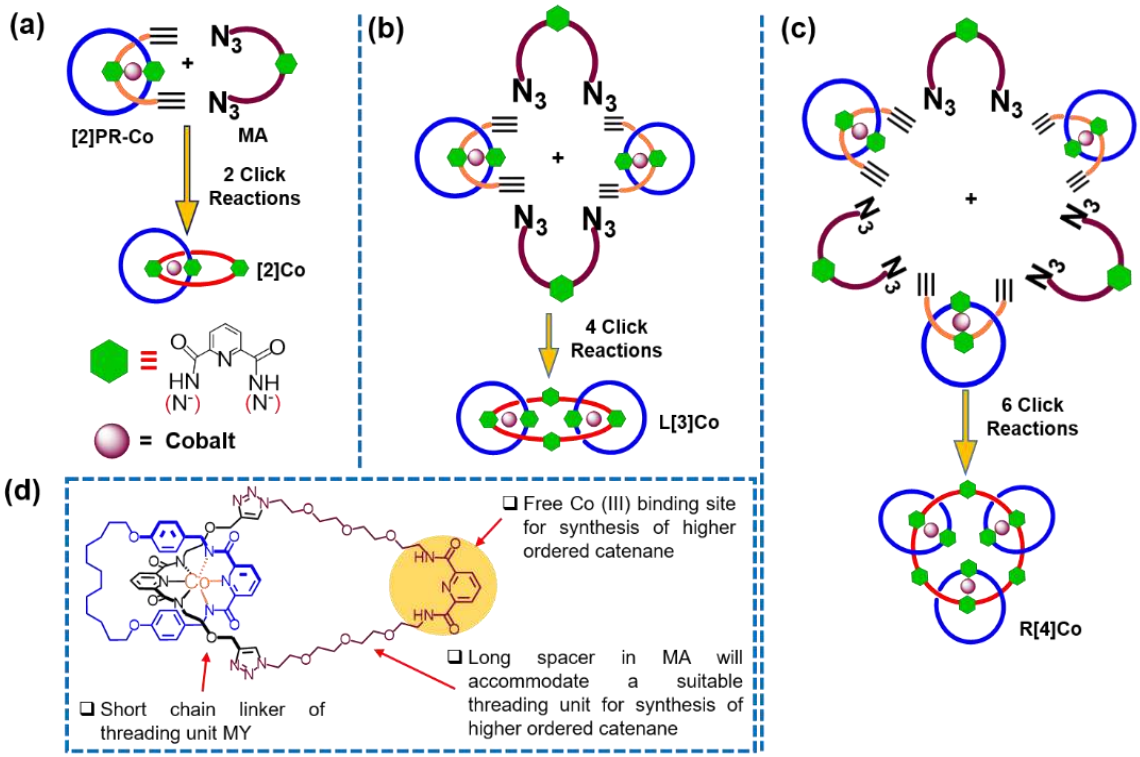

Figure 2.1. Cartoon representation for increasing formation of templated catenanes by ring-closing reactions between [2]pseudorotaxane and **MA** in various ratios (a) 2 click reaction results **[2]Co** (b) 4 click reactions results **L[3]Co** (c) 6 click reactions lead to formation of **R[4]Co** (d) explains choice of threading unit **MY** and **[2]Co** has free Co(III)-binding site for higher order catenane synthesis through post-functionalization.

2.3.2. Synthesis [2]pseudorotaxane from MC and MY:

Complexation reaction is performed by refluxing an equivalent amount of the macrocycle (**MC**), $Co(OAc)_2.4H_2O$, and Bu_4NOAc in MeOH for 2 h to give a pink color solution, followed by the addition of one equivalent of **MY** as a solution in methanol.

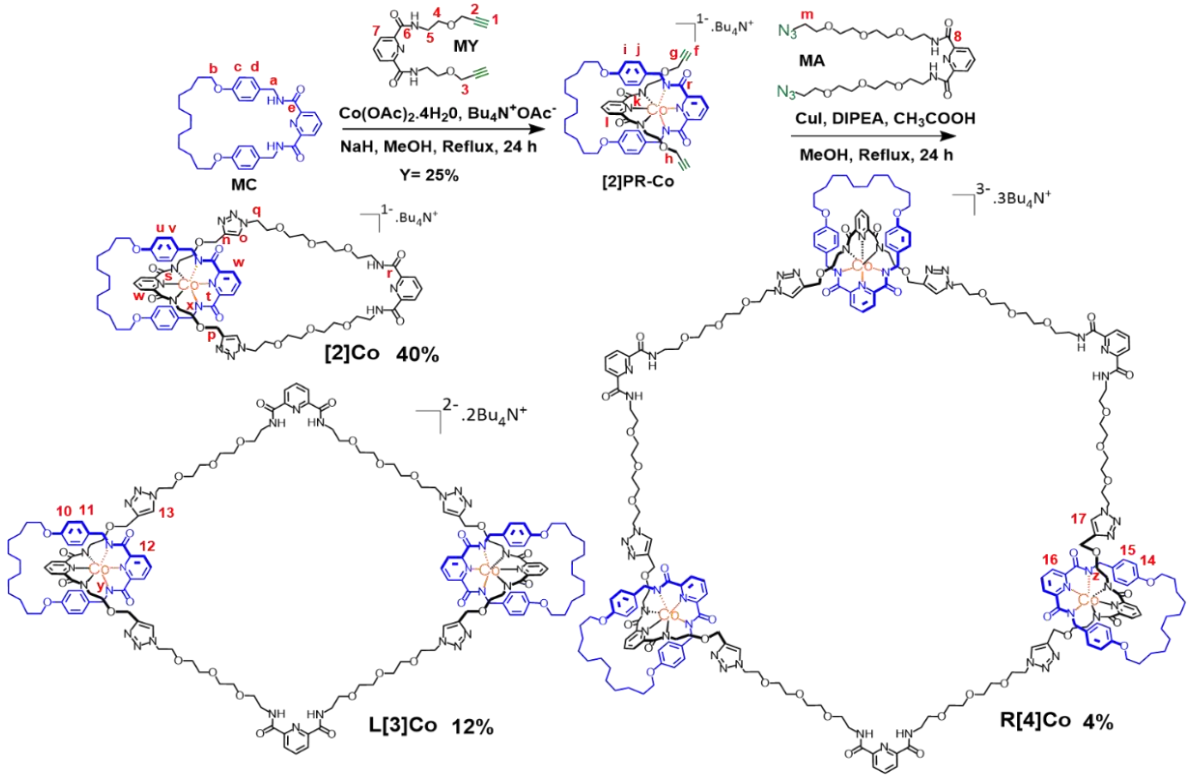

Scheme 2.2. Reaction scheme for the synthesis of [2]pseudorotaxane from its constituent subunits (**MC** and **MY**) and cobalt(III)-metalated catenanes **[2]Co**, **L[3]Co**, **R[4]Co** from [2]pseudorotaxane and **MA** via click reaction.

The sequence of addition is important to avoid or minimize the homodimer formation between **MY** ligands. Subsequently, addition of excess NaH in methanol shows a color change from pink to purple. Upon exposure to air under reflux conditions, the color change is observed from purple to green, indicating the conversion of labile Co(II) to non-labile Co(III). It may be noted that, the designed ligand supports to capture soft Co(II) but subsequently convert into hard Co(III) by air exposure after deprotonation of the amide nitrogen atoms. The product formation

is indicated by thin layer chromatography as a new spot (green colored) below the precursor units (**MC** and **MY**). The overall charge of the complex becomes 1^- due to the coordination of two doubly negative charged groups into Co(III), and the tetrabutyl ammonium ion acts as a counter cation. The pseudorotaxane (**[2]PR–Co**) could be purified by column chromatography (10 : 90 v/v MeOH: EtOAc) to get the product. It was found that some impurities could not be separated even through the column separation, as indicated by ^{1}H-NMR. However, these impurities could be washed off with ethyl acetate, and the product was obtained as a greenish semisolid with a 25% yield. **[2]PR–Co** was characterized by ^{1}H-NMR, ^{13}C-NMR, and mass spectroscopy.

Formation of **[2]PR–Co** from constituent monomer (**MY**) and macrocycle (**MC**) can be observed from ^{1}H-NMR proton signals, which comprise both **MC** and **MY** sub-unit proton signals (**scheme 2.2**) and mass spectra (**Figure 2.4**). The terminal-alkyne proton peak **1** (2.82 ppm) and methylene signal **3** (4.19 ppm) next to the triple bond (**Figure 2.2a**) of **MY** has become signal **f** (2.75 ppm) and signal **h** (3.5 ppm) for **[2[PR–Co** respectively (**Figure 2.2c**). In addition, benzene aromatic peaks **d** (7.21 ppm), **e** (6.82 ppm) of **MC** (**Figure 2.2b**) have become signal **l** (6.4 ppm) and **j** (6.25 ppm) for **[2[PR–Co** (**Figure 2.2c**). Moreover, the ^{1}H-NMR signals for the protons close to the coordination sphere get shifted upfield due to an increase in shielding effect caused by the perturbation from the complexation (**Figure 2.2**). Such a shielding effect has also been observed in previously reported knotted structures.[29–30] In addition, ^{13}C-NMR provides further evidence for the synthesis of entangled molecules, i. e. pseudorotaxane (**[2]PR–Co**). Two peaks at 76 and 80 ppm (**Figure 2.3a**) correspond to **MY** terminal-alkyne carbon are present in isolated **[2]PR–Co** (**Figure 2.3c**). Moreover, two sets of carbonyl carbons signals (one from **MC** and the other from **MY**) at 170.33 and 170 ppm are observed for **[2]PR–Co** (**Figure 2.3c**), suggests the product.

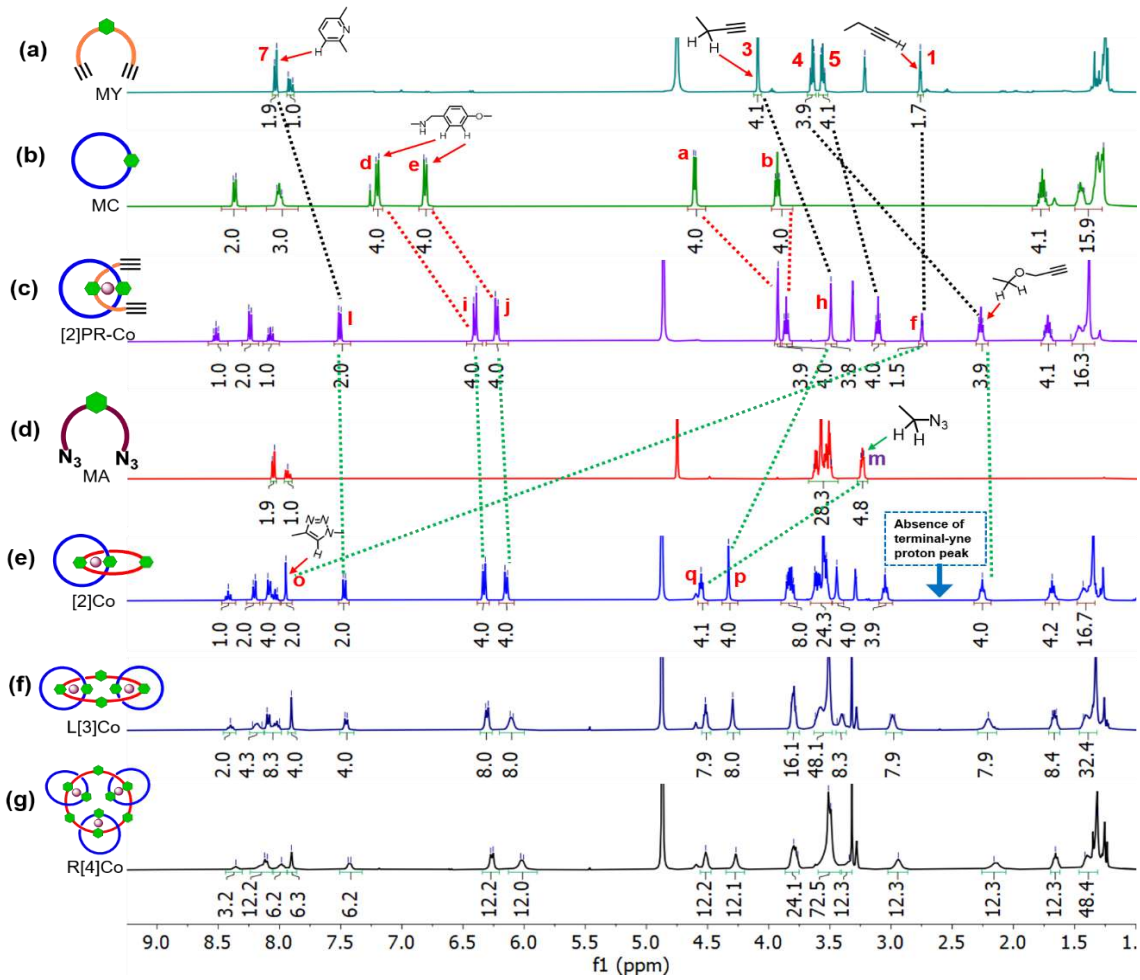

Figure 2.2. Comparison of ^{1}H-NMR peak shift for the formation of Co(III)-metalated catenane **[2]Co**, **L[3]Co**, **R[4]Co** from precursor **MC**, **MY** and **MA** (a) di-Yne ligand **MY** in CD_3OD (b) macrocycle **MC** in $CDCl_3$ (c) pseudorotaxane **[2]PR–Co** in CD_3OD (d) di-Azide ligand **MA** in CD_3OD (e) **[2]Co** in CD_3OD (f) linear **[3]Co** in CD_3OD (g) radial **[4]Co** in CD_3OD. Proton NMR for **MC** is recorded in $CDCl_3$ due to its poor solubility in CD_3OD at RT. NH^{-} protons getting exchanged with CD_3OD and are not seen here.

Further evidence for the product comes from mass spectroscopy. ESI^{+} mass spectra of **[2]PR–Co** (**Figure 2.4a**) includes clusters of isotopic distribution peaks at m/z 951.3342, the base peak (calcd. m/z for $C_{50}H_{58}CoN_6O_8$ [(**[2]PR–Co**)$^{1-}$+Na^{+} +H^{+}]$^{+}$ 951.3451). These signals correspond to 1^{+} charged states of **[2]PR–Co** and are in good agreement with the theoretically

calculated values. The peak for the counter cation tetrabutyl ammonium can also be observed at m/z of 242.2850 (**Section 2.6.2**).

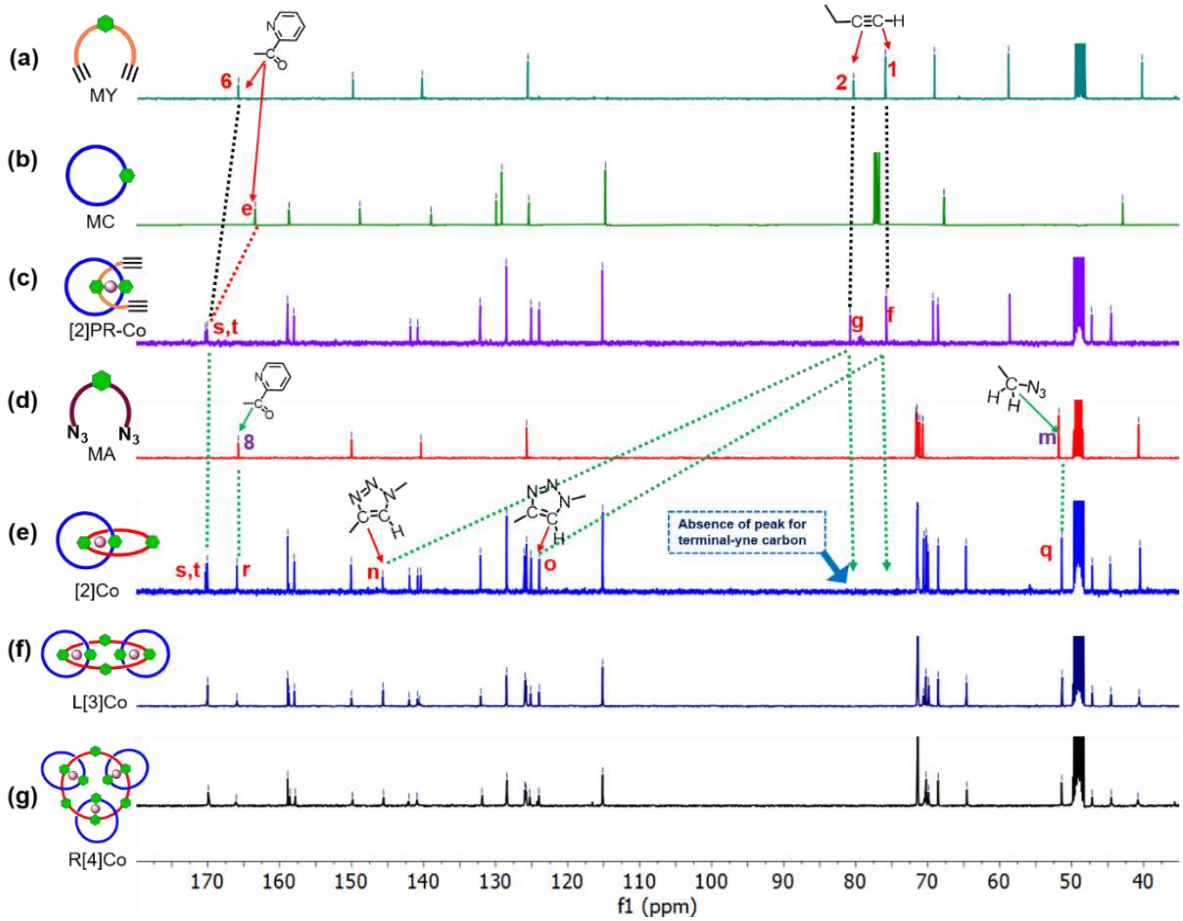

Figure 2.3. Comparison of partial ^{13}C-NMR peak shift for the synthesis of Co(III)-metalated catenane **[2]Co**, **L[3]Co**, **R[4]Co** from precursor macrocycle **MC**, **MY** and **MA** (a) di-Yne ligand **MY** (b) macrocycle **MC** (c) pseudorotaxane **[2]PR–Co** (d) di-Azide ligand **MA** (e) **[2]Co** (f) linear **[3]Co** (g) radial **[4]Co**. All spectra are recorded in CD_3OD except **MC** due to poor solubility in CD_3OD at RT. **MC** Spectra is recorded in $CDCl_3$.

2.3.3. Ring-closing of [2]PR–Co: Synthesis of templated catenanes

The final ring closing click reaction for the synthesis was performed by refluxing an equivalent amount of di-alkyne **[2]PR–Co** and di-azide ligand **MA** in the presence of CuI, CH_3COOH, and DIPEA in MeOH for 24 hours. Completion of the reaction was indicated by the

disappearance of **[2]PR–Co** and **MA**. A tlc of the reaction mixture with 55:45 (EtOAc: MeOH, v/v) revealed the formation of 3 major compounds and a trail of green-colored spots, which can be seen with naked eye as well as under UV light.

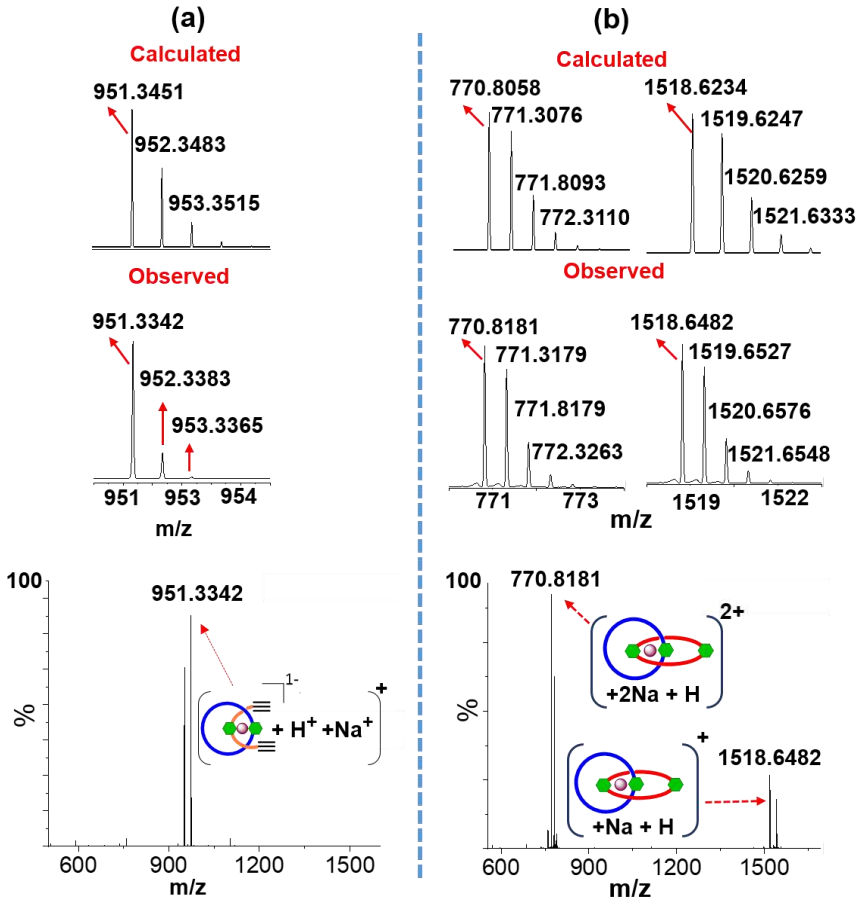

Figure 2.4. Characterization of (a) pseudorotaxane **[2]PR–Co** (b) Co(III)-metalated [2]catenane by ESI^+ mass spectra (bottom) with isotopic distribution peaks (top); theoretically calculated isotopic distribution peaks matching with experimentally observed one. Full spectra data are given in **section 2.6.2.**

These three spots were isolated using silica gel column chromatography with EtOAc: MeOH as eluent. The first spot isolated via column chromatography corresponds to **[2]Co** with 40% yield, followed by **L[3]Co** with 12% yield, and **R[4]Co** with a yield of 4%. The variation in the yield of catenanes may be attributed to an increase in bite angle, flexibility of the reacting

partners, and the reaction dynamics. Moreover, **[2]Co**, **L[3]Co**, and **R[4]Co** are formed via consecutive 2, 4, and 6 click reactions (**Figure 2.1**) between **[2]PR–Co** and **MA** might influence the yield. It is worth mentioning that Co(III) is not getting replaced by Cu(I) while performing click reaction in the ring closing step. Formation of templated catenane can be suggested by the absence of terminal-alkyne proton peak at 2.75 ppm in **[2]PR–Co** (**Figure 2.2e**) and appearance of a peak at 7.95 ppm (peak **o** in **Figure 2.2e**, which corresponds to triazole ring protons). Furthermore, construction of electron-withdrawing triazole ring caused a de-shielding effect to nearby protons, i. e., peak **h** (3.5 ppm for **[2]PR–Co**) is shifted to peak **p** (4.32 ppm) in the **[2]Co** (Figure 2). A similar de-shielding effect has also been seen for the **MA** ligand. The peak at 3.32 ppm (peak **m** from **MA**) shifted to 4.55 ppm (peak **q** in **[2]Co**) (**Figure 2.2**).

In ^{13}C-NMR spectra of **[2]Co**, peaks corresponding to terminal alkyne (77 and 79 ppm) are absent when compared to **[2]PR–Co** (**Figure 2.3e**). This indicates the accomplishment of ring closing leading to the formation of **[2]Co**, the [2]catenane still connected with the cobalt ion. This is further supported by appearance of peaks at 145.7 and 123 ppm (peaks **n** and **o** in **Figure 2.3e**) for quaternary and tertiary carbon of the triazole ring, respectively. Moreover, the peak from carbonyl carbon (peak **8** Figure **2.3d**) and peak for carbon next to the azide-group (peak **m** Figure **2.3d**) of **MA** are present in **[2]Co**, provides further evidence of completion of the ring closing reaction.

In positive mode ESI spectra, diagnostic peaks found at m/z 1518.6482 and 770.8181 are attributed to mono and di-cationic charged species produced from **[2]Co**. The isotopic distribution matches with the simulated mass data for **[2]Co**; calculated m/z for $C_{73}H_{94}CoN_{15}O_{16}Na$ [(**[2]Co**)$^{1-}$+ Na^+ + H^+]$^+$ is 1,518.6234 and for $C_{73}H_{94}CoN_{15}O_{16}Na_2$ [(**[2]Co**)$^{1-}$+ 2Na^+ + H^+]$^{2+}$ is 770.8058 (**Figure 2.4b**). This suggests the formation of **[2]Co**. The

peak for tetrabutyl ammonium can also be observed at m/z of 242.2850 (Full data are given in **Section 2.6.2**). The addition of one Na^+ ion in mass spectroscopy is a common phenomenon due to the use of sodium borosilicate glass/HCOONa for standardization. We are getting more Na^+ in the spectra, possibly due to the tetraethylene glycol units in the synthesized structures. Which is known to stabilize Na^+. Although a general rule towards the order of synthesized catenane and the number of Na^+ attached to it cannot be drawn, with an increase in tetraethylene glycol chain, the number of sodium is increasingly found to be added to the mass of the molecular ion.

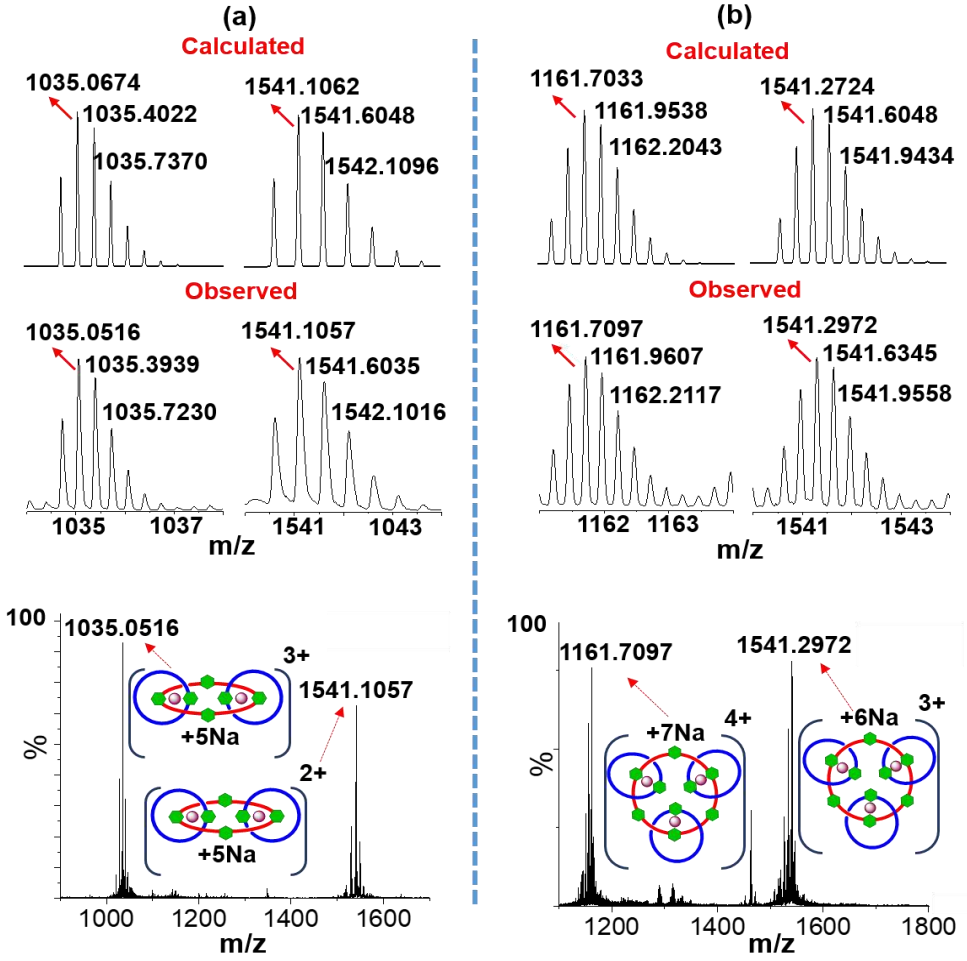

Figure 2.5. Full ESI^+ mass spectra (bottom) (a) **L[3]Co** catenane shows intense peaks at m/z 1035 and 1541, corresponds to 3^+ and 2^+ charged species, respectively; (b) **R[4]Co** shows intense peaks at m/z 1161 and 1541 corresponds to 4^+ and 3^+ ionic species respectively. Comparison between simulated and experimental isotopic distribution peaks given on the top.

The NMR spectra of catenanes **L[3]Co** and **R[4]Co** are like **[2]Co** due to their structural similarity (**Figure 2.2f**, **2.2g**). However, the proton NMR signals become broader for **L[3]Co** and **R[4]Co** because of conformational changes.[21,31] The identification of **L[3]Co** and **R[4]Co** is further evidenced with prominent peaks in ESI^+ mass spectra. For **L[3]Co**, group of isotopic distribution peaks at m/z 1541.1057 corresponds to a 2^+ charged species $[(\mathbf{L[3]Co})^{2-} + 4Na^+]^{2+}$ and at m/z 1035.0516 is attributed to a 3^+ charged species $[(\mathbf{L[3]Co})^{2-} + 5Na^+]^{3+}$.The corresponding simulated isotopic mass (calcd. m/z for $C_{146}H_{186}Co_2N_{30}O_{32}Na_4$ $[(\mathbf{L[3]Co})^{2-}+ 4Na^+]^{2+}$ 1541.1062 and m/z for $C_{146}H_{186}Co_2N_{30}O_{32}Na_5$ $[(\mathbf{L[3]Co})^{2-} + 4Na^+]^{2+}$ 1541.1062 and m/z for $C_{146}H_{186}Co_2N_{30}O_{32}Na_5$ $[(\mathbf{L[3]Co})^{2-} + 5Na^+]^{3+}$ 1035.0674) are also matching with the experimentally observed data (**Figure 2.5a**). Similarly, for **R[4]Co** 3^+ and 4^+ charged peaks can be readily identifiable at m/z 1541.2972 and m/z 1,161.7097, respectively (**Figure 2.5b**) and correctly match with calculated mass.

When analyzed under ESI negative mode, the radial catenane (**R[4]Co**) results in a base peak at m/z 1495.0839 (**Figure 2.6**) with isotopic distribution pattern which matches with the simulated mass spectra of $\mathbf{R[4]Co^{3-}}$ $C_{219}H_{279}Co_3N_{45}O_{48}$ is 4485.8837/3 = 1,495.2945), providing evidence that this species possesses triple negative charge. In addition, another product having four cobalt ion is formed in trace amount. The mass spectra (ESI negative mode) is matching with radial pre-[5]catenate complex (calcd. m/z for $[(\mathbf{R[5]Co})^{4-}$ $C_{292}H_{372}Co_4N_{60}O_{64}$ is 5981.5128/4 = 1,495.3755, found: 1,495.4163 (**Figure 2.7**) but could not be isolated by column chromatography in pure form for further characterization.

Diffusing various solvents into templated catenanes does not produce good crystals for diffraction, possibly due to the semisolid nature of the compound.

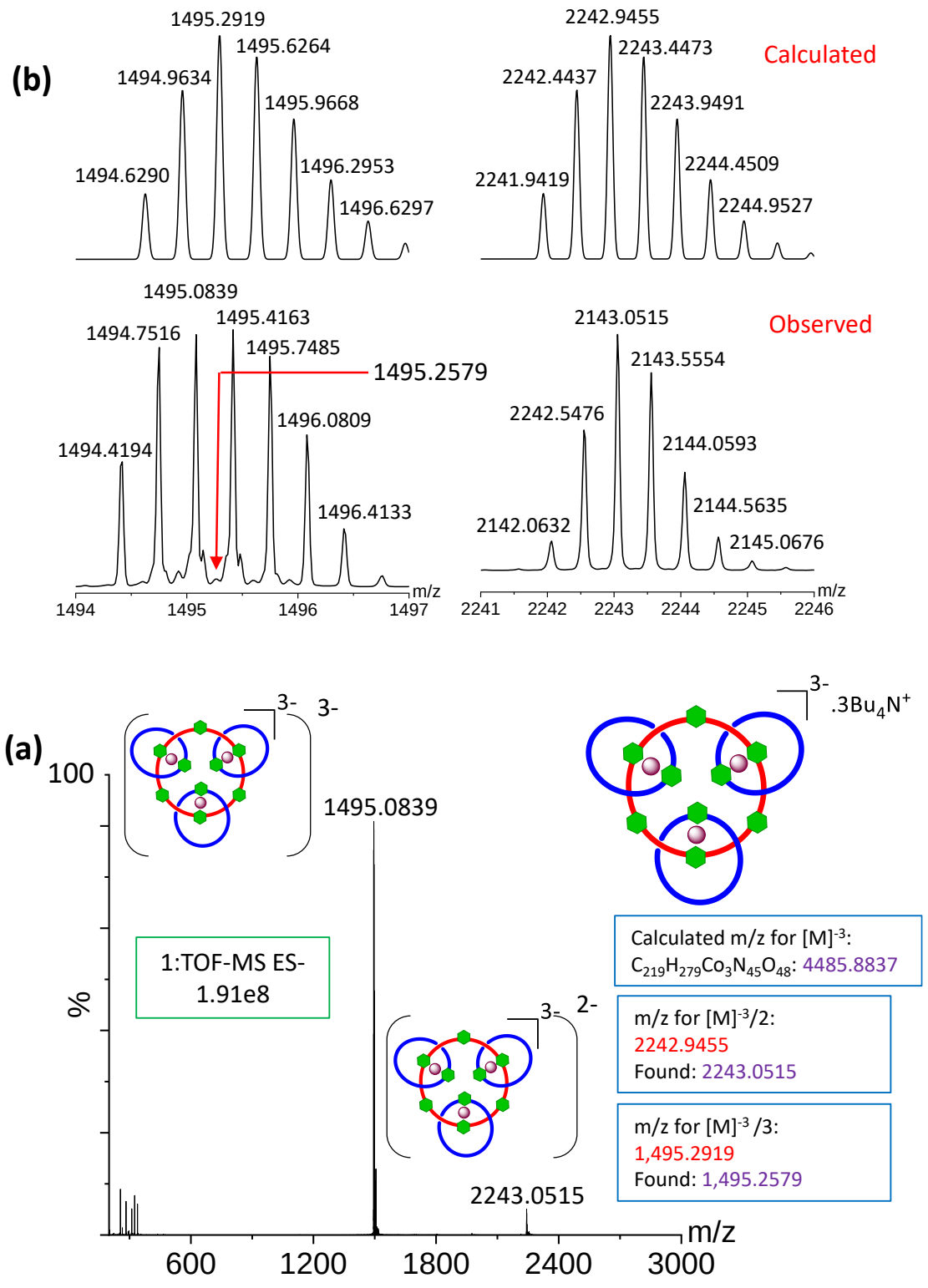

Figure 2.6. Mass spectra (ESI^-) analysis for synthesized **R[4]Co** (a) full spectra (b) comparison between calculated and experimentally observed isotopic distribution peaks.

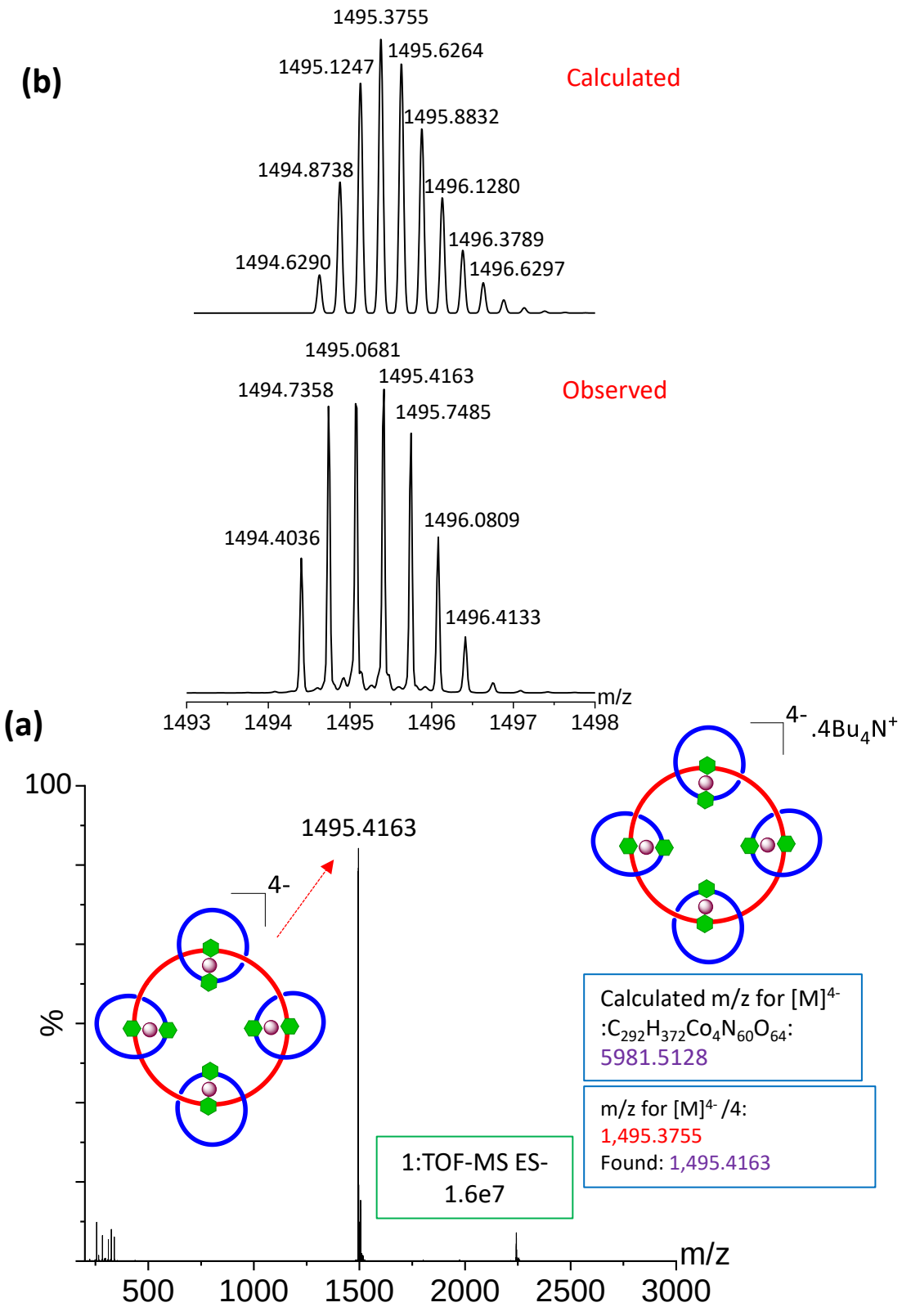

Figure 2.7. Mass spectra (ESI^-) analysis for synthesized **R[5]Co** (a) full spectra (b) comparison between calculated and experimentally observed isotopic distribution peaks.

2.3.4. Demetalation of Co(III): Isolation of fully organic catenane

Demetalation using Zn/CH_3COOH in MeOH was performed with each synthesized templated catenanes (**[2]Co**, **L[3]Co**, and **R[4]Co**) by stirring them for 30 minutes in the open air (**scheme 2.3**). This resulted in the removal of Co(III) metal from the coordination site, as can be confirmed visually by the disappearance of the green color from the reaction mixture. Column chromatography purification results in the isolation of desired completely organic catenanes **[2]**, **L[3]**, and **R[4]**, respectively, and evidenced from NMR and mass spectroscopy (**Figure 2.8, 2.9**).

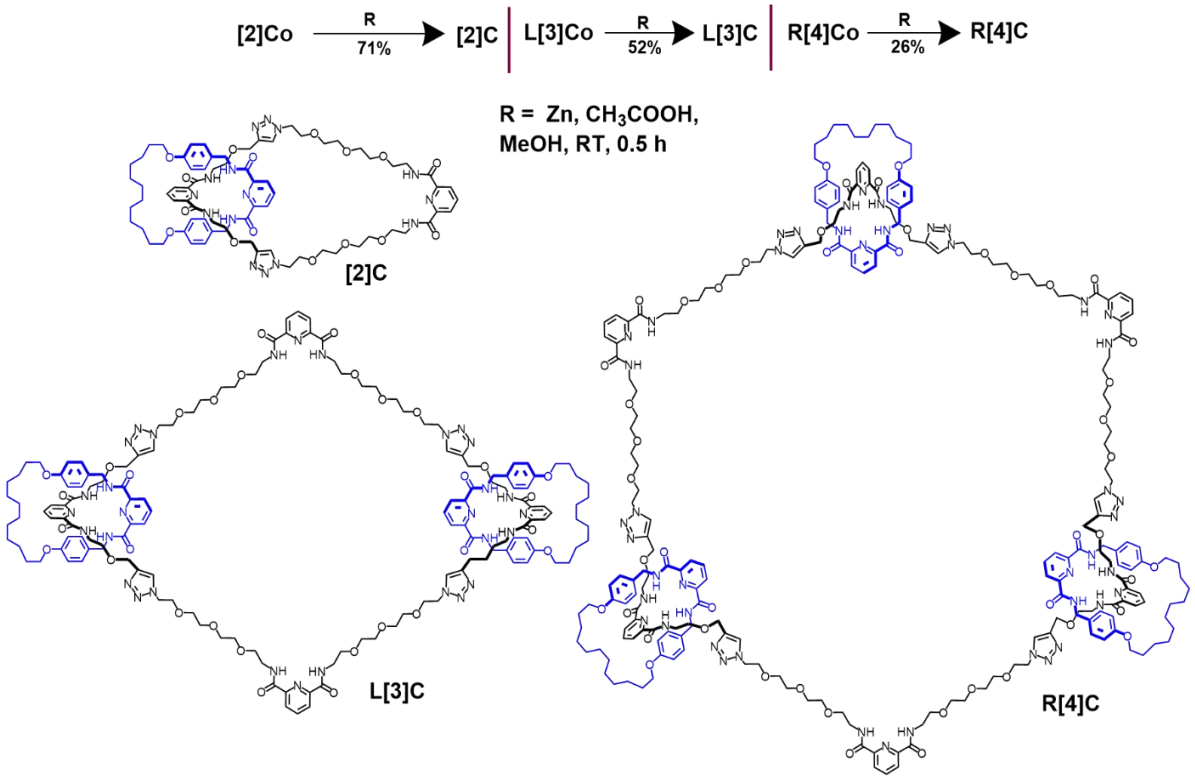

Scheme 2.3. Demetallation scheme for **[2]Co**, **L[3]Co** and **R[4]Co** to yield fully organic catenanes **[2]**, **L[3]**, and **R[4]**.

Mass spectral analysis of **[2]**, **L[3]** and **R[4]** (**Figure 2.8**) reveals presence of characteristics peaks for [(**[2]**) + $Na]^+$ at m/z 1462.6813, for [(**[2]**) + $2Na]^{2+}$ at m/z 742.847, for [(**L[3]**) + $2Na]^{2+}$ at m/z 1,463.1901, for [(**L[3]**) + $3Na]^{3+}$ at m/z 983.1306, for [(**R[4]**) + $3Na]^{3+}$ at m/z

1,463.3324 and [(**R[4]**) + 4Na]$^{4+}$ at m/z 1103.2644. The observed mass matches the simulated isotopic distribution (**Figure 2.8**).

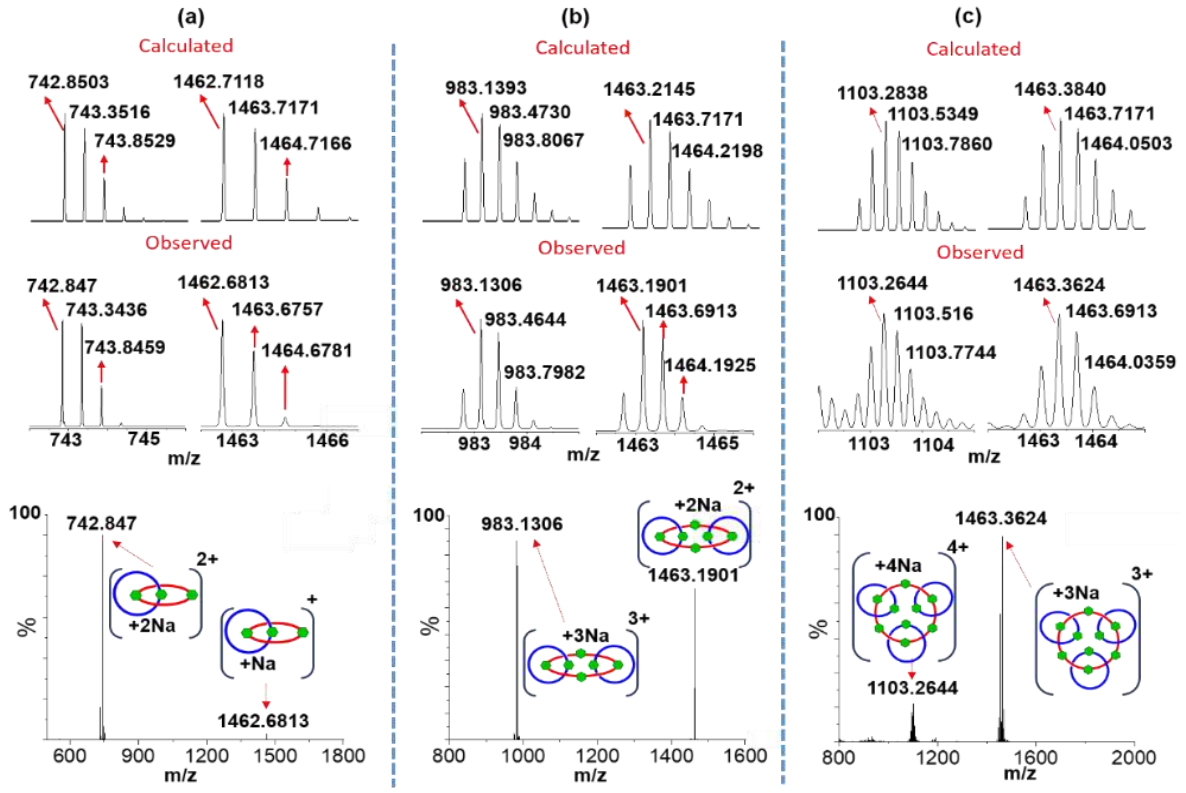

Figure 2.8. Similar to the metalated one, the fully organic catenanes show charged ion peaks 1^+, 2^+, 3^+, and 4^+ by addition of Na^+ ion in ESI^+ mass spectra (a) **[2]** (b) **L[3]** (c) **R[4]**. Spectra of desired region is given at bottom with isotopic distribution of probable structure and their comparison with simulated isotopic distribution peaks are given at top.

Comparison of proton NMR signal between the metalated and organic catenane shows that the shielded protons due to complex formation returned to their original position (as in ligands).Downfield shift in proton NMR is observed for the benzene proton of **MC** subunit of **[2]Co**, **L[3]Co**, and **R[4]Co** by 1 ppm (peak **u**, **v** of **[2]Co**, **10**, **11** of **[3]Co** and **15**, **14** of **R[4]Co**, **Figure 2.9**) and one methylene (CH_2) proton of $–N^––CH_2–CH_2–O–$ group of **MY** subunit by 2 ppm (peak **x** of **[2]Co**, **y** of **[3]Co** and **z** of **R[4]Co**) due to removal of metal ion (**Figure 2.9**). Similar de-shielding is also observed for the pyridine peaks of the **MY** subunit

(**w** of **[2]Co**, **12** of **[3]Co**, **16** of **R[4]Co**). The carbonyl carbons and carbon in close vicinity of the coordination sphere get shielded by 5−10 ppm upon demetallation and can be observed in the ^{13}C-NMR comparison between the metalated and fully organic catenanes (**Figure 2.10**).

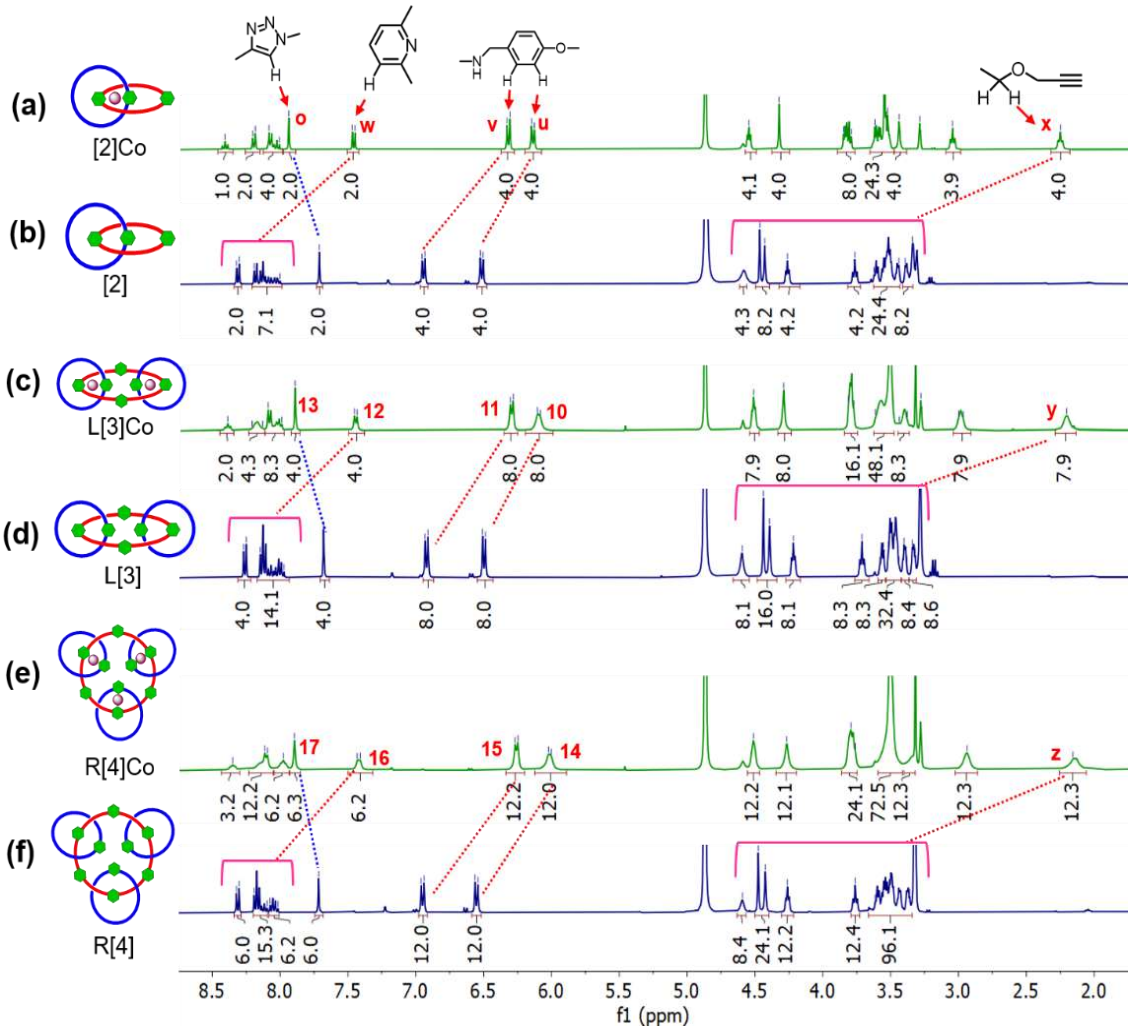

Figure 2.9. Partial proton NMR for comparison between metalated and fully organic catenane. Deshielding is observed upon removal metal from the cobalt(III)-metalated catenane (a) **[2]Co** (b) **[2]** (c) **L[3]Co** (d) **L[3]** (e) **R[4]Co** (f) **R[4]**. All spectra were recorded in CD_3OD. NH^- protons getting exchanged with CD_3OD and are not seen. Peak **x**, **y**, **z** has been assigned to methylene protons next to oxygen (–N–CH_2–C**H**$_2$–O–CH_2–CH≡CH) of the MY subunit of metalated catenane. However, it is possible that the same peak might be due to methylene proton next to the anionic nitrogen (–N–C**H**$_2$–CH_2–O–CH_2–CH≡CH) and vice versa.

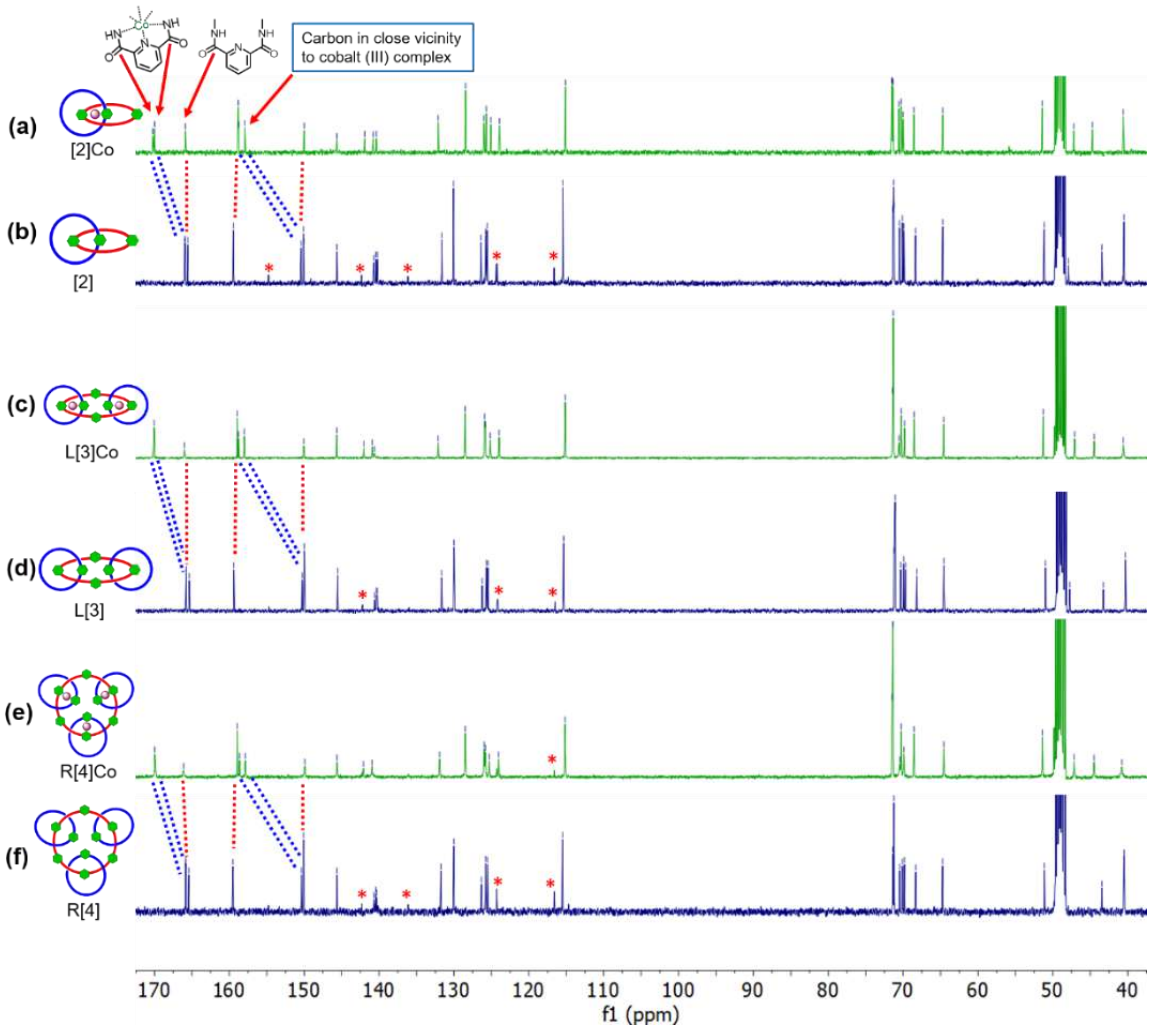

Figure 2.10. ^{13}C NMR comparison between metalated and fully organic catenane shows shielding effect of 5 ppm occurs at carbonyl carbon and carbon nearby metal coordination center (shielded by 10 ppm) upon removal of metal from metalated catenanes (a) **[2]Co** (b) **[2]** (c) **L[3]Co** (d) **L[3]** (e) **R[4]Co** (f) **R[4]**.

2.3.5. VT-NMR study for metalated linear [3]catenane (L[3]Co) and metalated radial [4]catenane(R[4]Co):

A variable temperature NMR of these complexes shows that the signal becomes broader with decrease in temp., whereas at higher temperature (45 °C), it is sharper, indicating the flexibility in the conformation.

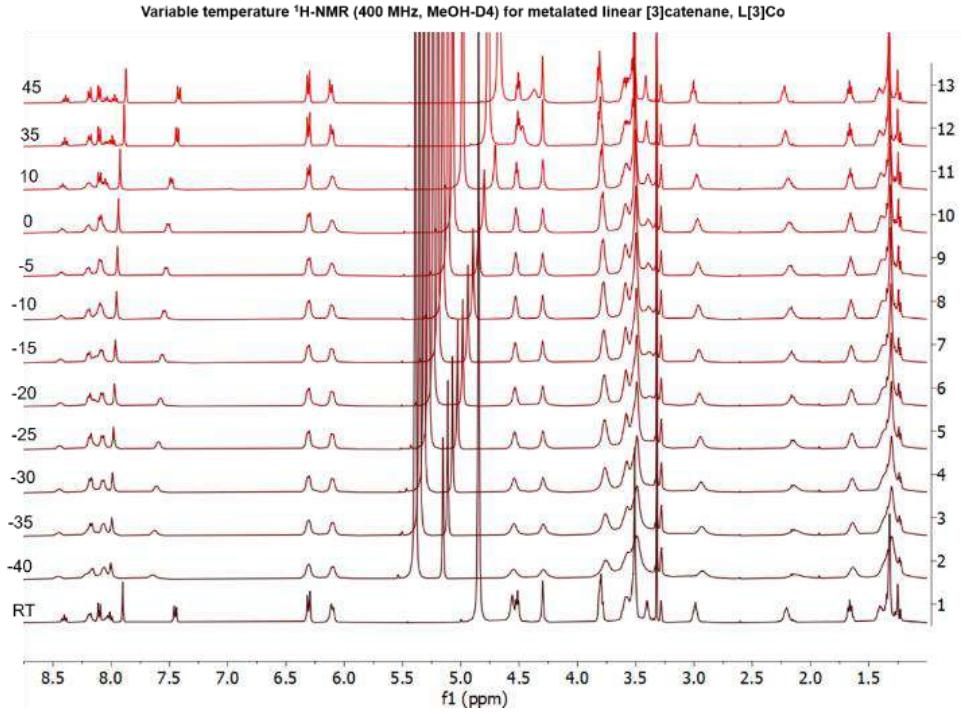

Figure 2.11. Variable temperature (in degree Celsius) ^{1}H-NMR for metalated linear [3]catenane. Data recorded from -40 ˚C to 45 ˚C. At lower temperature broadening of NMR signals and at higher temperature sharpening of NMR signals was observed.

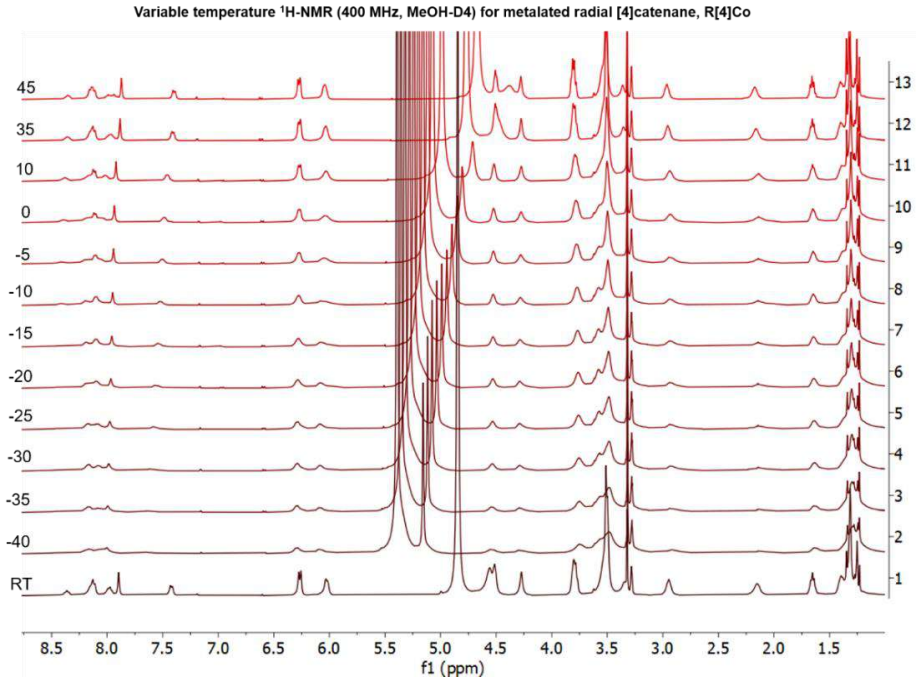

Figure 2.12. Variable temperature (in degree Celsius) ^{1}H-NMR for metalated radial [4]catenane. Data recorded from -40 ˚C to 45 ˚C. At lower temperature broadening of NMR signals and at higher temperature sharpening of NMR signals was observed.

2.3.6. MS-MS experiment on [2]catenane ([2]C), linear [3]catenane (L[3]C) and radial [4]catenane (R[4]C):

These organic catenanes is further analyzed by MS/MS fragmentation method (**Figure 2.13, 2.14, 2.15**). These experiments shows that the rings attached in the structures and the macrocycle hosting them could be found in the spectra, further supports the catenanes.

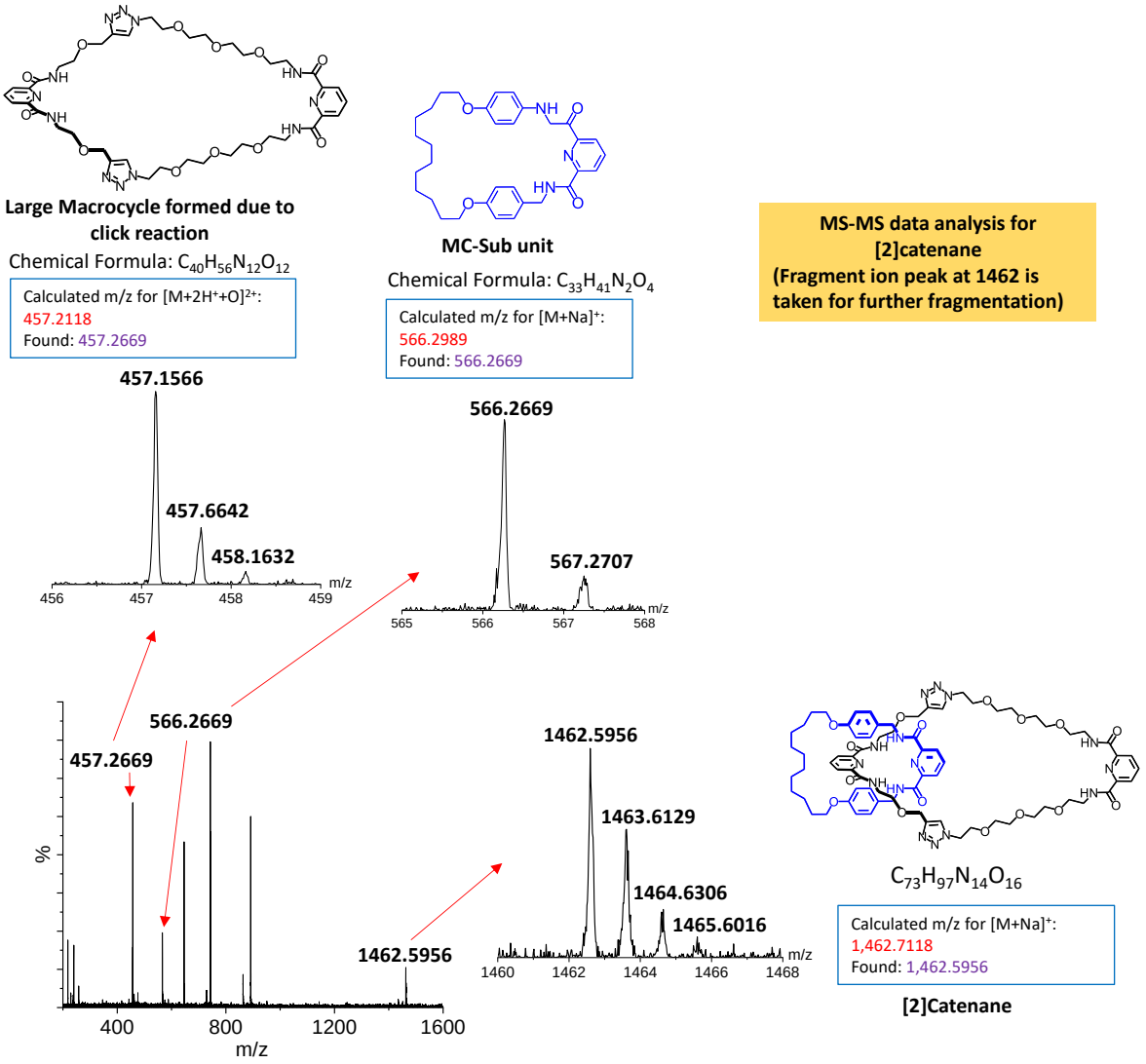

Figure 2.13. MS-MS data analysis for [2]catenane in ESI^{+} mode shows mass of its constituent macrocycles.

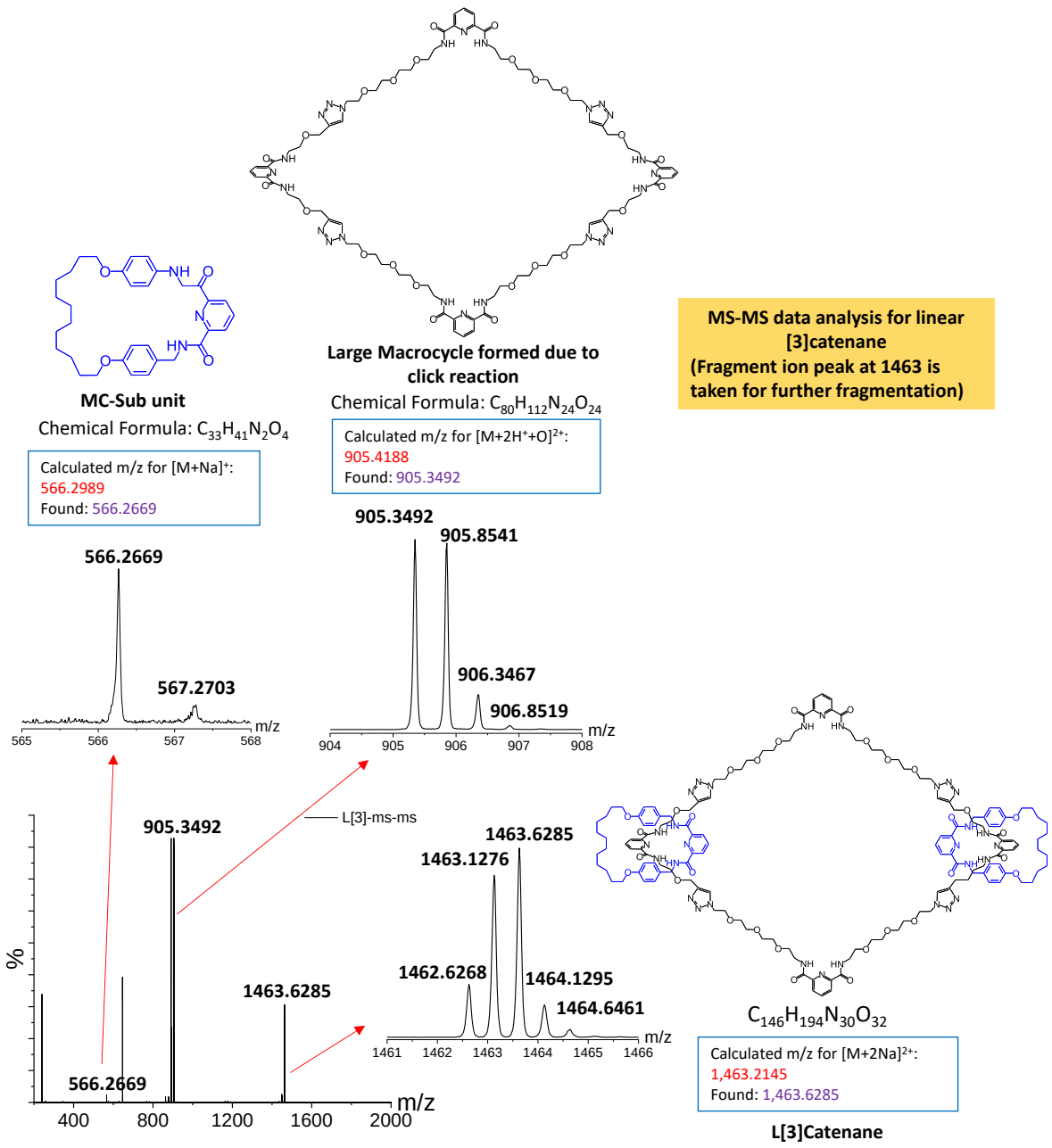

Figure 2.14. MS-MS data analysis for linear [3]catenane in ESI^+ mode shows mass of its constituent macrocycles.

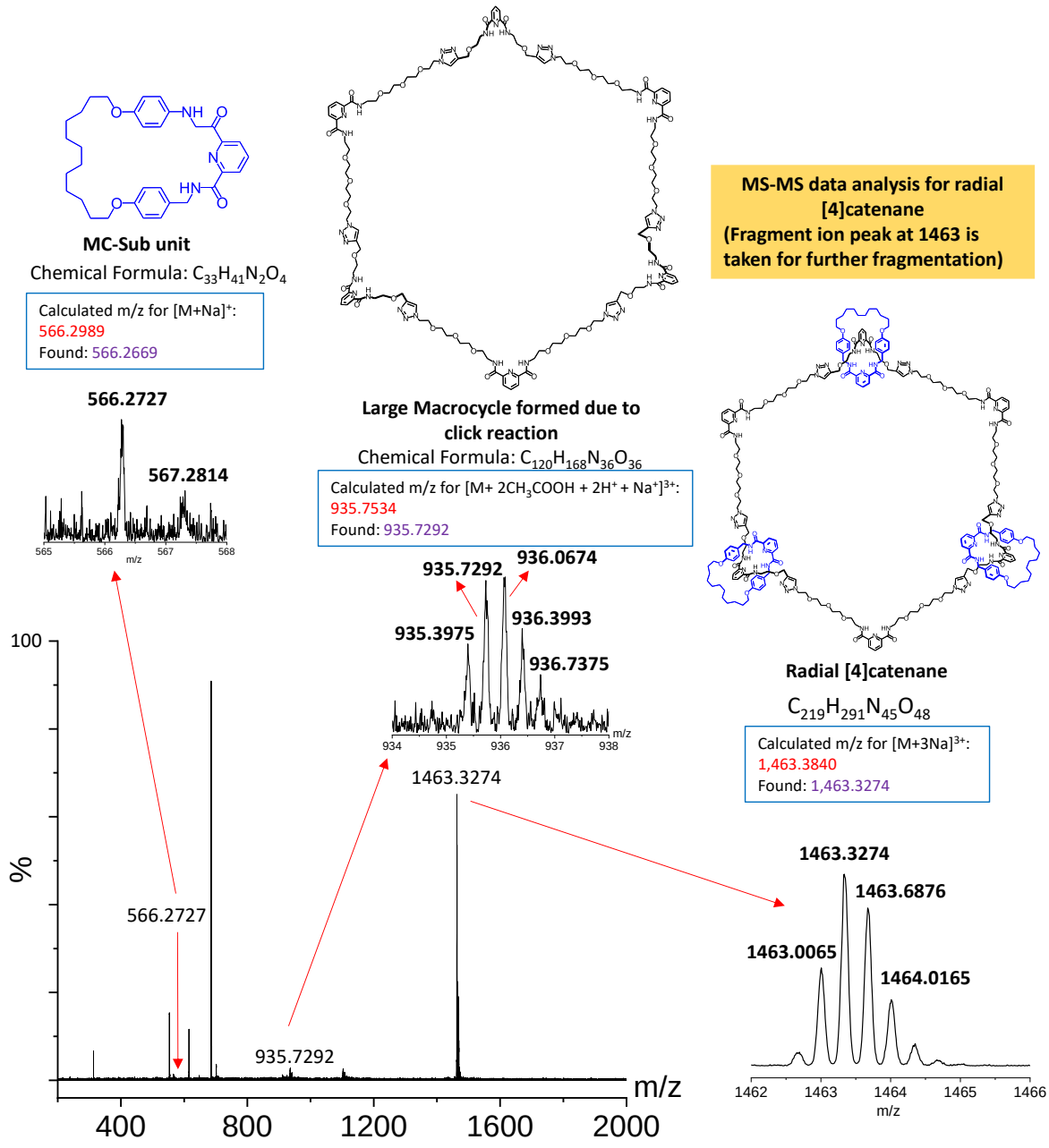

Figure 2.15. MS-MS data analysis for radial [4]catenane in ESI^+ mode shows mass of its constituent macrocycles.

2.4. Conclusions:

In conclusion, cobalt(III)-metalated (**[2]Co**, **L[3]Co**, and **R[4]Co)** catenanes have been synthesized using the coupling of bis(alkyne) functionalized pseudorotaxane (**[2]PR–Co**) and bis-azide functionalized ligand (**MA**) using click reaction as the ring-closing step. Isolated yield

for the **[2]Co**, **L[3]Co**, and **R[4]Co** catenanes are 40%, 12%, and 4%, respectively. Hydrogenation with Zn/CH_3COOH to give **[2]**, **L[3]** and **R[4]** catenanes with a reaction yield 71%, 52% and 26% from **[2]Co**, **L[3]Co** and **R[4]Co** respectively. This synthetic strategy of increasingly formed catenane using hard cobalt(III)-metal complex and via covalent bond formation strategy through CuAAC (Alkyne–Azide cycloaddition) reaction, will provide a methodology with multiple mechanical bonds being formed for the construction of newer supramolecular topologies and will allow access to a new group of interlocked MIMs. Moreover, the free binding site present in the Co(III)-templated [2]catenanes (**[2]Co)** may be used further to synthesize higher-order catenane via post-functionalization.

2.5. Experimental Section:

2.5.1. Reagents and Instruments: $SOCl_2$, 4-Methoxybenzylamine, 63% HBr, Propargyl bromide, Et_3N, Cobalt(II)acetate tetrahydrate and NaH has been purchased from Spectrochem, India Pvt. Ltd. 2,6-Pyridinedicarboxylic acid is used from Himedia, India Pvt. Ltd. K_2CO_3, 1,12-dibromododecane, Trifluroacetic acid, Ethylene glycol, p-Tolunesulfonyl choride, NaN_3, 4-dimethylaminopyridine, PPh_3, Tetraethylene glycol and Copper(I)iodide has been brought from Sigma Aldrich. N, N-diisopropylethylamine and acetic acid has been taken from SRL Chemicals and Tetrabutylammonium acetate is from Alpha Aeser. Common organic solvent such as Hexane, EtOAc, CH_3CN, DCM, DMF, THF and methanol has been purchased from Merck and used without further purification. Silica gel (100-200 mesh) has been used in Column Chromatography for the purification of synthesized compounds. Anhydrous MeOH, DCM, Acetonitrile, THF, DMF has been prepared by common laboratory methods. Deuterated solvents $CDCl_3$ has been used from Sigma Aldrich and CD_3OD from Euriso-top Chemicals. ^{1}H-NMR and ^{13}C-NMR spectra has been recorded in a Bruker 400 MHz and 700 MHz

Spectrometer. Variable temperature NMR has been recorded in JEOL 400 MHz instrument. Mass spectra has been recorded in Water ESI-MS Spectrometer.

2.5.2. Synthesis of monomer M2:

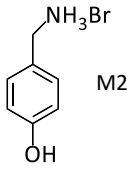

Monomer **M2** was synthesized according to reported literature procedure,[32] by taking 4-methoxybenzylamine (25 g, 182 mmol) and adding to it 48% HBr (106 mL) in dropwise manner with stirring, under ice bath. At this stage a precipitate was formed. Since an extremely exothermic reaction occurs, the addition was done slowly. The mixture was stirred to reflux at 120 ˚C for 12 h before being cooled to room temperature and concentrated to dryness, giving a light pink solid. The solid product residue was washed with MeCN three times to remove brown colored impurity. Then the product **M2** (violet solid) was collected by filtration and dried under vacuum. Yield: 32.6 g, 86%.

^{1}H-NMR (400 MHz, CD_3OD) δ in ppm: 7.32-7.30 (d, 2H), 6.87-6.80 (d, 2H), 4.03 (s, 2H).

^{13}C-NMR (100 MHz, CD_3OD) δ in ppm: 159.55, 131.65, 124.95, 116.84, 44.05.

HR-MS (ESI$^+$): Calcd. m/z for $C_7H_{10}NO$ $[M\text{-}Br^-]^+$ 124.0758, found 124.0786.

2.5.3. Synthesis of monomer M3:

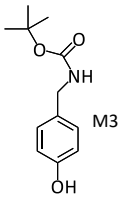

Monomer **M3** was synthesized following literature procedure.[32] 4-Hydroxybenzylamine, **M2** (20 g, 98 mmol), $NaHCO_3$ (32.93 g, 392 mmol, 4 equivalent) and anhydrous MeOH (60 mL) was added in a round bottom flask. To this, Boc-anhydride (24.76 mL, 107.8 mmol) was added under argon atmosphere. The reaction mixture was stirred at RT for 24 hours, filtered and the

solvent was removed under reduced pressure. Later, the oily residue was purified by silica column chromatography (EtOAc: Hexane, from 1:9 to 3:7 v/v) to get light yellow wax **M3** 39.883 g (yield 91%).

^{1}H-NMR (400 MHz, $CDCl_3$) δ in ppm: 7.10-7.08 (d, 2H), 6.78-6.76 (d, 2H), 6.51 (s, br 1H), 4.88 (s, br, H), 4.22-4.20 (d, 2H), 1.46 (s, 9H).

^{13}C-NMR (100 MHz, $CDCl_3$) δ in ppm: 156.12, 155.44, 130.26, 128.86, 115.48, 79.76, 44.17, 28.20.

HR-MS (ESI$^+$): Calcd. m/z for $C_{12}H_{17}NO_3Na$ $[M+Na]^+$ 246.1103, found 246.1176.

2.5.4. Synthesis of monomer M4:

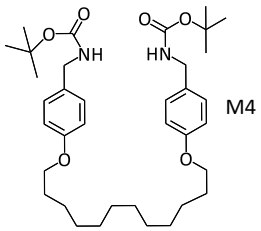

1,12-Dibromododecane (15.25 g, 30.71 mmol) was added with stirring to a solution of monomer **M3** (14.40 g, 64.51 mmol) and anhydrous K_2CO_3 (251.9 g 34.81 mmol) in anhydrous CH_3CN under N_2 atmosphere. The reaction mixture was refluxed at 85 ˚C for 20 hours. After completion of reaction, solvent was evaporated and the reaction mixture was added with EtOAc and H_2O, and work up was performed. The organic layer was dried with anhydrous Na_2SO_4 and filtered and evaporated to get white solid substance. The compound was recrystallized with DCM: EtOAc (2:3). The crude product was taken in a beaker and to it EtOAc was added and heated to get saturated solution. To it 2/3 of DCM was added and left to crystallize. Later, crystals were washed with EtOAc to get pure product **M4**. (yield 75%)

^{1}H-NMR (400 MHz, $CDCl_3$) δ in ppm: 7.19-7.17 (d, 4H), 6.85-6.83 (d, J = 8.2 Hz, 4H), 4.78 (s, br, 2H), 4.24-4.22 (d, 4H), 3.95-3.91 (t, J = 8 Hz, 4H), 1.80-1.76 (m, 4H), 1.45 (s, 16H), 1.29 (s, 18H).

^{13}C-NMR (100 MHz, $CDCl_3$) δ in ppm: 158.46, 155.82, 130.75, 128.80, 114.56, 79.35, 68.03, 44.18, 29.52, 29.35, 29.23, 28.39, 26.00.

HR-MS (ESI$^+$): Calcd. m/z for $C_{36}H_{59}N_2O_6$ $[M\text{-}Boc+H]^+$ 412.3265, found 412.2701.(HR-MS of monomer M4 gives peak of monomer M5 due to fragmentation, see **section 2.6.2**)

2.5.5. Synthesis of monomer M5:

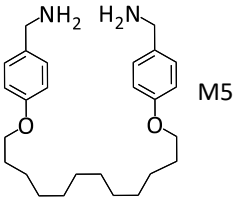

M5

To 1.5 g (2.44 mmol) of **M4**, 3.74 ml (20 equivalent) of trifluoroacetic acid and 80 mL anhydrous DCM was added in a 250 mL RB flask. The reaction mixture was stirred at room temperature for 4 hours. After completion of reaction, 50 mL H_2O was added to stop the reaction and stirred for 30 minutes. Later, on addition of 100 mL DCM to it, the amine salt (triflet) comes to aqueous layer. The water layer was separated from aqueous layer by using a separating funnel and transferred to 1000 mL beaker and added large amount of DCM. Then, to this mixture 1N NaOH solution was added until a basic pH is obtained. The mixture was stirred, at this stage all triflate salt has converted to free amine and remained in DCM layer. A final work up was performed to remove the water layer from the mixture. The DCM layer was dried with anhydrous Na_2SO_4, filtered and evaporated to dryness to get monomer **M5** (white solid) in quantitative yield. It was immediately dissolved in anhydrous DCM and proceed for next cyclization reaction without further characterization. Formation of free amine product can be confirmed by ninhydrin.

2.5.6. Synthesis of 2,6-Pyridinedicarbonyl dichloride:

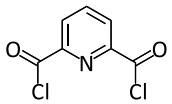

2,6-Pyridinedicarbonyl dichloride

Dipicolinic acid (5 g, 29.9186) is dissolved in 32 mL of $SOCl_2$ in 100 mL round bottom flask. The reaction mixture was stirred to reflux at 120 ˚C for 24 hours. Completion of reaction can be observed by the appearance of pink color solution. After cooling to room temperature, excess $SOCl_2$ is evaporated under high vacuum to yield the desired product **2,6-pyridinedicarbonyl dichloride** (white to pink solid). The product is moisture and air sensitive and stored in a sealed environment at 4 ˚C.(quantitative yield)

2.5.7. Synthesis of macrocycle MC:

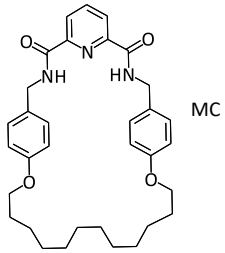

Macrocyclization was performed by following reported literature procedure under high dilution.[33] To a 1000 mL RB flask having monomer **M5** (1 g, 2.42 mmol), was added 600 mL of anhydrous DCM under N_2 atmosphere. This solution was then kept in an ice bath and to it, triethylamine (0.75 mL, 5.4 mmol) was injected and stirred. To this reaction mixture, 2,6-pyridinedicarbonyl dichloride (0.494 g, 2.42 mmol) dissolved in 30 mL of anhydrous DCM was added dropwise over a 10 minutes under ice bath conditions. It was then stirred for 18 hours after bringing it to room temperature. The solvent was removed under reduced pressure and the crude was purified by silica gel column chromatography using EtOAc: DCM (30:70) as eluent to get the desired product **MC** (white solid) in 50% yield, 0.66 g.

^{1}H-NMR (400 MHz, $CDCl_3$) δ in ppm: 8.38-8.36 (d, 2H), 8.02-7.98 (t, 3H), 7.21-7.19 (d, 4H), 6.82-6.80 (d, 4H), 4.61-7.59 (d, 4H), 3.94-3.91 (t, 4H), 1.79 (p, *J* = 8 Hz, 4H), 1.46-1.26 (m, 16H).

^{13}C-NMR (100 MHz, $CDCl_3$) δ in ppm: 163.32, 158.62, 148.78, 138.88, 129.84, 129.07, 125.30, 114.67, 77.32, 67.68, 42.84, 28.86, 28.72, 28.40, 28.22, 25.44.

HR-MS (ESI$^+$): Calcd. m/z for $C_{33}H_{42}N_3O_4$ $[M+H]^+$ 544.3180, found 544.3212.

2.5.8. Synthesis of monomer M7:

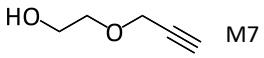

M7

Monomer **M7** was synthesized according to reported procedure.[34] Ethylene glycol (20 g, 322.2 mmol) and propargyl bromide (19.16 g or 15.95 mL, 161.1 mmol) were mixed in a 100 mL RB flask and it was brought to 0 ˚C. To it powder NaOH (7.73 g, 193.3 mmol) were added under N_2 atmosphere at 0 ˚C. It was brought to room temperature and the reaction mixture was stirred at 45 ˚C for 3 hours to give pale yellow precipitate. The reaction mixture was washed with DCM several times and filtered off the solid residue. The DCM part was dried with anhydrous Na_2SO_4 and evaporated to dryness. It was purified by column chromatography (eluent EtOAc: Hexane 1:1) to give pale yellow liquid (5.88 g, 36%) product **M7**.

^{1}H-NMR (400 MHz, $CDCl_3$) δ in ppm: 4.21-4.20 (d, *J* = 4 Hz, 2H), 3.78-3.76 (t, 2H), 3.65-3.64 (t, 2H), 2.46-2.45 (t, *J* = 2.36 Hz, 1H).

^{13}C-NMR (100 MHz, $CDCl_3$) δ in ppm: 79.43, 74.70, 71.17, 61.71, 58.41.

HR-MS (ESI$^+$): Calcd. m/z for $C_5H_8O_2$ $[M]^+$ 100.0525, found 100.0796.

2.5.9. Synthesis of monomer M8:

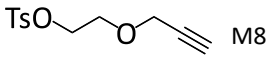

M8

Monomer **M8** was synthesized according to reported procedure.[35] Monomer **M7** (15 g, 149.8 mmol), tosyl chloride (57.12 g, 299.6 mmol), triethylamine (125.37 mL, 898.9 mmol) were mixed and to it DCM (400 mL) was added under N_2 atmosphere at 0 ˚C. The reaction mixture was stirred at room temperature for 1 hour. Again the reaction mixture was brought to 0 ˚C and DMAP (0.915 g, 0.05 equivalent, 7.49 mmol) was added. Later, the reaction mixture was stirred at room temperature for 2 hours. As soon as reaction stops, the extra solvent is evaporated under reduced pressure, crude residues is extracted with DCM, combined DCM

were dried over anhydrous Na_2SO_4, concentrated and purified by column chromatography (with Hexane: EtOAc, 70:30 solvent system) to produce pale yellow liquid product **M8** (31.5 g, 82.7%).

^{1}H-NMR (400 MHz, $CDCl_3$) δ in ppm: 7.81-7.79 (d, 2H), 7.35-7.33 (d, 2H), 4.20-4.17 (dd, 2H), 4.12-4.11 (d, *J* = 2.2 Hz, 2H), 3.73-3.71 (dd, 2H), 2.45-2.43 (s, 3H), 2.41 (t, *J* = 2.32 Hz, 1H).

^{13}C-NMR (100 MHz, $CDCl_3$) δ in ppm: 144.86, 132.84, 129.81, 127.98, 75.04, 68.84 67.09, 58.35, 21.64.

HR-MS (ESI$^+$): Calcd. m/z for $C_{12}H_{14}O_4SNa$ $[M+Na]^+$ 277.0501, found 277.0616.

2.5.10. Synthesis of monomer M9:

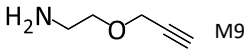

M9

Conversion of **M8** to **M9** is achieved by in-situ reaction without isolating the azide monomer. Monomer **M8** (3 g, 11.79 mmol) and NaN_3 (0.843 g, 12.9 mmol) were dissolved in 30 mL 0f anhydrous DMF in round bottom flask. The reaction mixture was allowed to heat at 55 ˚C constantly for 10 hours exactly. It was, cooled to room temperature and PPh_3 (7.73 g, 29.79 mmol) was added to the reaction mixture along with 50 mL of anhydrous THF and H_2O (0.318 ml, 17.69 mmol). The reaction mixture is further stirred for 12 hours. The amine formed is confirmed by ninhydrin test. The extra solvent is evaporated under reduced pressure and the crude is subjected to column chromatography using DCM: MeOH in 90:10 ratio to get gray colored sticky liquid product **M9** with 38% yield (0.45 g). It was immediately dissolved in anhydrous DCM and used for next reaction without further characterization. The In situ method is adopted to control the degradation of intermediate, small length azide produced in this process.

2.5.11. Synthesis of monomer MY:

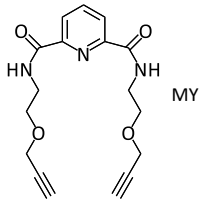

To a solution of monomer **M9** (1.29 g, 12.9 mmol) in anhydrous DCM (60 mL) at 0 ˚C under an atmosphere of N_2, Et_3N (2.16 mL, 15.48 mmol) was added. To this solution, 2,6-pyridinedicarbonyl dichloride (1.18 g, 0.45 equivalent, 5.8 mmol) dissolved in anhydrous DCM (20 mL) was added dropwise over 10 minutes at 0 ˚C. The final solution was stirred for 18 hours at room temperature before being concentrated in vacuum. The crude residue was purified by silica-gel column chromatography using DCM: MeOH, 99:1 as eluent to get desired product **MY** with 73% yield (1.45 g).

^{1}H-NMR (400 MHz, $CDCl_3$) δ in ppm: 8.35-8.33 (d, 2H), 8.20 (t, 2H), 8.02 (t, 1H), 4.22 (d, *J* = 2.36 Hz, 4H), 3.78-3.71 (m, 8H), 2.49 (t, *J* = 2.48 Hz, 2H).

^{13}C-NMR (100 MHz, $CDCl_3$) δ in ppm: 163.59, 148.73, 138.89, 124.98, 79.41, 74.97, 68.76, 58.37, 39.31.

HR-MS (ESI$^+$): Calcd. m/z for $C_{17}H_{20}N_3O_4$ $[M+H]^+$ 330.1446, found 330.1472.

2.5.12. Synthesis of monomer M11:

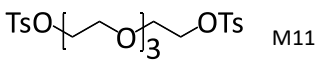

Tetraethylene glycol (20 g, 102.9 mmol), tosyl chloride (78.51 g, 411.8 mmol), triethylamine (172.4 mL, 1235.4 mmol) was dissolved in DCM under N_2 atmosphere at 0 ˚C and the reaction mixture was allowed to stir for one hour at RT. Again the reaction mixture was brought to 0 ˚C and to it, DMAP (1.257 g, 0.1 equivalent, 10.29 mmol) was added. Then, the reaction mixture was stirred at room temperature for 2 hours. As soon as reaction stops, the extra solvent is evaporated under reduced pressure, crude residues is extracted with DCM, combined DCM

were dried over anhydrous Na_2SO_4, concentrated and purified by column chromatography (with Hexane: EtOAc, 50:50 v/v) to produce pale yellow liquid product **M11** (34 g, 65.7%). **^{1}H-NMR** (400 MHz, $CDCl_3$) δ in ppm: 7.79-7.77 (d, 4H), 7.34-7.32 (d, 4H), 4.16-4.13 (m, 4H), 3.68-3.67 (dd, 4H), 3.55 (s, 8H), 2.43 (s, 6H).

^{13}C-NMR (100 MHz, $CDCl_3$) δ in ppm: 144.79, 132.94, 129.80, 127.93, 70.68, 70.50, 69.22, 68.64, 21.60.

HR-MS (ESI$^+$): Calcd. m/z for $C_{22}H_{31}O_9S_2$ $[M+H]^+$ 503.1398, found 503.1434.

2.5.13. Synthesis of monomer M12:

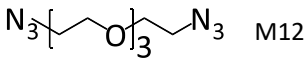

M12

Monomer **M11** (13.5 g, 26.88 mmol) and NaN_3 (13.98 g, 215.08 mmol) was dissolved in anhydrous DMF under N_2 atmosphere. The reaction mixture was stirred at 80 ˚C for 18 hours. The DMF is evaporated to dryness under reduced pressure followed by extraction with (3 x 400 mL) Ethyl acetate, dried in Na_2SO_4 and purified by column chromatography using 1:1 Hexane :EtOAc as eluent to get desired product (colorless liquid) **M12** in 82% yield (5.4 g). The product formed can be visualize over thin layer chromatography by dipping developed TLC plate into PPh_3 solution (THF: H_2O, 1:1) followed by evaporation of excess PPh_3 by exposing the TLC plate to a heat gun and then performing ninhydrin test. The formed amine product shows positive test (purple colored spot) on the TLC plate.

^{1}H-NMR (400 MHz, $CDCl_3$) δ in ppm: 3.68-3.66 (m, 12H), 3.39-3.37 (t, 4H).

^{13}C-NMR (100 MHz, $CDCl_3$) δ in ppm: 77.66, 69.99, 50.81.

HR-MS (ESI$^+$): Calcd. m/z for $C_8H_{16}N_6O_3Na$ $[M+Na]^+$ 267.1232, found 267.1186.

2.5.14. Synthesis of monomer M13:

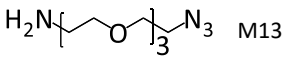

M13

Monomer **M12** (4.85 g, 19.85 mmol), PPh_3 (5.2 g, 19.85 mmol) and H_2O (0.536 mL, 29.78 mmol) were dissolved in (100 mL) THF under N_2 atmosphere. The reaction mixture was stirred at room temperature for 12 hours. Later, it was evaporated to dryness under reduced pressure and purified by column chromatography using DCM: MeOH: Et_3N (90:10:0.25) as eluent to yield off-white thick liquid product **M13** (2.3 g, yield 53%). TLC vizualisation of product was done using ninhydrin test.

^{1}H-NMR (400 MHz, $CDCl_3$) δ in ppm: 3.68-3.64 (m, 8H), 3.56-3.53 (t, 2H), 3.41-3.38 (t, 2H), 2.89 (t, 2H), 2.60 (s, 4H).

^{13}C-NMR (100 MHz, $CDCl_3$) δ in ppm: 72.29, 70.61, 70.57, 70.54, 70.18, 69.97, 50.64, 41.37.

HR-MS (ESI$^+$): Calcd. m/z for $C_8H_{19}N_4O_3$ $[M+H]^+$ 219.1452, found 219.1487.

2.5.15. Synthesis of monomer MA:

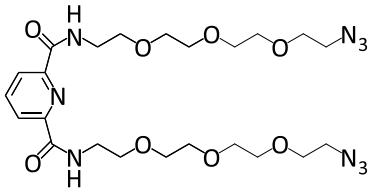

MA

To a solution of monomer **M13** (1.7 g, 7.78 mmol) in anhydrous DCM (60 mL) at 0 ˚C under N_2 atmosphere, Et_3N (1.3 mL, 9.34 mmol) was added. To this reaction mixture, a solution of 2,6-pyridinedicarbonyl dichloride (0.725 g, 3.5 mmol) in anhydrous DCM (20 mL) was added dropwise over 10 minutes while keeping the solution at 0 ˚C. The reaction mixture is stirred at room temperature for 18 hours before being concentrated in vacuum. The crude residue was purified by column chromatography (DCM: MeOH: 95:5 as eluent) to give off-white thick liquid **MA** (1.825 g, 90%).

^{1}H-NMR (400 MHz, CD_3OD) δ in ppm: 8.81 (s, 2H), 8.34-8.32 (d, 2H), 8.03-7.99 (t, 1H), 3.71-3.60 (m, 28H), 3.36-3.34 (t, 4H).

^{13}C-NMR (100 MHz, CD_3OD) δ in ppm: 163.85, 148.82, 138.74, 124.77, 70.57, 70.52, 70.41, 70.21, 70.10, 69.97, 50.59, 39.45.

HR-MS (ESI$^+$): Calcd. m/z for $C_{23}H_{37}N_9O_8Na$ $[M+Na]^+$ 590.2688, found 590.266.

2.5.16. Synthesis of pseudo [2]rotaxane ([2]PR-Co):

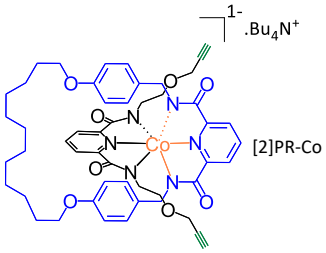

Cobalt metal complexation was performed according to reported literature procedure.[36] To a 100 mL two-neck round bottom flask equipped with stir bar, **MC** (0.33 g, 0.6 mmol), $Co(OAc)_2.(H_2O)_4$ (0.151 g, 0.6 mmol) and $Bu_4N^+OAc^-$ (0.183 g, 0.6 mmol) was transferred and it was purged with anhydrous methanol (25 mL) under inert atmosphere. The mixture was refluxed at 80 ˚C (performed by using a condenser, sealed with a rubber septum on top of it) for 1 hours under inert atmosphere to obtain a clear pale pink solution. To this mixture, 0.199 g (0.6 mmol) of monomer **MY** (dissolved in anhydrous MeOH 25 mL) was injected under reflux conditions. This reaction mixture was further refluxed for 1 hour under inert atmosphere. In another RB flask, sodium methoxide was prepared by the slow addition of 25 mL anhydrous methanol into NaH (1 g) at 0 ˚C) and injected into the reaction mixture at reflux conditions. This results a color change to deep purple. Later, on exposure to air (performed by removing the septum), the solution turned to green and it was further refluxed for 24 hours. Later, the solvent was evaporated to dryness and the residue is subjected to SiO_2 column chromatography using EtOAC: MeOH (84:14 v/v) as solvent. Collected green colored cobalt complex product from column chromatography was further washed with EtOAc repeatedly to remove unwanted impurities and resulted pure **[2]PR-Co** in 25% yield (0.14 g).

^{1}H-NMR (400 MHz, CD_3OD) δ in ppm: 8.54-8.51 (t, 1H), 8.26-8.24 (d, 2H), 8.09 (t, 1H), 7.53-7.51 (d, 2H), 6.42-6.40 (d, 4H), 6.25-6.22 (d, 4H), 3.93 (s, 4H), 3.88-3.85 (t, 4H), 3.50 (s, 4H), 3.13-3.10 (t, 4H), 2.76-2.75 (t, *J* = 2.48 Hz, 2H), 2.29-2.26 (t, 4H), 1.76-1.69 (p, 4H), 1.54-1.39 (m, 16H).

^{13}C-NMR (100 MHz, CD_3OD) δ in ppm: 170.33, 170.08, 158.92, 158.02, 141.86, 140.85, 132.17, 128.55, 125.10, 123.96, 115.18, 80.79, 75.77, 69.29, 68.59, 47.23, 44.55, 30.27, 30.14, 29.81, 29.59, 26.57.

HR-MS (ESI$^+$): Calcd. m/z for $C_{50}H_{58}CoN_6O_8$ $[M^-+H^++Na^+]^+$ 951.3451, found 951.3342.

2.5.17. Synthesis of [2]Co, L[3]Co, R[4]Co via click reaction:

Click reaction was performed using reported literature procedure[37] in high dilution conditions. To a 250 mL RB flask **[2]PR-Co** (0.3 g, 0.32 mmol), monomer **MA** (0.183 g, 0.32 mmol), CH_3COOH (0.388 g, 6.46 mmol), DIPEA (0.835, 6.46 mmol) and CuI (1.23 g, 6.46 mmol) were transferred. Then 180 mL of anhydrous MeOH was added into it. The mixture is refluxed for 24 h under N_2 atmosphere. Four more similar batches of reactions were performed using another 1.2 g of [2]PR-Co. All batches were collected, MeOH was removed under reduced pressure and the resulting material was purified using column chromatography (Ethyl acetate: Methanol 55:45) to result **[2]Co**, **L[3]Co** and **R[4]Co** successively. Higher order catenane has more polarity (due to increased number of triazole rings) than the lower one and hence, will get collects at the end of the column. All catenane having cobalt metal are green in colored and sticky liquid in nature. After collecting the metalated catenanes from column, they were further purified by washing with hexane and EtOAc to remove undesired impurities and results in pure product **[2]Co**, **L[3]Co** and **R[4]Co** with yield of 40% (0.96 g), 12% (0.29 g) and 4% (0.096 g) respectively. Characterization of metalated catenane by ^{1}H-NMR, ^{13}C-NMR and ESI-MS has been discussed below.

2.5.18. Characterization of cobalt(III)-templated linear [2]catenane ([2]Co):

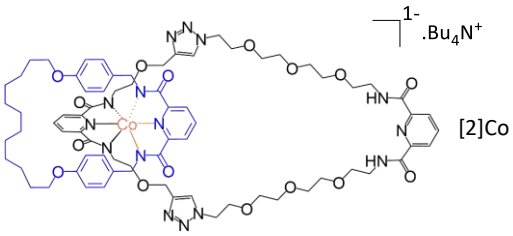

^{1}H-NMR (400 MHz, CD_3OD) δ in ppm: 8.42 (t, 1H), 8.21-8.19 (d, 2H), 8.09-8.02 (m, 4H), 7.95 (s, 2H), 7.48-7.46 (d, 2H), 6.33-6.31 (d, 4H), 6.15-6.13 (d, 4H), 4.55 (t, 4H), 4.32 (s, 4H), 3.85-3.79 (m, 8H), 3.62-3.52 (m, 24H), 3.44 (s, 4H), 3.04 (t, 4H), 2.25 (t, 4H), 1.68 (p, 4H), 1.42-1.34 (m, 16H).

^{13}C-NMR (100 MHz, CD_3OD) δ in ppm: 170.30, 170.07, 165.94, 158.89, 158.81, 158.00, 150.08, 145.70, 141.98, 140.85, 140.42, 132.13, 128.48, 126.03, 125.73, 125.11, 123.94, 115.14, 71.49, 71.45, 71.38, 71.33, 70.55, 70.23, 69.97, 68.55, 64.70, 51.39, 47.17, 44.67, 40.54, 30.29, 30.13, 29.83, 29.59, 26.56.

HR-MS (ESI$^+$): Calcd. m/z for $C_{73}H_{94}CoN_{15}O_{16}Na$ $[M^-+Na^++H^+]^+$ 1,518.6234, found 1,518.6482 and for $C_{73}H_{94}CoN_{15}O_{16}Na_2$ $[M^-+2Na^++H^+]^{2+}$ 770.8058, found 770.8181.

2.5.19. Characterization of cobalt(III)-templated linear [3]catenane (L[3]Co):

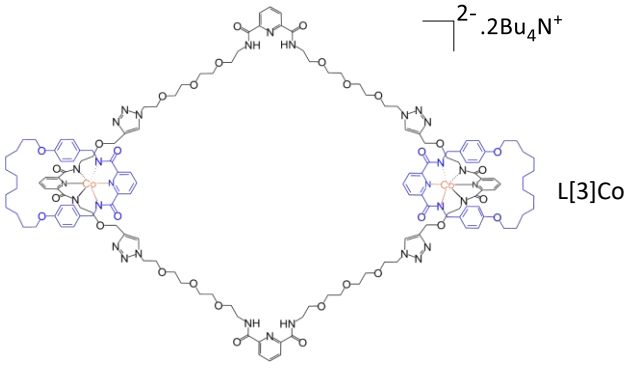

^{1}H-NMR (400 MHz, CD_3OD) δ in ppm: 8.40 (t, 2H), 8.22-8.14 (m, 4H), 8.10-8.00 (m, 8H), 7.9 (s, 4H), 7.46-7.44 (d, 4H), 6.31-6.29 (d, 8H), 6.11-6.09 (d, 8H), 4.51 (t, 8H), 4.29 (s, 8H), 3.81-3.77 (m, 8H), 3.61-3.50 (m, 48H), 3.44-3.38 (br, 8H), 3.00-2.96 (br, 8H), 2.20 (br, 8H), 1.67-1.64 (p, J = 7.8 Hz, 8H), 1.42-1.32 (m, 16H).

^{13}C-NMR (100 MHz, CD_3OD) δ in ppm: 170.00, 165.95, 158.89, 158.71, 157.95, 150.02, 145.63, 142.01, 140.86, 140.58, 132.07, 128.49, 125.90, 125.78, 125.13, 123.96, 115.14, 71.45, 71.34, 70.59, 70.26, 69.85, 68.54, 64.62, 51.33, 47.15, 44.53, 40.63, 30.27, 30.13, 29.81, 29.58, 26.55.

HR-MS (ESI$^+$): Calcd. m/z for $C_{146}H_{186}Co_2N_{30}O_{32}Na_4$ $[M^{2-}+4Na^+]^{2+}$ 1,541.1062, found 1,541.1057 and for $C_{146}H_{186}Co_2N_{30}O_{32}Na_5$ $[M^{2-}+5Na^+]^{3+}$ 1,035.0674, found 1,035.0516.

2.5.20. Characterization of cobalt(III)-templated radial [4]catenane (R[4]Co):

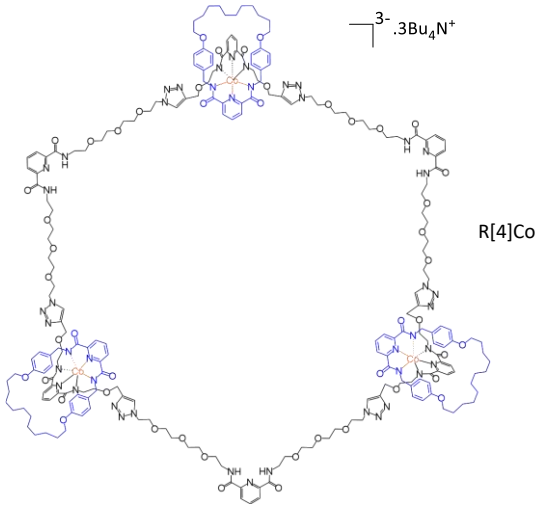

^{1}H-NMR (400 MHz, CD_3OD) δ in ppm: 8.36 (t, 3H), 8.12-8.10 (m, 12H), 7.98 (t, 6H), 7.9 (s, 6H), 7.44-7.42 (d, 6H), 6.27-6.25 (d, 12H), 6.03-6.01 (d, 12H), 4.52 (br, 12H), 4.27 (br,12H), 3.80-3.76 (m, br, 12H), 3.51-3.49 (m, br 72H), 3.44 (br, 12H), 2.94 (br, 12H), 2.16 (br, 12H), 1.66 (p, 12H), 1.41-1.31 (br, 48H).

^{13}C-NMR (100 MHz, CD_3OD) δ in ppm: 169.92, 166.05, 158.89, 158.59, 157.84, 149.88, 145.58, 142.06, 140.93, 131.89, 128.44, 125.93, 125.79, 125.27, 124.01, 115.15, 71.45, 71.35, 70.43, 70.24, 69.89, 68.56, 64.57, 51.40, 47.18, 44.50, 40.79, 30.25, 30.15, 29.79, 29.58, 26.54.

HR-MS (ESI$^+$): Calcd. m/z for $C_{219}H_{279}Co_3N_{45}O_{48}Na_6$ $[M^{3-}+6Na^+]^{3+}$ 1,541.2724, found 1,541.2972 and for $C_{219}H_{279}Co_3N_{45}O_{48}Na_7$ $[M^{3-}+7Na^+]^{4+}$ 1,161.7033, found 1,161.7097.

HR-MS (ESI$^-$): Calcd. m/z for $C_{219}H_{279}Co_3N_{45}O_{48}$ $[M]^{3-}$ 1495.2919, found 1,495.2579.

2.5.21. General procedure for de-metalation of cobalt complex:

Removal of cobalt metal from metalated catenane was done according to reported literature procedure.[37] Required amount of metalated catenane was transferred to a RB flask and to it anhydrous MeOH and CH_3COOH (5 ml each) was added followed by addition of activated Zinc. The reaction mixture was stirred for 30 minutes in open air. Complete disappearance of green color from the reaction mixture can be used as an indication for completion of reaction. Later, solvent was removed to dryness using rotatory evaporator and 30 mL of $CHCl_3$ was added. To it, 1:1 mixture of 12.5 mL of 17.5% ammonia solution and 12.5 mL of saturated Na_4EDTA was added. The mixture was stirred for 30 minutes and work up was performed with $CHCl_3$ and water 3 times. Organic layer was collected and again work up was performed using brine solution. Later organic layer was collected, dried with anhydrous Na_2SO_4, evaporated to dryness and purified by column chromatography using EtOAC: MeOH as eluent. 12.5 mL of saturated Na_4EDTA was prepared by mixing 5 g of EDTA with 2.73 g of NaOH and making the volume up to 12.5 mL with water and stirring it well. Activated Zinc was prepared by taking 10 g of Zinc powder in a RB flask and washing it with 2N HCl three times followed by washing with DI water, ethanol, acetone, diethyl ether two times each and drying in hot air oven at 100 ˚C for 15 minutes.

2.5.22. Synthesis of [2]catenane ([2]):

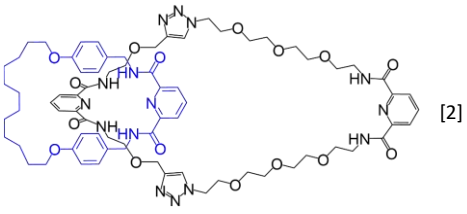

Activated Zinc (50 mg) was used for removal of cobalt from **[2]Co** (35 mg). It was purified by column using EtOAc: MeOH (75:25) to get 24 mg of [2]catenane (**[2])** with yield of 71%.

^{1}H-NMR (400 MHz, CD_3OD) δ in ppm: 8.33-8.32 (d, 2H), 8.20-8.01 (m, 7H), 7.72 (s, 2H), 6.97-6.94 (d, 4H), 6.54-6.51 (d, 4H), 4.59 (s, 4H), 4.47-4.44 (d, 8H), 4.27 (t, 4H), 3.77 (t, 4H), 3.63-3.45 (m, 24H), 3.40-3.35 (m, 8H), 1.66-1.59 (p, 4H), 1.36-1.28 (m, 16H).

^{13}C-NMR (100 MHz, CD_3OD) δ in ppm: 165.93, 165.89, 165.52, 159.43, 150.37, 150.06, 150.04, 145.62, 140.68, 140.38, 140.20, 131.59, 130.04, 126.36, 125.76, 125.69, 125.53, 115.43, 71.33, 71.24, 71.22, 71.19, 70.45, 70.07, 69.86, 68.32, 64.69, 51.15, 47.91, 43.42, 40.48, 32.15, 30.72, 30.50, 30.10, 29.84, 29.63, 26.73.

HR-MS (ESI^{+}): Calcd. m/z for $C_{73}H_{97}N_{15}O_{16}Na$ $[M+Na]^{+}$ 1,462.7118, found 1,462.6813 and for $C_{73}H_{97}N_{15}O_{16}Na_2$ $[M+Na]^{2+}$ 742.8503, found 742.847.

2.5.23. Synthesis of linear [3]catenane (L[3]):

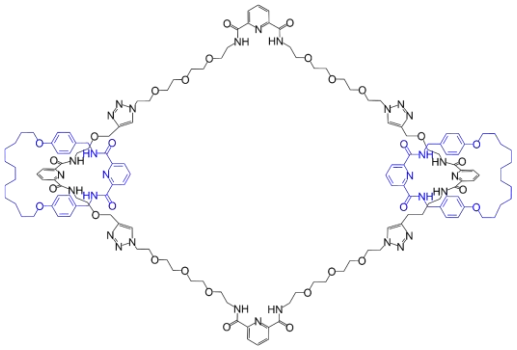

L[3]

Activated Zinc (100 mg) was used for removal of cobalt from **L[3]Co** (50 mg). It was purified by column using 65:35 EtOAc: MeOH to get 25 mg of L[3]catenane (**L[3])** with yield of 52%.

^{1}H-NMR (400 MHz, CD_3OD) δ in ppm: 8.28-8.26 (d, 4H), 8.15-7.98 (m, 14H), 7.68 (s, 4H), 6.94-6.91 (d, 8H), 6.51-6.49 (d, 8H), 4.59 (s, 8H), 4.44-4.39 (d, 16H), 4.22 (t, 8H), 3.71 (t, 8H), 3.58-3.55 (m, 8H), 3.51-3.44 (m, 32H), 3.40-3.38 (m, 8H), 3.34-3.32 (m, 8H), 1.60-1.53 (p, 8H), 1.34-1.25 (m, 32H).

^{13}C-NMR (100 MHz, CD_3OD) δ in ppm: 165.84, 165.81, 165.40, 159.46, 150.33, 150.04, 145.59, 140.66, 140.43, 140.31, 131.73, 130.07, 126.31, 125.76, 125.74, 125.55, 115.46, 71.34,

71.20, 70.45, 70.06, 69.81, 68.30, 64.69, 51.13, 47.89, 43.41, 40.47, 32.15, 30.74, 30.60, 30.20, 30.09, 29.91, 29.69, 26.80.

HR-MS (ESI^{+}): Calcd. m/z for $C_{146}H_{194}N_{30}O_{32}Na_2$ $[M+2Na]^{2+}$ 1,463.2145, found 1,463.1901 and for $C_{146}H_{194}N_{30}O_{32}Na_3$ $[M+3Na]^{3+}$ 983.1393, found 983.1306.

2.5.24. Synthesis of radial [4]catenane (R[4]):

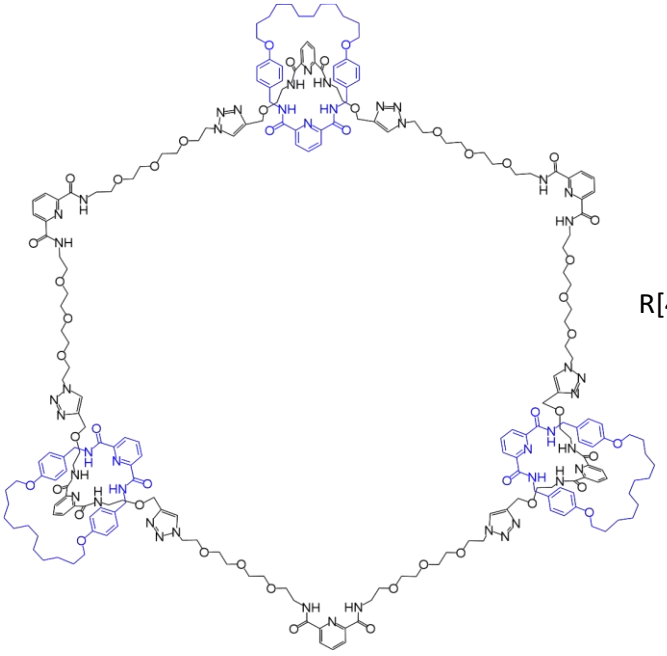

R[4]

Activated Zinc (220 mg) was used for removal of cobalt from **R[4]Co** (80 mg). It was purified by column using 55:45 EtOAc: MeOH to get 20 mg of R[4]catenane (**R[4]**) with yield of 26%.

^{1}H-NMR (400 MHz, CD_3OD) δ in ppm: 8.32-8.30 (d, 6H), 8.19-8.10 (m, 15H), 8.07-8.02 (m, 6H), 7.72 (s, 6H), 6.96-6.94 (d, 12H), 6.56-6.54 (d, 12H), 4.59 (s, 8H), 4.48-4.42 (d, 24H), 4.26 (t, 12H), 3.76 (t, 12H), 3.61-3.36 (m, 96H), 1.63-1.59 (p, 12H), 1.35-1.30 (m, 48H).

^{13}C-NMR (100 MHz, CD_3OD) δ in ppm: 165.85, 165.82, 165.42, 159.51, 150.37, 150.08, 145.62, 140.68, 140.45, 140.33, 131.73, 130.03, 126.33, 125.78, 125.51, 115.50, 71.37, 71.26, 71.22, 70.46, 70.10, 69.83, 68.33, 64.74, 51.14, 43.45, 40.49, 32.15, 30.75, 30.63, 30.47, 30.23, 30.09, 29.95, 29.73, 26.84.

HR-MS (ESI$^+$): HR-MS (ESI$^+$): Calcd. m/z for $C_{219}H_{291}N_{45}O_{48}Na_3$ $[M+3Na]^{3+}$ 1,463.3840, found 1,463.3624 and for $C_{219}H_{291}N_{45}O_{48}Na_4$ $[M+4Na]^{4+}$ 1103.2839, found 1103.2644.

2.6. Spectral data:

2.6.1. ^{1}H, and ^{13}C NMR Spectra:

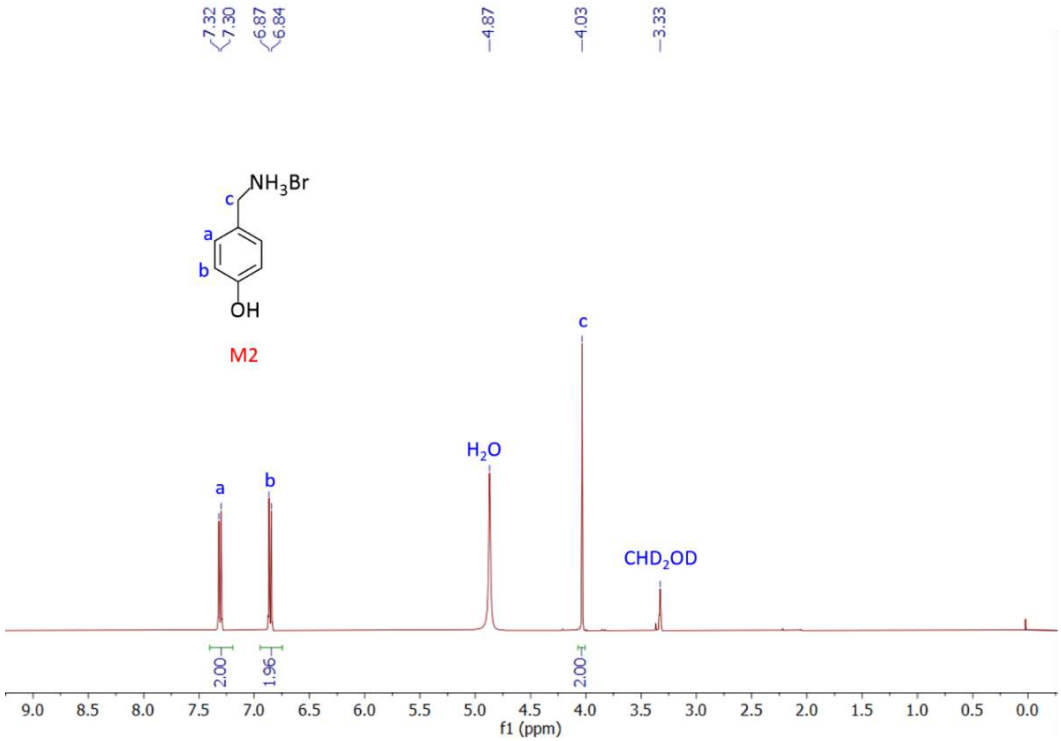

Figure 2.16. ^{1}H-NMR spectra of monomer-2 in MeOH-D$_4$ (400 MHz).

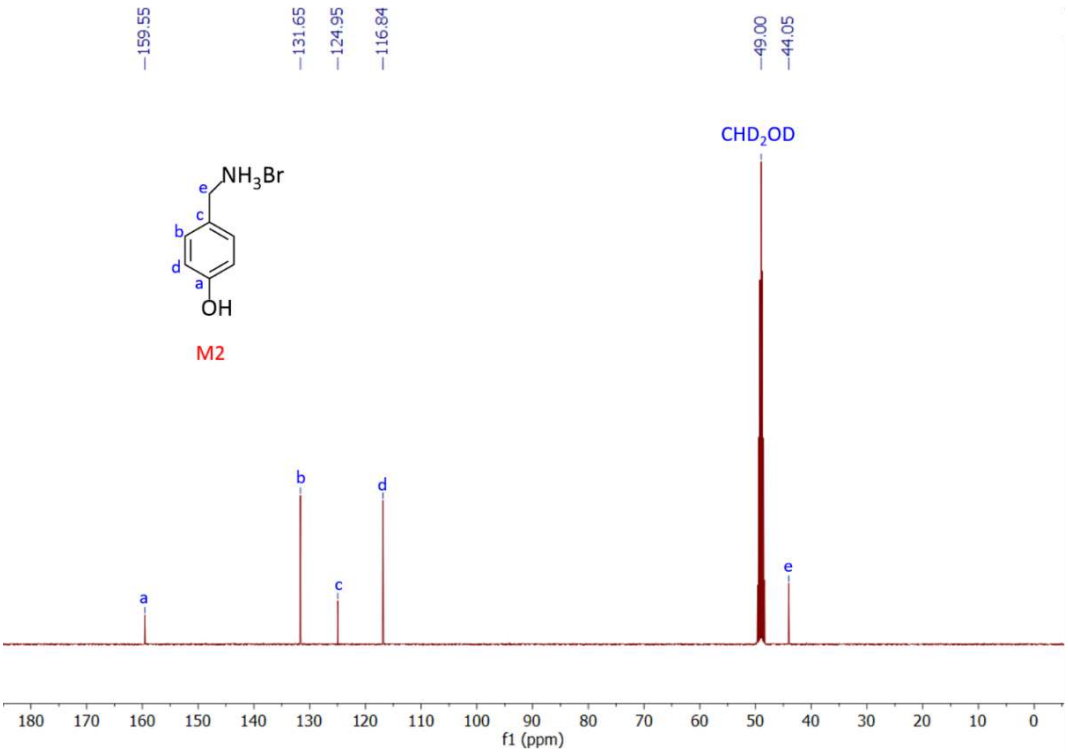

Figure 2.17. ^{13}C-NMR spectra of monomer-2 in MeOH-D$_4$ (100 MHz).

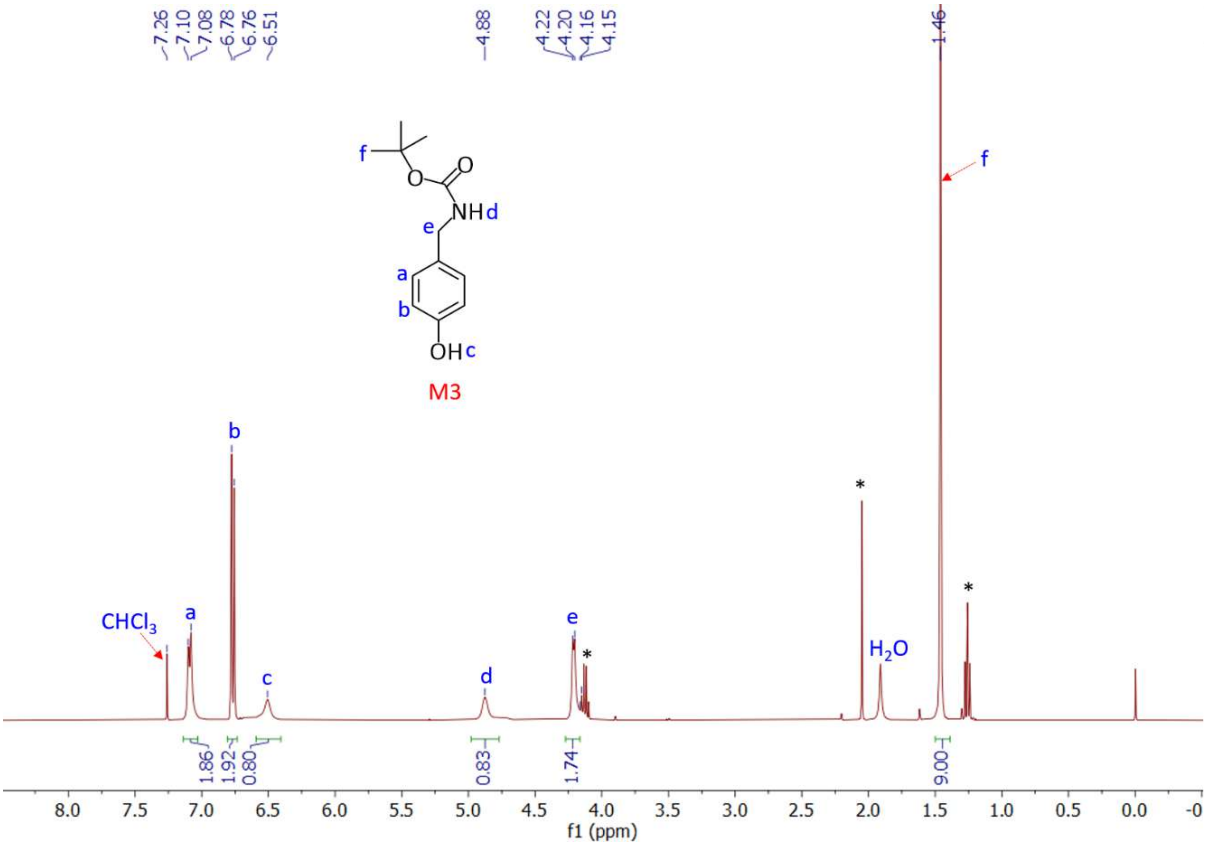

Figure 2.18. ^{1}H-NMR spectra of monomer-3 in $CDCl_3$ (400 MHz).

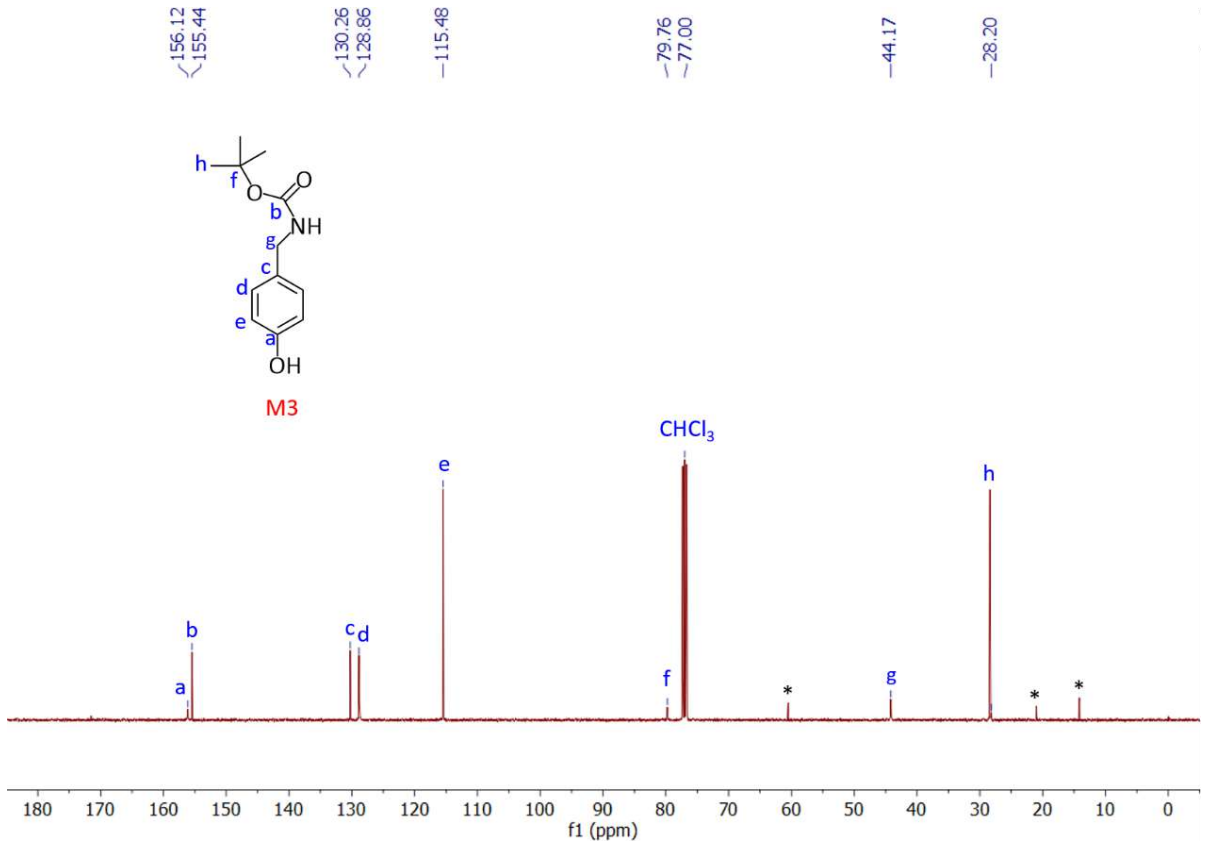

Figure 2.19. ^{13}C-NMR spectra of monomer-3 in $CDCl_3$ (100 MHz).

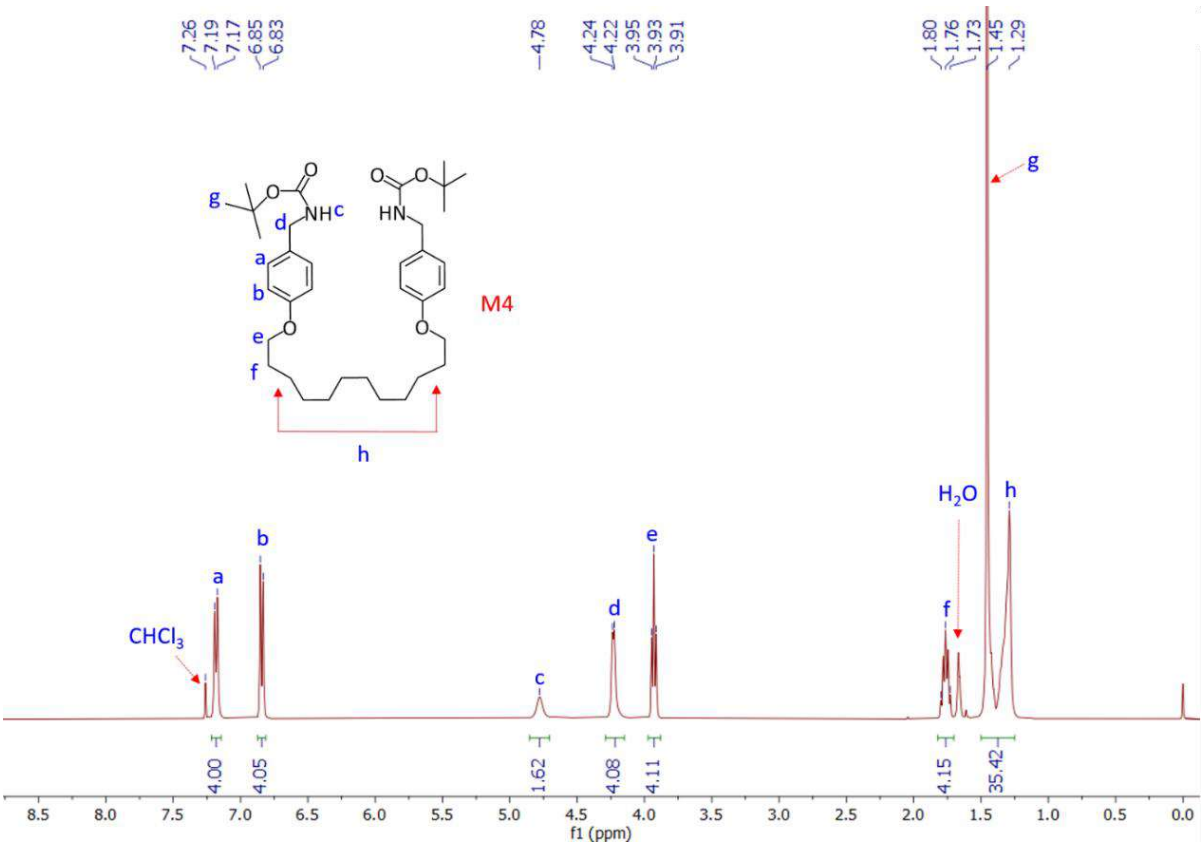

Figure 2.20. ^{1}H-NMR spectra of monomer-4 in $CDCl_3$ (400 MHz).

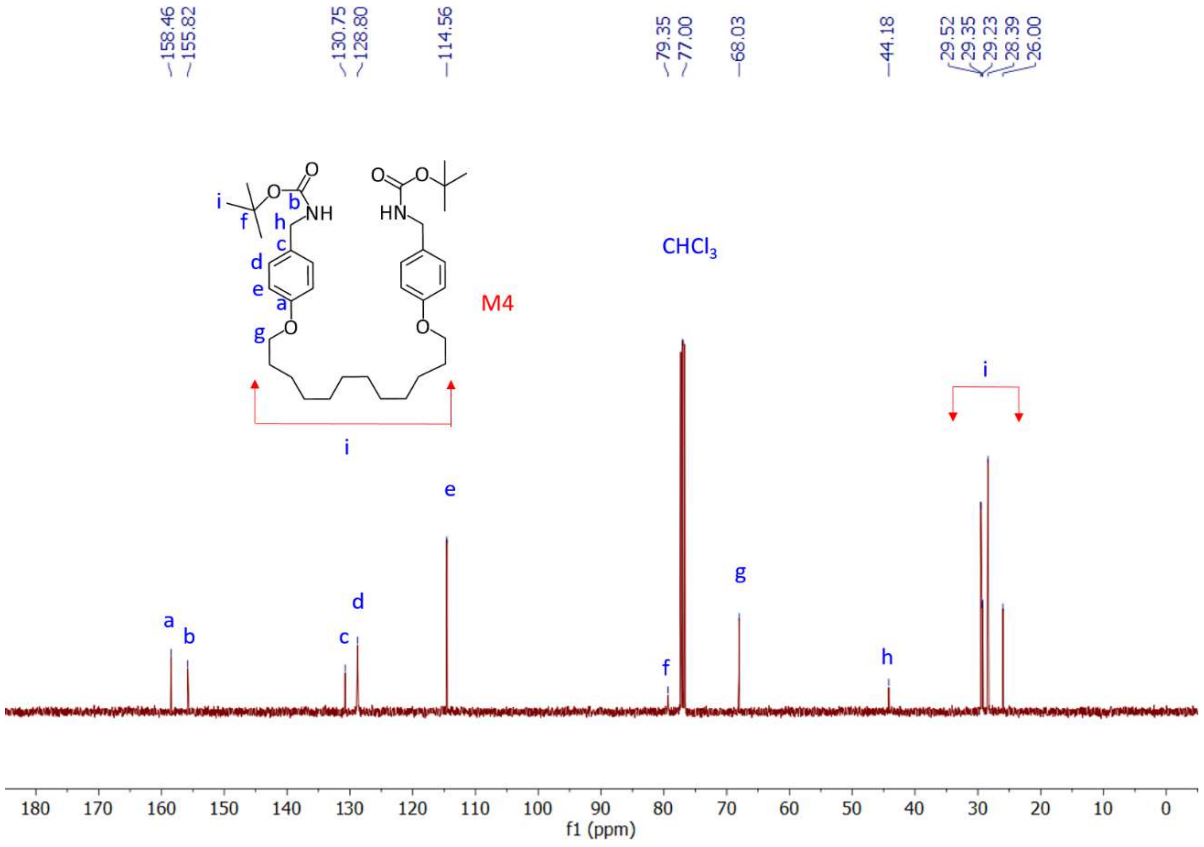

Figure 2.21. ^{13}C-NMR spectra of monomer-4 in $CDCl_3$ (100 MHz).

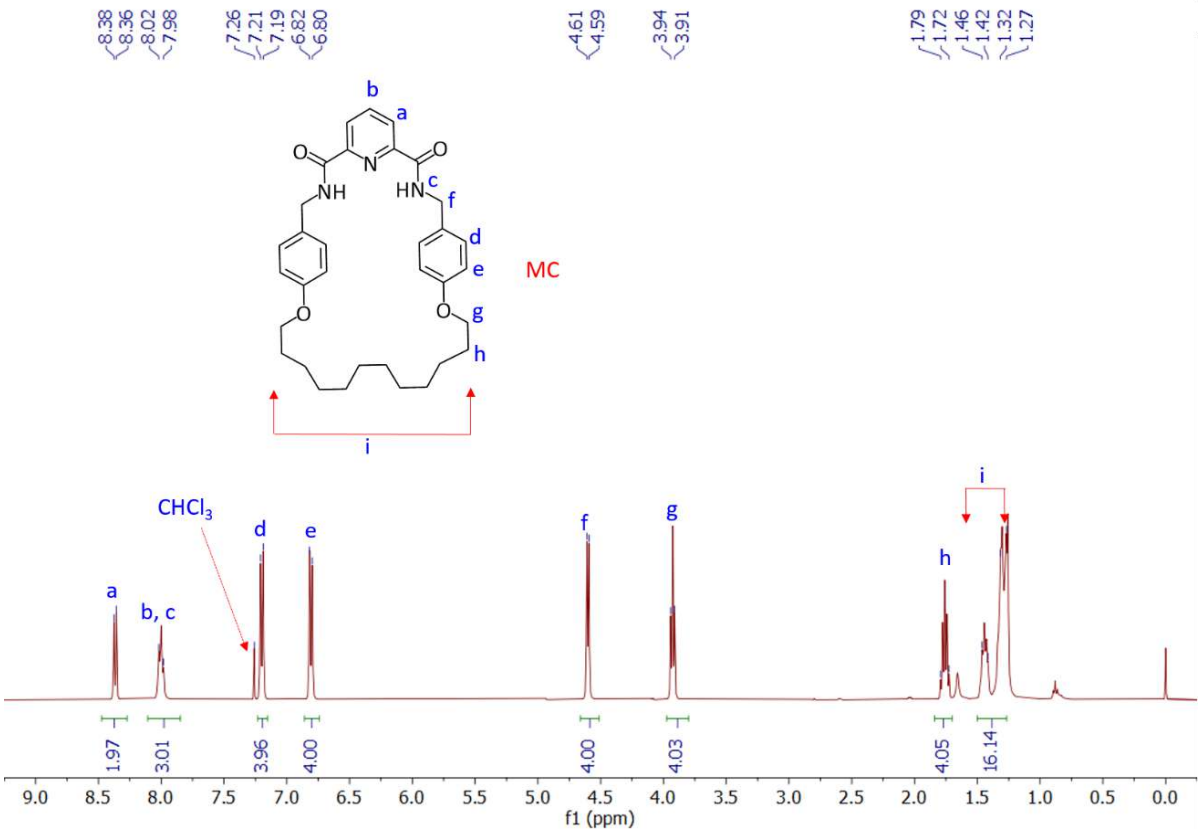

Figure 2.22. ^{1}H-NMR spectra of macrocycle MC in $CDCl_3$ (400 MHz).

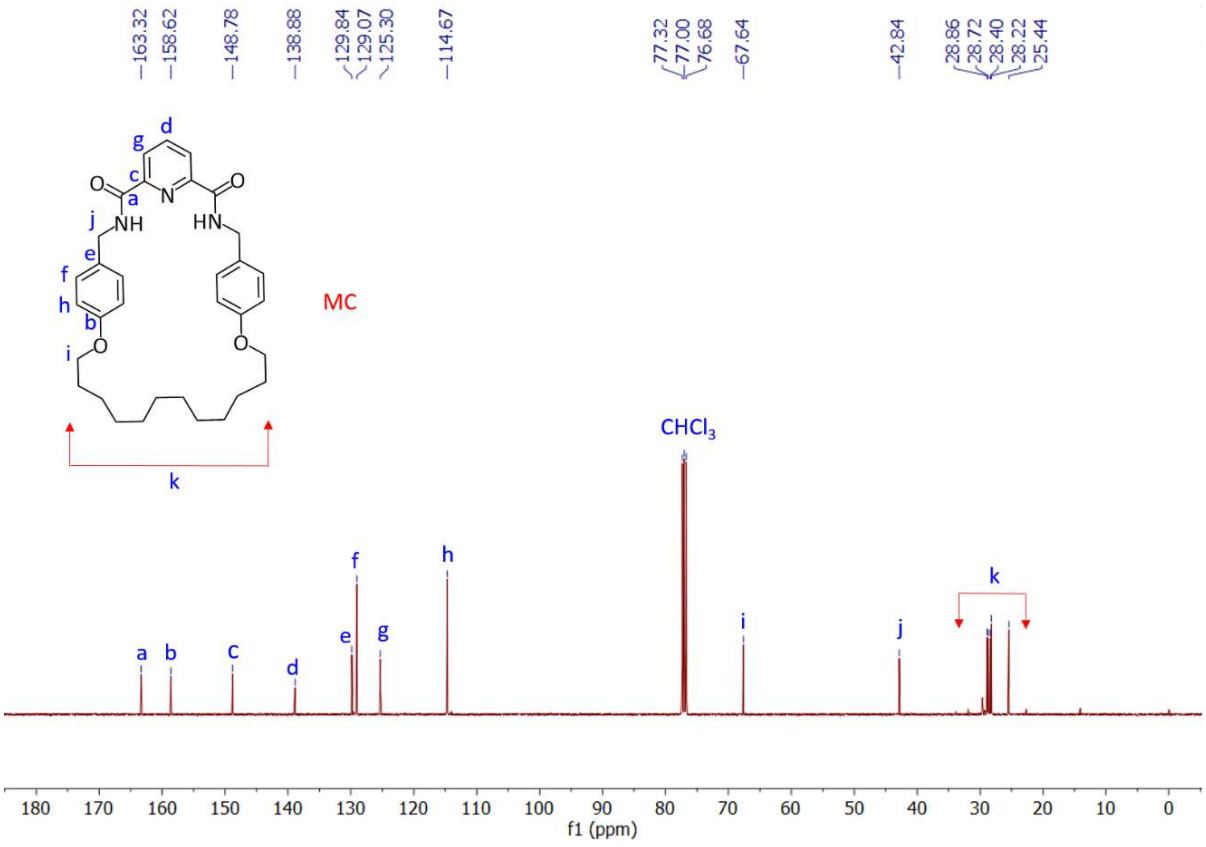

Figure 2.23. ^{13}C-NMR spectra of macrocycle MC in $CDCl_3$ (100 MHz).

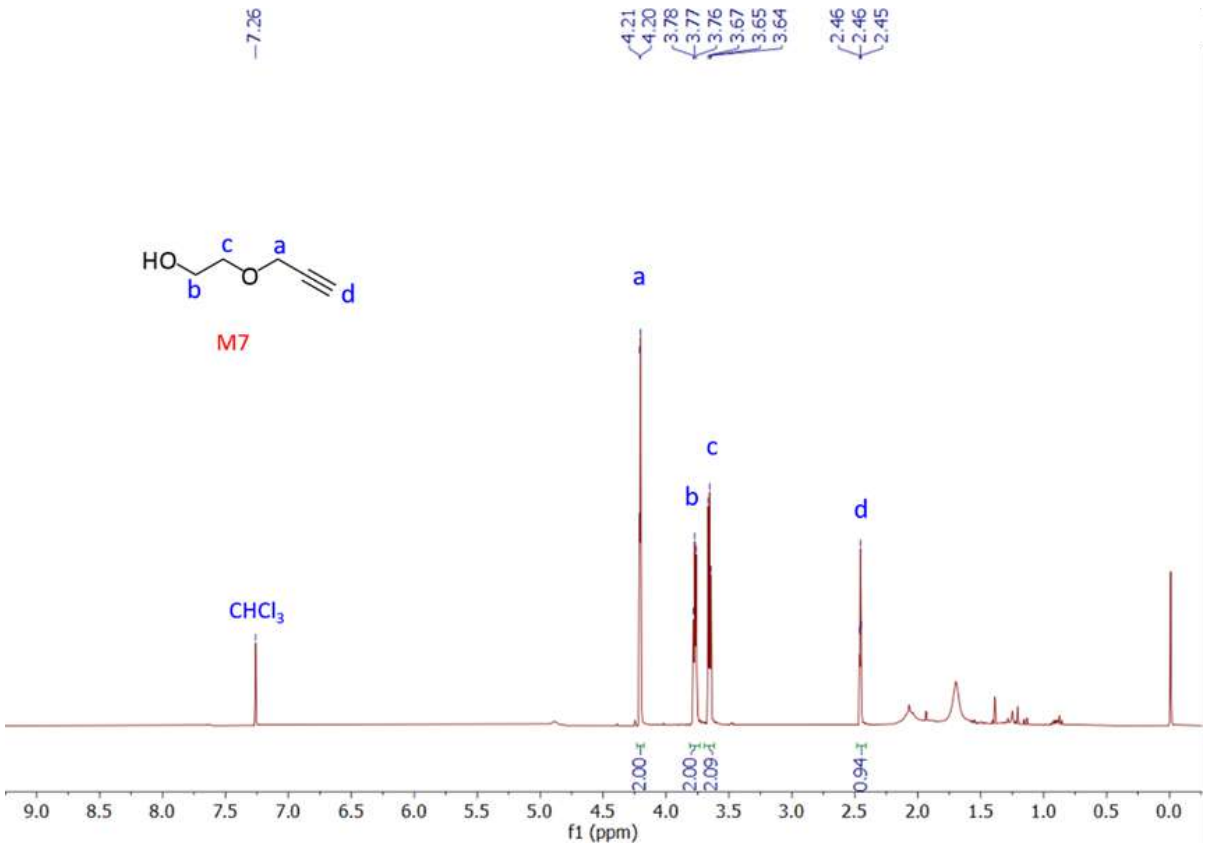

Figure 2.24. ^{1}H-NMR spectra of monomer-7 in $CDCl_3$ (400 MHz).

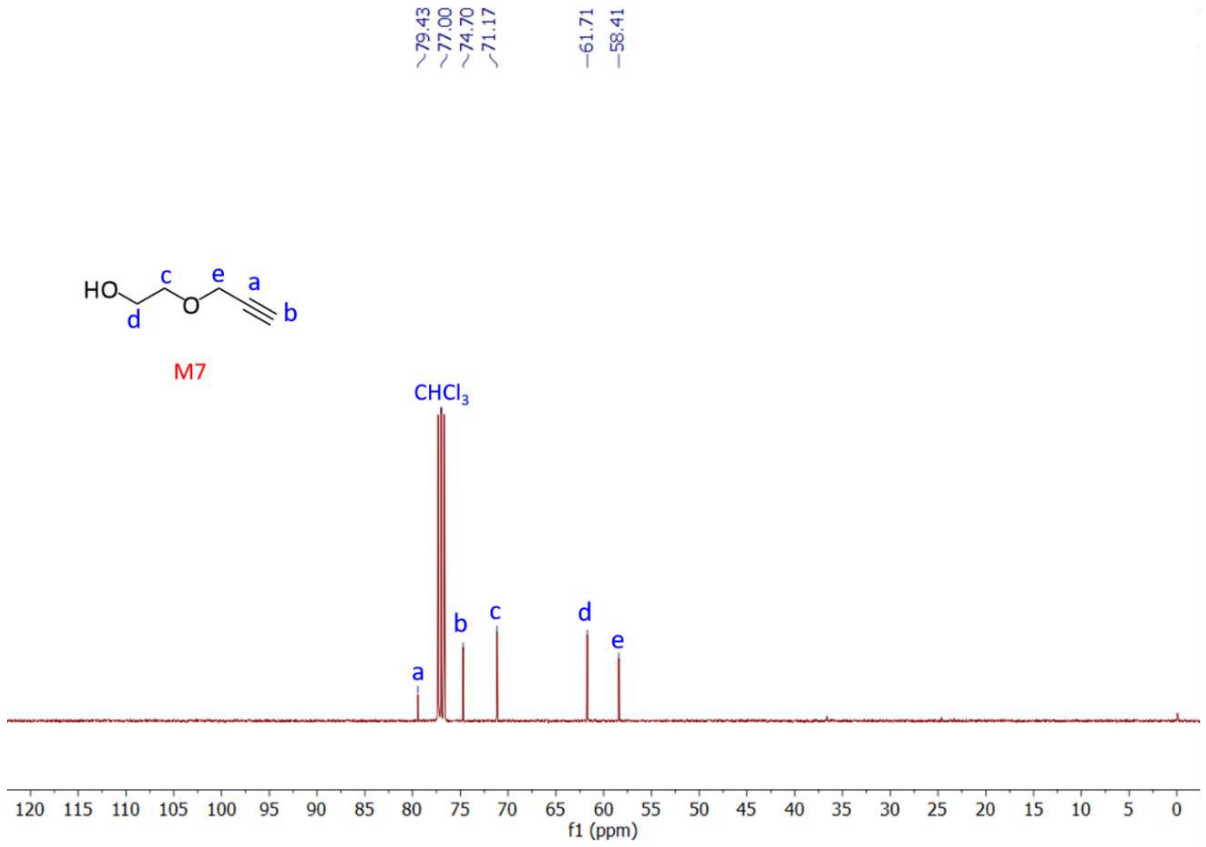

Figure 2.25. ^{13}C-NMR spectra of monomer-7 in $CDCl_3$ (100 MHz).

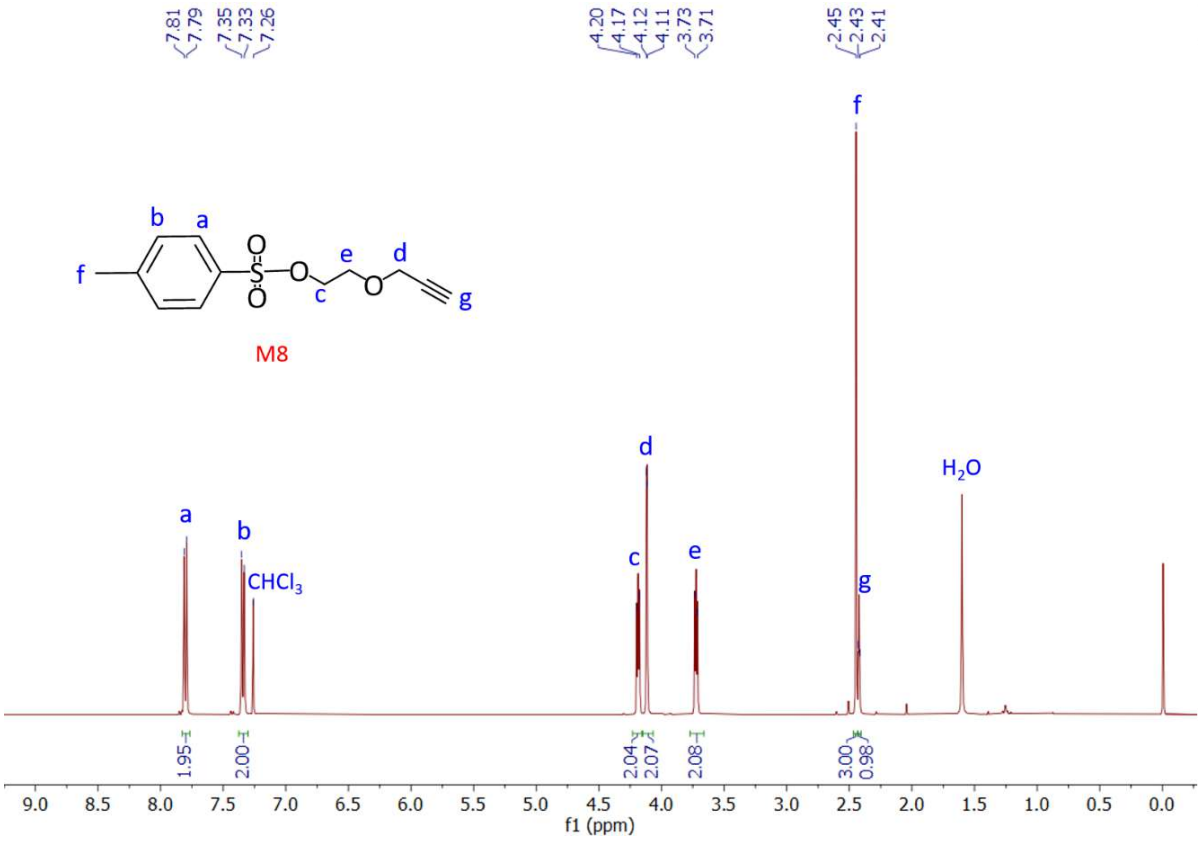

Figure 2.26. ^{1}H-NMR spectra of monomer-8 in $CDCl_3$ (400 MHz).

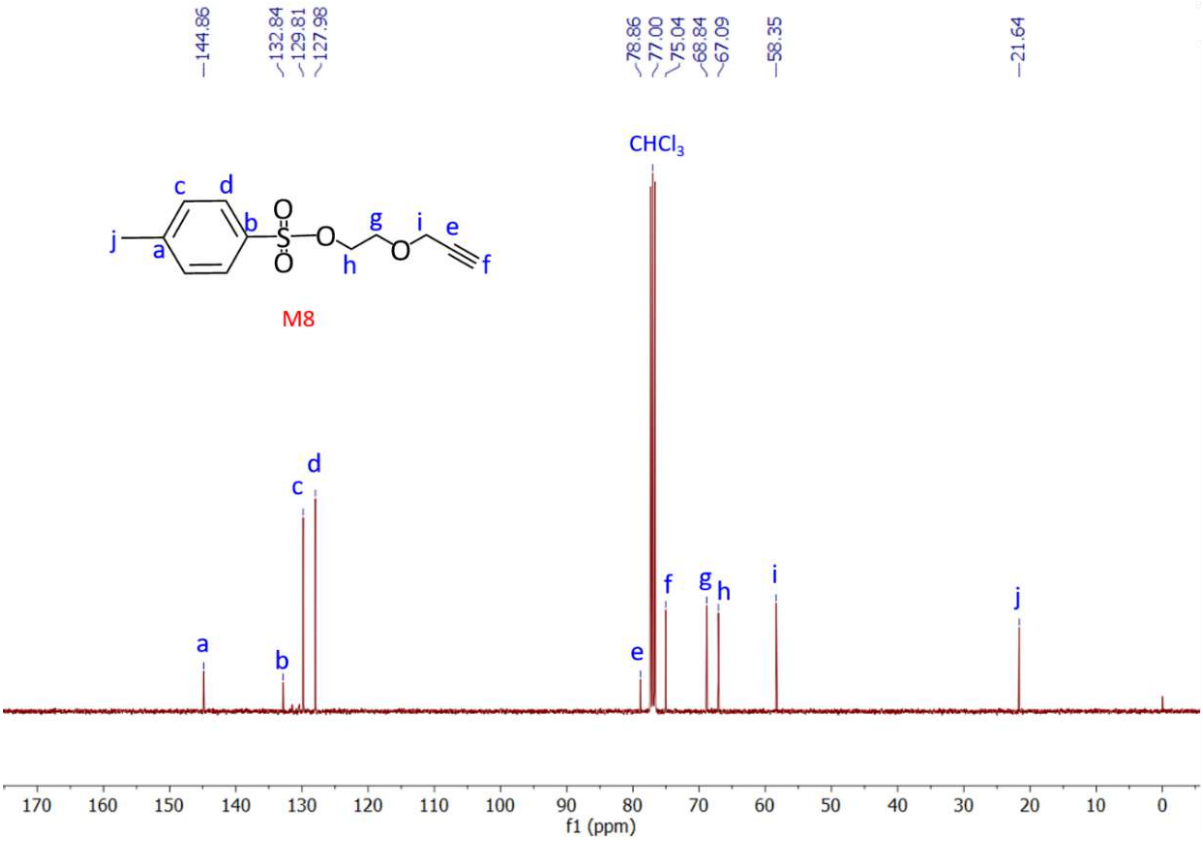

Figure 2.27. ^{13}C-NMR spectra of monomer-8 in $CDCl_3$ (100 MHz).

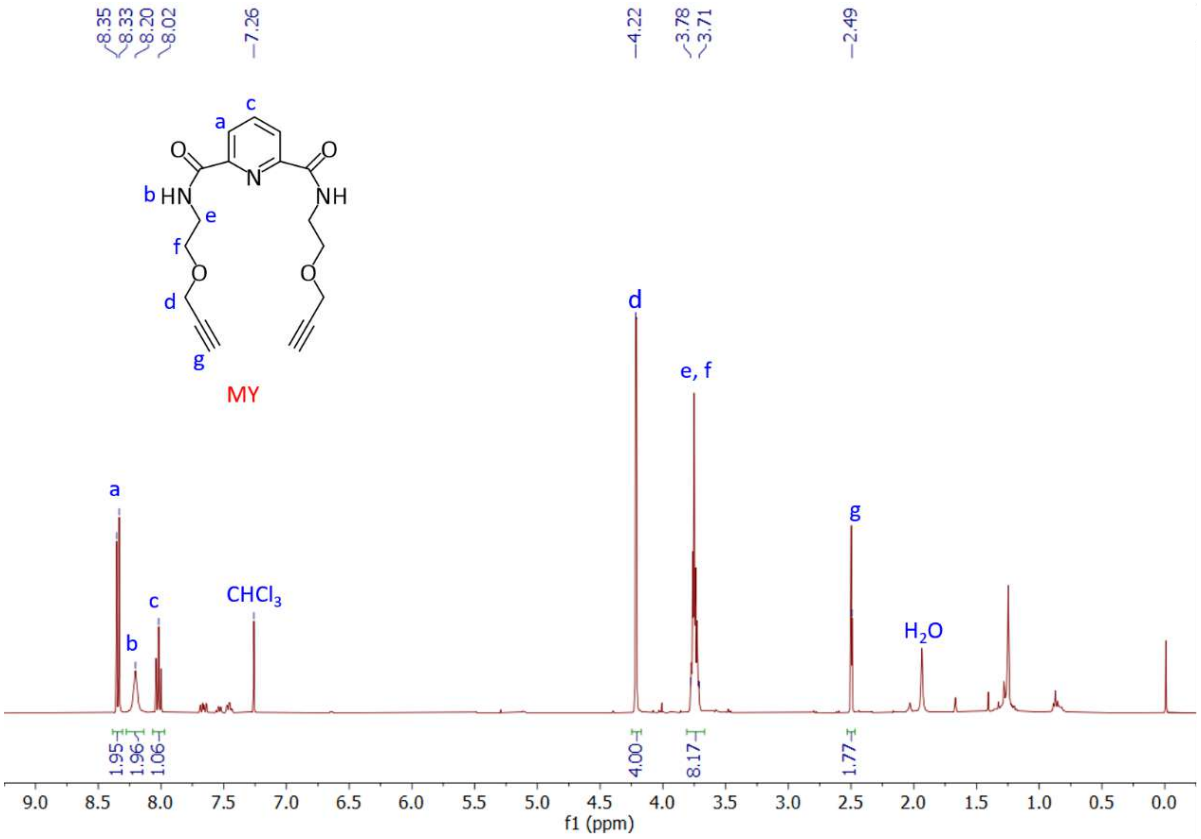

Figure 2.28. ^{1}H-NMR spectra of monomer MY in $CDCl_3$ (400 MHz).

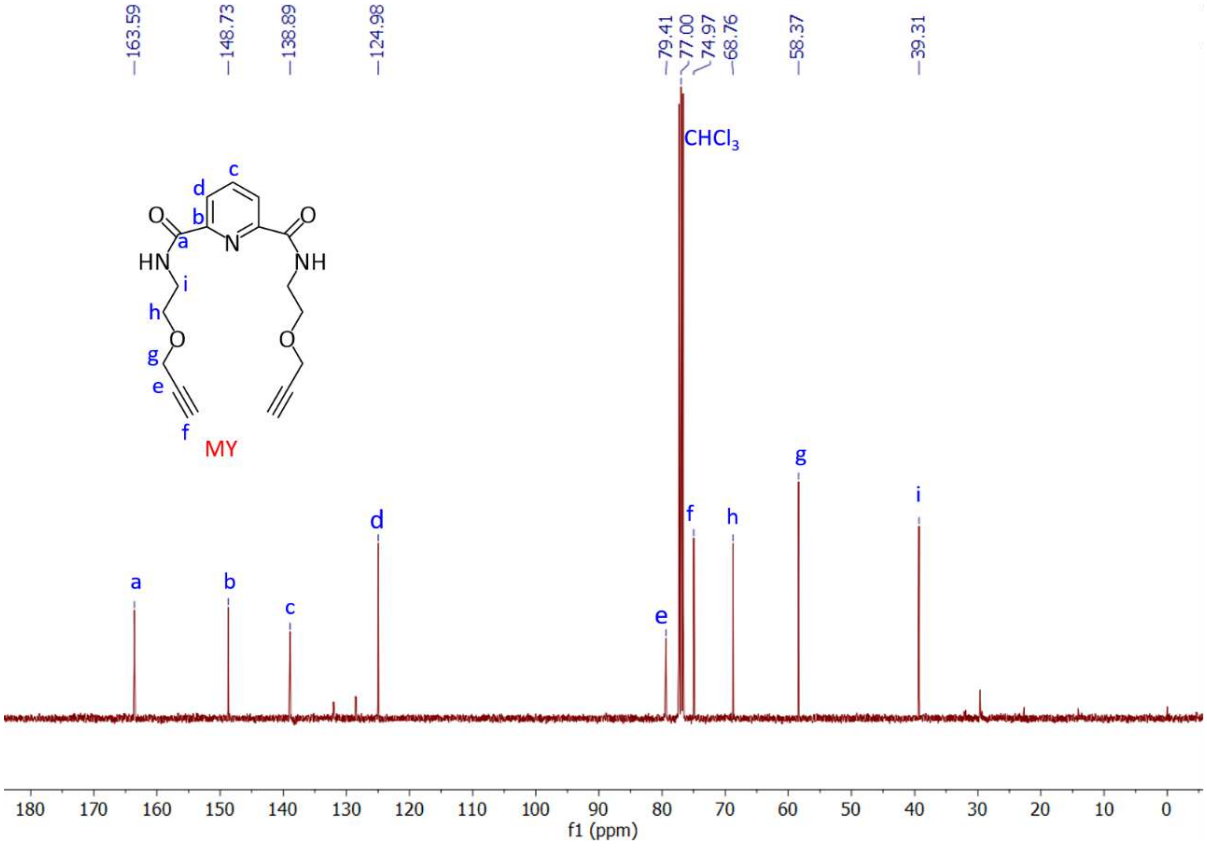

Figure 2.29. ^{13}C-NMR spectra of monomer MY in $CDCl_3$ (100 MHz).

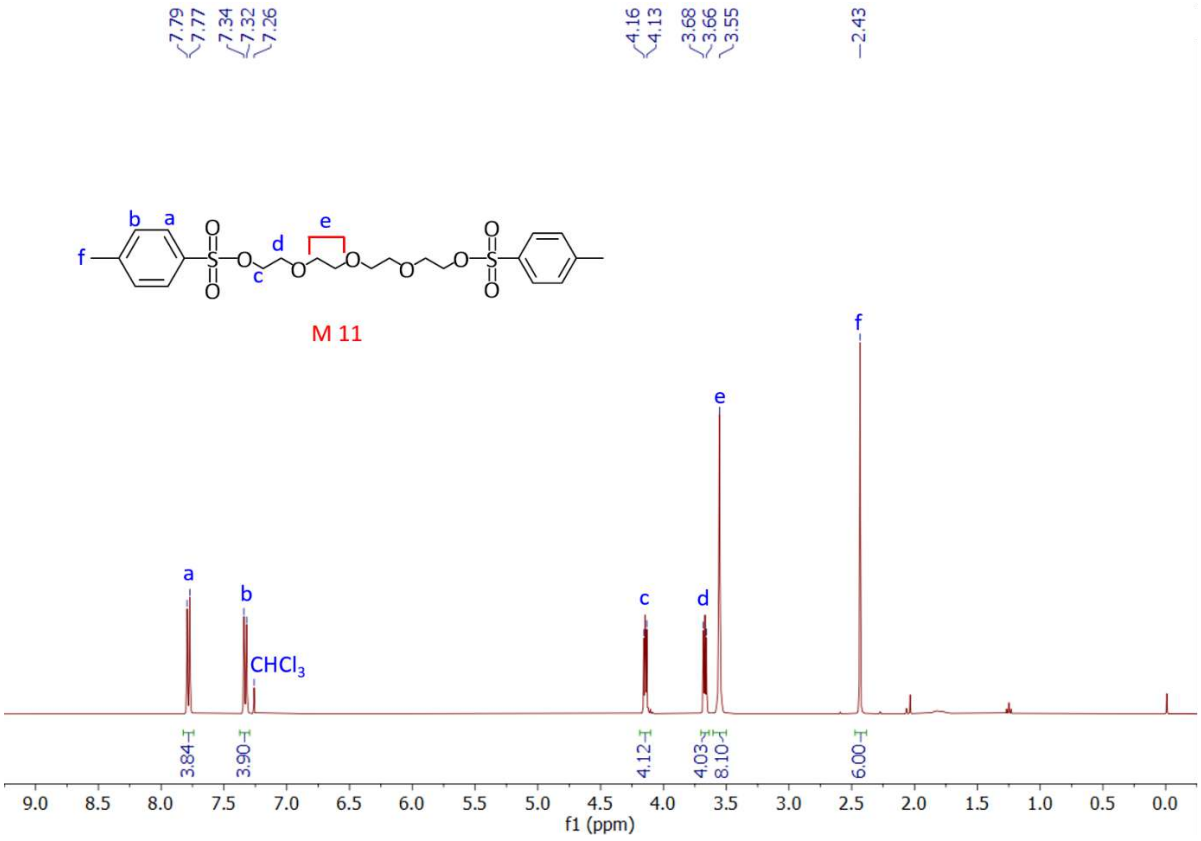

Figure 2.30. ^{1}H-NMR spectra of monomer-11 in $CDCl_3$ (400 MHz).

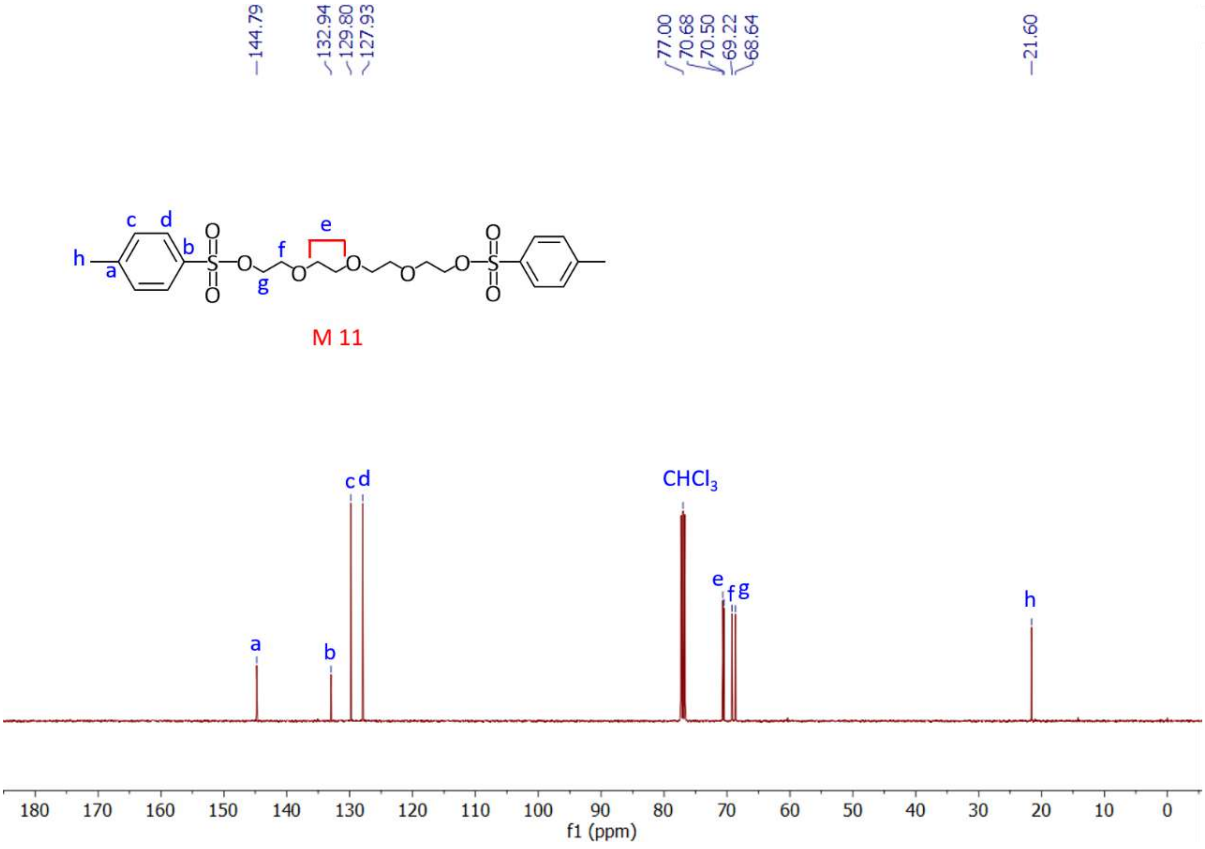

Figure 2.31. ^{13}C-NMR spectra of monomer-11 in $CDCl_3$ (100 MHz).

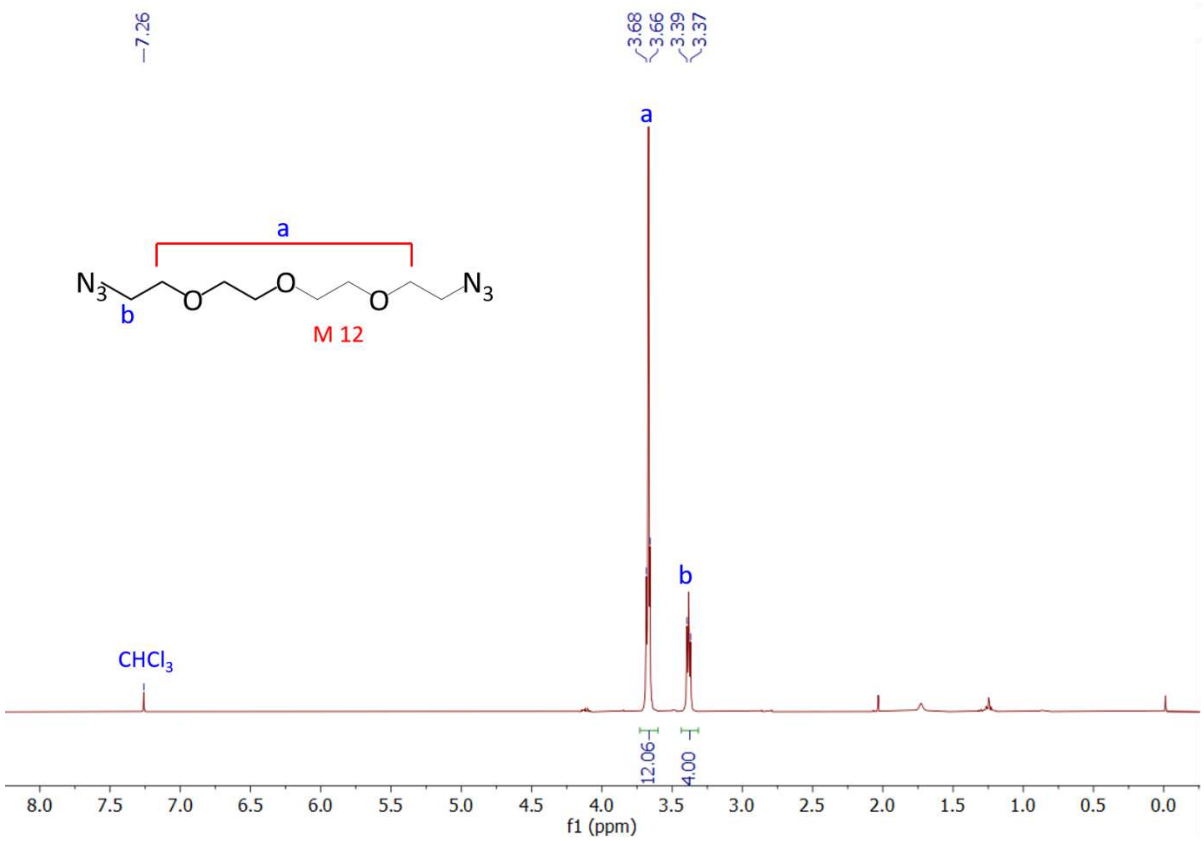

Figure 2.32. ^{1}H-NMR spectra of monomer-12 in $CDCl_3$ (400 MHz).

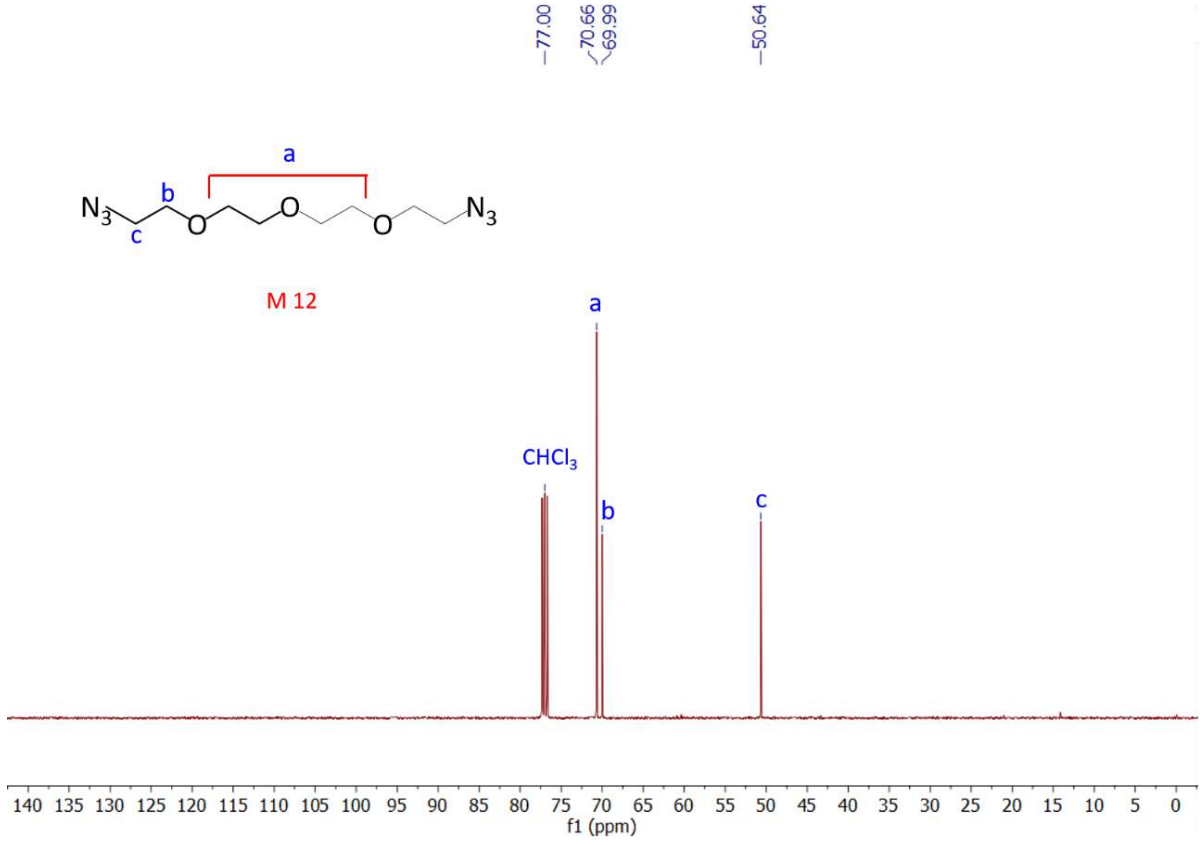

Figure 2.33. ^{13}C-NMR spectra of monomer-12 in $CDCl_3$ (100 MHz).

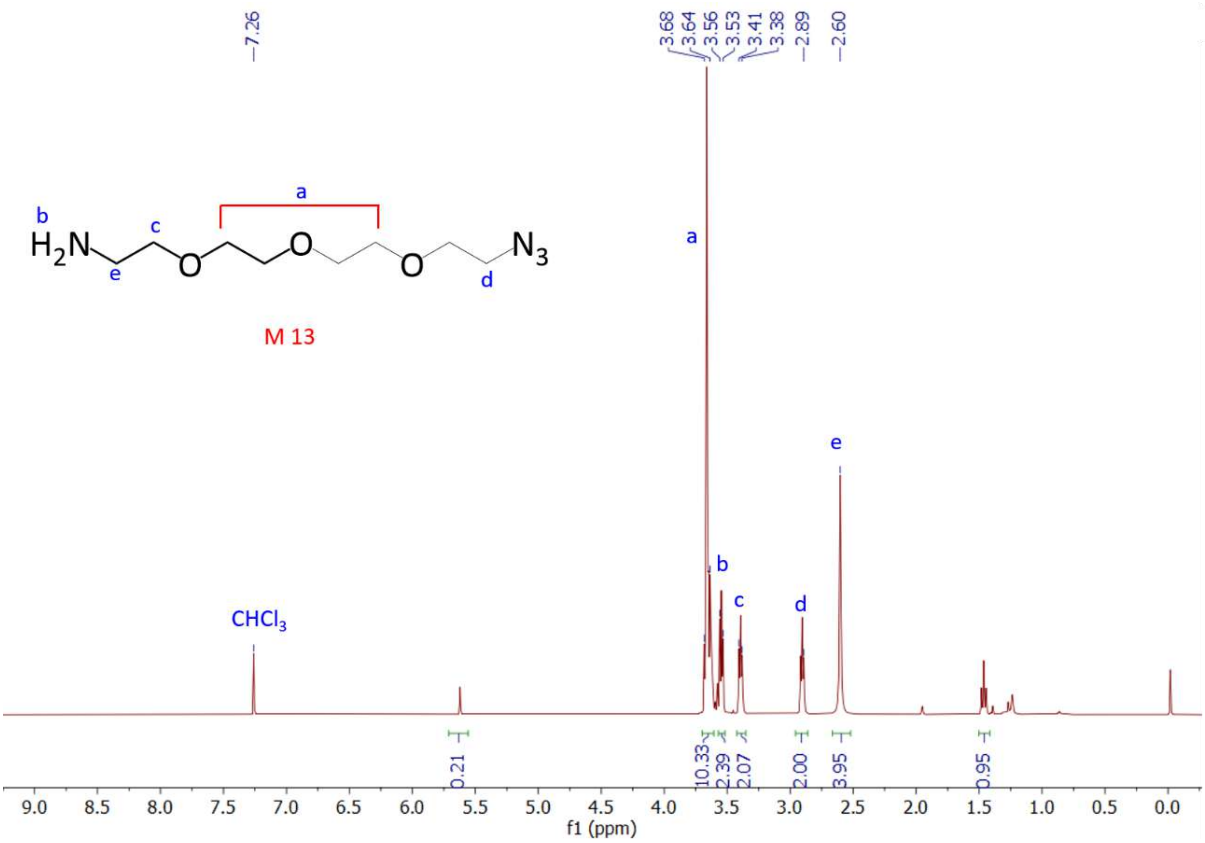

Figure 2.34. ^{1}H-NMR spectra of monomer-13 in $CDCl_3$ (400 MHz).

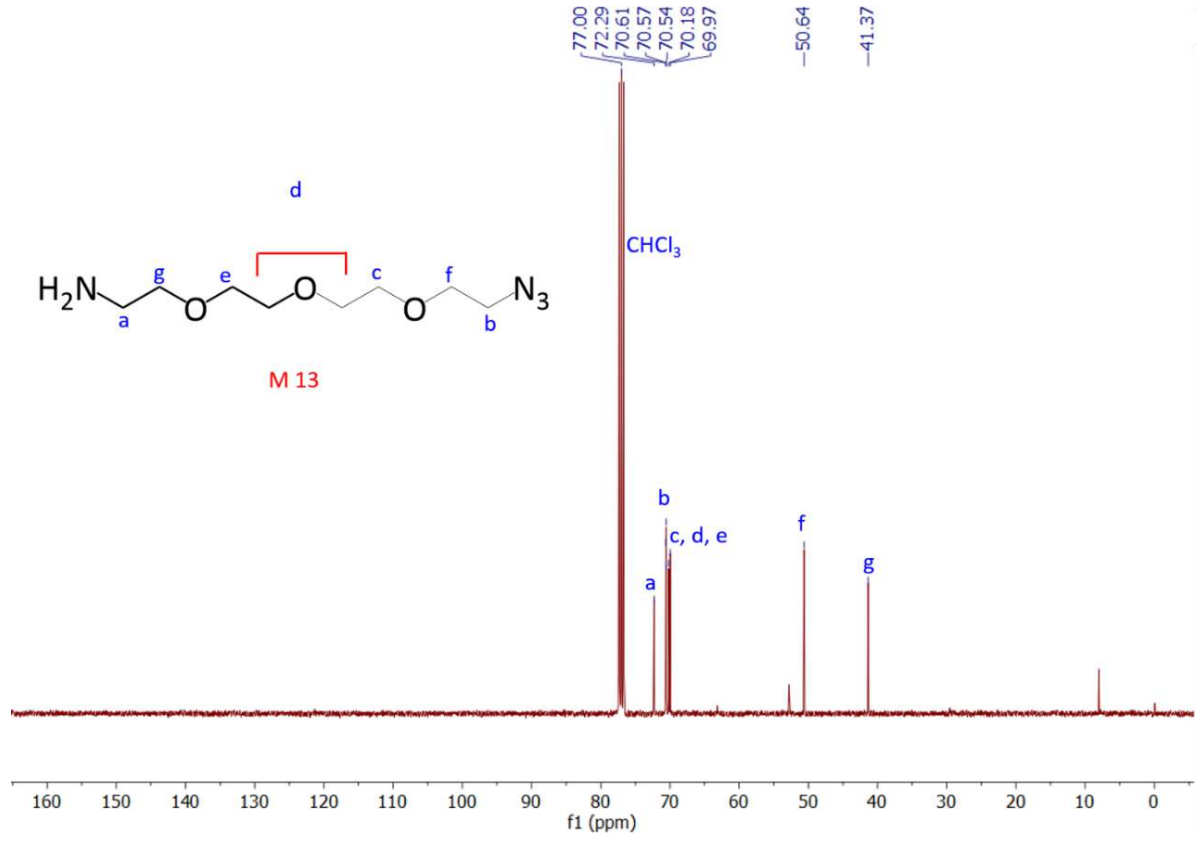

Figure 2.35. ^{13}C-NMR spectra of monomer-13 in $CDCl_3$ (100 MHz).

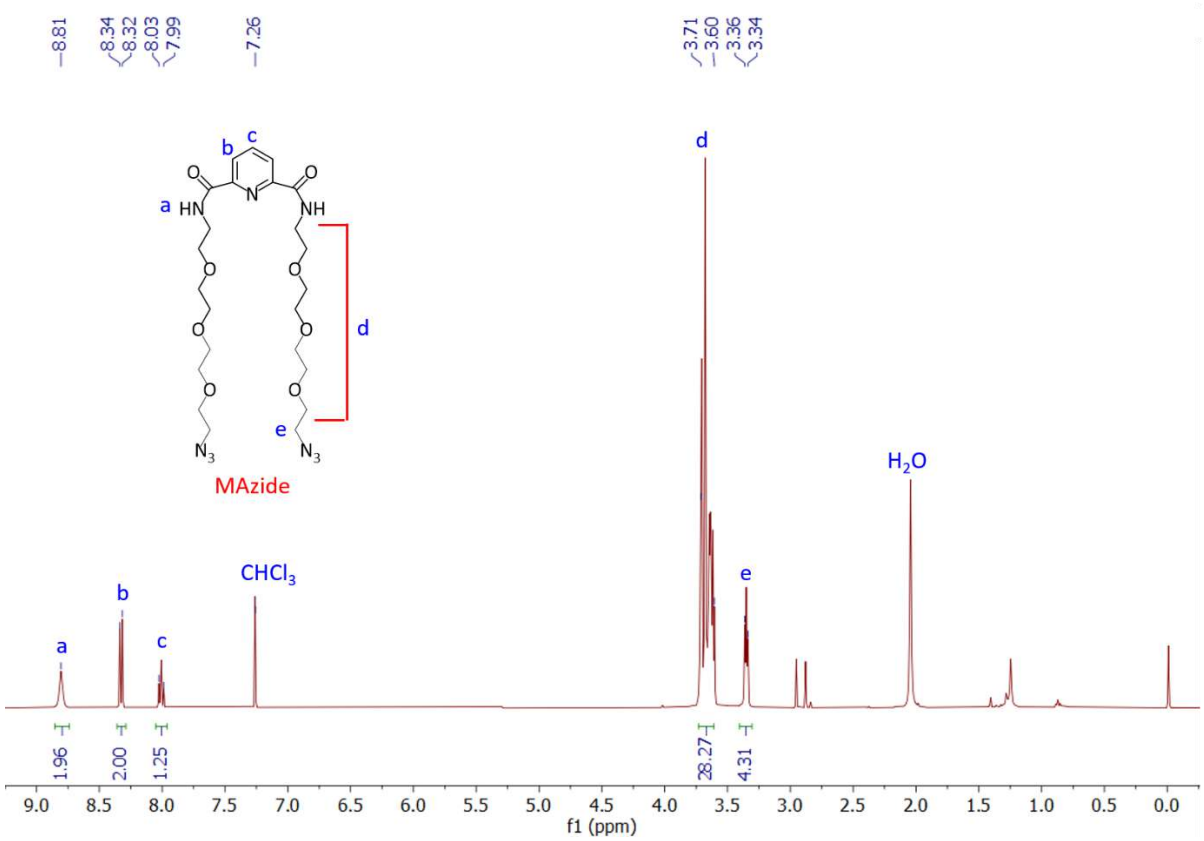

Figure 2.36. ^{1}H-NMR spectra of monomer MA in $CDCl_3$ (400 MHz).

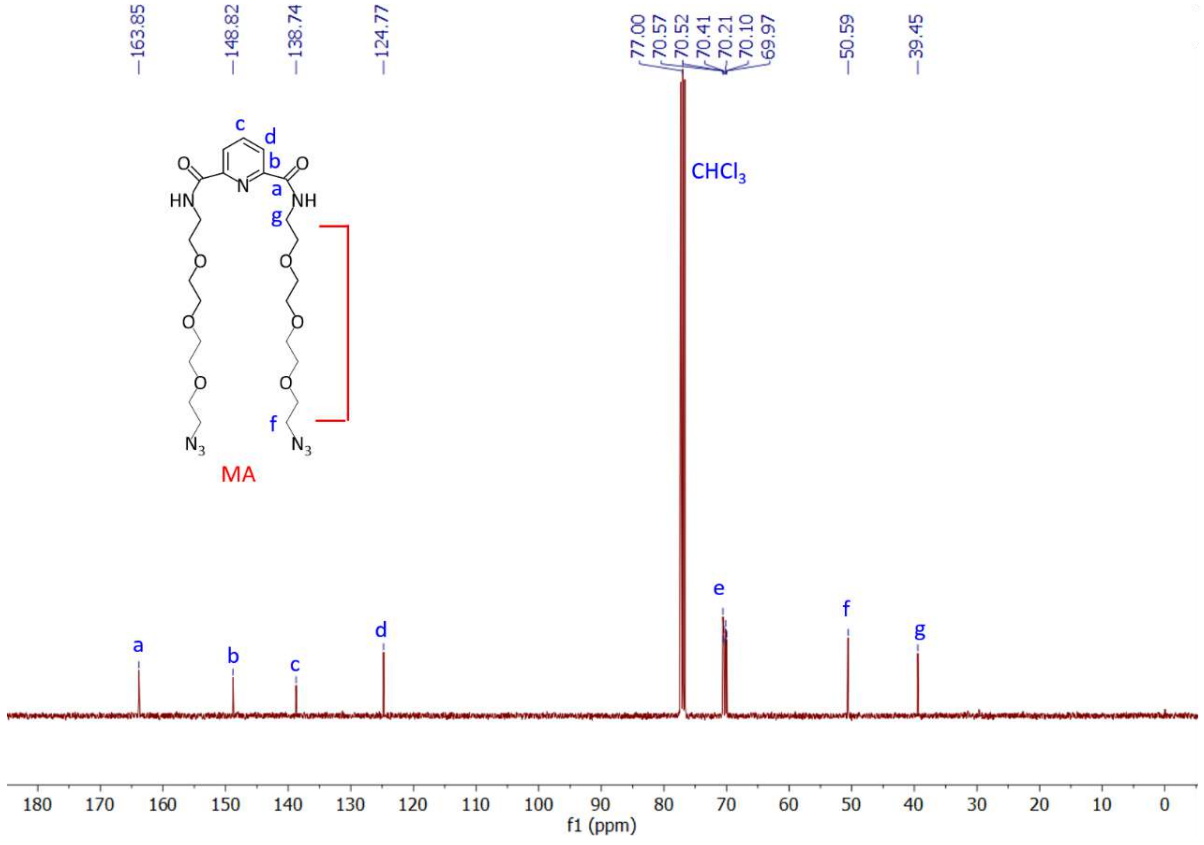

Figure 2.37. ^{13}C-NMR spectra of monomer MA in $CDCl_3$ (100 MHz).

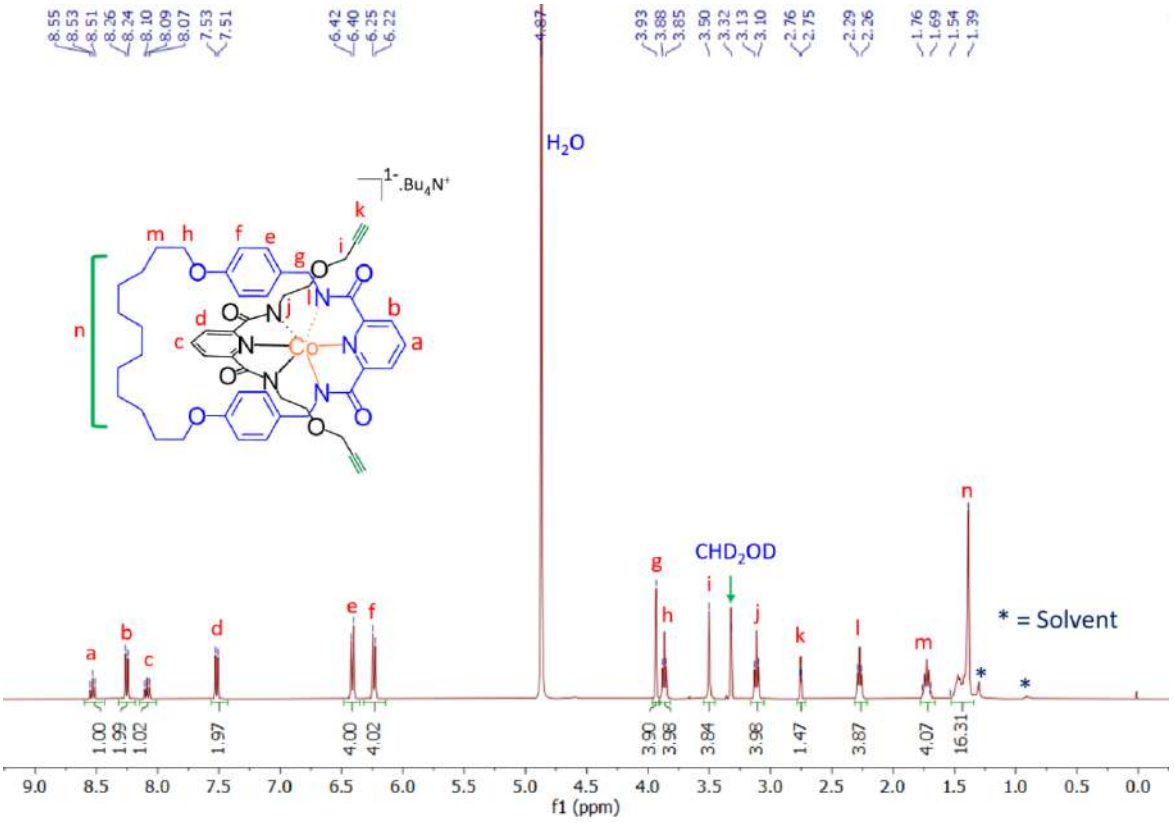

Figure 2.38. ^{1}H-NMR spectra of pseudo-rotaxane [2]PR-Co in MeOH-D$_4$ (400 MHz). NH-protons getting exchanged with CD$_3$OD and are not seen here.

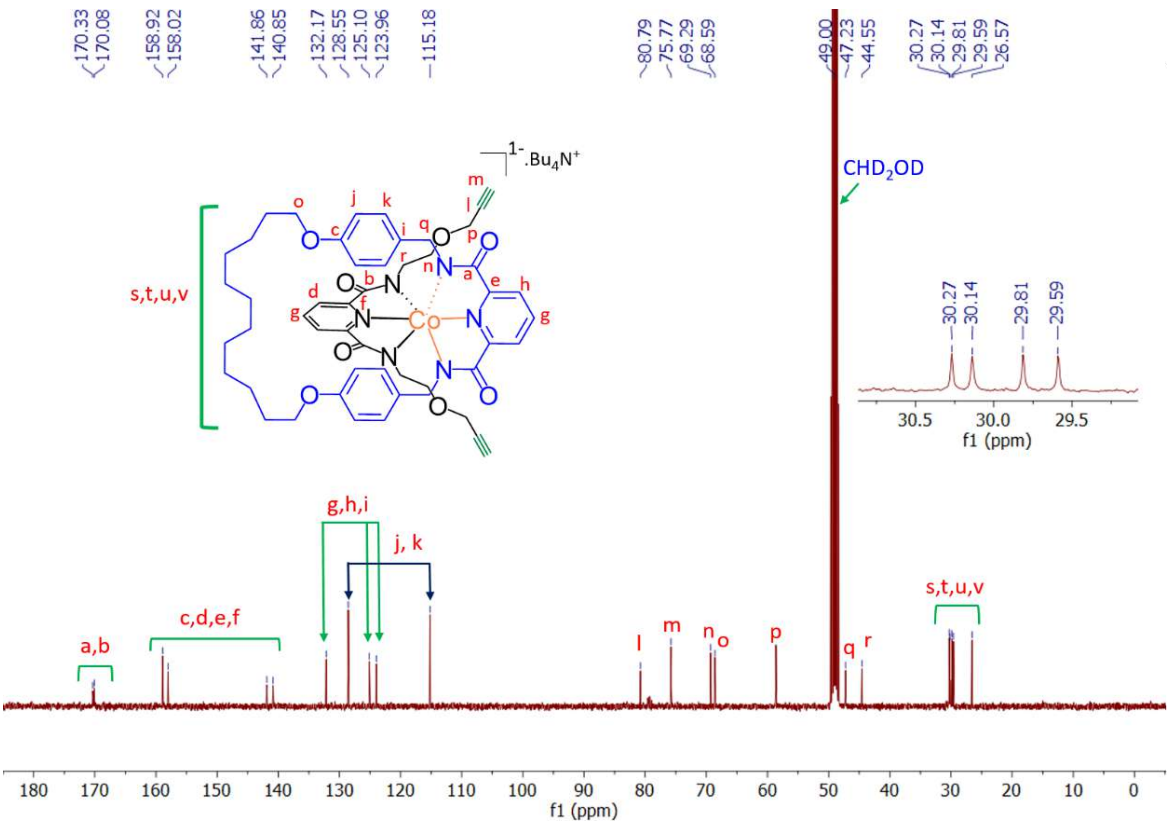

Figure 2.39. ^{13}C-NMR spectra of pseudo-rotaxane [2]PR-Co in MeOH-D$_4$ (100 MHz).

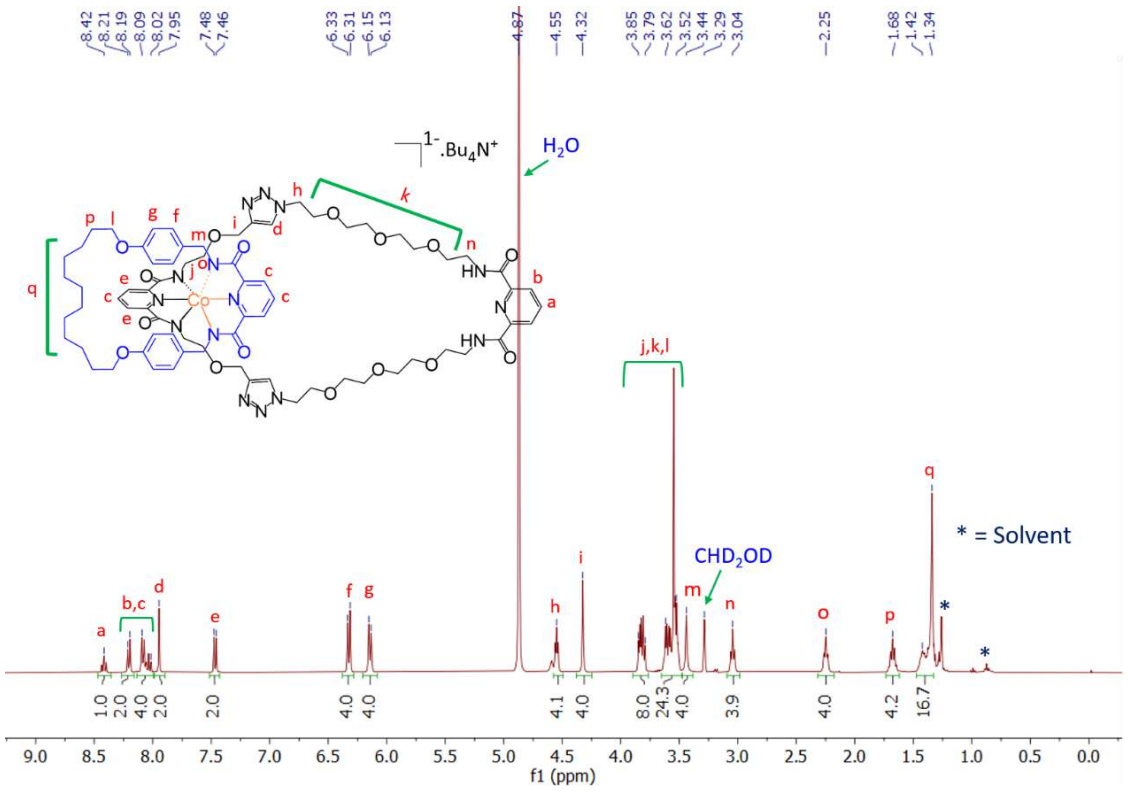

Figure 2.40. ^{1}H-NMR spectra of cobalt(III)-templated catenane [2]Co in MeOH-D$_4$ (400 MHz). NH- protons getting exchanged with CD$_3$OD and are not seen here.

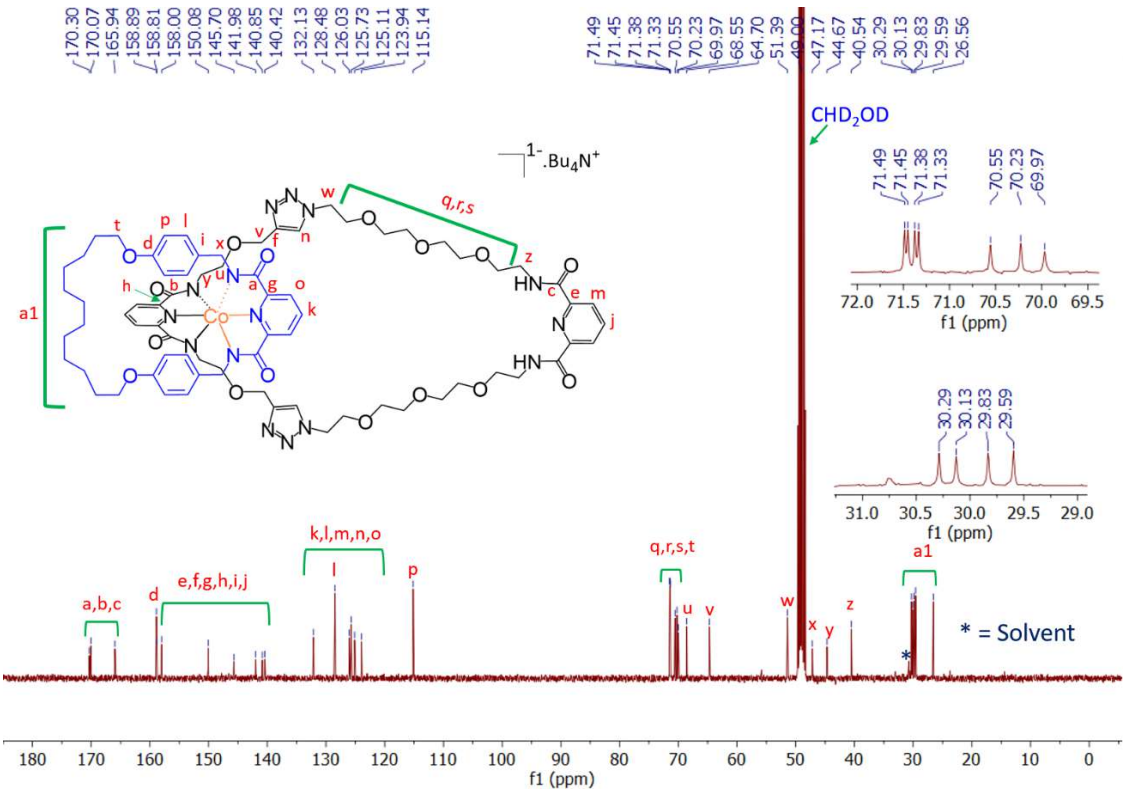

Figure 2.41. ^{13}C-NMR spectra of cobalt(III)-templated catenane [2]Co in MeOH-D$_4$ (100 MHz).

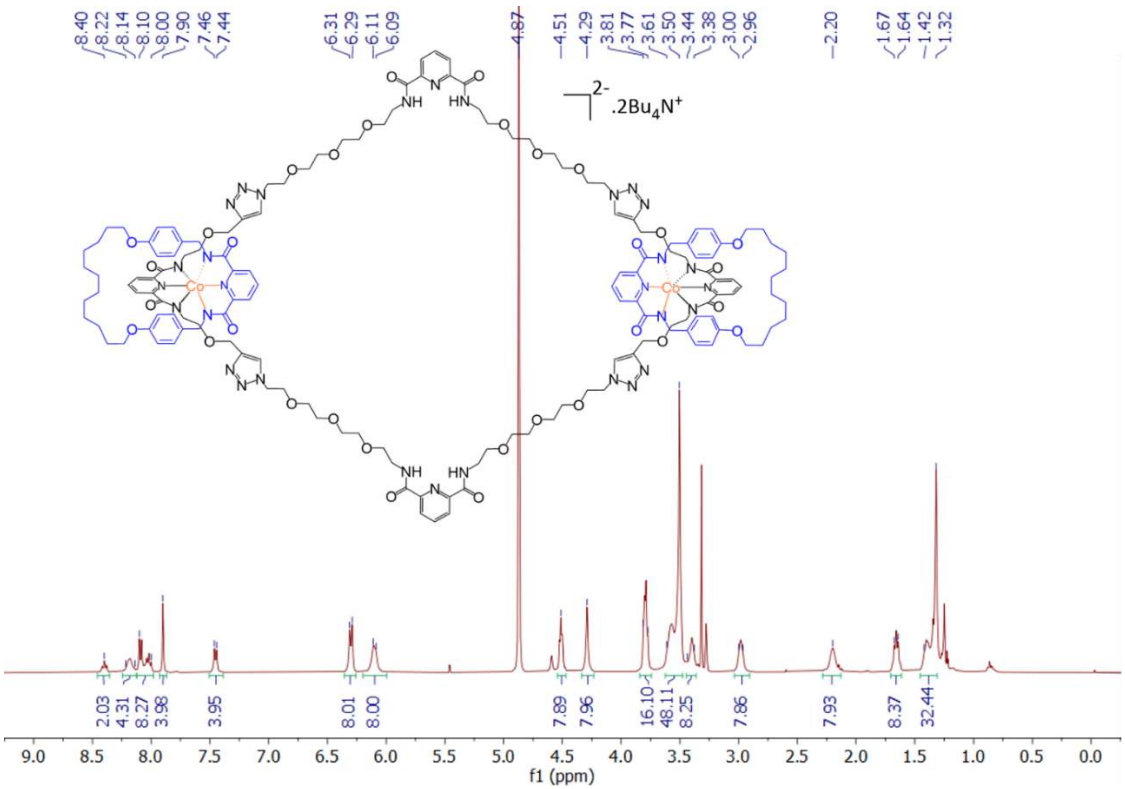

Figure 2.42. ^{1}H-NMR spectra of cobalt(III)-templated catenane L[3]Co in MeOH-D$_4$ (400 MHz). NH- protons getting exchanged with CD$_3$OD and are not seen here.

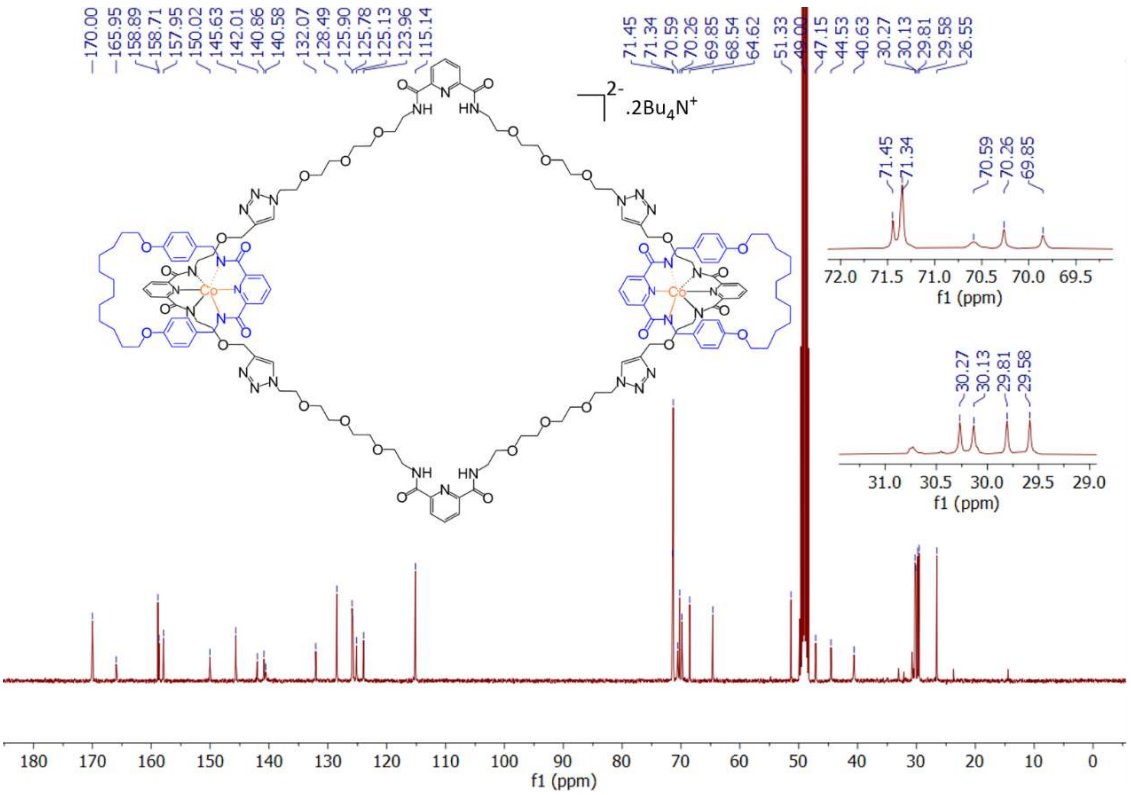

Figure 2.43. ^{13}C-NMR spectra of cobalt(III)-templated catenane L[3]Co in MeOH-D$_4$ (100 MHz).

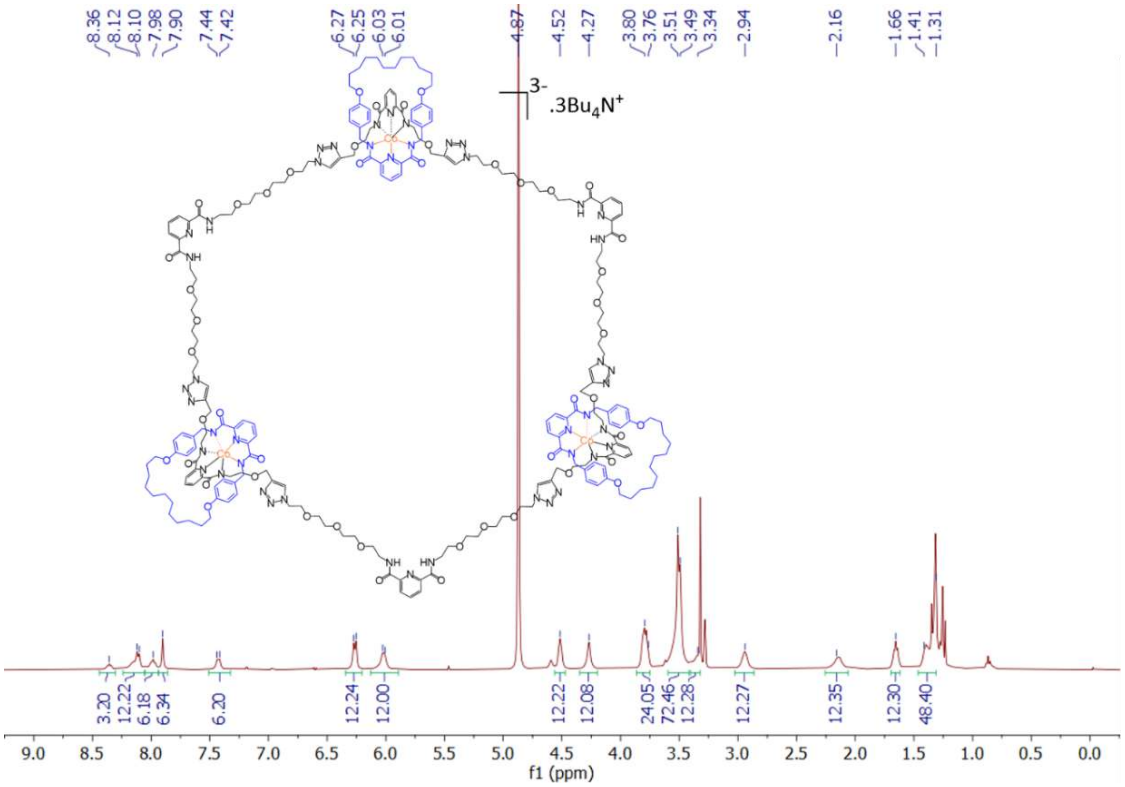

Figure 2.44. ^{1}H-NMR spectra of cobalt(III)-templated catenane R[4]Co in MeOH-D_4 (400 MHz). NH- protons getting exchanged with CD_3OD and are not seen here.

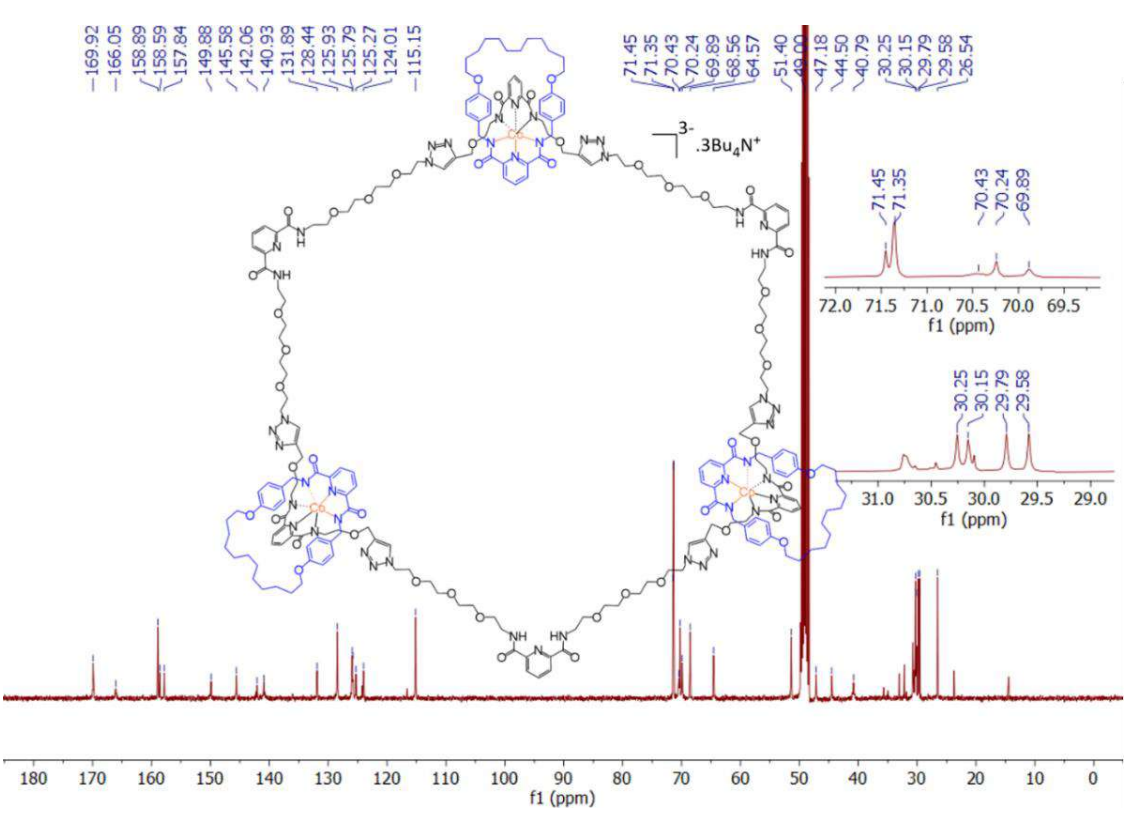

Figure 2.45. ^{13}C-NMR spectra of cobalt(III)-templated catenane R[4]Co in MeOH-D_4 (100 MHz).

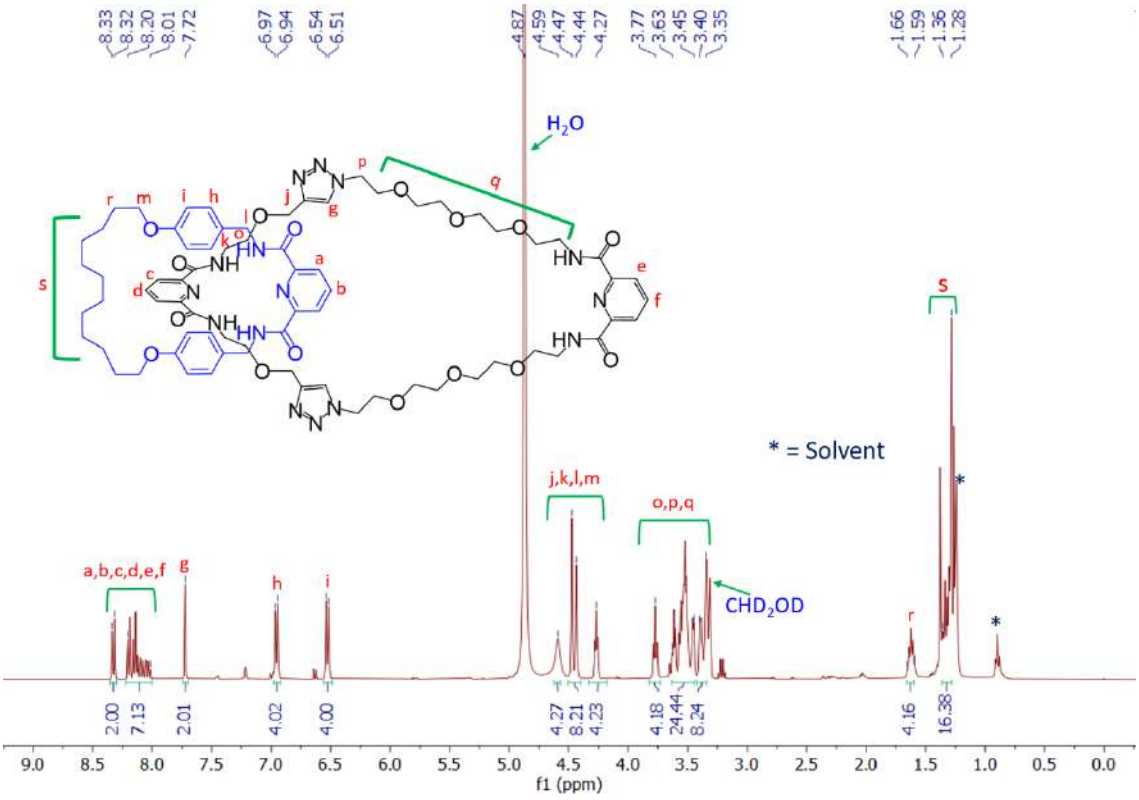

Figure 2.46 ^{1}H-NMR spectra of [2]catenane in MeOH-D_4 (400 MHz). NH- protons getting exchanged with CD_3OD and are not seen here.

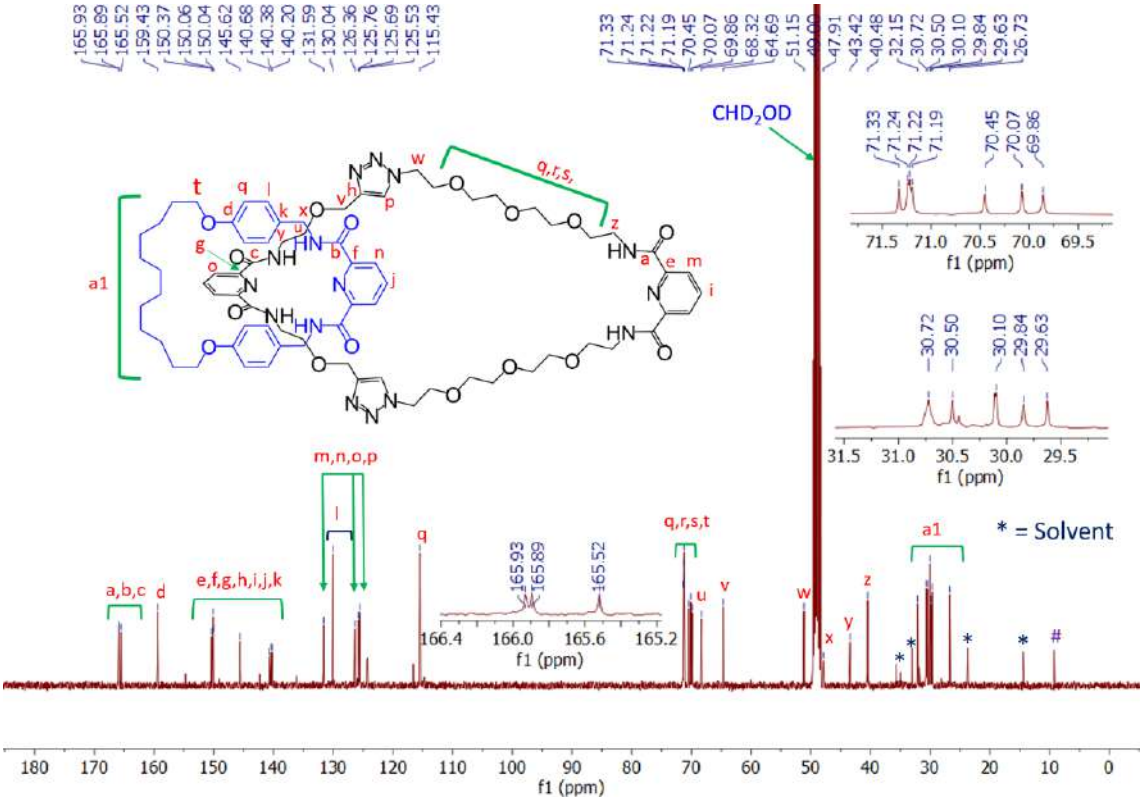

Figure 2.47. ^{13}C-NMR spectra of [2]catenane in MeOH-D_4 (100 MHz).

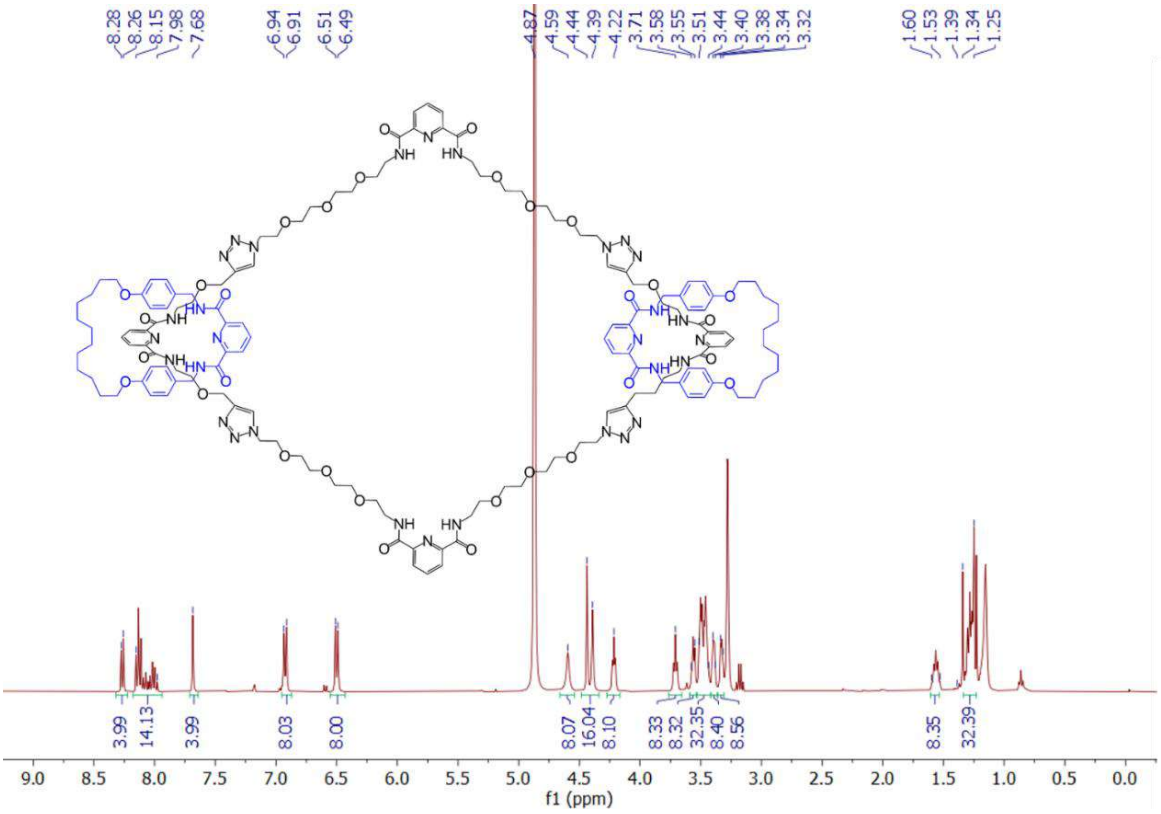

Figure 2.48. ^{1}H-NMR spectra of linear [3]catenane in MeOH-D_4 (400 MHz). NH- protons getting exchanged with CD_3OD and are not seen here.

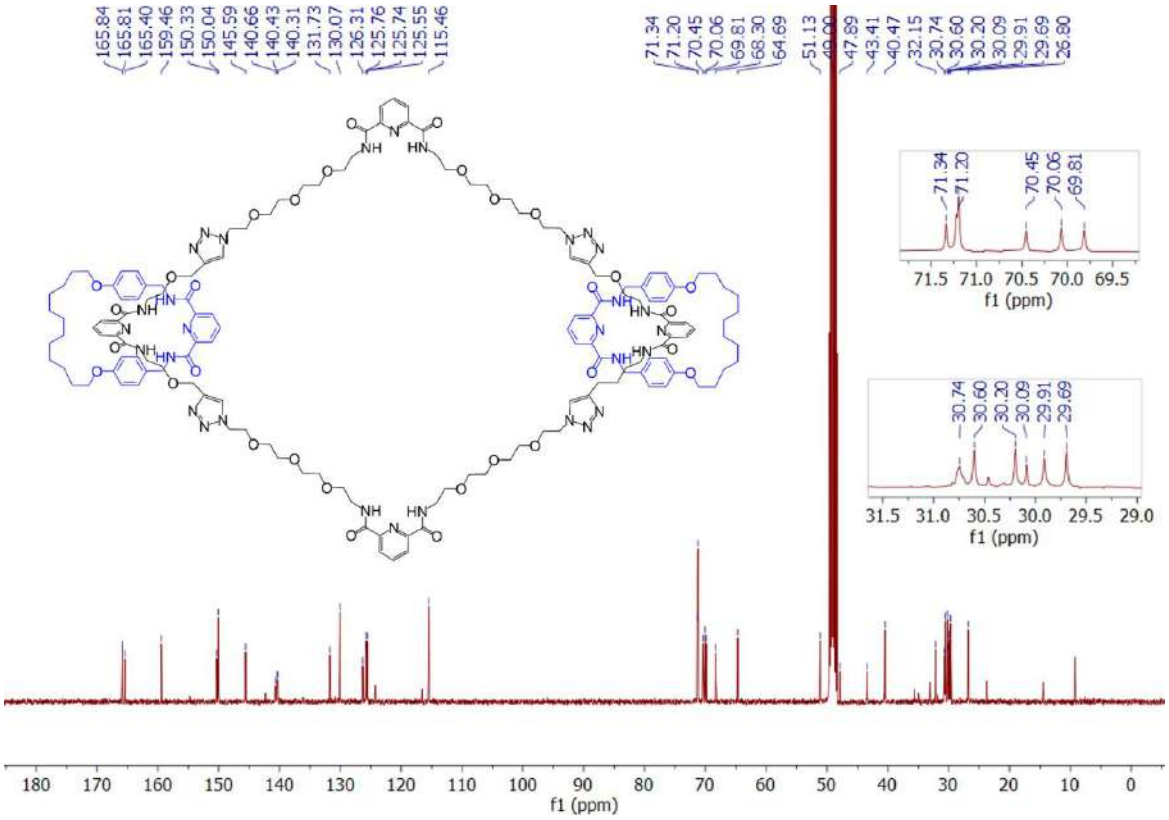

Figure 2.49. ^{13}C-NMR spectra of linear [3]catenane in MeOH-D_4 (100 MHz).

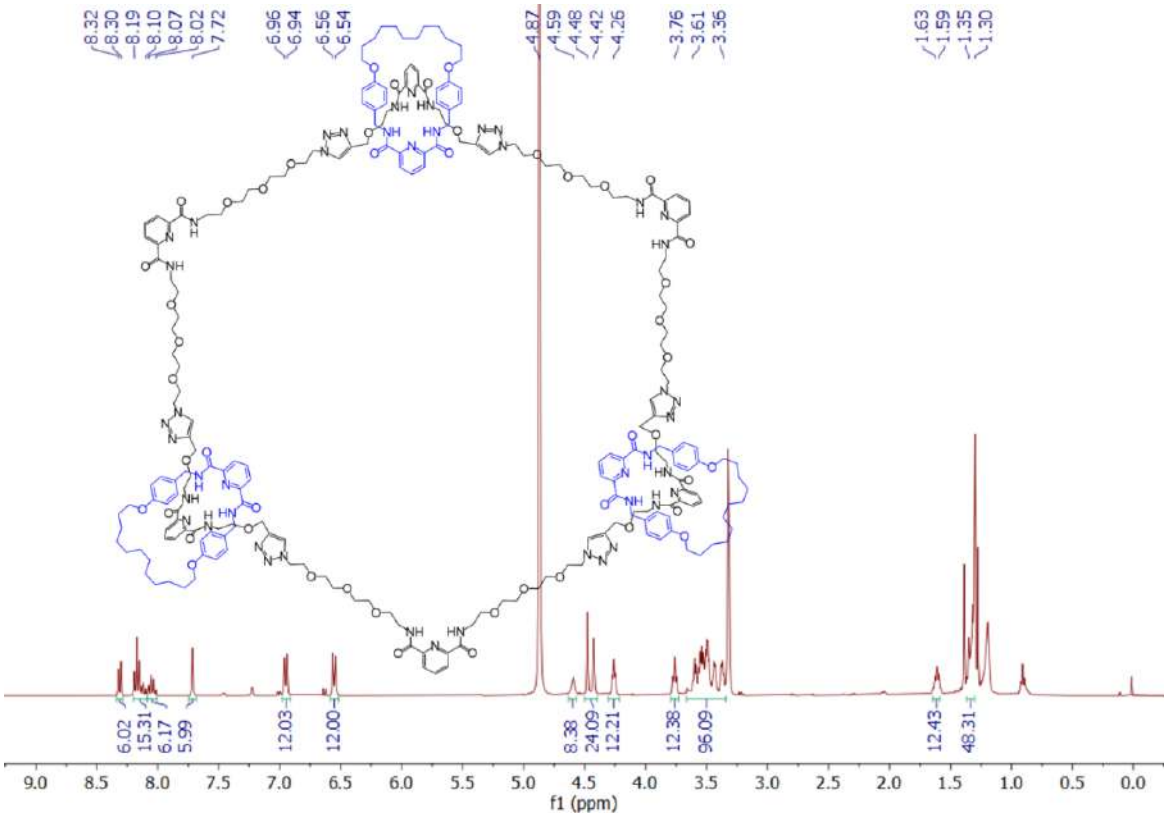

Figure 2.50. ^{1}H-NMR spectra of radial [4]catenane in MeOH-D_4 (400 MHz). NH- protons getting exchanged with CD_3OD and are not seen here.

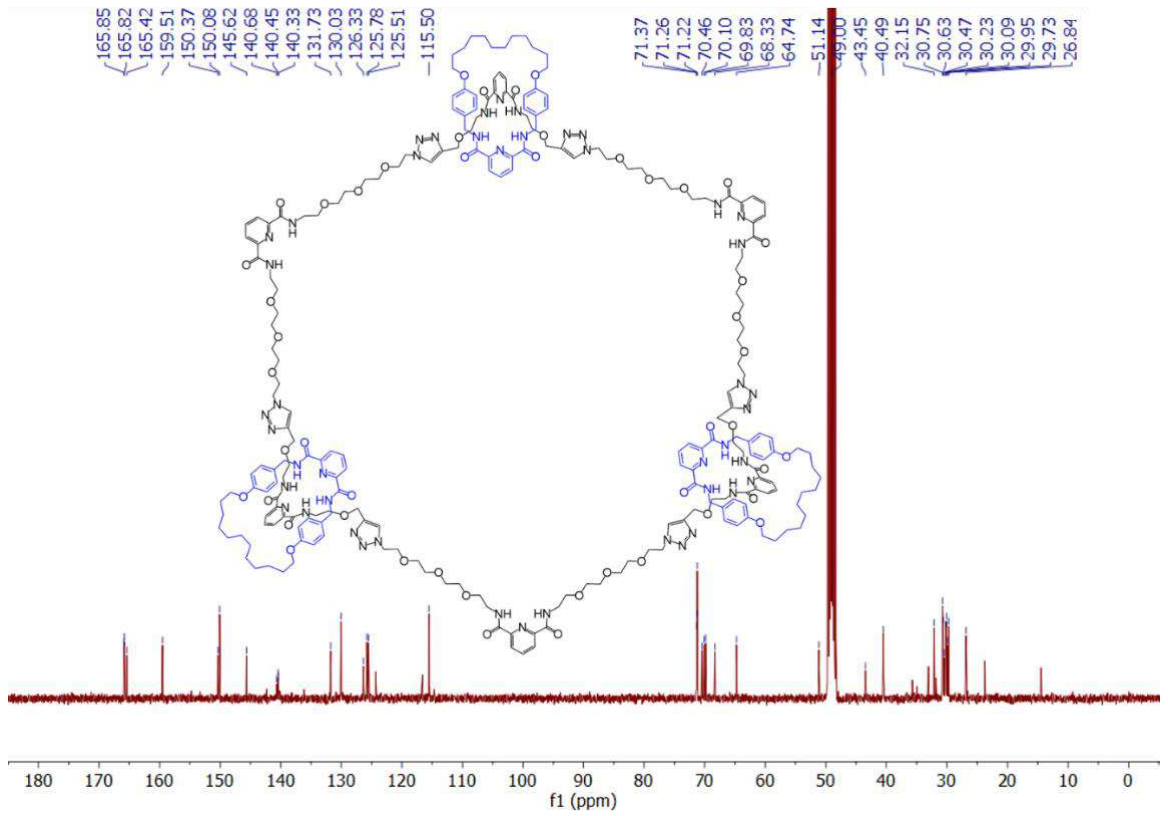

Figure 2.51. ^{13}C-NMR spectra of radial [4]catenane in MeOH-D_4 (100 MHz).

2.6.2. Mass Spectra:

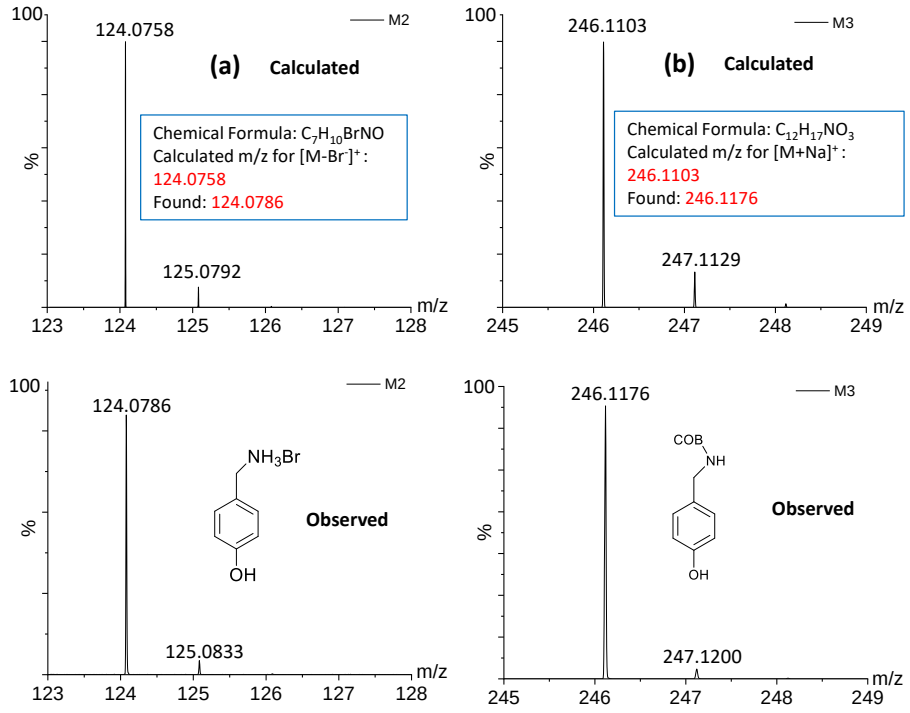

Figure 2.52. Mass spectra (ESI^+) analysis (a) for M2 (b) for M3; bottom: experimentally observed, top: theoretically calculated.

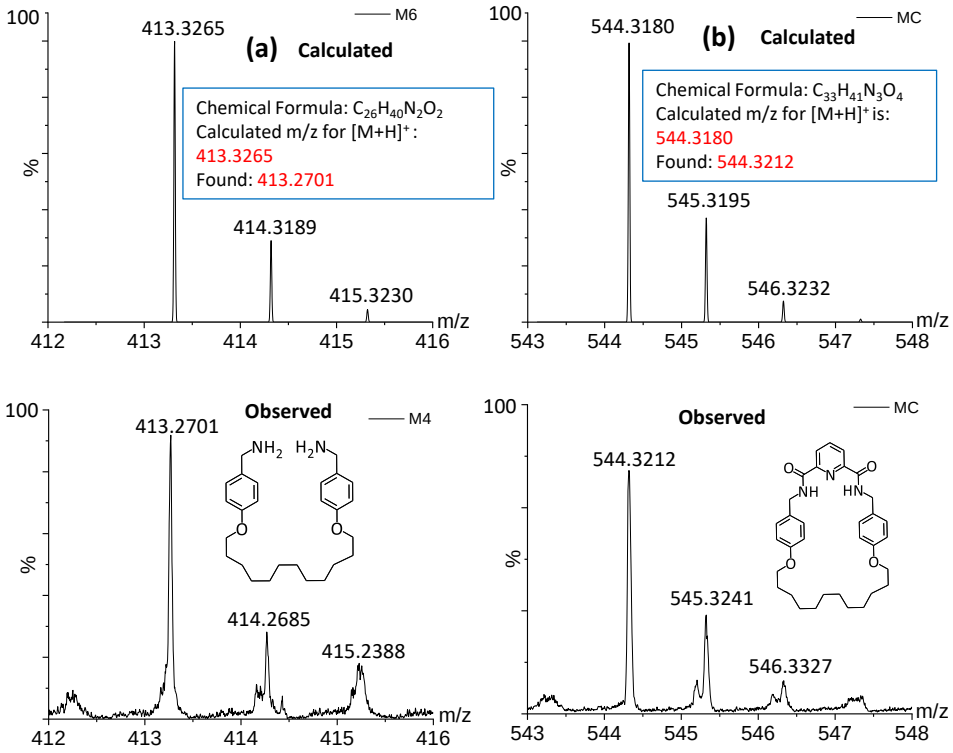

Figure 2.53. Mass spectra (ESI^+) analysis (a) for M5 (b) for MC; bottom: experimentally observed, top: theoretically calculated.

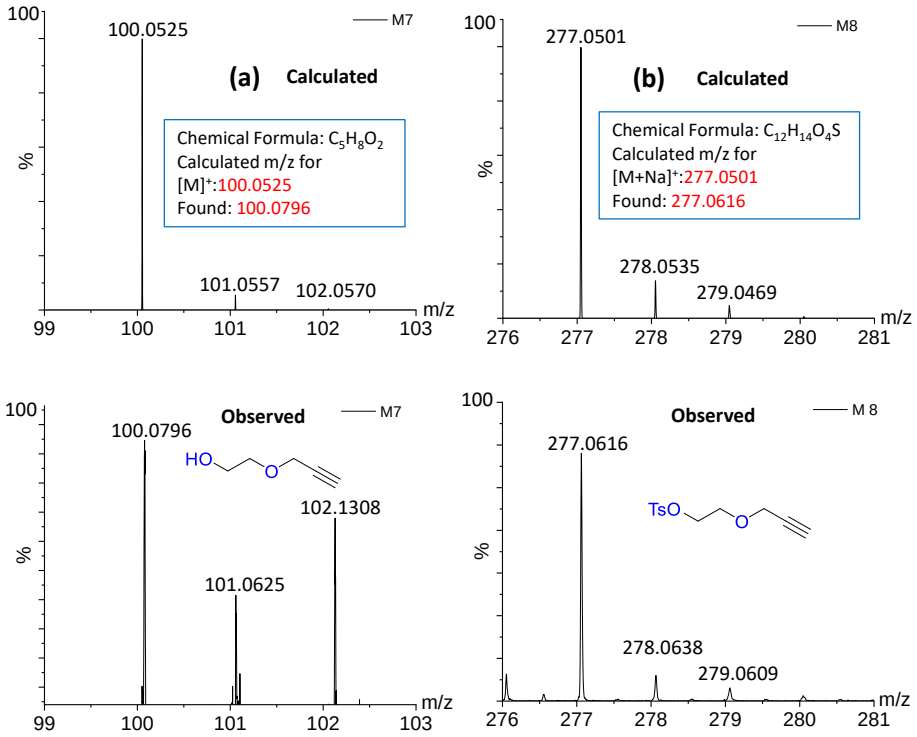

Figure 2.54. Mass spectra (ESI^+) analysis (a) for M7 (b) for M8; bottom: experimentally observed, top: theoretically calculated.

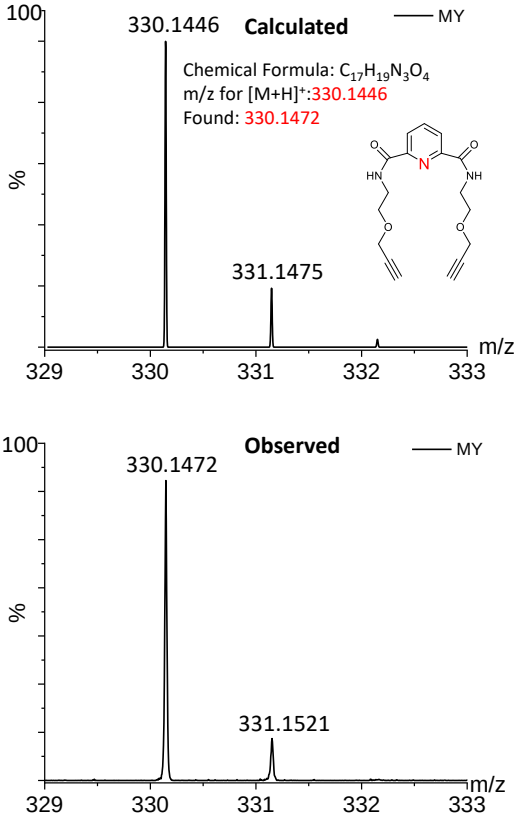

Figure 2.55. Mass spectra (ESI^+) analysis for MY; bottom: experimentally observed, top: theoretically calculated.

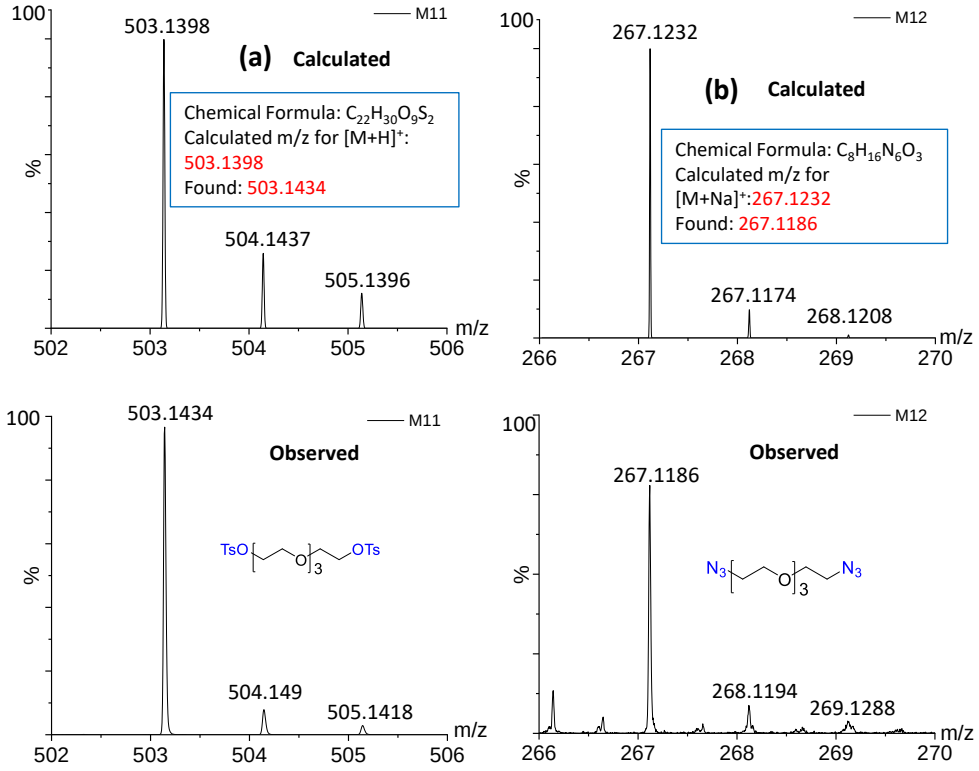

Figure 2.56. Mass spectra (ESI$^+$) analysis (a) for M11 (b) for M12; bottom: experimentally observed, top: theoretically calculated.

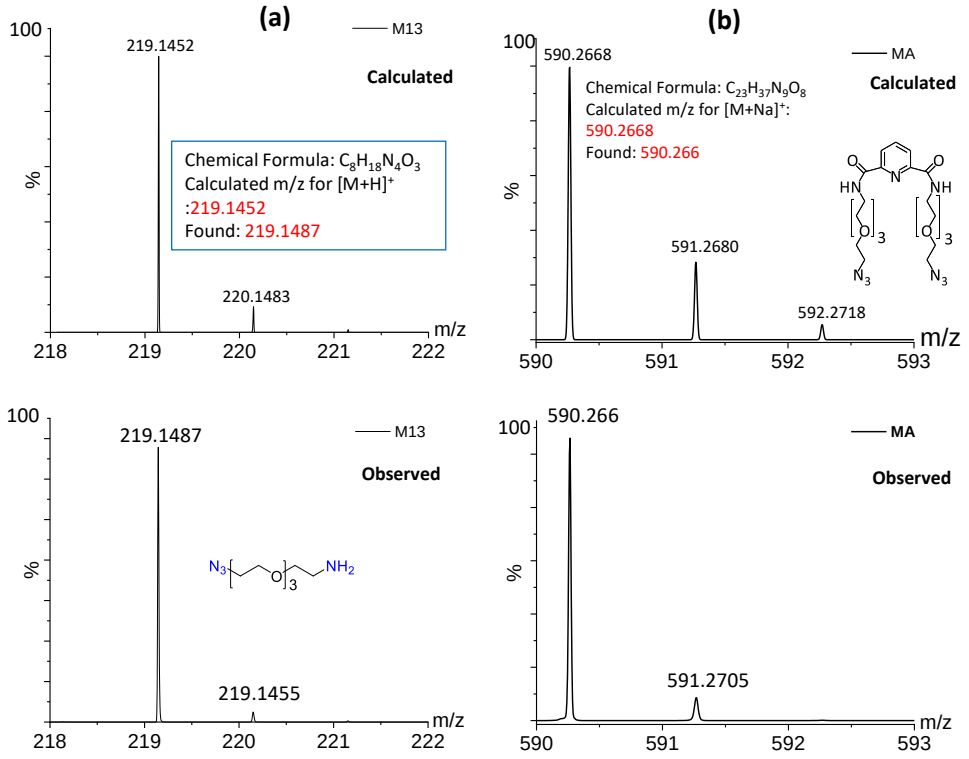

Figure 2.57. Mass spectra (ESI$^+$) analysis (a) for M13 (b) for MA; bottom: experimentally observed, top: theoretically calculated.

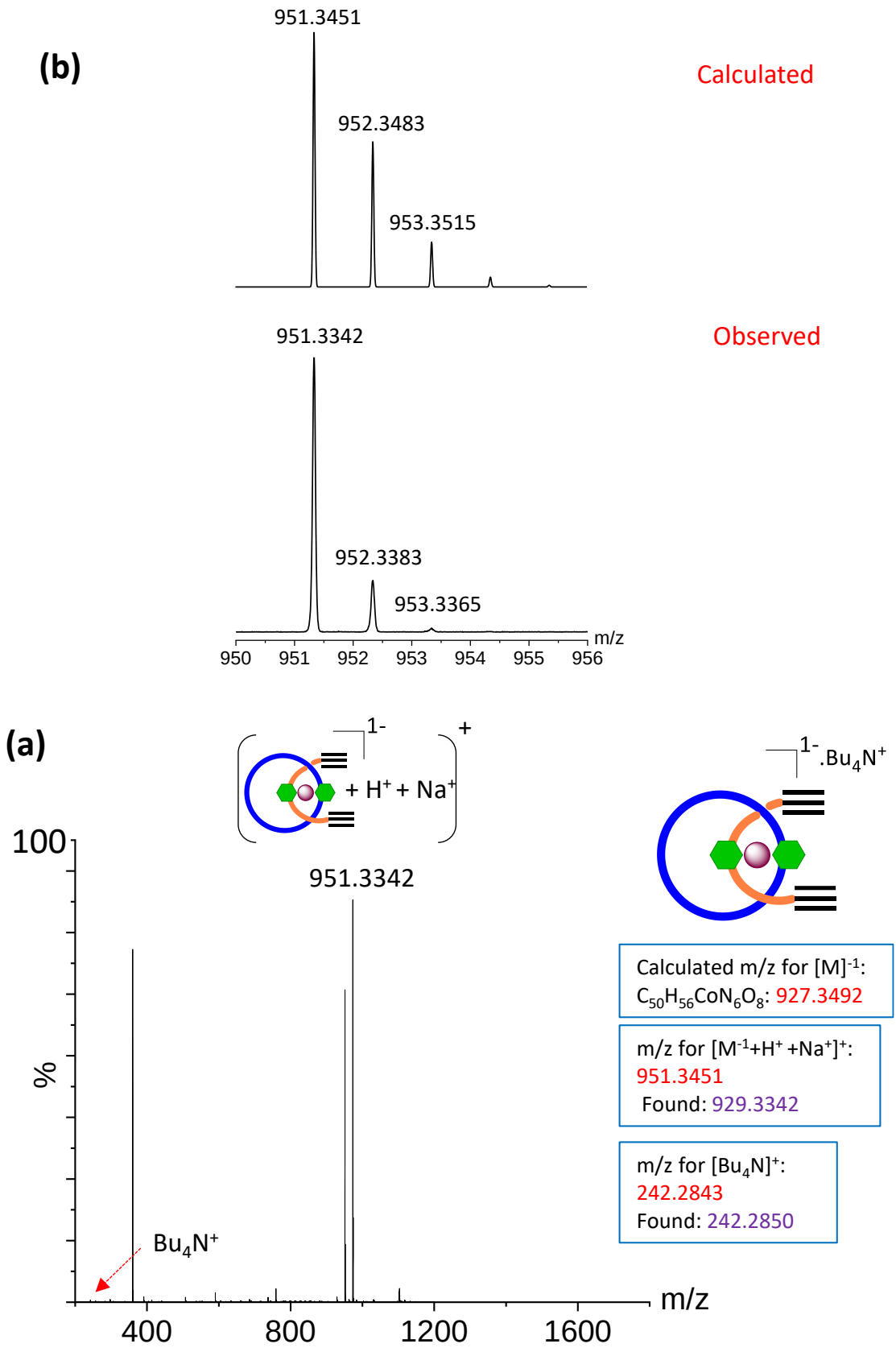

Figure 2.58. Mass spectra (ESI^+) analysis for synthesized [2]PR-Co (a) full spectra (b) comparison between calculated and experimentally observed isotopic distribution peaks.

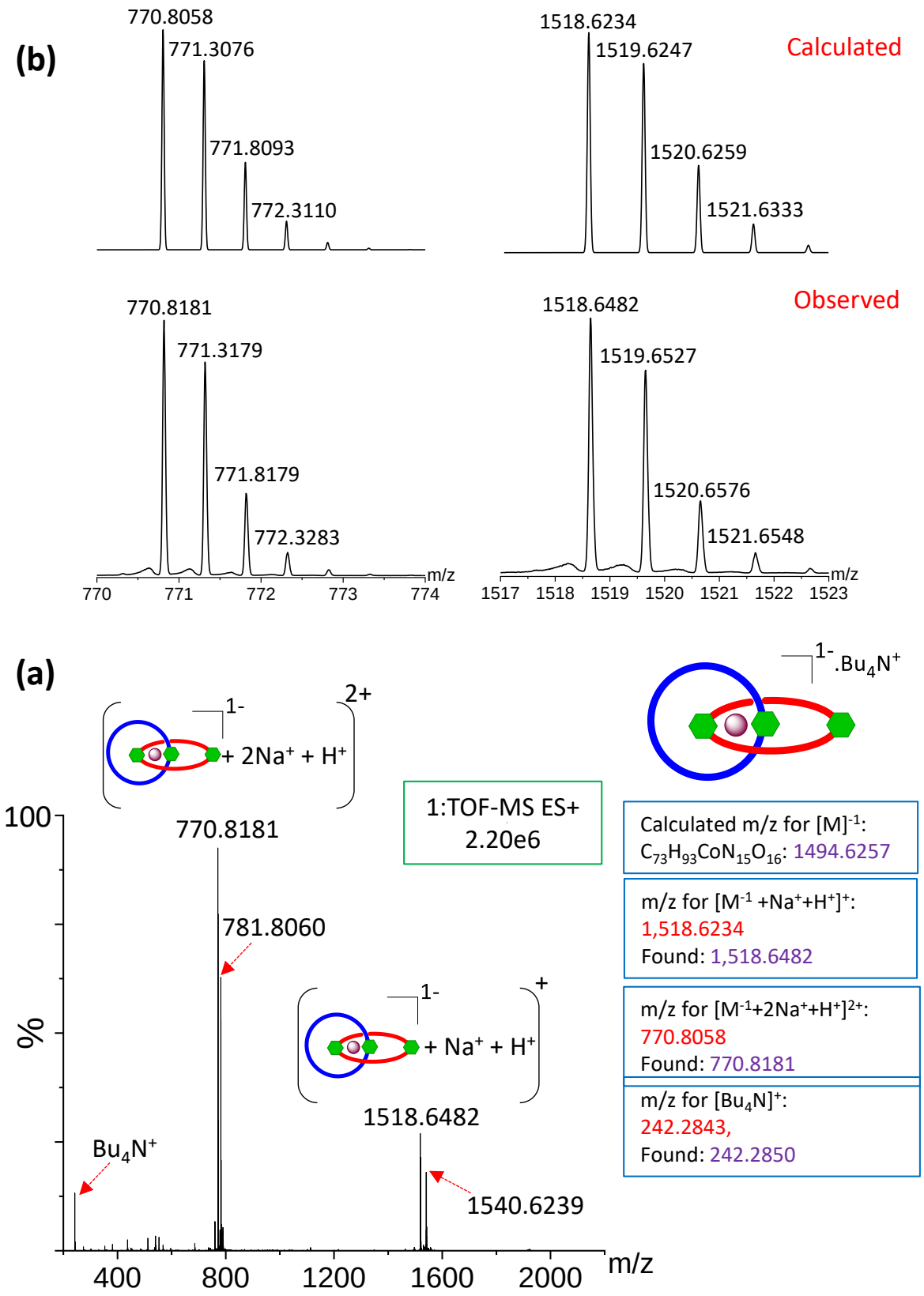

Figure 2.59. Mass spectra (ESI^+) analysis for synthesized [2]Co (a) full spectra (b) comparison between calculated and experimentally observed isotopic distribution peaks.

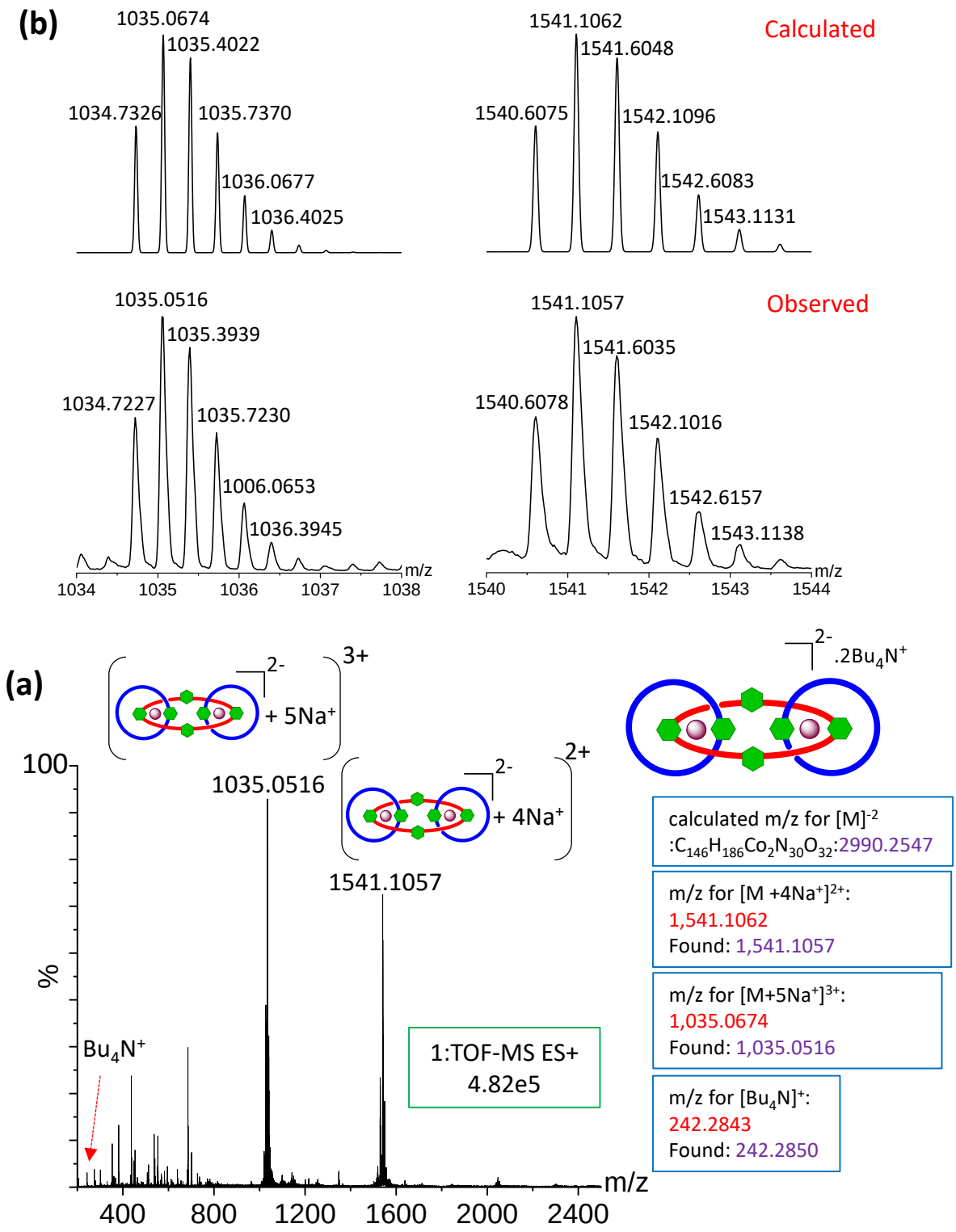

Figure 2.60. Mass spectra (ESI^+) analysis for synthesized L[3]Co (a) full spectra (b) comparison between calculated and experimentally observed isotopic distribution peaks.

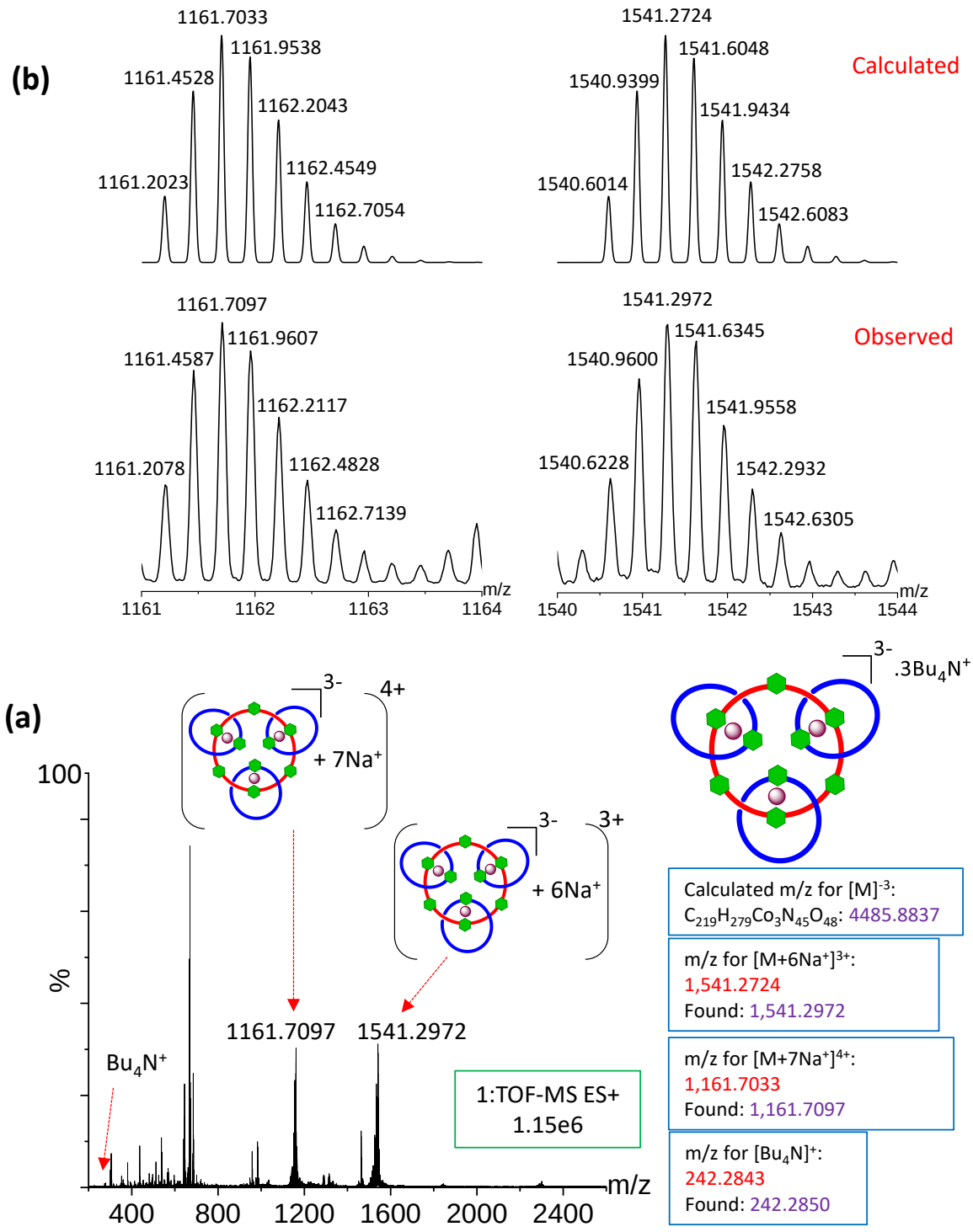

Figure 2.61. Mass spectra (ESI^+) analysis for synthesized R[4]Co (a) full spectra (b) comparison between calculated and experimentally observed isotopic distribution peaks.

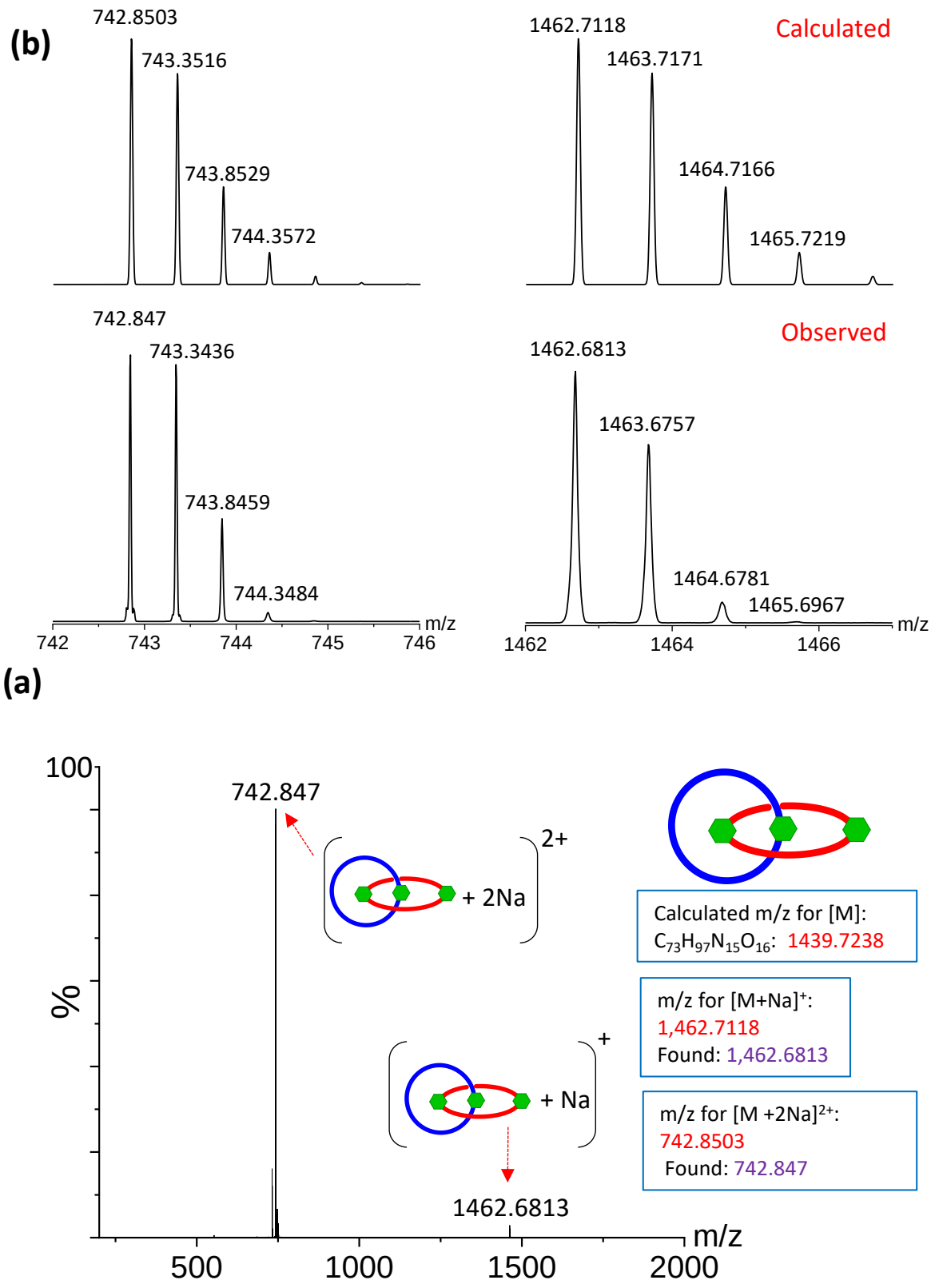

Figure 2.62. Mass spectra (ESI^+) analysis for synthesized [2]catenane (a) full spectra (b) comparison between calculated and experimentally observed isotopic distribution peaks.

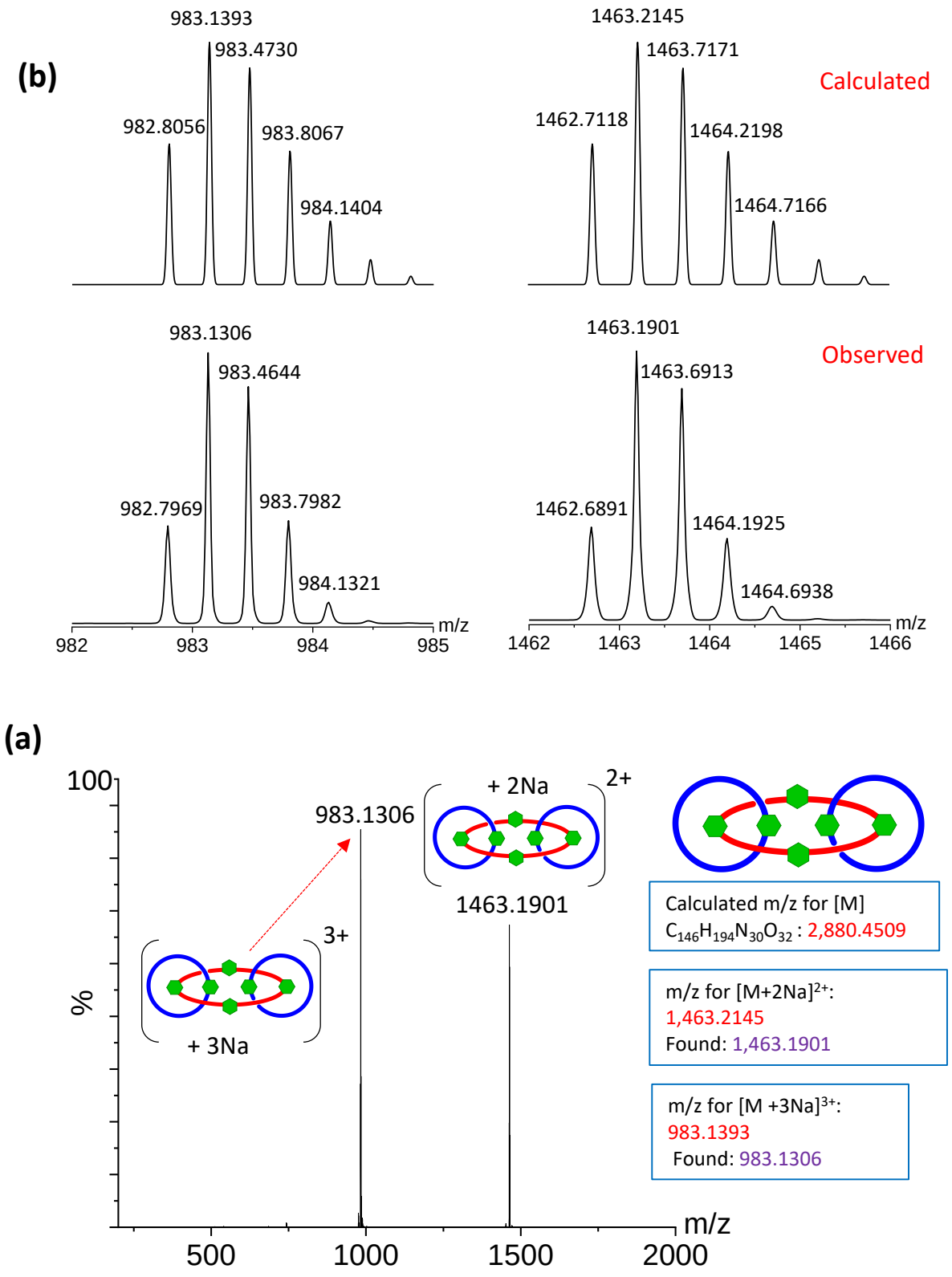

Figure 2.63. Mass spectra (ESI$^+$) analysis for synthesized L[3]catenane (a) full spectra (b) comparison between calculated and experimentally observed isotopic distribution peaks.

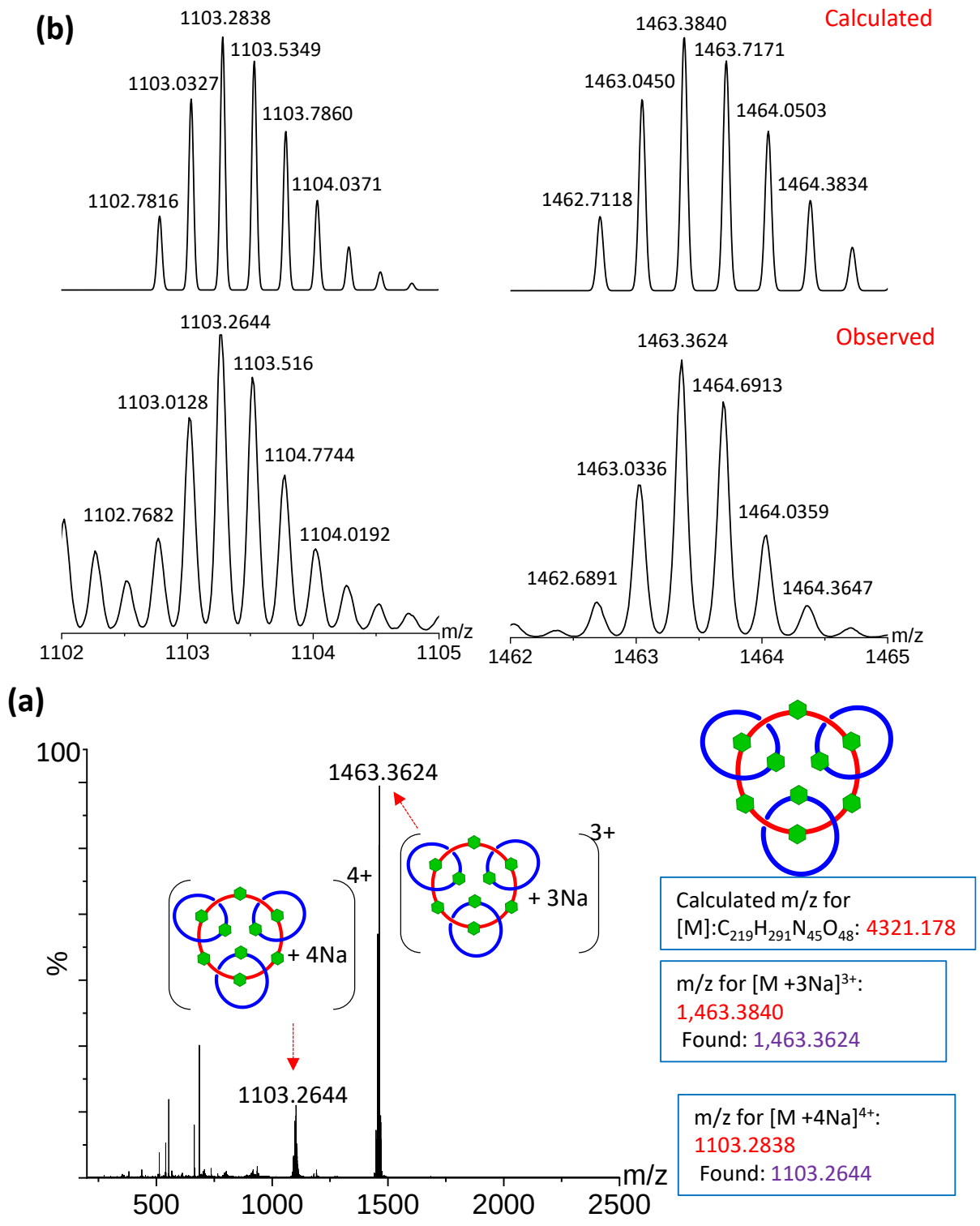

Figure 2.64. Mass spectra (ESI^+) analysis for synthesized R[4]catenane (a) full spectra (b) comparison between calculated and experimentally observed isotopic distribution peaks.

2.7. Reference:

1. a) K. Senthilkumar, M. Kondratowicz, T. Lis, P. J. Chmielewski, J. Cybinska, J. L. Zafra, J. Casado, T. Vives, J. Crassous, L. Favereau, M. Stepien, *J. Am. Chem. Soc.* **2019**, *141*, 7421–7427; b) A. Bu, Y. Zhao, H. Xiao, C. H. Tung, L. Z. Wu, H. Cong, *Angew. Chem. Int. Ed.* **2022**, *61*, e202209449.
2. a) M. G. L. v d Heuvel, C. Dekker, *Science* **2007**, *317*, 333–336; b) Z. Qu, J. Fang, Y. X. Wang, Y. Sun, Y. Liu, W. H. Wu, W. B. Zhang, *Nat. Commun.* **2023**, *14*, 3480; c) G. Li, L. Wang, L. Wu, Z. Guo, J. Zhao, Y. Liu, R. Bai, X. Yan, *J. Am. Chem. Soc.* **2020**, *142*, 14343–14349.
3. D. A. Leigh, J. K. Y. Wong, F. o Dehez, F. Zerbetto, *Nature* **2003**, *424*, 174–179
4. Binks, C. Tian, S. D. P. Fielden, I. J. Vitorica-Yrezabal, D. A. Leigh, *J. Am. Chem. Soc.* **2022**, *144*, 15838–15844.
5. H. Min Tay, T. G. Johnson, A. Docker, M. J. Langton, P. D. Beer, *Angew. Chem. Int. Ed.* **2023**, *62*, e202312745.
6. L. Fang, C. Wang, A. C. Fahrenbach, A. Trabolsi, Y. Y. Botros, J. F. Stoddart, *Angew. Chem. Int. Ed.* **2011**, *50*, 1805–1809.
7. a) R. Mitra, H. Zhu, S. Grimme, J. Niemeyer, *Angew. Chem. Int. Ed.* **2017**, *56*, 11456–11459; b) L. Zhu, J. Li, J. Yang, H. Y. Au-Yeung, *Chem. Sci.* **2020**, *11*, 13008–13014.
8. Y. Jiao, L. Dordevic, H. Mao, R. M. Young, T. Jaynes, H. Chen, Y. Qiu, K. Cai, L. Zhang, X. Y. Chen, Y. Feng, M. R. Wasielewski, S. I. Stupp, J. F. Stoddart, *J. Am. Chem. Soc.* **2021**, *143*, 8000–8010.
9. X. Mo, Y. Deng, S. K. Lai, X. Gao, H. L. Yu, K. H. Low, Z. Guo, H. L. Wu, H. Y. Au-Yeung, E. C. M. Tse, *J. Am. Chem. Soc.* **2023**, *145*, 6087–6099.
10. A. Bessaguet, Q. Blancart-Remaury, P. Poinot, I. Opalinski, S. Papot, *Angew. Chem. Int. Ed.* **2023**, *62*, e202216787.

11. Xie, C. Y. Wang, N. Chen, Z. Cao, G. Wu, B. Yin, Y. Li, *Angew. Chem. Int. Ed.* **2023**, *62*, e202309605.
12. M. Steudel, E. Ubasart, L. Leanza, M. Pujals, T. Parella, G. M. Pavan, X. Ribas, M. von Delius, *Angew. Chem. Int. Ed.* **2023**, *62*, e202309393.
13. a) Y. Wang, J. Gong, X. Wang, W. J. Li, X. Q. Wang, X. He, W. Wang, H. B. Yang, Angew. Chem. Int. Ed. 2022, 61, e202210542; b) N. Pairault, F. Rizzi, D. Lozano, E. M. G. Jamieson, G. J. Tizzard, S. M. Goldup, *Nat. Chem.* **2023**, *15*, 781–786.
14. N. Hoyas Perez, J. E. M. Lewis, *Org. Biomol. Chem.* **2020**, *18*, 6757–6780.
15. a) H. Y. Au-Yeung, C. C. Yee, A. W. Hung Ng, K. Hu, *Inorg. Chem.* **2018**, 57, 3475–3485; b) J. E. Beves, B. A. Blight, C. J. Campbell, D. A. Leigh, R. T. McBurney, Angew. Chem. Int. Ed. **2011**, *50*, 9260–9327.
16. Wu, P. M. Rauscher, X. Lang, R. J. Wojtecki, J. J. d Pablo, M. J. A. Hore, S. J. Rowan, *Science* **2017**, *358*, 1434–1439.
17. J. Liu, M. Wu, L. Wu, Y. Liang, Z. B. Tang, L. Jiang, L. Bian, K. Liang, X. Zheng, Z. Liu, *Angew. Chem. Int. Ed.* **2023**, *62*, e202314481.
18. E. Dehkordi, V. Luxami, G. D. Pantos, *J. Org. Chem.* **2018**, *83*, 11654–11660.
19. a) M. Gauthier, K. Fournel-Marotte, C. Clavel, P. Waeles, P. Laurent, F. Coutrot, *Angew. Chem. Int. Ed.* **2023**, *62*, e202310643; b) Z. Meng, Y. Han, L. N. Wang, J. F. Xiang, S. G. He, C. F. Chen, *J. Am. Chem. Soc.* 2015, 137, 9739–9745; c) L. Steemers, M. J. Wanner, M. Lutz, H. Hiemstra, J. H. van Maarseveen, Nat. Commun. 2017, 8, 15392; d) K. D. Hanni, D. A. Leigh, Chem. Soc. Rev. 2010, 39, 1240–1251; e) S. Prusty, M. B. Podh, C. S. Purohit, ChemistrySelect 2018, 3, 9690–9693.
20. a) K. Wang, C. C. Yee, H. Y. Au-Yeung, *Chem. Sci.* **2016**, *7*, 2787–2792; b) S. M. Goldup, D. A. Leigh, T. Long, P. R. McGonigal, M. D. Symes, J. Wu, *J. Am. Chem. Soc.* **2009**, *131*, 15924–15929; c) A. W. H. Ng, Y. H. Leung, H. Y. Au-Yeung, *Org.*

Chem. Front. **2021**, *8*, 2182–2189; d) A. W. H. Ng, S. K. Lai, C. C. Yee, H. Y. Au-Yeung, *Angew. Chem. Int. Ed.* **2022**, *61*, e202110200; e) J. D. Megiatto Jr., D. I. Schuster, *Chem. Eur. J.* **2009**, *15*, 5444–5448.

21. D. A. Leigh, F. Schaufelberger, L. Pirvu, J. H. Stenlid, D. P. August, J. Segard, *Nature* **2020**, *584*, 562–568.
22. D. A. Leigh, L. Pirvu, F. Schaufelberger, *J. Am. Chem. Soc.* **2019**, *141*, 6054–6059
23. Bitsch, C. O. Dietrich-Buchecker, A.-K. Khémiss, J.-P. Sauvage, A. V. Dorsselaer, *J. Am. Chem. Soc.* **1991**, *113*, 4023–4025.
24. T. Higashi, K. Morita, X. Song, J. Zhu, A. Tamura, N. Yui, K. Motoyama, H. Arima, J. Li, *Commun. Chem.* **2019**, *2*, 78, https://doi.org/10.1038/s42004-019-0180-x.
25. M. Okada, A. Harada, *Macromolecules* **2003**, *36*, 9701–9703.
26. T. A. Barendt, L. Ferreira, I. Marques, V. Felix, P. D. Beer, *J. Am. Chem. Soc.* **2017**, *139*, 9026–9037.
27. a) D. Whang, K.-M. Park, J. Heo, P. Ashton, K. Kim, *J. Am. Chem. Soc.* **1998**, *120*, 4899–4900; b) S. Li, J. Huang, F. Zhou, T. R. Cook, X. Yan, Y. Ye, B. Zhu, B. Zheng, P. J. Stang, *J. Am. Chem. Soc.* **2014**, *136*, 5908–5911.
28. a) M. T. Nguyen, D. P. Ferris, C. Pezzato, Y. Wang, J. F. Stoddart, Chem **2018**, *4*, 2329–2344; b) C. F. Chang, C. J. Chuang, C. C. Lai, Y. H. Liu, S. M. Peng, S. H. Chiu, *Angew. Chem. Int. Ed.* **2012**, *51*, 10094–10098; c) A. W. H. Ng, C. C. Yee, H. Y. Au-Yeung, *Angew. Chem. Int. Ed.* **2019**, *58*, 17375–17382.
29. D. A. Leigh, P. J. Lusby, R. T. McBurney, A. Morelli, A. M. Z. Slawin, A. R. Thomson, D. B. Walker, *J. Am. Chem. Soc.* **2009**, *131*, 3762–3771.
30. Zhang, G. Gil-Ramirez, A. Markevicius, C. Browne, I. J. Vitorica-Yrezabal, D. A. Leigh, *J. Am. Chem. Soc.* **2015**, *137*, 10437–10442.

31. F. Ayme, J. E. Beves, D. A. Leigh, R. T. McBurney, K. Rissanen, D. Schultz, *Nat. Chem.* **2012**, *4*, 15–20

32. (a) S. Basu, B. Ellinger, S. Rizzo, C. Deraeve, M. Schurmann, H. Preut, H. D. Arndt, H. Waldmann, *Proc Natl Acad Sci U S A* **2011**, *108*, 6805-6810; (b) T. Prakasam, M. Lusi, M. Elhabiri, C. Platas-Iglesias, J. C. Olsen, Z. Asfari, S. Cianferani-Sanglier, F. Debaene, L. J. Charbonniere, A. Trabolsi, *Angew. Chem. Int. Ed.* **2013**, *52*, 9956-9960.

33. A.-M. L. Fuller, D. A. Leigh, P. J. Lusby, A. M. Z. Slawin, D. B. Walker, *J. Am. Chem. Soc.* **2005**, *127*, 12612-12619.

34. T. Mayer, M. E. Maier, *Eur. J. Org. Chem.* **2007**, *2007*, 4711-4720.

35. J. Cao, Y. Liu, L. Zhang, F. Du, Y. Ci, Y. Zhang, H. Xiao, X. Yao, S. Shi, L. Zhu, H. F. Kung, J. Qiao, J. Radioanal. Nucl. Chem. **2017**, *312*, 263-276.

36. D. A. Leigh, P. J. Lusby, R. T. McBurney, A. Morelli, A. M. Z. Slawin, A. R. Thomson, D. B. Walker, *J. Am. Chem. Soc.* **2009**, *131*, 3762-3771.

37. C. Shao, X. Wang, Q. Zhang, S. Luo, J. Zhao, Y. Hu, *J. Org. Chem.* **2011**, *76*, 6832-6836.

Chapter 3: Template Assisted Synthesis of Linear [5]Catenane by Post-Functionalization of Templated [2]Catenane and Using Click Reaction

3.1. Abstract:

Polymers with all mechanically interlocked rings, such as linear [n]catenanes, have great potential as functional materials due to possible higher degrees of freedom that may contribute to their flexibility but remain elusive. All the synthetic methods used to prepare such a polymer yield mixtures of products. In the absence of higher molecular weight linear [n]catenanes, emphasis on synthesizing low molecular weight oligomers is being pursued.

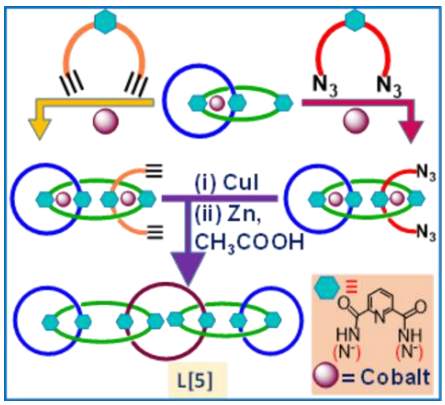

In this chapter, we have described the synthesis of a linear [5]catenane by post-functionalizing a Co(III)-templated [2]catenane having a pyridine-diamide unit free for further metal ion coordination. Two molecules were synthesized with suitable threading groups: one, two terminal azide groups, and two, with two terminal alkyne groups to form two [3]pseudorotaxane

utilizing Co(III)-coordination. These units were then joined, forming a macrocycle, using click reaction, giving the desired metalated linear [5]catenane in 40% yield. Removal of metal ions leads to linear [5]catenane. In addition, the formation of linear [3] and [2]catenane are also observed. All synthesized structures have been isolated by column chromatographic technique and characterized by ^{1}H-NMR, ^{13}C-NMR, and mass spectroscopy.

3.2. Introduction:

Mechanically interlocked molecules (MIMs), such as catenanes, are emerging as new materials as they show applications such as in memory devices, [1] ion transport, [2] molecular switch, [3] molecular motor, [4] catalysis, [5] including their use as catalyst in click reaction, [6] guest molecule encapsulation, [7] and sensors, [8] to name a few. In addition, the mechanical bond in catenane imparts stereochemistry [9] and improves mechanical properties. [10] Although various methods exist for simple catenane synthesis, [11] higher-ordered catenanes, particularly linear polycatenane, pose an intriguing synthetic challenge to chemists. One of the challenges is that the ring-closing reactions utilized to make the mechanical bond generate non-interlocked by-products, thereby reducing yield. [12] A few other challenges are isolation of the intermediate catenated structures in pure form and the formation of by-products such as topological isomeric products. Nevertheless, formation of multiple mechanical bonds is achieved due to newer synthetic strategies. [13] Thus, construction of previously unknown structures was possible, [14] and novel functions of these materials due to entanglement were discovered. [15]

Synthesis of such topological architectures is achieved by designing and exploring novel templating centers,[16] utilizing different tectons,[17] implementing novel synthetic strategy,[18] and utilizing different reactions for the ring-closing step.[16a,18b,19] Yet, only a few higher-ordered ($n > 4$) catenane have been synthesized. [5]catenane, named olympiadane, was the first high-ordered catenane synthesized by Stoddart's group utilizing strong π-π interaction between

electron-deficient viologens and electron-rich aromatic rings for threading, followed by covalent capture to close the ring.[20] Iwamoto's group synthesized linear [5]catenane using hydrogen bonding between ether and ammonium ion for threading and Grubb's method for ring-closing.[21] Recently, Jonathan and co-workers used zip-tie strategy along with orthogonal templating, utilizing phenanthroline and terpyridine groups for one-pot synthesis of linear [4], [5], [6], [7] and [8]catenane.[13c,22] The branched [8]catenane geometry is another significant topology.[23] The highest linear catenane achieved so far is a 26-mer by Rowan and co-workers.[24] Although most of these syntheses rely on a metal template followed by ring-closing, the choice of templating unit is limited to phenanthroline, terpyridine, and bipyridine. Only a few reports utilized non-ionic pyridine-diamide,[16a,25] anionic pyridine-diamide,[17a,26] di-benzimidazole pyridine[24] and thiazolothiazole pyridine[15,16b] unit as coordination site.

Pyridine-diamide based anionic template with suitable metal ion provides a non-labile site ideal for synthesizing catenane that can be used further for higher-ordered catenanes, but only a few reports exist.[25b] Recently, our group reported the synthesis of [2], linear [3], and radial [4]catenane by using a pyridine-diamide based anionic templation center and utilizing click reaction as the ring closing step.[17a] The reported Co(III)-templated [2]catenane (**[2]Co-C** in **Scheme 3.1**) has a free pyridine-diamide moiety for further functionalization.[26] In this chapter, we report the synthesis, isolation, and characterization of a linear [5]catenane, utilizing the metalated [2]catenane as the starting material.

3.3. Results and Discussion:

The overall synthesis is depicted in **Scheme 3.1**. The metalated [2]catenane (**[2]Co-C**) is synthesized as reported previously.[17a] As can be seen from the design, two types of macrocycles are used for synthesizing the targeted liner [5]catenane. The terminal ones are already in the starting material (**[2]Co-C**).

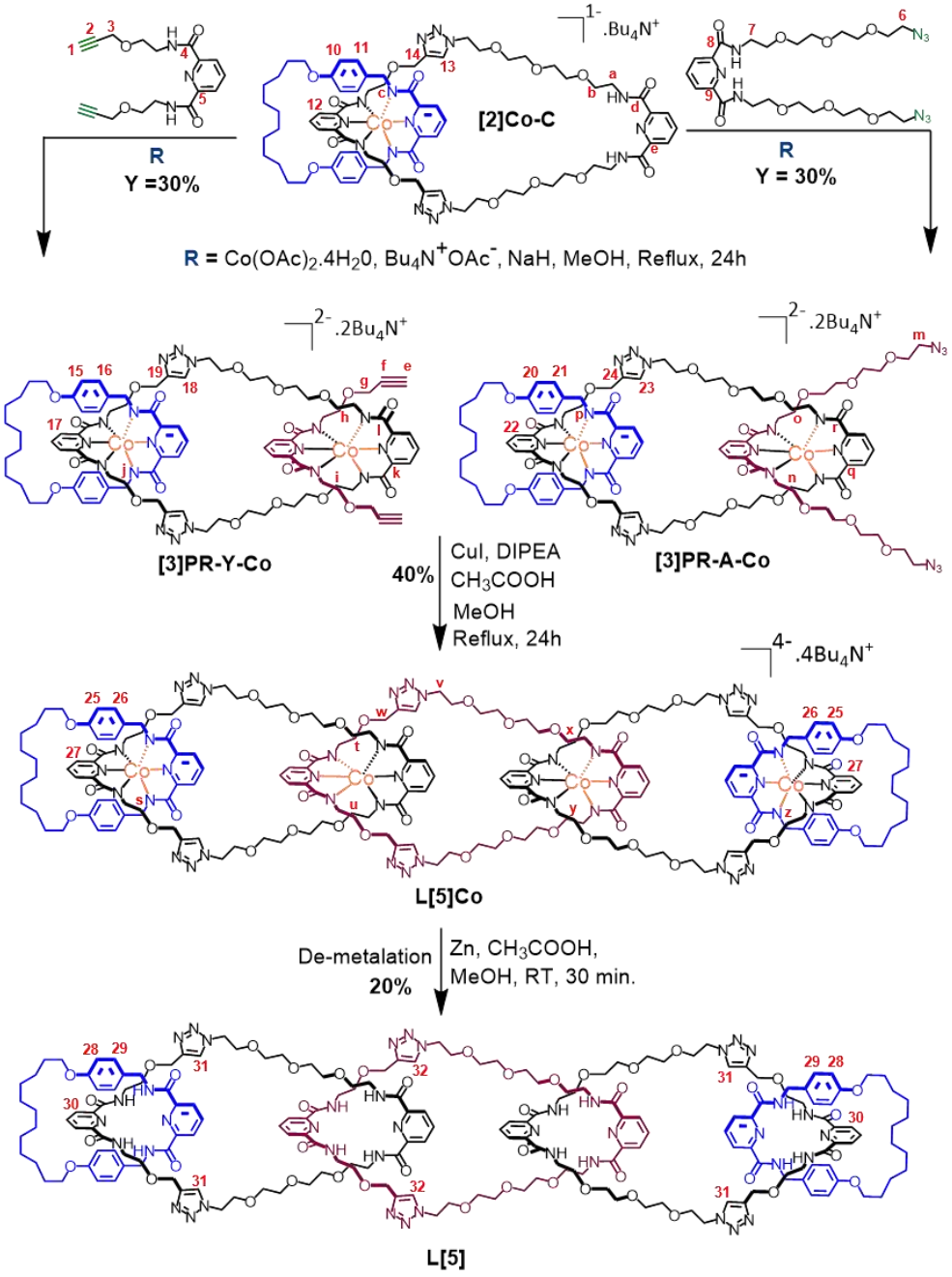

Scheme 3.1. Reaction scheme for the synthesis of linear [5]catenane from Co(III)-templated [2]catenane precursor **[2]Co-C**, di-alkyne ligand **LY**, and di-azide ligand **LA**. It is to be noted that **[3]PR-Y-Co** and **L[5]Co** has been isolated as mixture with their corresponding non-entangled isomers namely **[3]PR-Y-Co**-Isomer and **L[5]Co**-Isomer. But for simplification only the entangled isomer is shown.

But the central macrocycles are achieved by design and synthesis of one long-chain di-azide [3]pseudorotaxane and another short-chain di-alkyne [3]pseudorotaxane followed by ring-

closing click reaction to form linear [5]pre-catenate complex. This complex is then demetallated to get the linear [5]catenane.

3.3.1. Synthesis of di-alkyne terminus [3]pseudorotaxane, ([3]PR-Y-Co):

For this synthesis, reaction was performed by refluxing 1 equivalent each of **[2]Co-C**, $Co(OAc)_2.4H_2O$, and $Bu_4N^+OAc^-$ in MeOH for 2.5 h under strict anaerobic conditions to give a dark green color solution. After this time, a solution of ligand **LY** (as in Scheme 3.1) in MeOH was added, and the reflux continued for 2.5 hours under the same condition. Then, a methanolic solution of NaH (producing sodium methoxide) was added, and the reaction mixture was allowed to reflux further for 24 hours in open air that oxidized Co(II) to Co(III) oxidation state. It may be noted that the sequential addition of threading partner **[2]Co-C** and **LY** is essential for higher yield of the coupling product, pseudorotaxane **[3]PR-Y-Co** and decrease in the formation of metalated dimmer of **LY**. In a vertical tlc experiment (with EtOAc: MeOH, 65 : 35 v/v eluent), three major green-colored spots were observed with distinctive R_f values. The reaction mixture was subjected to column chromatographic separation. All these spots were isolated and washed with hexane and EtOAc to get green-colored pure products each in 30% yield. Characterizing the second isolated product (R_f = 0.4) by ^{1}H-NMR, ^{13}C-NMR, and mass spectroscopy confirms as pseudorotaxane **[3]PR-Y-Co** along with its non-entangled isomer namely **[3]PR-Y-Co**-Isomer (**Scheme 3.2**). The third isolated spot (R_f = 0.1) has a ^{1}H-NMR, ^{13}C-NMR spectral pattern similar to that of **[2]Co-C** but different mass spectra. However, the demetallation experiment (explained later) confirms the third isolated product is a dimer of **[2]Co-C** (namely **[2]Co-D**). Moreover, the first green colored compound was characterized as self-complexed product between the threading ligand **LY**.

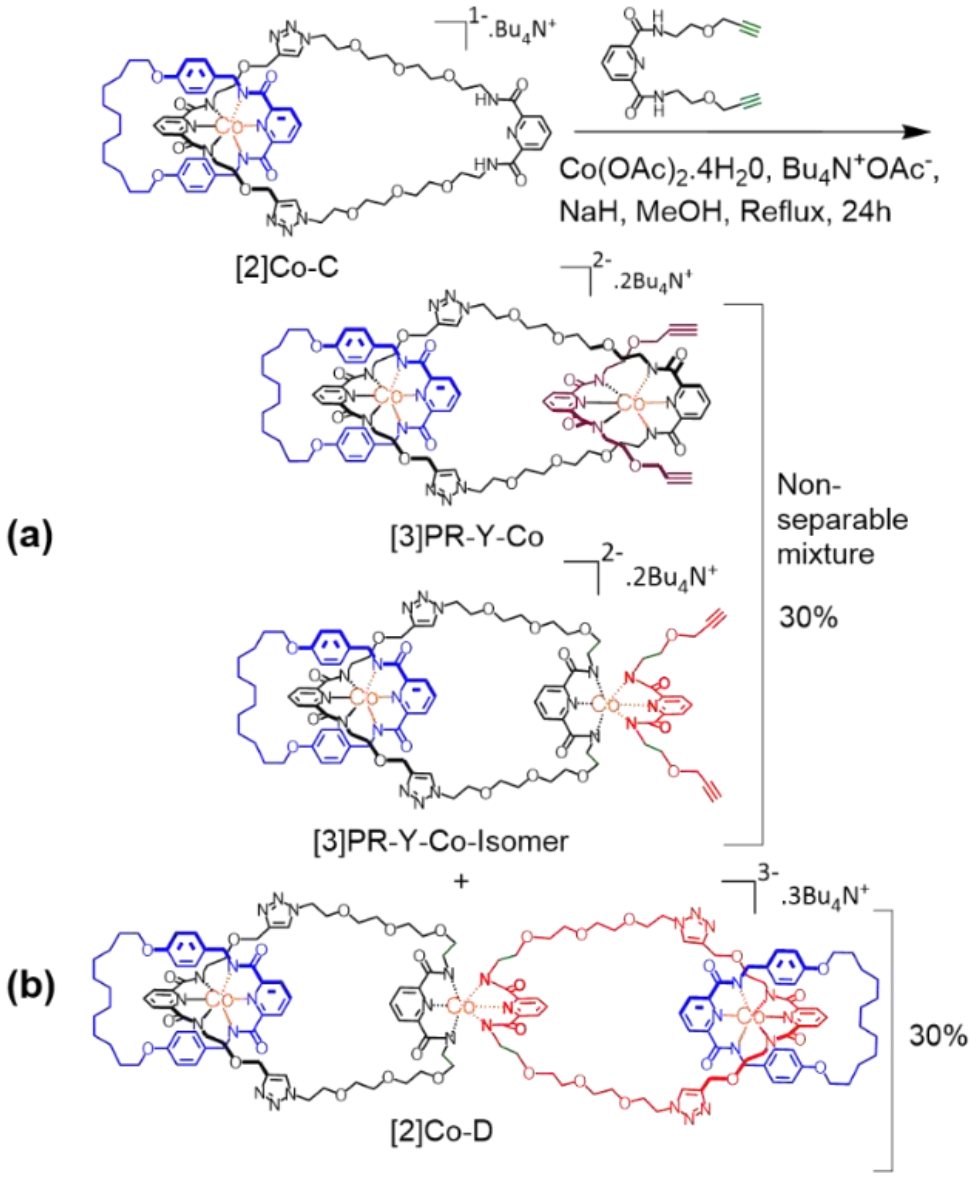

Scheme 3.2. Reaction scheme showing non-entangled isomers being formed in the di-alkyne [3]pseudorotaxane synthesis (a) entangled and non-entangled isomers of **[3]PR-Y-Co** (b) metalated [2]catenane dimer **L[2]Co**-D.

Proton NMR spectra of **[3]PR-Y-Co** possess two terminal alkyne protons peak at 2.7 ppm (peak **e**, Figure **3.1d**) and two methylene protons next to triple bond (–O–C**H**$_2$–CH≡CH, peak **g**, Figure **3.1d**) of di-alkyne ligand **LY**. Also, benzene protons of metalated [2]catenane (**[2]Co-C**) are at 6.15 and 6.33 ppm (peaks **15** and **16**, respectively). Thus suggesting **[3]PR-Y-Co** comprised of both metalated [2]catenane and threaded with di-alkyne ligand **LY**.

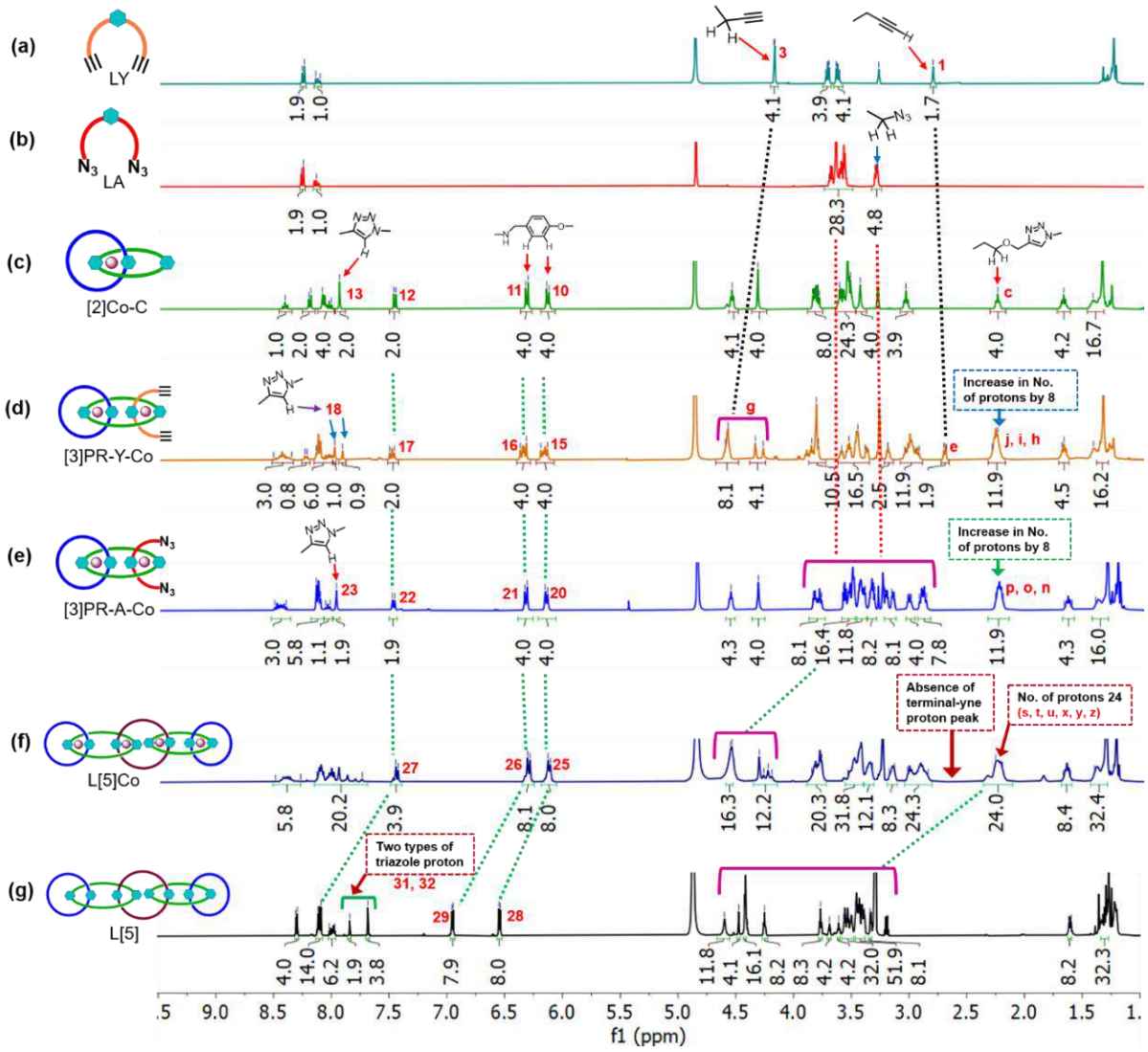

Figure 3.1. ^{1}H-NMR peak shift comparison for the synthesis of linear [5]catenane from its precursor molecule **[2]Co-C**, **LY**, **LA** (a) di-alkyne ligand **LY** (b) di-azide ligand **LA** (c) metalated [2]catenane **[2]Co-C** (d) di-alkyne terminus [3]pseudorotaxane **[3]PR-Y-Co** (e) di-azide terminus [3]pseudorotaxane **[3]PR-A-Co** (f) templated linear pre-[5]catenate complex **L[5]Co** (g) fully organic linear [5]catenane **L[5]**. All spectra were recorded in CD_3OD. Note that both **[3]PR-Y-Co** and **L[5]Co** have their corresponding isomers as a mixture, but only the entangled isomers are shown here. With CD_3OD, NH-protons are getting exchanged and are not seen here. Peak **j**, **i**, **h**, **p**, **o**, **n**, **s**, **t**, **u**, **x**, **y**, **z** has been assigned to methylene proton next to oxygen (–N–CH_2–C**H**$_2$–O–CH_2–CH≡CH) of LY subunit of metalated entangled structures. However, it is probable that the same peak might have arisen due to methylene proton next to anionic nitrogen (–N–C**H**$_2$–CH_2–O–CH_2–CH≡CH) and vice versa.

Moreover, due to complexation at the pyridine-diamide center of **[2]Co-C** with ligand **LY**, eight methylene (–CH_2–) protons (4 from each precursor) in close vicinity of the newly formed Co(III)-complex were shielded. As a result, the number of proton signals at 2.26 ppm (peak **j**, **i**, **h**, **Figure 3.1d**) has increased by eight. Similar shielding was also observed in our previous report after metalation.[17a] **[3]PR-Y-Co** could not be isolated in the pure form via column chromatography as can be observed from the proton NMR signals at 6.15, 6.33, 7.48 ppm (peak **15**, **16**, **17**, **Figure 3.1d**, and **Section 3.6.1**). Two isomeric products were possibly formed, as shown in **Scheme 3.2a**, but could not be separated. As a result, the ^{1}H-NMR shows signals of two doublets (**Section 3.6.1**) for the benzene protons (peak **15**, **16**, **Figure 3.1d**) rather than one doublet. Two different ^{1}H-NMR signals for the triazole protons at 7.91 and 7.98 ppm (peak **18**) appear rather than one, suggesting the formation of a product mixture (**Figure 3.1d**, **Scheme 3.2a**). Additional confirmation that **[3]PR-Y-Co** as an isomeric mixture came while performing demetallation of **L[5]Co** and is discussed in the later part.

Evidence for the synthesis of **[3]PR-Y-Co** also came from the ^{13}C-NMR analysis. Similar to ^{1}H-NMR, ^{13}C-NMR of **[3]PR-Y-Co** comprises signals for terminal alkyne carbons of precursor di-alkyne ligand **LY** (peak **1** and **2**, **Figure 3.2a**) at 76.06 and 80.76 ppm (peak **e** and **f** respectively **Figure 3.2d**). Also, a peak at 58.67 ppm (peak **g**) corresponds to methylene proton next to the terminal alkyne group (–O–**C**$\mathbf{H_2}$–CH≡CH) of **LY** subunit of **[3]PR-Y-Co** is present. These data suggest the presence of **LY** subunit in **[3]PR-Y-Co**. Evidence of **[2]Co-C** subunit in **[3]PR-Y-Co** came from the presence of benzene carbon peak of **[2]Co-C** (peak **10**, **11**, **Figure 3.2c**) at 115.19 and 118.53 ppm (peak **15**, **16** respectively, **Figure 3.2d**). Moreover, the carbonyl carbons (peak **4** of **LY**, peak **d** of **[2]Co-C**) and quaternary pyridine carbons (peak **5** of **LY**, peak **e** of **[2]Co-C**) got de-shielded by 4 ppm and 9 ppm, respectively when complexed to form **[3]PR-Y-Co** (peak **l** and **k** respectively).

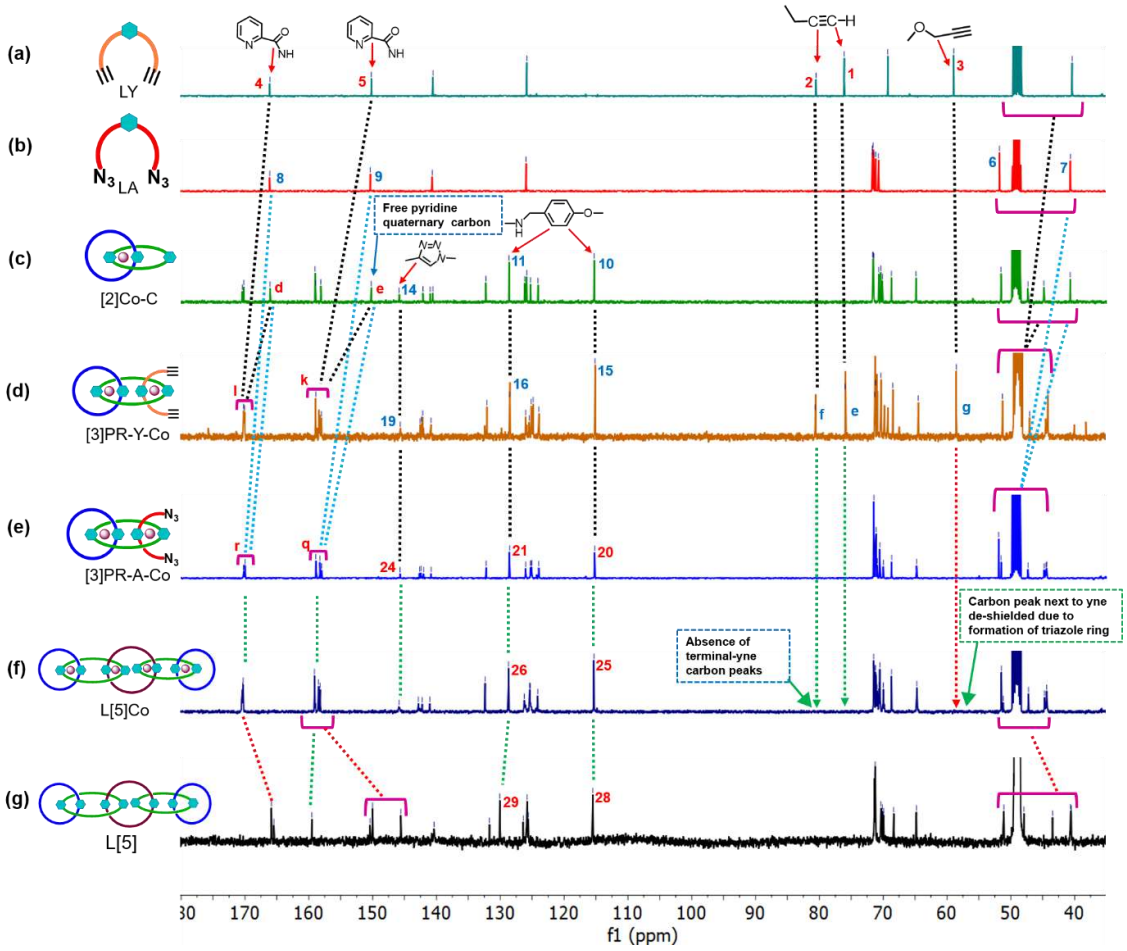

Figure 3.2. ^{13}C-NMR peak shift comparison for synthesis of linear [5]catenane from its precursor molecule **[2]Co-C**, **LY**, **LA** (a) di-alkyne ligand **LY** (b) di-azide ligand **LA** (c) metalated [2]catenane **[2]Co-C** (d) di-alkyne terminus [3]pseudorotaxane **[3]PR-Y-Co** (e) di-azide terminus [3]pseudorotaxane **[3]PR-A-Co** (f) templated linear pre-[5]catenane complex **L[5]Co** (g) fully organic linear [5]catenane **L[5]**. All spectra recorded in CD_3OD. Note that both **[3]PR-Y-Co** and **L[5]Co** have their corresponding isomers as a mixture, but only the entangled isomers are shown here.

Such de-shielding has also been observed in previously reported works and is common in metal complexes.[17a,25b] In addition, minor de-shielding is observed for the aliphatic carbons in the close vicinity of the newly formed Co(III)-metal complex compared to the non-complex structure (**Figure 3.2**). Further evidence for synthesis of **[3]PR-Y-Co** came from ESI positive mass analysis. It shows cluster of prominent isotopic distribution peaks at m/z 963.8205 (calcd.

m/z for $C_{90}H_{110}Co_2N_{18}O_{20}Na_2$ [(**[3]PR-Y-Co**)$^{2-}$+2H$^+$+2Na$^+$]$^{2+}$ is 963.8298). The theoretically calculated isotopic distribution pattern matches the experimentally found distribution pattern (**Figure 3.3a**), indicating formation of **[3]PR-Y-Co**. In the mass spectra, counter cation tetrabutyl ammonium can be seen at m/z 242.2850 (**Section 3.6.2**).

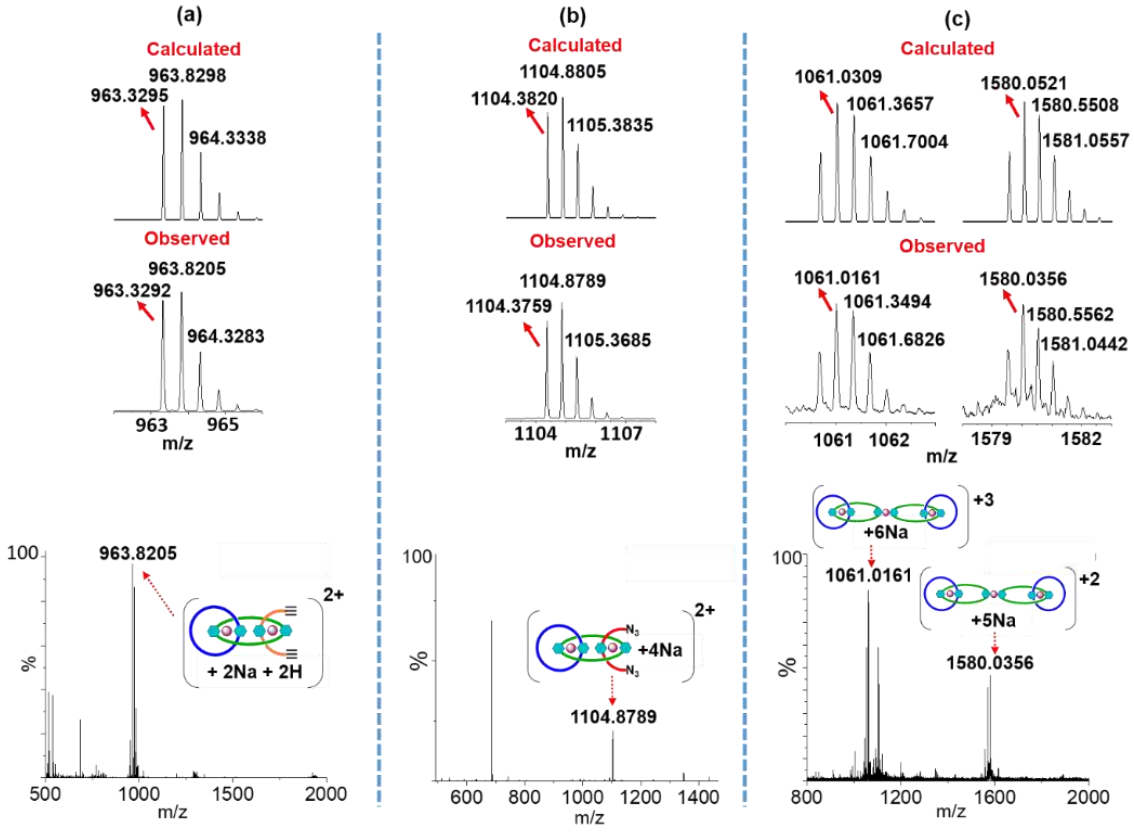

Figure 3.3. ESI$^+$ mass spectra for synthesized [3]pseudorotaxanes and dimer of metalated [2]catenane (a) di-alkyne terminus **[3]PR-Y-Co** (b) di-azide terminus **[3]PR-A-Co** (c) **[2]Co-D**. Expanded spectra of the desired peak (Isotopic distribution pattern) and simulated isotopic distribution are shown above.

3.3.2. Formation of dimer of metalated [2]catenane [2]Co-D during synthesis of [3]PR-Y-Co:

The third green-colored prominent spot **[2]Co-D** (**Scheme 3.2b** and **Figure 3.4**) from the reaction between metalated [2]catenane **[2]Co-C** and di-alkyne terminal ligand **LY** was

isolated with 30% yield and characterized by ^{1}H-NMR, ^{13}C-NMR and mass spectroscopy. It was observed that in CD_3OD, both ^{1}H-NMR and ^{13}C-NMR signals of **[2]Co-D** are similar to that of Co(III)-metalated [2]catenane **[2]Co-C (Figure 3.5, 3.6, Section 3.6.1)**. Mass spectra of **[2]Co-D** were recorded to confirm its structure further. Two prominent peaks with 2^{+} and 3^{+} charged states appear at m/z 1580.0356 and 1161.0161, respectively. These two peaks correspond to dimer of metalated [2]catenane (**Figure 3.3c**) with theoretical calculated isotopic distribution (calcd. m/z for $C_{146}H_{182}Co_3N_{30}O_{32}Na_5$ [(**[2]Co-D**)$^{3-}$+5Na^{+}]$^{2+}$ is 1580.0521 and for $C_{146}H_{182}Co_3N_{30}O_{32}Na_5$ [(**[2]Co-D**)$^{3-}$+6Na^{+}]$^{3+}$ is 1061.0309) matching with the experimentally observed mass.

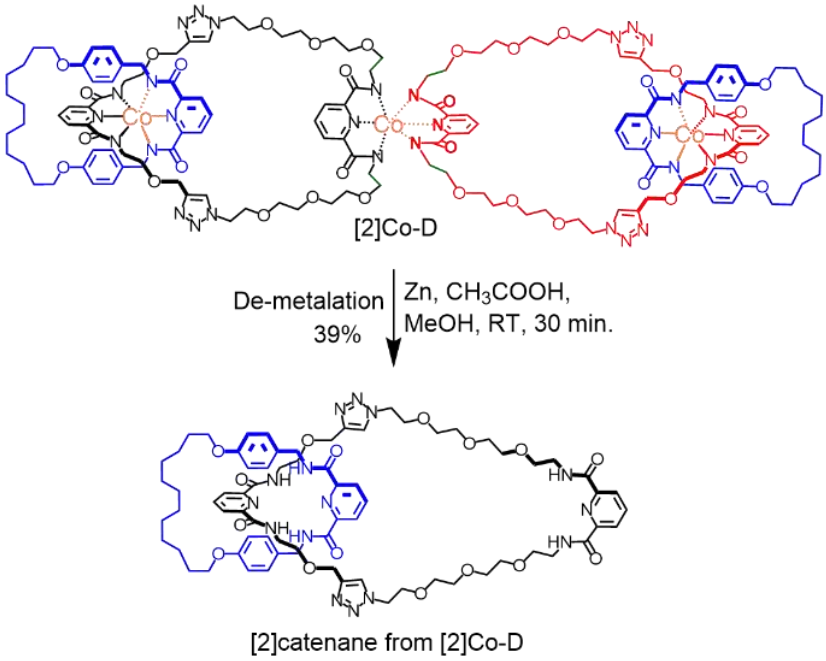

Scheme 3.3. Reaction scheme for demetallation of the dimer of metalated [2]catenane **[2]Co-D** resulting [2]catenane.

We performed a de-metalation experiment using Zn/CH_3COOH to confirm this product. When Co(III)-metals are removed from **[2]Co-D**, the product (**Scheme 3.3**) is [2]catenane (with 39% yield) as confirmed by ^{1}H-NMR, ^{13}C-NMR and ESI^{+} spectroscopy (**Figure 3.5**, **3.6**, **3.8,**

Section 3.6.1). This macrocyclic structure (as in **[2]Co-D**) can be used with suitable modification for synthesizing higher-ordered catenane using a zip-tie strategy developed by Jonathan's group.

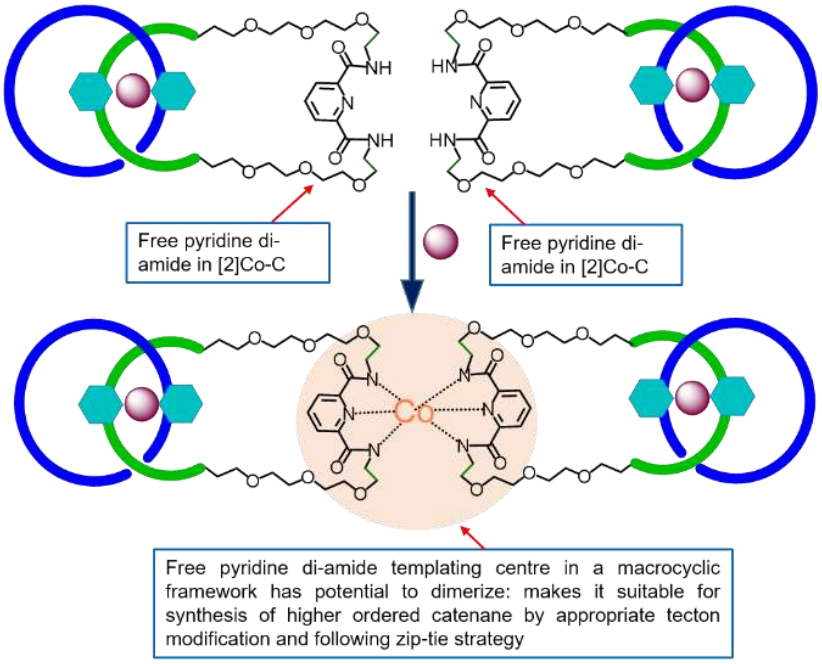

Figure 3.4. The pyridine-diamide unit acts as a templating center that forms an unusual non-entangled macrocyclic metal complex.

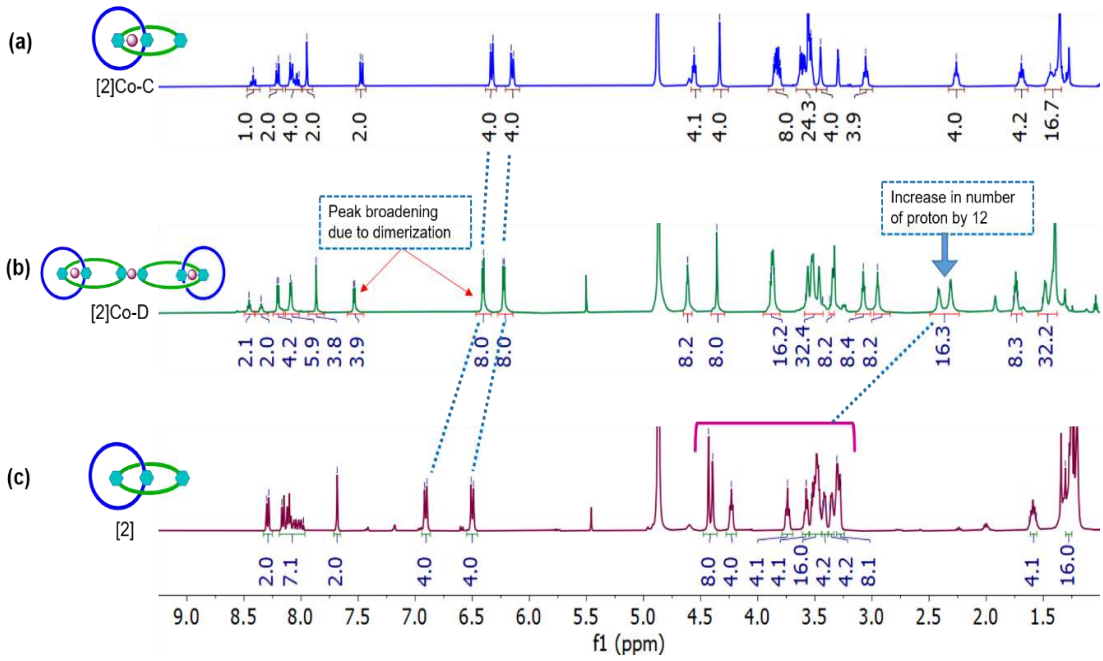

Figure 3.5. Partial ^{1}H-NMR comparison for the synthesis of linear **[2]Co**-dimer (**[2]Co-D**) from corresponding **[2]Co**-monomer. De-metalation **[2]Co-D** results fully organic [2]catenane.

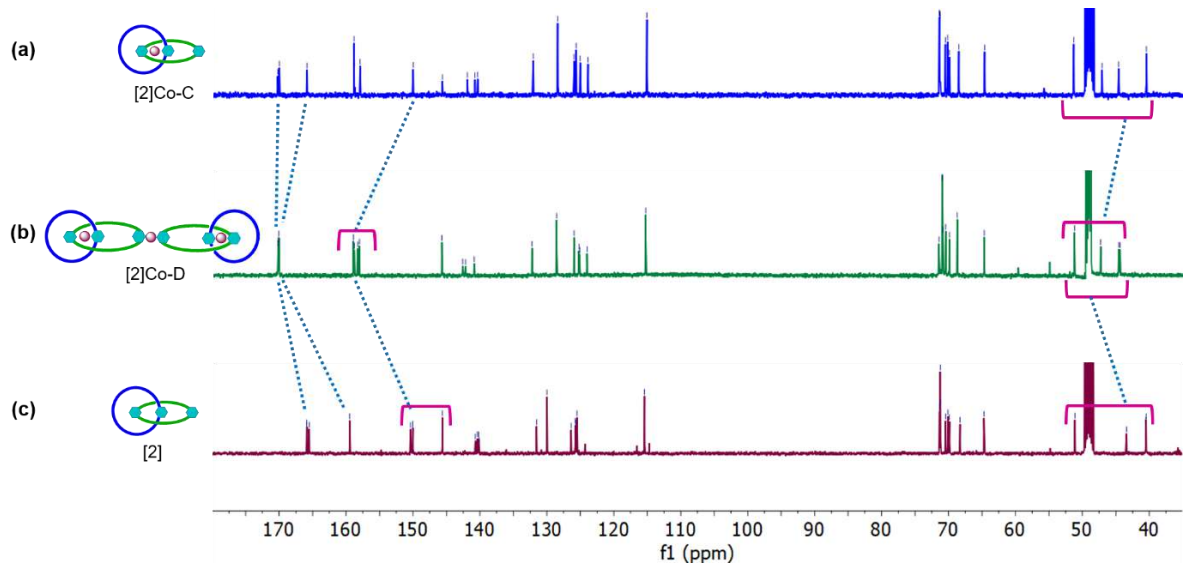

Figure 3.6. Partial ^{13}C-NMR comparison for the synthesis of linear **[2]Co**-dimer (**[2]Co-D)** from corresponding **[2]Co**-monomer. De-metalation **[2]Co-D** results fully organic [2]catenane.

3.3.3. Synthesis of di-azide terminus [3]pseudorotaxane, ([3]PR-A-Co):

[3]PR-A-Co was synthesized similarly to **[3]PR-Y-Co**, by reacting pyridine-diamide functionalized di-azide terminal ligand **LA** and metalated [2]catenane **[2]Co-C** having a free pyridine-di-amide center in presence of $Co(OAc)_2.4H_2O$ and $Bu_4N^+OAc^-$ and NaH in MeOH. Similar to **[3]PR-Y-Co**, here also three major green-colored spots were observed on a tlc (with MeOH: EtOAc 40: 60 v/v eluent), and each of these spots could be isolated by column chromatography with 30% yield (**Scheme 3.4**). The moderate polar product (R_f = 0.3) corresponds to di-azide terminus [3]pseudorotaxane **[3]PR-A-Co**, and the product formed with high polarity (R_f = 0.1) corresponds to a dimer of **[2]Co-C** as suggested by ^{1}H-NMR, ^{13}C-NMR, and ESI^+ mass spectroscopy. Moreover, the low polar (R_f = 0.8) self-complexed product between LA ligand has been observed and isolated first from the column chromatography.

Evidence of complexation reaction between **[2]Co-C** and **LA** came from the shielding effect observed for eight methylene (–CH_2–) protons (4 from each reacting partner) in close vicinity of the newly formed Co(III)-complex. As a result, number of protons at 2.27 ppm increased by eight (peak **p**, **o**, **n**, Figure **3.1e**).

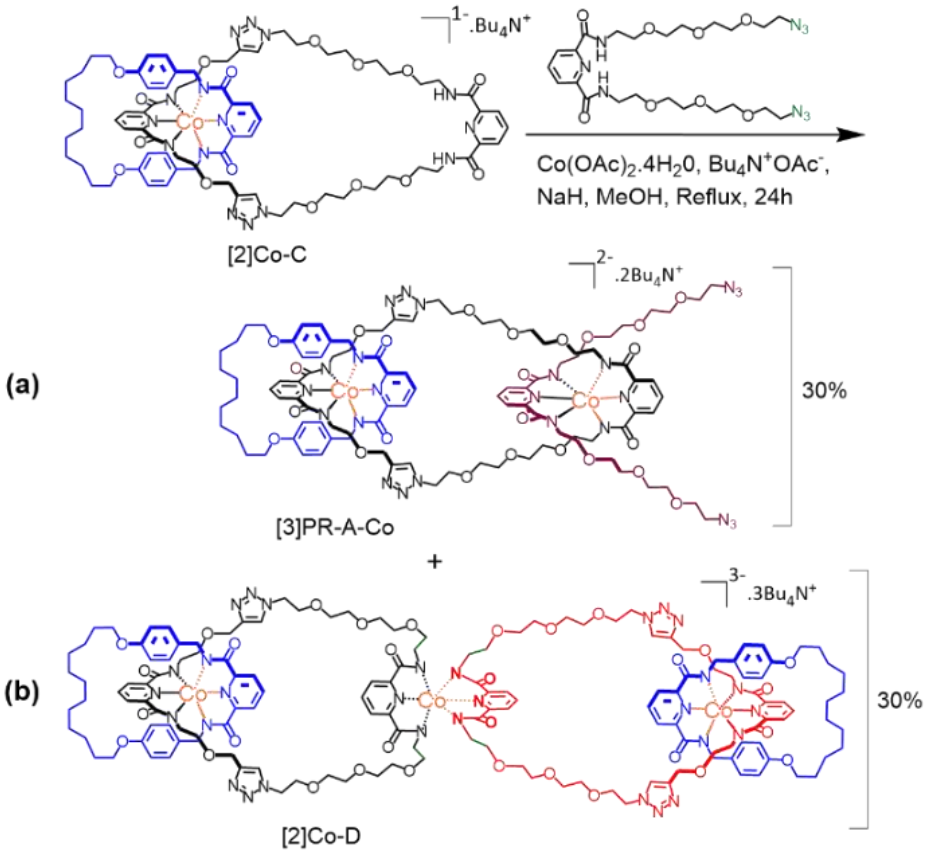

Scheme 3.4. Reaction scheme showing the formation of (a) **[3]PR-A-Co** and (b) **[2]Co-D**. The complex **[3]PR-A-Co** is used further.

Moreover, proton NMR spectra of **[3]PR-A-Co** comprise NMR signals of its constituent subunits, such as **[2]Co-C** and di-azide ligand **LA**. At 6.18 and 6.33 ppm benzene protons (peak **20** and **21**, respectively), at 7.49 ppm pyridine protons (peak **22**, **Figure 3.1e**), and at 7.97 ppm triazole proton (peak **23**) of [2]Co-C subunit of **[3]PR-A-Co** appears. Also, Both aliphatic and aromatic peaks of **LA** are present in **[3]PR-A-Co**, as observed by the increase in the number

of protons in ^{1}H-NMR spectra. In addition, unlike the di-alkyne counterpart, the di-azide [3]pseudorotaxane was isolated in pure form without any other isomeric product, as can be seen from the ^{1}H-NMR spectra with one doublet appearing for the benzene and pyridine protons (peak **20**, **21**, **22**, **Figure 3.1e**, **Section 3.6.1**) and only one peak appears for triazole protons (peak **23**, Figure **3.1e**).

A further indication of the formation of **[3]PR-A-Co** is provided by ^{13}C-NMR analysis that comprises of signals from **[2]Co-C** and **LA** subunits (**Figure 3.2e**). Benzene carbon peaks of **[2]Co-C** subunit appears at 115.16 and 128.52 ppm (peak **20**, **21**, **Figure 3.2e**), and quaternary carbons of the triazole ring of **[2]Co-C** subunit appear at 145.7 ppm (peak **24**, **Figure 3.2e**). As in **[3]PR-Y-Co**, in **[3]PR-A-Co**, the carbonyl carbon (peak **r**, **Figure 3.2e**) and pyridine quaternary carbon (peak **q, Figure 3.2e**) of recently formed Co(III)-complex got de-shielded by 4 and 9 ppm respectively with respect to the corresponding signals of subunit **[2]Co-C** (peak **d**, **e**, **Figure 3.2c**) and **LA** (peak **8**, **9, Figure 3.2b**). In addition, minor de-shielding is also observed for the aliphatic carbons near the newly formed Co(III)-complex (**Figures 3.2e** and **3.2b**). Such de-shielding further suggests complex formation at free pyridine-di-amide center between **[2]Co-C** and **LA**.

In ESI^{+} mass analysis, **[3]PR-A-Co** shows a diagnostic di-cationic peak at m/z 1104.8789 with isotopic distribution matching with the theoretically calculated mass (calcd. m/z for $C_{96}H_{126}Co_2N_{24}O_{24}Na_4$ [(**[3]PR-A-Co**)$^{2-}$ + $4Na^{+}$]$^{2+}$ is 1104.8805)(**Figure 3.3b**). This further suggests the formation of **[3]PR-A-Co**. In mass spectra, the counter cation tetrabutyl ammonium can be seen at m/z = 242.2850 (**Section 3.6.2**).

3.3.4. Synthesis of metalated linear [5]catenane via click reaction:

Click reaction was performed by refluxing one equivalent of each **[3]PR-Y-Co** and **[3]PR-A-Co** in the presence of CuI, DIPEA, and CH_3COOH in anhydrous MeOH for 24 hours.

Completion of the reaction was indicated by the disappearance of both reaction partners by tlc and appearance of a new deep green-colored spot. The reaction mixture was subjected to SiO_2 column chromatography with eluent EtOAc: MeOH (35 : 65, v/v) to isolate the deep green-colored semisolid product with a 40% yield. Characterization by ^{1}H-NMR, ^{13}C-NMR, ESI^{+}, and ESI^{-} mass spectroscopy suggests this product as Co(III)-metalated linear [5]catenane **L[5]Co**.

In addition, a trail of green color at the base of tlc plate can be seen. Possibly various other by-products form during the ring closing reaction but could not be identified.

^{1}H-NMR suggest the ring closing click reaction between **[3]PR-Y-Co** and **[3]PR-A-Co** leading to the formation of **L[5]Co** due to the disappearance of signals (**Figure 3.1f**) for both terminal alkyne protons peak of **[3]PR-A-Co** sub-unit at 2.7 ppm. In addition, the peak at 2.27 ppm (peak **s**, **t**, **u**, **x**, **y**, **z**, **Figure 3.1f**) corresponds to 24 protons (12 from **[3]PR-Y-Co** and 12 from **[3]PR-A-Co**), suggesting the presence of both the sub-units in **L[5]Co**. Moreover, due to the formation of triazole rings, nearby protons (peak **w**, **v**, **Scheme 3.1**) got de-shielded, increasing the number of protons between 4.21 and 4.57 ppm by eight. Notably, no shift in NMR signals for the benzene and pyridine protons of both the reaction partners (peak **25**, **26**, and **27**, **Figure 3.1f**, **Scheme 3.1**) could be observed. As **[3]PR-Y-Co** is an isomeric mixture, synthesized **L[5]Co** is also an isomeric mixture of entangled and non-entangled isomer (**L[5]Co-Isomer**, **Scheme 3.5**). Note that, for simplification in the discussion only **L[5]Co** is mentioned. This can be inferred from the complex pattern of ^{1}H-NMR peaks **25**, **26**, and **27** (**Figure 3.1f**), and further evidenced by demetallation and discussed in the demetallation section of L[5]Co.

More evidence of **L[5]Co** formation is drawn from the ^{13}C-NMR analysis. The peaks corresponding to terminal alkyne carbon of **[3]PR-Y-Co** (peak **e**, **f**, **Figure 3.2d**) are absent in ^{13}C-NMR spectra of **L[5]Co** (**Figure 3.2f**) suggests absence of non-reacting alkyne terminus.

De-shielding effect of triazole ring on nearby carbon can also be observed, as the peak corresponding to carbon next to the triazole ring in **[3]PR-Y-Co** sub-unit is not seen at 58.67 ppm and merged with the peaks around 65–70 ppm. Signals for benzene carbons can be seen at 115.17 and 128.53 ppm (peaks **25**, and **26**, respectively, **Figure 3.2f**) without any change.

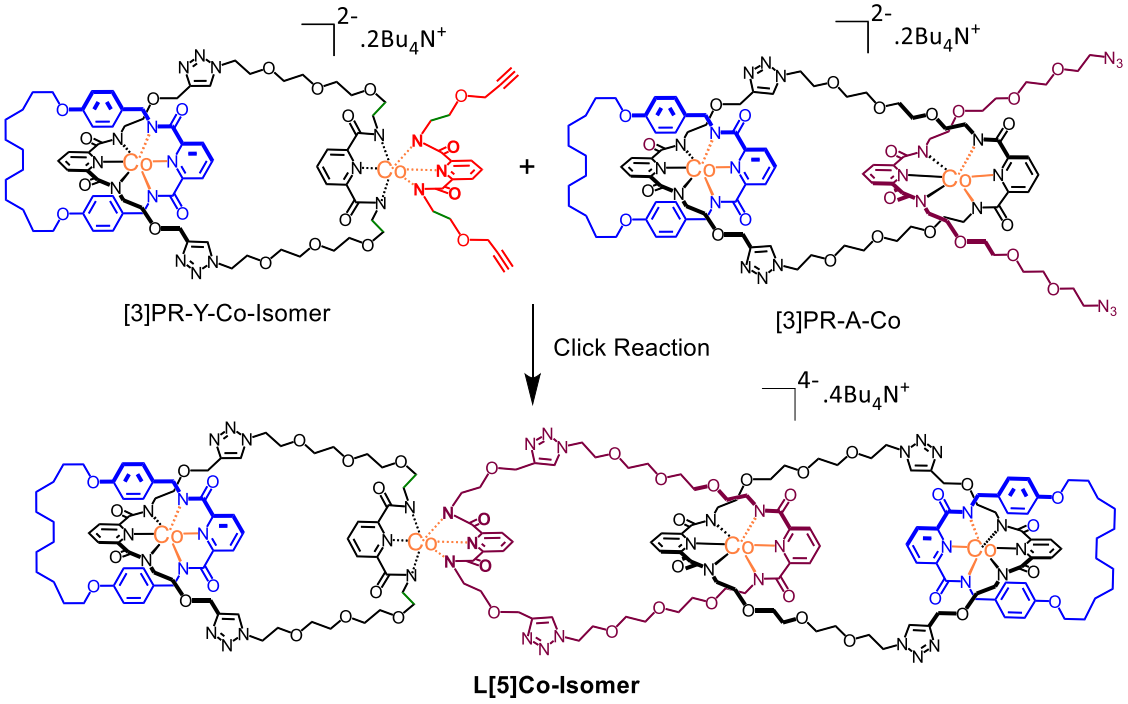

Scheme 3.5. Reaction scheme and structure for the formation of a non-entangled isomer of **L[5]Co** (**L[5]Co-Isomer**) from the reaction between **[3]PR-Y-Co-Isomer** and **[3]PR-A-Co**.

L[5]Co was further characterized using both ESI^+ and ESI^- mass spectroscopy. In a positive mode mass spectra, the metalated linear [5]catenane shows characteristic peaks at m/z 1386.1505 and 1045.3530. These two peaks correspond to 3^+ and 4^+ charged states of **L[5]Co** generated due to the addition of sodium ions from HCOONa used during the mass experiment. The theoretically calculated mass matches the experimentally observed for both the charged states. For 3^+ charge state calcd. m/z for $C_{186}H_{234}Co_4N_{42}O_{44}Na_7$ $[(\mathbf{L[5]Co})^{4-} + 7Na^+]^{3+}$ is 1386.1366 and for 4^+ charge state calcd. m/z for $C_{186}H_{234}Co_4N_{42}O_{44}Na_8$ $[(\mathbf{L[5]Co})^{4-}+8Na^+]^{3+}$

is 1045.3483 (**Figure 3.7a**). The peak for tetrabutyl ammonium counter cation can be seen at m/z 242.2850 (**Section 3.6.2**). Further, ESI negative mode mass spectra analysis reveals peak corresponds to 4^- charge state with m/z 999.3553 indicating the product. The overall tetra-anionic nature of the molecule is due to the deprotonated amides and four Co(III) ions. The isotopic distribution peaks are matching with the theoretically calculated mass (**Section 3.6.2**) (calcd. m/z for $C_{186}H_{234}Co_4N_{42}O_{44}$ (**L[5]Co**)$^{4-}$ is 999.3670).

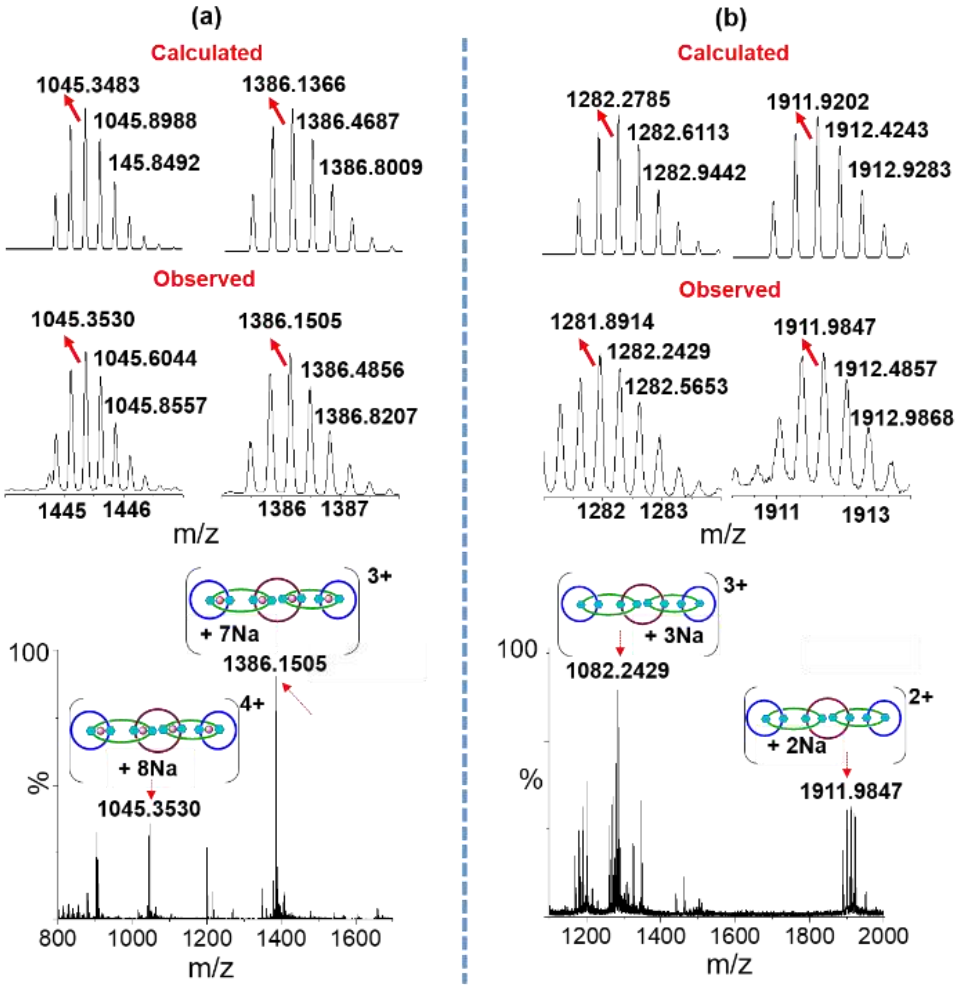

Figure 3.7. ESI^+ mass spectra for (a) metalated linear [5]catenane **L[5]Co** and (b) fully organic linear [5]catenane **L[5]**. Both show positively charged peaks due to the addition of Na^+. Full spectra are given at the bottom, with isotopic distribution at the top. Simulated isotopic distribution matches with experimentally observed mass. Note that both **L[5]Co** has its corresponding isomers **L[5]Co**-Isomer as a mixture, but the mass of the entangled isomers is shown here.

3.3.5. Demetalation of metalated linear [5]catenane to form fully organic linear [5]catenane:

We performed the demetallation of Co(III) ions from metalated linear [5]catenane to form fully organic linear [5]catenane in CH_3COOH: MeOH (v/v, 1 : 1 ratio) with activated Zn dust and stirring the solution for 30 minutes in open air.

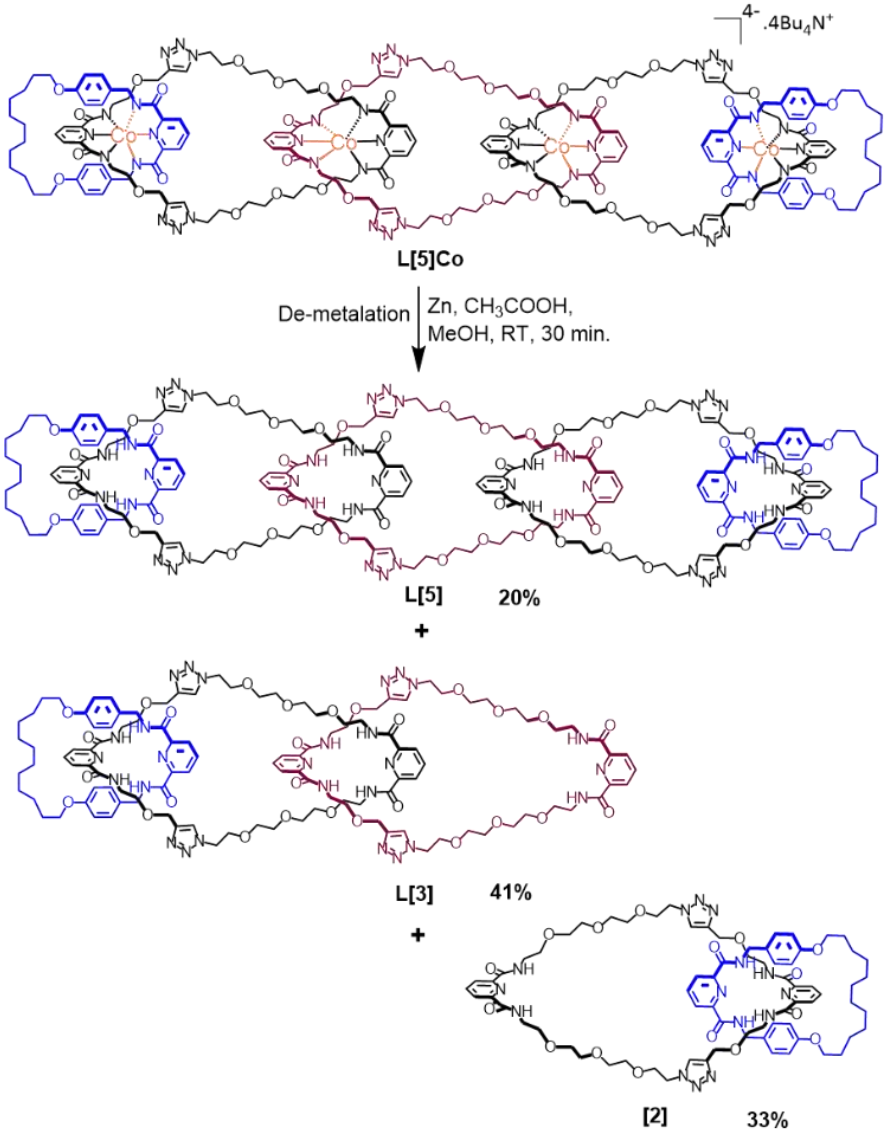

Scheme 3.6. Reaction scheme for demetallation of **L[5]Co** leading to formation of linear [5], linear [3], and [2]catenane. As **L[5]Co** is an isomeric mixture of entangled and non-entangled isomers of **[3]PR-Y-Co** sub-unit. Note that both **L[5]Co** has its corresponding isomers **L[5]Co**-Isomer as a mixture, but only the entangled isomers is shown here.

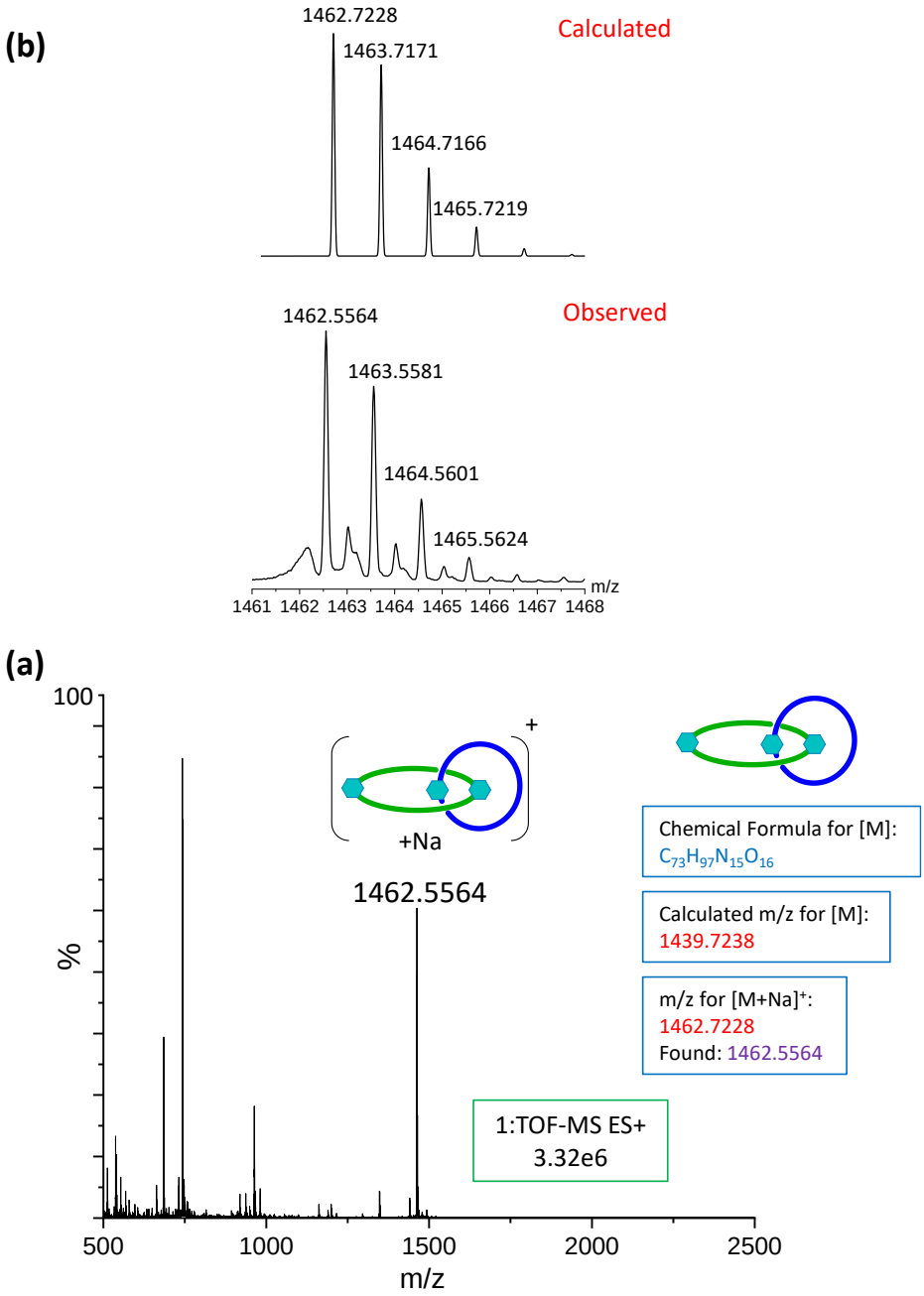

Figure 3.8. Mass spectra (ESI^+) analysis for synthesized **[2]C** (a) full spectra (b) comparison between calculated and experimentally observed isotopic distribution peaks.

Disappearance of deep green color of the reaction mixture is observed, indicating removal of Co(III) ions from the complex. Three major spots were visible on a tlc under UV light. The products were subjected to silica gel column chromatography with EtOAc: MeOH eluent (45 :

55, v/v) and isolated. All three isolated products were obtained as semisolids. These were characterized by ^{1}H-NMR, ^{13}C-NMR, and ESI^{+} mass spectroscopy.

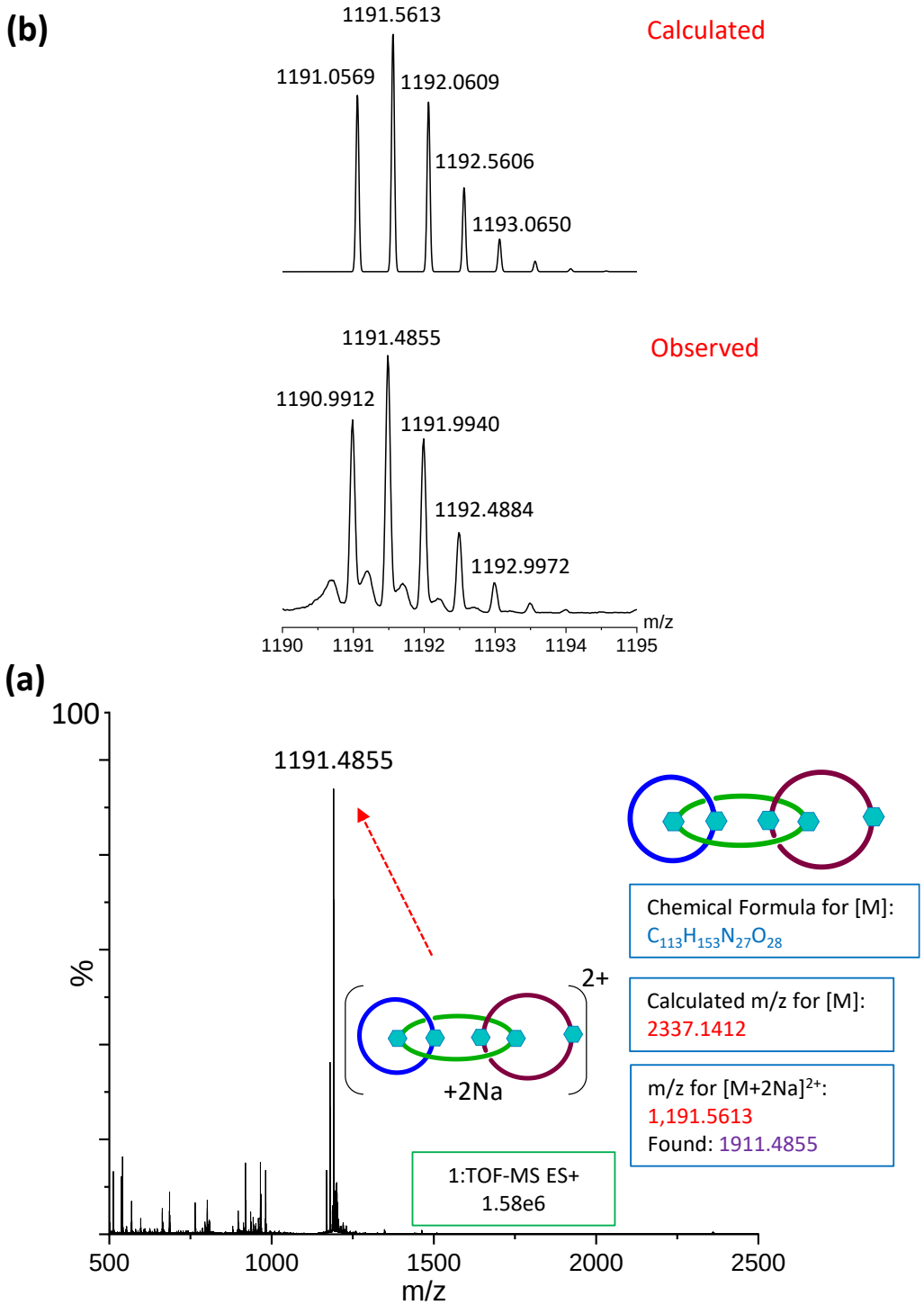

Figure 3.9. Mass spectra (ESI^{+}) analysis for synthesized **L[3]C** (a) full spectra (b) comparison between calculated and experimentally observed isotopic distribution peaks.

The first isolated product (R_f = 0.8) was characterized to be a [2]catenane, the second isolated product is a linear [3]catenane (R_f = 0.5), and the last high polar product (R_f = 0.4) is the desired linear [5]catenane. The yield for the respective catenanes are 33%, 41%, and 20%, respectively (**Scheme 3.6**). The mass of the [2]catenane, and linear [3]catenane are found at m/z 1462.5564 ([**M** + Na]$^{+}$) and 1191.4855 ([**M** + 2Na]$^{2+}$) respectively matching with the calculated mass (**Figure 3.8**, **3.9**). Further, the ^{1}H and ^{13}C NMR also matches with the products. The details are present in **Section 3.6.1**.

The formation of [2]catenane and linear [3]catenane can be explained due to the formation of a mixture of products in the previous step (**Schemes 3.1** and **3.6**). As described earlier, during the formation of **[3]PR-Y-Co**, an isomeric non-entangled product is also forming (**[3]PR-Y-Co**-Isomer). **[3]PR-Y-Co**-isomer when reacts with **[3]PR-A-Co** leads to formation of a cobalt complex ([**L[5]Co**-Isomer] containing metalated [2] and linear [3]catenate complex (**Scheme 3.5**). De-metalation of this product ([**L[5]Co**-Isomer) leads to the formation of [2] and linear [3]catenane.

The desired linear [5]catenane is characterized ^{1}H, ^{13}C NMR and mass spectroscopy. In fully organic linear [5]catenane, the protons near to the pyridine-diamide templating center are de-shielded compared to the metalated complex **L[5]Co** (**Figure 3.1g**). Such de-shielding occurs due to removal of metal ion is reported previously.[25b] Moreover, the benzene and pyridine protons also de-shielded by an average of 0.5 ppm (peak **28**, **29**, **Figure 3.1g**). One set of proton peaks (peak **31**, **32**, Figure **3.1g**) at 7.68 ppm (4 protons) and another set at 7.84 ppm (2 protons) belonging to triazole rings suggests that **L[5]** has two types of triazole rings. Two major changes are observed in the ^{13}C-NMR of **L[5]** from **L[5]Co**. The carbonyl and quaternary carbon of pyridine-diamide center gets shielded, while the aliphatic carbons in close vicinity to the metal center gets shielded by 3.69 ppm (**Figure 3.2g**).

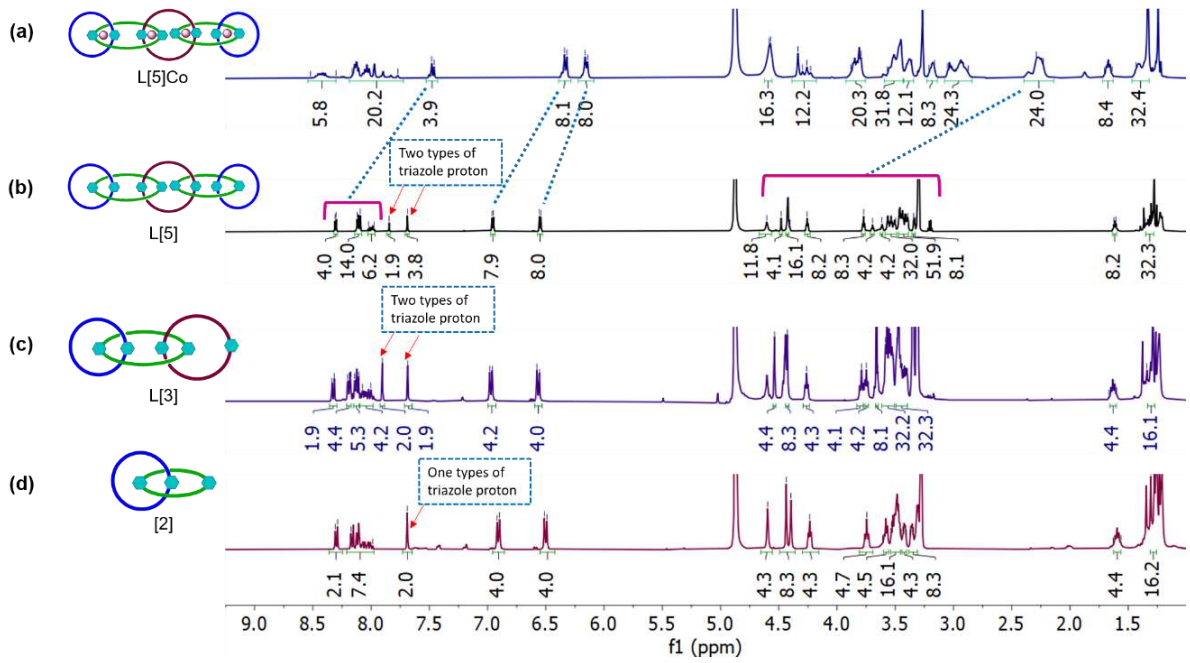

Figure 3.10. Partial ^{1}H-NMR comparison for demetalation of **L[5]Co** leading to formation of solely organic linear [5], linear [3] and [2]catenane.

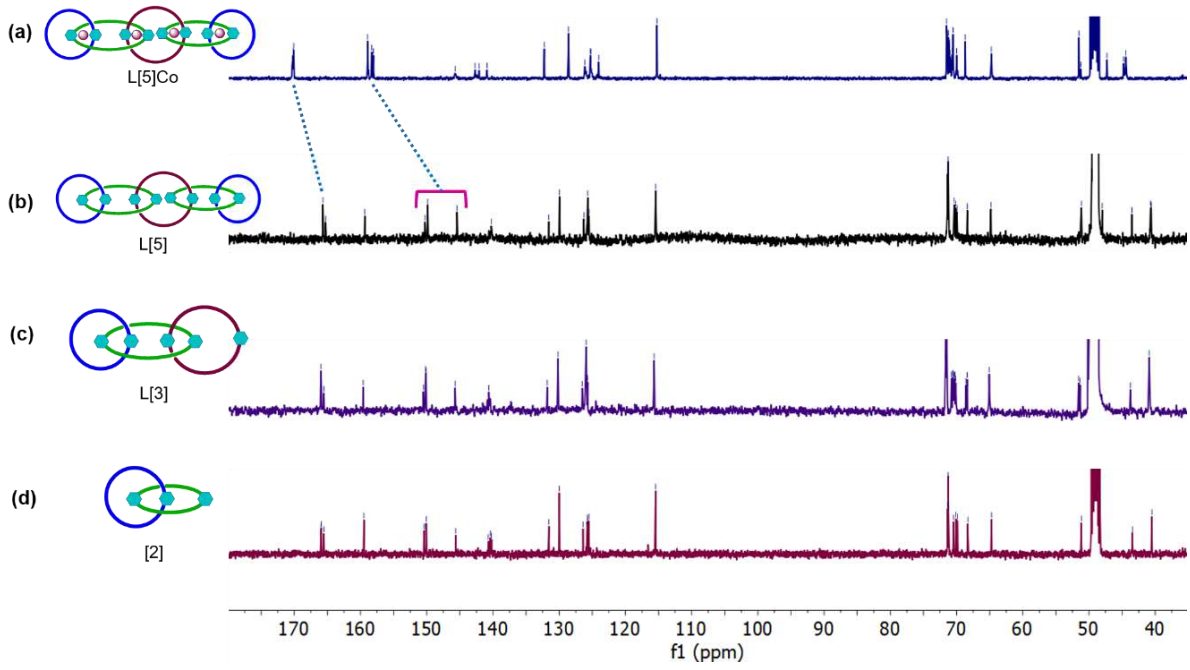

Figure 3.11. Partial ^{13}C-NMR comparison for demetalation of **L[5]Co** leading to formation of solely organic linear [5], linear [3] and [2]catenane.

Further confirmation of isolation of solely organic linear [5]catenane came from mass spectra (**Figure 3.7b**). Clusters of isotopic distribution peaks were observed in mass spectra of **L[5]** at m/z 1911.9847 and 1082.2429 correspond to 2^+ and 3^+ charged ions of **L[5]** and are matching with the theoretically calculated isotopic distribution pattern (calcd. m/z for $C_{186}H_{250}N_{42}O_{44}Na_2$ [**L[5]** + $2Na^+$]$^{2+}$ is 1911.9202 and calcd. m/z for $C_{186}H_{250}N_{42}O_{44}Na_3$ [**L[5]** + $3Na^+$]$^{3+}$ is 1282.2785).

3.3.6. VT-NMR experiment for metalated linear [5]catenane:

Variable temperature (VT) proton NMR spectra were recorded for L[5]Co. This study suggests the molecule is conformationally flexible at room temperature (**Figure 3.12**).

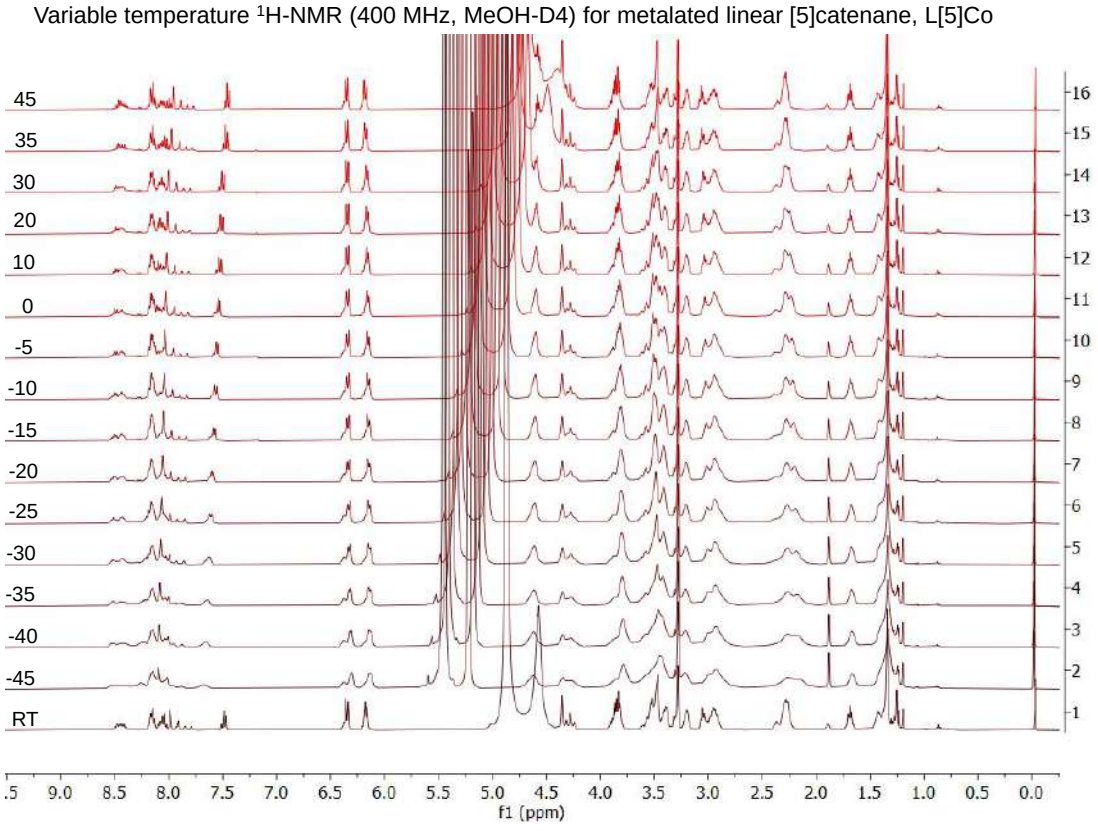

Figure 3.12. Variable temperature (in degree Celsius) ^{1}H-NMR for metalated linear [5]catenane. Data recorded from -45 ˚C to 45 ˚C. At lower temperature broadening of NMR signals and at higher temperature sharpening of NMR signals was observed.

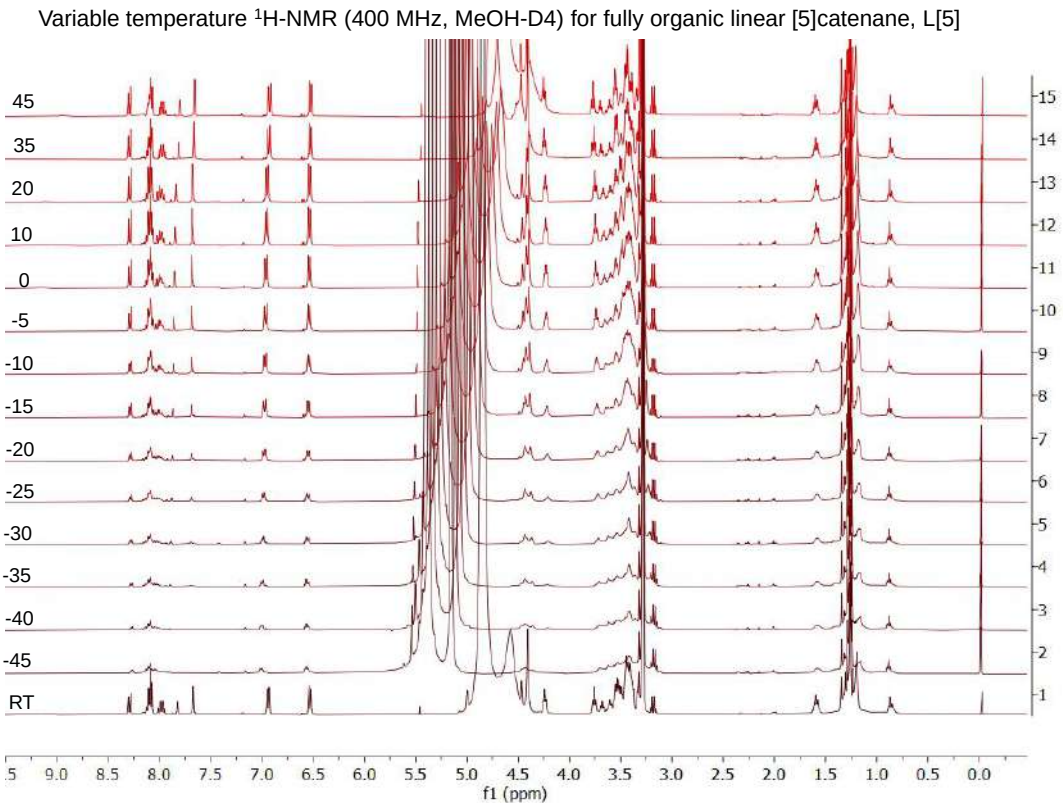

Figure 3.13. Variable temperature (in degree Celsius) ^{1}H-NMR for fully organic linear [5]catenane. Data recorded from -45 ˚C to 45 ˚C. At lower temperature broadening of NMR signals and at higher temperature sharpening of NMR signals was observed.

Moreover, variable temperature NMR suggest that **L[5]** is conformationally flexible in nature and remain in dynamic equilibrium among various conformations at RT (**Figure 3.13**).As higher order linear [n]catenane are known to show more co-conformational flexibility compared to their lower ordered catenane and corresponding templated catenane.[13c] To have an insight, we have further compared VT-NMR data among synthesized **[2]** (**Figure 3.14**) and **L[5]Co** and **L[5]** catenane. As the temperature is lowered from 45 ˚C to –45 ˚C, pronounced broadening was observed (below−5 ˚C) due to conformational rigidity attained in the low temperature for **L[5]** compared to the **[2]** and **L[5]Co**. This suggests **L[5]** is more prone to conformational changes compared to the **[2]** and **L[5]Co**.

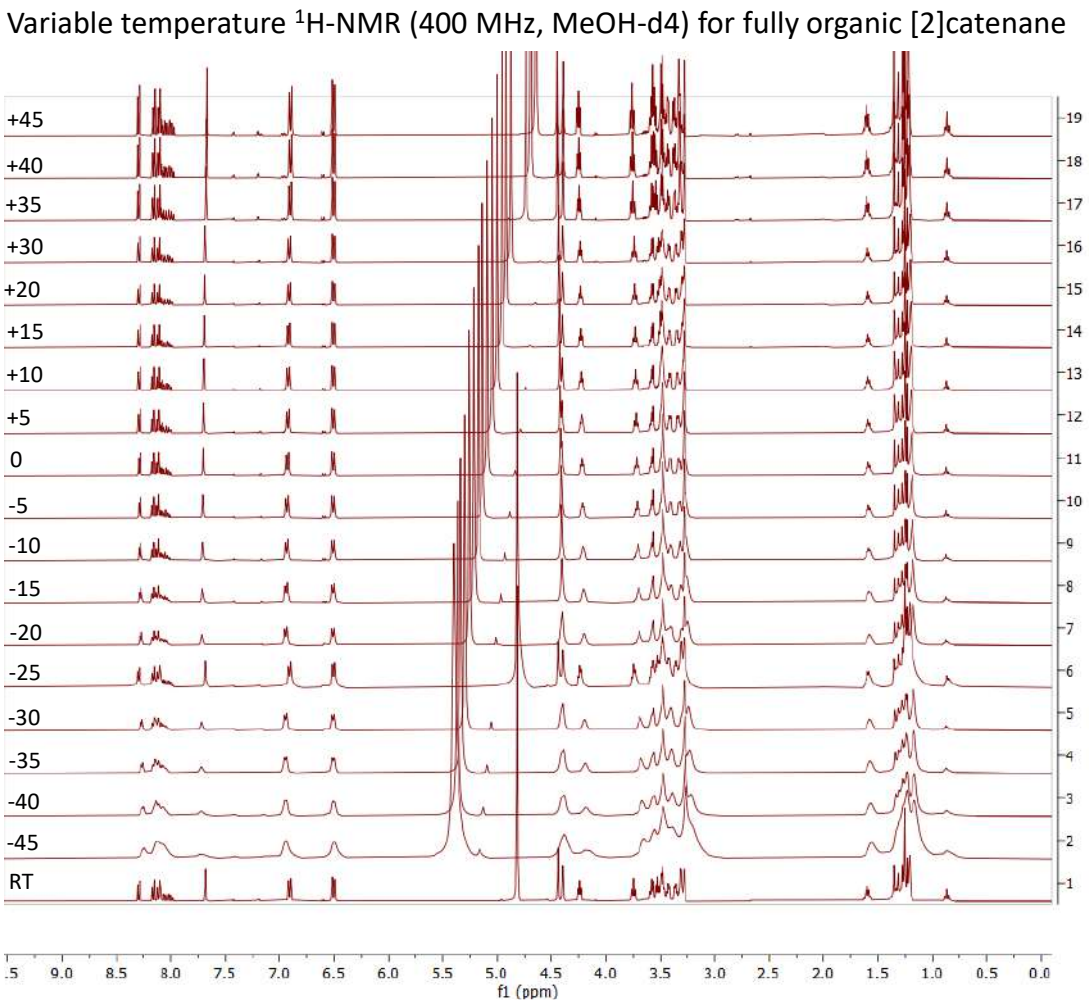

Figure 3.14. Variable temperature (in degree Celsius) ^{1}H-NMR for fully organic [2]catenane. Data recorded from -45 ˚C to 45 ˚C. At lower temperature broadening of NMR signals and at higher temperature sharpening of NMR signals was observed.

3.3.7. MS/MS Experiment on Linear [5]catenane L[5]:

Evidence of entanglement of all 5 rings in **L[5]** and all 3 rings in **L[3]** can be observed from the MS/MS experiment. For **L[5]**, further fragmentation of base peak at m/z 1911.8274), corresponding to the M^{2+} ion, produces fragments of **[4]**, **[3]** and **[2]** catenanes and corresponding macrocycles (**Figure 3.15**). Also MS/MS data for **L[3]**, shows peaks for [2]catenane and corresponding macrocycles (**Figure 3.16**)

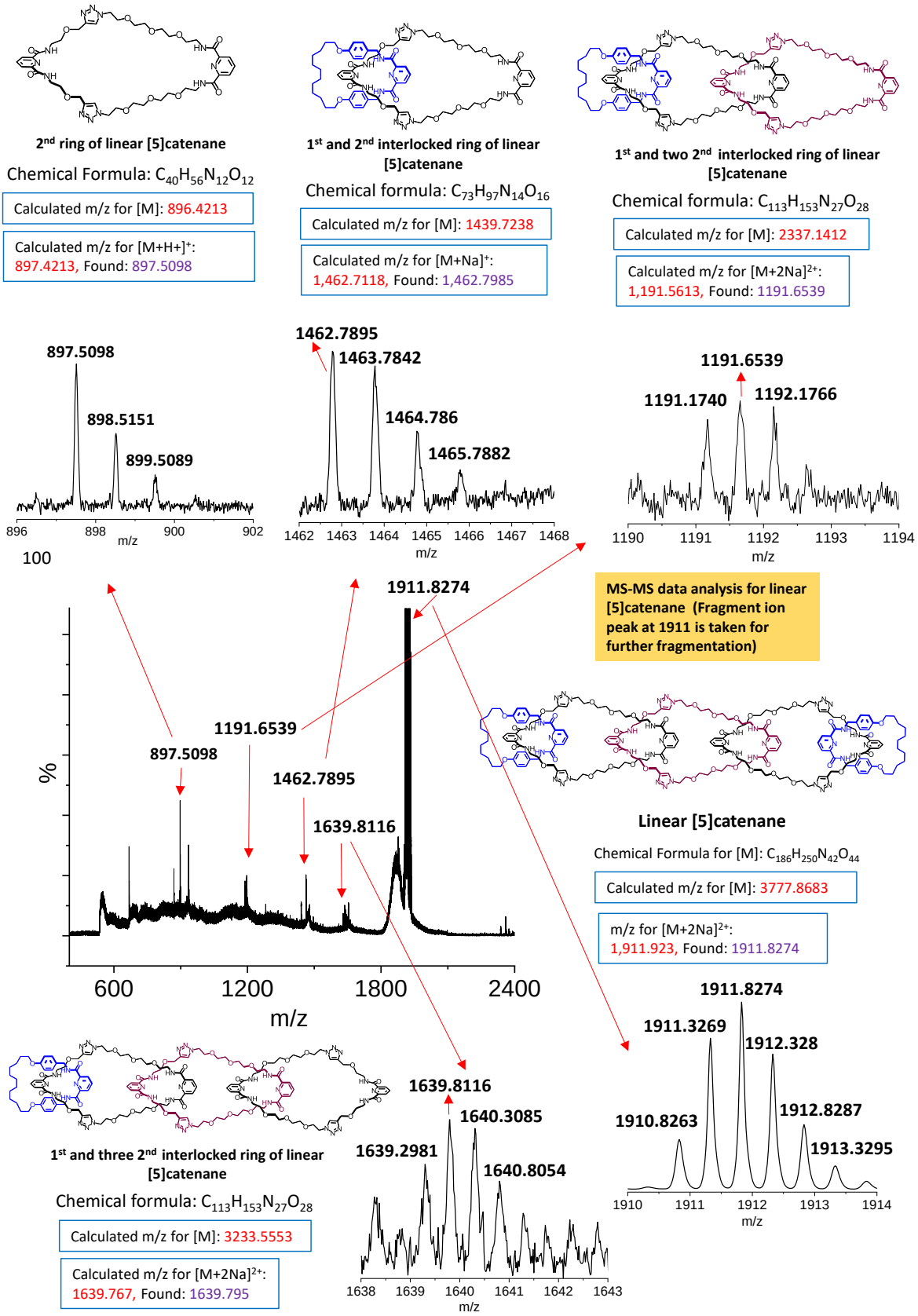

Figure 3.15. Ms-Ms spectra (ESI^+) analysis for synthesized linear [5]catenane shows mass for constituent macrocycles.

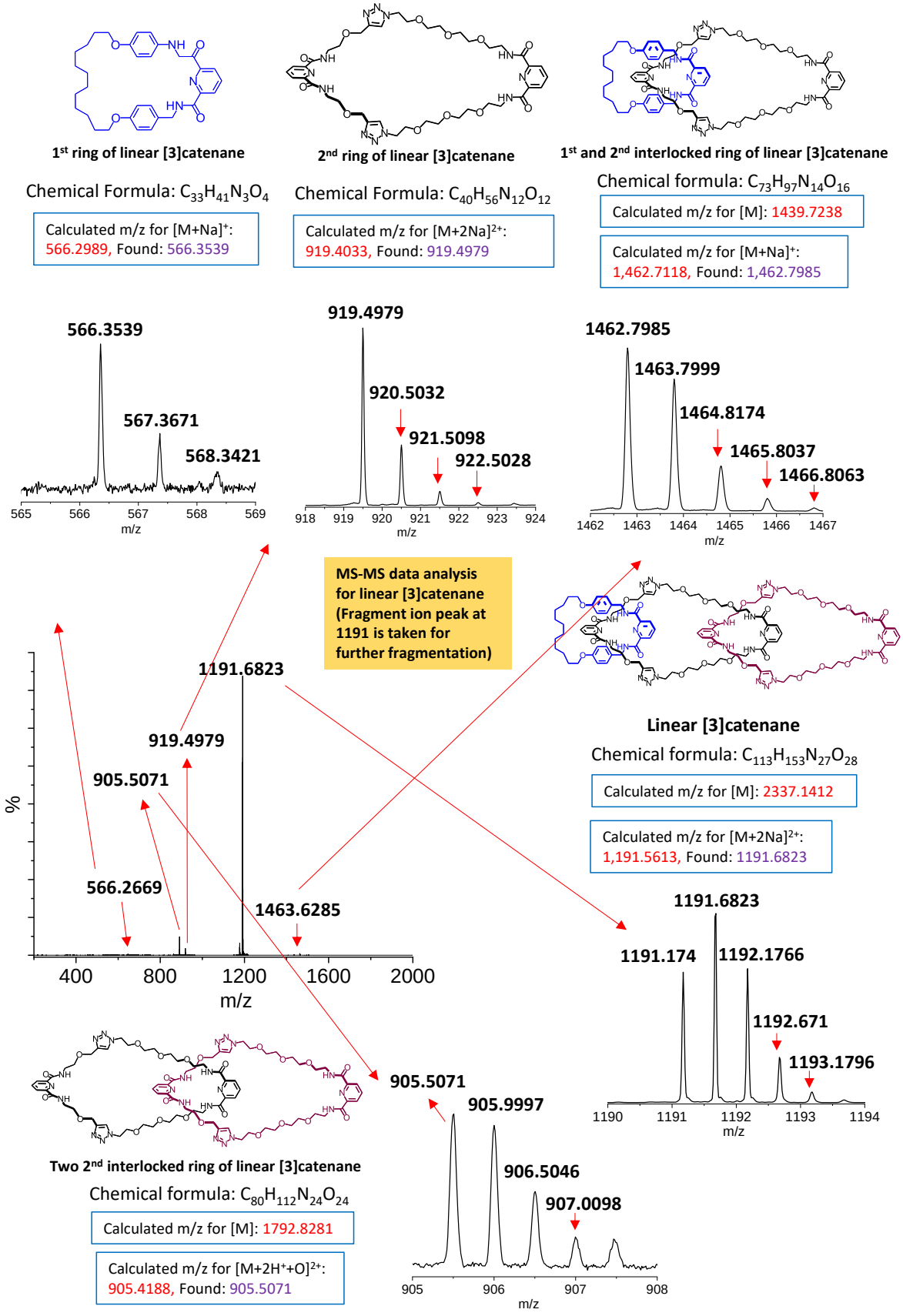

Figure 3.16. Ms-Ms spectra (ESI^+) analysis for synthesized linear [3]catenane shows mass for constituent macrocycles.

3.4. Conclusions:

In conclusion, post-functionalization of a Co(III)-metalated pre-[2]catenate complex having a free pyridine-diamide binding center has been explored for the synthesis of higher ordered catenane using click reaction in ring closing step. **[2]Co-C** is threaded with two different threading units using anionic Co(III)-template to synthesize two [3]pseudorotaxanes namely **[3]PR-Y-Co** (having two terminal alkyne groups) and **[3]PR-A-Co** (having two terminal azide groups). Click reaction was performed between **[3]PR-Y-Co** and **[3]PR-A-Co** to form a macrocycle leading to a linear Co(III)-templated pre-[5]catenanate complex in 40% yield. Demetallation of this complex with Zn/CH_3COOH leads to a linear [5]catenane in 20% yield. This linear [5]catenane comprises of two types of macrocycles; three central macrocycles (same structure) and two terminal macrocycles (same structure). This method establishes anionic non-labile pyridine-diamide templating center as potential candidate for higher order catenane synthesis with multiple mechanical bonds. Interestingly, metal complexes of catenanes are also formed. These complexes can be suitably modified to make higher catenane with zip-tie strategy.

3.5. Experimental Section:

3.5.1. Reagents and Instruments:

Synthesis of di-azide ligand **LA**, di-alkyne ligand **LY** and Co(III)-metalated [2]catenane (**[2]Co-C**) has been discussed in reported literature procedure.[28] Threading of **[2]Co-C** to give [3]pseudorotaxane **[3]-PR-Y-Co** and **[3]PR-A-Co** has been synthesized following literature procedure similar to that of [2]pseudorotaxane in reported literature.[28-29] Click reaction has been performed following literature procedure.[28] Cobalt(II)acetate tetrahydrate and NaH has

been purchased from Spectrochem, India Pvt. Ltd. Copper(I)iodide has been brought from Sigma Aldrich. N, N-diisopropylethylamine and acetic acid has been taken from SRL Chemicals and Tetrabutylammonium acetate is from Alpha Aeser. Common organic solvent such as Hexane, EtOAc, DCM and methanol has been purchased from Merck and used without further purification. Silica gel (100-200 mesh) has been used in column chromatography for the purification of synthesized compounds. Anhydrous MeOH, DCM, has been prepared by common laboratory methods. Deuterated MeOH, has been purchased from Euriso-top Chemicals. ^{1}H-NMR and ^{13}C-NMR spectra has been recorded in a Bruker 400 MHz and 700 MHz Spectrometer and Jeol 400 MHz. Mass spectra has been recorded in Water ESI-MS Spectrometer.

3.5.2. Synthesis of pseudorotaxane with di-alkyne terminal, [3]PR-Y-Co:

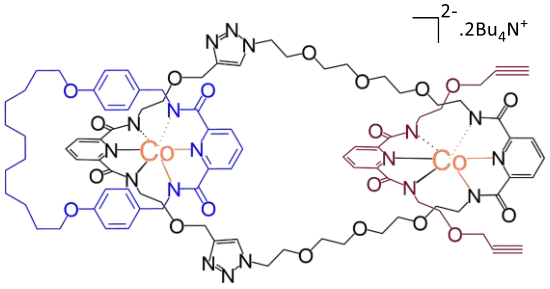

[3]PR-Y-Co

To a 100 mL two-neck round bottom flask equipped with stir bar, metalated [2]catenane **[2]Co-C** (0.268 g, 0.179 mmol), $Co(OAc)_2.(H_2O)_4$ (0.0446 g, 0.179 mmol) and $Bu_4N^+OAc^-$ (0.054 g, 0.179 mmol) was transferred and it was purged with anhydrous methanol (25 mL) under inert atmosphere. The mixture was refluxed at 80 ˚C (performed by using a condenser, sealed with a rubber septum on top of it) for 2.5 hours under inert atmosphere to obtain a clear green solution. To this mixture, 0.059 g (0.179 mmol) of di-alkyne ligand **LY** (dissolved in 25 mL anhydrous MeOH) was injected under reflux conditions. This reaction mixture was further refluxed for 2.5 hour under inert atmosphere. In another RB flask, sodium methoxide was

prepared (by the slow addition of 25 mL anhydrous methanol into 1 g NaH at 0 ˚C) and injected into the reaction mixture at reflux conditions. This results a color change to deep green. Later, the reaction mixture was allowed to oxidize by exposing to air (performed by removing the septum) and refluxed for 24 hours at this stage. Then, solvent was evaporated to dryness and the residue is subjected to SiO_2 column chromatography using EtOAC: MeOH (65:35 v/v) as solvent. Collected green colored cobalt complex product from column chromatography was further washed with hexane and EtOAc repeatedly to remove unwanted impurities and resulted mixture of **[3]PR-Y-Co** and its non-entangled isomeric product **[3]PR-Y-Co**-isomer in 30% yield (0.102 g).

^{1}H-NMR: (400 MHz, CD_3OD) δ in ppm: 8.51-8.36 (m, 3H), 8.24-8.22 (d, 1H), 8.14-8.01 (m, 6 H), 7.98 (s, 1H), 7.92 (s, 1H), 7.49 (t, 2H), 6.38-6.33 (2d, 4H), 6.20-6.15 (2d, 4H), 4.61-4.59 (m, 8H), 4.35-4.28 (2s, 4H), 3.86-3.80 (m, 10H), 3.60-3.40 (m, 16H), 3.21 (s, 2H), 3.06-2.93 (m, 12H), 2.72-2.70 (t, 2H), 2.30-2.26 (m, 12H), 1.70-1.68 (m, 4H), 1.43-1.34 (m, 16H).

^{13}C-NMR: (100 MHz, CD_3OD) δ in ppm: 170.22, 170.05, 158.93, 158.04, 145.68, 142.59, 142.36, 142.19, 140.87, 132.13, 128.58, 126.08, 125.51, 125.20, 124.89, 123.99, 115.19, 80.76, 76.06, 71.44, 71.31, 70.46, 68.59, 64.62, 58.67, 51.43, 47.18, 44.35, 30.28, 30.15, 29.83, 29.60, 26.57.

HR-MS (ESI$^+$): Calcd. m/z for $C_{90}H_{110}Co_2N_{18}O_{20}Na_2$ $[(M^{2-}+2H^+ +2Na^+]^{+2}$ is 963.8298, found 963.8205.

Furthermore, in the synthesis of **[3]PR-Y-Co**, another green colored product is observed to be formed and isolated via column chromatography which is having higher polarity than **[3]PR-Y-Co**. This product is dimer of **[2]Co-C** namely **[2]Co-D** and isolated with 30% yield. Detail characterization for **[2]Co-D** is discussed below.

3.5.3. Synthesis of pseudorotaxane with di-azide terminal, [3]PR-A-Co:

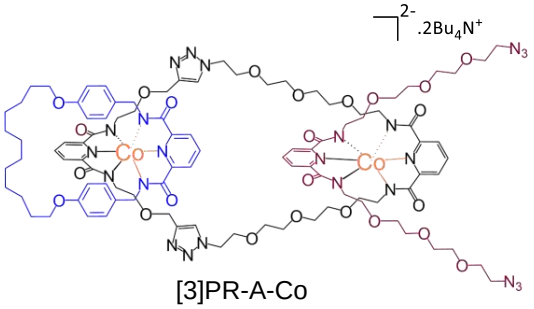

[3]PR-A-Co

To a 100 mL two-neck round bottom flask equipped with stir bar, metalated [2]catenane **[2]Co-C** (0.252 g, 0.168 mmol), $Co(OAc)_2.(H_2O)_4$ (0.0419 g, 0.168 mmol) and $Bu_4N^+OAc^-$ (0.0508 g, 0.168 mmol) was transferred and it was purged with anhydrous methanol (25 mL) under inert atmosphere. The mixture was refluxed at 80 ˚C (performed by using a condenser, sealed with a rubber septum on top of it) for 2.5 hours under inert atmosphere to obtain a clear green solution. To this mixture, 0.0956 g (0.168 mmol) of di-azide ligand **LA** (dissolved in anhydrous MeOH 25 mL) was injected under reflux conditions. This reaction mixture was further refluxed for 2.5 hour under inert atmosphere. In another RB flask, sodium methoxide was prepared (by the slow addition of 25 mL anhydrous methanol into 1 g NaH at 0 ˚C) and injected into the reaction mixture at reflux conditions. This results a color change to deep green. Later, the reaction mixture was allowed to oxidase by exposing to air (performed by removing the septum) and refluxed for 24 hours at this stage. Then, solvent was evaporated to dryness and the residue is subjected to SiO_2 column chromatography using EtOAC: MeOH (60:40 v/v) as solvent. Collected green colored cobalt complex product from column chromatography was further washed with hexane and EtOAc repeatedly to remove unwanted impurities and resulted pure **[3]PR-A-Co** in 30% yield (0.11 g).

^{1}H-NMR: (400 MHz, CD_3OD) δ in ppm: 8.50-8.41 (m, 3H), 8.15-8.11 (m, 6H), 8.05 (t, 1H), 7.98 (s, 2H), 7.49-7.47 (d, 2H), 6.36-6.33 (d, 4H), 6.18-6.16 (d, 4H), 4.58 (t, 4H), 4.35 (s, 4H),

3.88-3.81 (m, 8H), 3.62-3.52 (m, 16H), 3.49-3.43 (m, 12H), 3.39-3.35 (m, 8H), 3.26-3.23 (m, 8H), 3.20-3.18 (2t, 8H), 3.05 (t, 4H), 2.96-2.90 (m, 8H), 2.31-2.24 (m, 12H), 1.72-1.65 (m, 4H), 1.45-1.35 (m, 16).

^{13}C-NMR: (100 MHz, CD_3OD) δ in ppm: 170.30, 170.23, 170.04, 158.93, 158.85, 158.30, 158.03, 145.71, 142.66, 142.43, 142.01, 140.84, 132.19, 128.53, 126.00, 125.24, 125.13, 125.06, 123.95, 115.17, 71.38, 71.36, 71.31, 71.09, 71.05, 71.01, 70.98, 70.81, 70.42, 69.87, 68.56, 64.65, 51.76, 51.39, 47.16, 44.64, 44.35, 44.22, 30.29, 30.14, 29.83, 29.60, 23.72.

HR-MS (ESI$^+$): Calcd. m/z for $C_{96}H_{126}Co_2N_{24}O_{24}Na_4$ $[M^{2-}+4Na^+]^{+2}$ is 1104.8805, found 1104.8789.

Similar to **[3]PR-Y-Co**, also in the synthesis of **[3]PR-A-Co**, dimer of **[2]Co-C** is formed with 30% yield and has higher polarity than **[3]PR-A-Co**.

3.5.4. Formation of [2]catenane dimer, [2]Co-D:

While synthesis of both [3]pseudorotaxanes, **[2]Co-C** gets dimerized at the free pyridine-diamide centre to form **[2]Co-D** with 30% yield (0.0769 g).

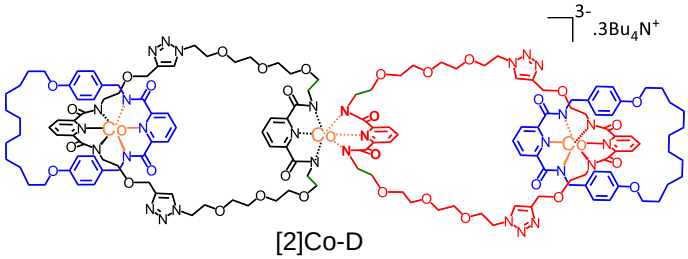

[2]Co-D

^{1}H-NMR: (700 MHz, CD_3OD) δ in ppm: 8.46 (t, 2H), 8.36 (t, 2H), 8.22-8.20 (d, 4H), 8.11-8.09 (m, 6H), 7.87 (s, 4H), 7.55-7.53 (d, 4H), 6.42-6.40 (d, 8H), 6.23-6.22 (d, 8H), 4.61 (t, 8H),

4.36 (s, 8H), 3.89-3.85 (m, 16H), 3.58-3.43 (m, 32H), 3.36-3.33 (m, 8H), 3.07 (t, 8H), 2.95 (t, 8H), 2.41-2.31 (2t, 16H), 1.75-1.72 (m, 8H), 1.50-1.39 (m, 32H).

^{13}C-NMR: (175 MHz, CD_3OD) δ in ppm: 170.25, 170.18, 170.09, 158.96, 158.81, 158.30, 158.05, 145.72, 142.60, 142.19, 140.87, 132.22, 128.56, 125.94, 125.22, 125.10, 124.00, 115.23, 71.37, 70.88, 70.77, 70.36, 69.81, 68.64, 64.60, 51.10, 47.18, 44.46, 44.30, 30.29, 30.14, 29.84, 29.61, 26.58.

HR-MS (ESI$^+$): Calcd. m/z for $C_{146}H_{182}Co_3N_{30}O_{32}Na_5$ $[M^{3-}+5Na^+]^{+2}$ is 1580.0521, found 1580.0356 and for $C_{146}H_{182}Co_3N_{30}O_{32}Na_3$ $[M^{3-}+6Na^+]^{+3}$ is 1061.0309, found 1061.0161.

3.5.5. Ring closing click reaction to form metalated linear [5]catenane L[5]Co:

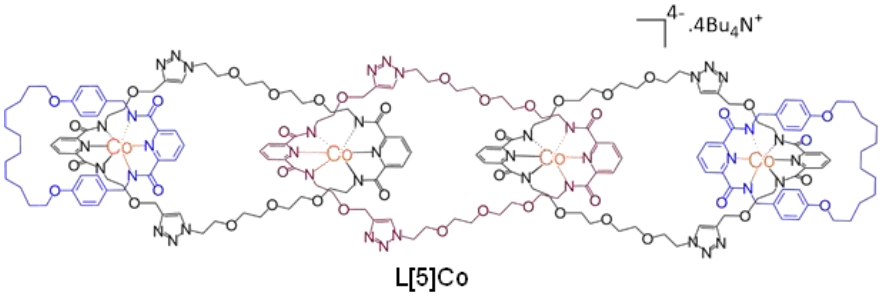

L[5]Co

Click reaction was performed using reported literature procedure[1] under high dilution conditions. To a 250 mL RB flask, di-alkyne pseudorotaxane **[3]PR-Y-Co** (0.1 g, 0.053 mmol), di-azide pseudorotaxane **[3]PR-A-Co** (0.1126 g, 0.053 mmol), CH_3COOH (0.0638 mL, 1.063 mmol), DIPEA (0.1821 mL, 1.063 mmol) and CuI (0.2026 g, 1.063 mmol) were transferred. Then 90 mL of anhydrous MeOH was added into it. The mixture was refluxed for 24 h under N_2 atmosphere. MeOH was removed under reduced pressure and the resulting material was purified using column chromatography (Ethyl acetate: Methanol 35:65) to result metalated linear [5]catenane **L[5]Co**. The collected portion was washed with hexane and EtOAC to remove undesired impurities and pure green colored semisolid product **L[5]Co** was

isolated with yield of 40% (0.086 g). It is to be noted that isolated product also comprise of **L[5]Co-**Isomer, but for simplification only L[5]Co is mentioned.

^{1}H-NMR (400 MHz, CD_3OD) δ in ppm: 8.51-8.30 (m, 6H), 8.16-7.77 (m, 20H), 7.50-7.45 (m, 4H), 6.33-6.31 (2d, 8H), 6.16-6.14 (2d, 8H), 4.58-4.56 (m, 16H), 4.33-4.22 (m, 12H), 3.87-3.79 (m, br, 20H), 3.60-3.44 (m, br, 32 H), 3.41-3.35 (m, br, 12H), 3.20-3.16 (m, br, 8H), 3.04-2.87 (m, br, 24H), 2.28-2.22 (m, br, 24H), 1.70-1.63 (m, 8H), 1.43-1.32 (m, 32H).

^{13}C-NMR (100 MHz, CD_3OD) δ in ppm: 170.15, 170.06, 158.90, 158.83, 158.27, 158.01, 145.67, 142.65, 142.04, 140.85, 132.19, 128.53, 126.07, 125.23, 125.14, 123.96, 115.17, 71.39, 71.27, 71.10, 70.98, 70.86, 70.54, 70.41, 69.86, 68.59, 64.63, 51.39, 51.11, 47.16, 44.64, 44.31, 30.28, 30.13, 29.82, 29.59, 26.55.

HR-MS (ESI^+): Calcd. m/z for $C_{186}H_{234}Co_4N_{42}O_{44}Na_7$ $[M^{4-}+7Na^+]^{+3}$ is 1386.1366, found 1386.1505 and for $C_{186}H_{234}Co_4N_{42}O_{44}Na_8$ $[M^{4-}+8Na^+]^{+4}$ is 1,045.3483, found 1045.3630.

HR-MS (ESI^-): Calcd. m/z for $C_{186}H_{234}Co_4N_{42}O_{44}$ $[M^{4-}]^{-3}$ is 1,332.8250, found 1,332.7611and for $C_{186}H_{234}Co_4N_{42}O_{44}$ $[M^{4-}]^{-4}$ is 999.3670, found 999.3553.

3.5.6. Demetalation of L[5]Co to form fully organic linear [5]catenane:

Removal of cobalt metal from metalated linear [5]catenane was done according to reported literature procedure.[28-29] 0.05 g of **L[5]Co** was transferred to a RB flask and to it anhydrous MeOH and CH_3COOH (5 ml each) were added followed by addition of activated Zinc (0.2 g). The reaction mixture was stirred for 30 minutes in open air. Complete disappearance of green color from the reaction mixture can be used as an indication for completion of reaction. Later, solvent was removed to dryness using rotatory evaporator and 30 mL of $CHCl_3$ was added. To it 1:1 mixture of 12.5 mL of 17.5% ammonia solution and 12.5 mL of saturated Na_4EDTA was added. The mixture was stirred for 30 minutes and work up was performed with $CHCl_3$ and water 3 times. Organic layer was collected and again work up was performed using brine

solution. Later, organic layer was collected, dried with anhydrous Na_2SO_4, evaporated to dryness and purified by column chromatography using EtOAC: MeOH as eluent (55: 45 v/v) to isolate three colorless stick solid demetalated products. The low polarity or first isolated from column chromatography is a fully organic [2]catenane with 33% yield (6 mg). the second isolated product via column chromatography was linear [3]catenane with 41% yield (12 mg). The last isolated product was the desired product, linear [5]catenane **L[5]** with 20% yield (10 mg). Three product were formed because **[3]PR-Y-Co** subunit of **L[5]Co** composed of isomeric mixture. Detail characterization of all three catenane by ^{1}H-NMR, ^{13}C-NMR and ESI-MS has been discussed **section 3.6.1** and **3.6.2**.

12.5 mL of saturated Na_4EDTA was prepared by mixing 5 g of EDTA with 2.73 g of NaOH and making the volume up to 12.5 mL with water and stirring it well. Activated Zinc was prepared by taking 10 g of Zinc powder in a RB flask and washing it with 2N HCl three times followed by washing with DI water, ethanol, acetone, diethyl ether two times each and drying in hot air oven at 100 ˚C for 15 minutes.

3.5.7. Characterization of fully organic linear [5]catenane:

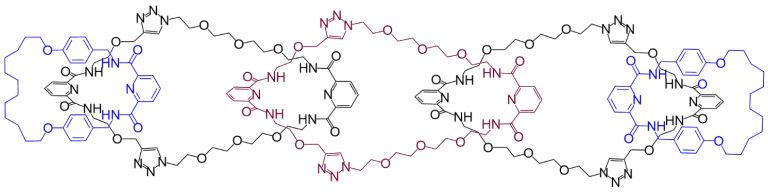

L[5]

^{1}H-NMR: (700 MHz, CD_3OD) δ in ppm: 8.31-8.30 (d, 4H), 8.12-8.09 (m, 14H), 8.02-7.97 (m, 6H), 7.84 (s, 2H), 7.68 (s, 4H), 6.96-6.95 (d, 8H), 6.55-6.54 (d, 8H), 4.60 (s, br, 12H), 4.47 (s, 4H), 4.42-4.40 (m, 16H), 4.25 (t, 8H), 3.76 (t, 8H), 3.69 (t, 4H), 3.61 (t, 4H), 3.56-3.49 (m, 32H), 3.46-3.38 (m, 52H), 3.34-3.32 (t, 8H), 1.62-1.60 (m, 8H), 1.35-1.27 (m, 32H).

^{13}C-NMR: (175 MHz, CD_3OD) δ in ppm: 165.86, 165.47, 159.51, 150.40, 150.02, 145.58, 140.38, 131.69, 130.06, 126.39, 125.79, 125.61, 115.51, 71.34, 71.25, 70.34, 70.13, 70.00, 69.90, 68.34, 64.79, 51.09, 47.93, 43.45, 40.62, 40.54, 30.76, 30.54, 30.14, 29.89, 29.66, 26.77.

HR-MS (ESI$^+$): Calcd. m/z for $C_{186}H_{250}N_{42}O_{44}Na_2$ $[M+2Na^+]^{+2}$ is 1,911.9202, found 1911.9847 and for $C_{186}H_{250}N_{42}O_{44}Na_3$ $[M+3Na^+]^{+3}$ is 1,282.2785, found 1,282.2429.

3.5.8. Characterization of fully organic linear [3]catenane:

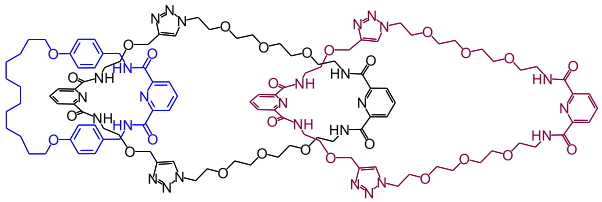

L[3]

^{1}H-NMR: (400 MHz, CD_3OD) δ in ppm: 8.33-8.31 (d, 2H), 8.20-8.17 (m, 4H), 8.14-8.10 (m, 5H), 8.07-8.00 (m, 4H), 7.90 (s, 2H), 7.68 (s, 2H), 6.98-6.95 (d, 4H), 6.57-6.55 (d, 4H), 4.53 (s, 4H), 4.45-4.42 (2d, 8H), 4.26 (t, 4H), 3.78 (t, 4H), 3.74 (t, 4H), 3.66-3.65 (m, 8H), 3.58-3.51 (m, 32H), 3.48-3.39 (m, 32H), 1.66-1.59 (m, 4H), 1.34-1.28 (m, 16H).

^{13}C-NMR: (100 MHz, CD_3OD) δ in ppm: 165.92, 165.49, 159.53, 150.42, 150.09, 150.03, 145.64, 140.53, 131.69, 130.06, 126.39, 125.80, 125.59, 115.51, 71.44, 71.35, 71.24, 70.51, 70.33, 70.23, 70.11, 70.01, 69.89, 68.34, 68.14, 64.82, 51.30, 51.08, 43.44, 40.62, 30.76, 30.54, 30.14, 29.90, 29.66, 26.77.

HR-MS (ESI$^+$): Calcd. m/z for $C_{113}H_{153}N_{27}O_{28}Na_2$ $[M+2Na^+]^{+2}$ is 1,191.5613, found 1911.4855

3.5.9. Characterization of fully organic [2]catenane:

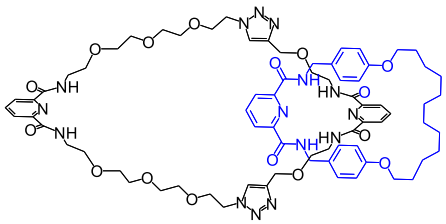

[2]

^{1}H-NMR: (400 MHz, CD_3OD) δ in ppm: 8.31-8.29 (d, 2H), 8.17-7.99 (m, 7H), 7.69 (s, 2H), 6.92-6.90 (d, 4H), 6.51-6.49 (d, 4H), 4.60 (s, 4H), 4.44-4.40 (2s, 8H), 4.24 (t, 4H), 3.75 (t, 4H), 3.58 (t, 4H) 3.53-3.45 (m, 16H), 3.44-3.41 (m, 4H), 3.37-3.34 (m, 8H), 1.63-1.56 (m, 4H), 1.31-1.26 (m, 16H).

^{13}C-NMR: (100 MHz, CD_3OD) δ in ppm: 165.95, 165.91, 165.55, 159.48, 150.40, 150.08, 150.05, 145.63, 140.71, 140.40, 140.22, 131.55, 129.99, 126.40, 125.76, 125.69, 125.52, 115.43, 71.36, 71.26, 71.22, 70.45, 70.11, 69.88, 68.29, 64.73, 51.15, 43.43, 40.51, 30.76, 30.52, 30.12, 30.08, 29.87, 29.63, 26.75.

HR-MS (ESI^{+}): Calcd. m/z for $C_{73}H_{97}N_{15}O_{16}Na$ $[M+Na^{+}]^{+}$ is 1462.7228, found 1462.5564.

3.5.10. Demetalation of [2]Co-D to give fully organic [2]catenane:

Removal of cobalt metal from dimer of metalated [2]catenane was done as in like **L[5]Co**. 0.11 g of **[2]Co-D** was transferred to a RB flask and to it anhydrous MeOH and CH_3COOH (5 ml each) were added followed by addition of activated zinc (0.3 g). The reaction mixture was stirred for 30 minutes in open air. Complete disappearance of green color from the reaction mixture can be used as an indication for completion of reaction. Later, solvent was removed to dryness using rotatory evaporator and 30 mL of $CHCl_3$ was added. To it 1:1 mixture of 12.5 mL of 17.5% ammonia solution and 12.5 mL of saturated Na_4EDTA was added. The mixture

was stirred for 30 minutes and work up was performed with $CHCl_3$ and water 3 times. Organic layer was collected and again work up was performed using brine solution. Later, organic layer was collected, dried with anhydrous Na_2SO_4, evaporated to dryness, and purified by column chromatography using EtOAC: MeOH as eluent (75: 25 v/v) to isolate colorless stick solid [2]catenane products with 73% yield (0.038 g).

^{1}H-NMR: (400 MHz, CD_3OD) δ in ppm: 8.30-8.28 (d, 2H), 8.17-7.98 (m, 7H), 7.68 (s, 2H), 6.92-6.90 (d, 4H), 6.51-6.49 (d, 4H), 4.43-4.40 (as, 8H), 4.23 (t, 4H), 3.74 (t, 4H), 3.58 (t, 4H), 3.53-3.45 (m, 16H), 3.43-3.40 (m, 4H), 3.37-3.34 (m, 4H), 3.31-3.28 (m, 8H), 1.62-1.56 (m, 4H), 1.31-1.25 (m, 16H).

^{13}C-NMR: (100 MHz, CD_3OD) δ in ppm: 165.90, 165.86, 165.51, 159.45, 150.37, 150.06, 150.03, 145.60, 140.69, 140.38, 140.20, 140.13, 131.55, 129.99, 126.38, 125.75, 125.68, 125.49, 115.42, 71.34, 71.23, 71.20, 70.44, 70.09, 69.86, 68.27, 64.72, 51.12, 43.42, 40.52, 40.48, 30.75, 30.50, 30.47, 30.11, 29.85, 29.62, 26.73.

HR-MS (ESI$^+$): Calcd. m/z for $C_{73}H_{97}N_{15}O_{16}Na$ $[M+Na^+]^+$ is 1462.7228, found 1462.5564.

3.6. Spectra:

3.6.1. ^{1}H and ^{13}C NMR spectra:

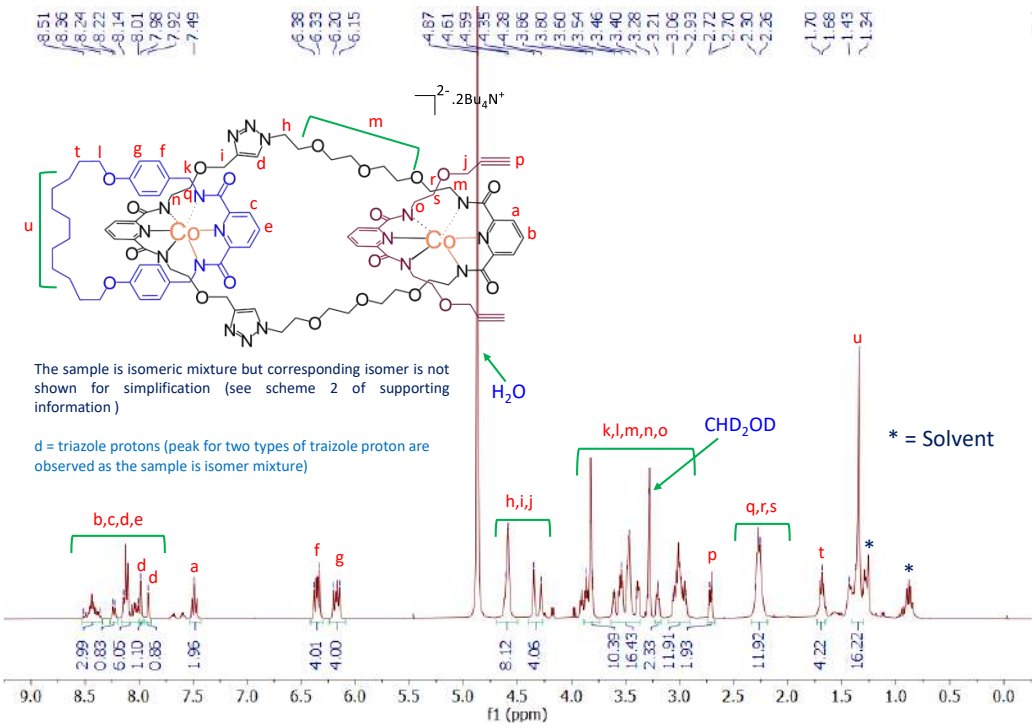

Figure 3.17. ^{1}H-NMR spectra of **[3]PR-Y-Co** in MeOH-D$_4$ (400 MHz).

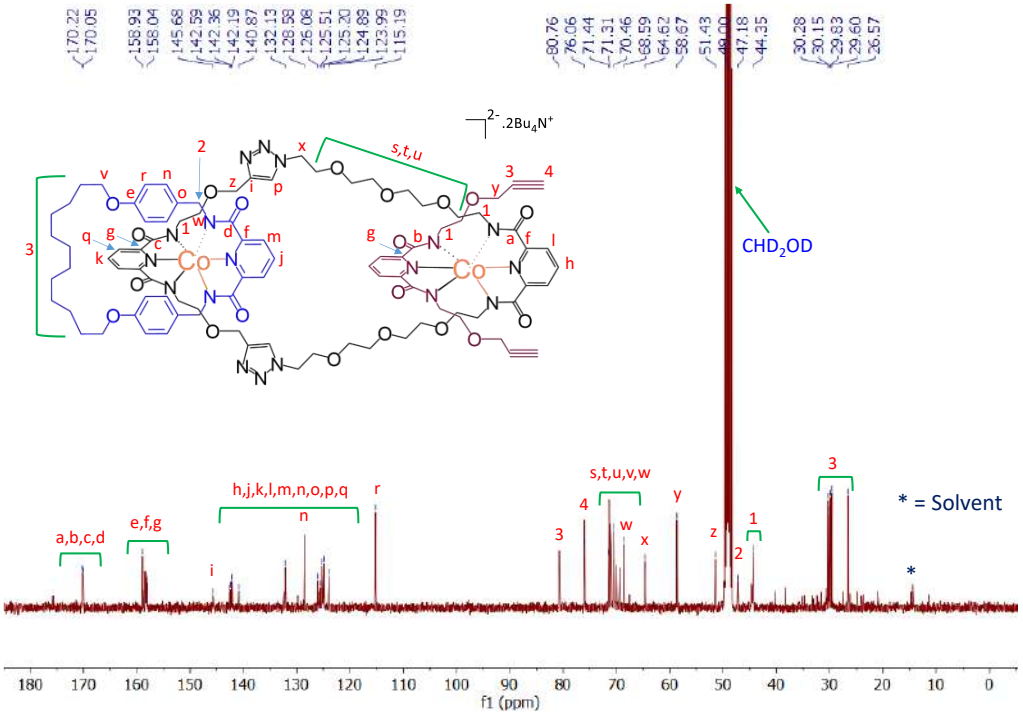

Figure 3.18. ^{13}C-NMR spectra of **[3]PR-Y-Co** in MeOH-D$_4$ (100 MHz).

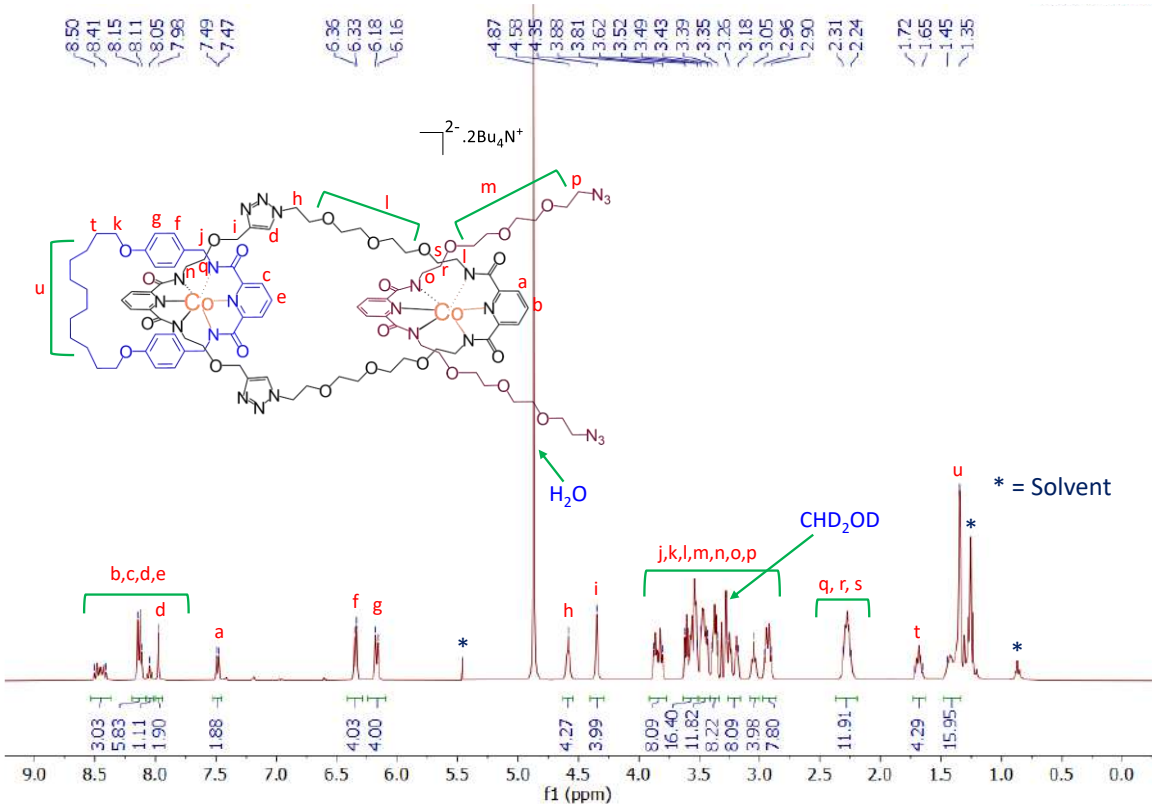

Figure 3.19. ^{1}H-NMR spectra of **[3]PR-A-Co** in MeOH-D4 (400 MHz).

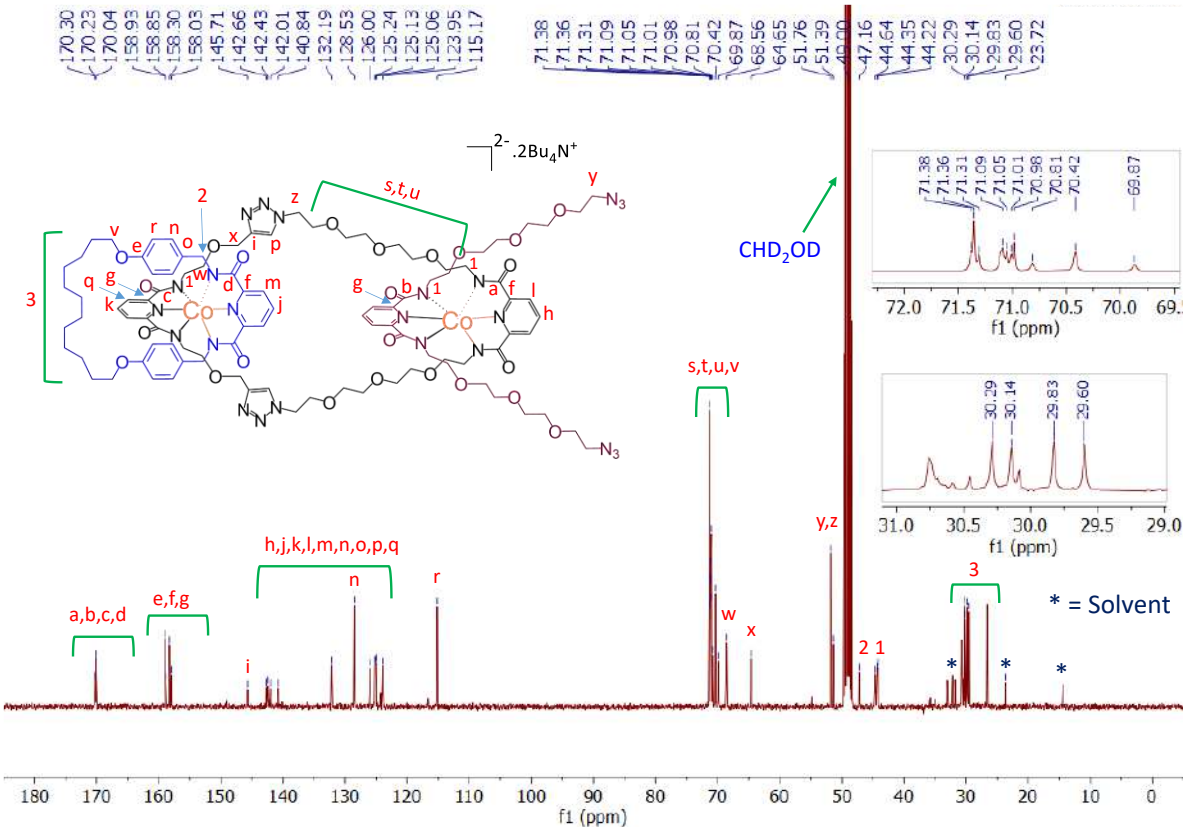

Figure 3.20. ^{13}C-NMR spectra of **[3]PR-A-Co** in MeOH-D4 (100 MHz).

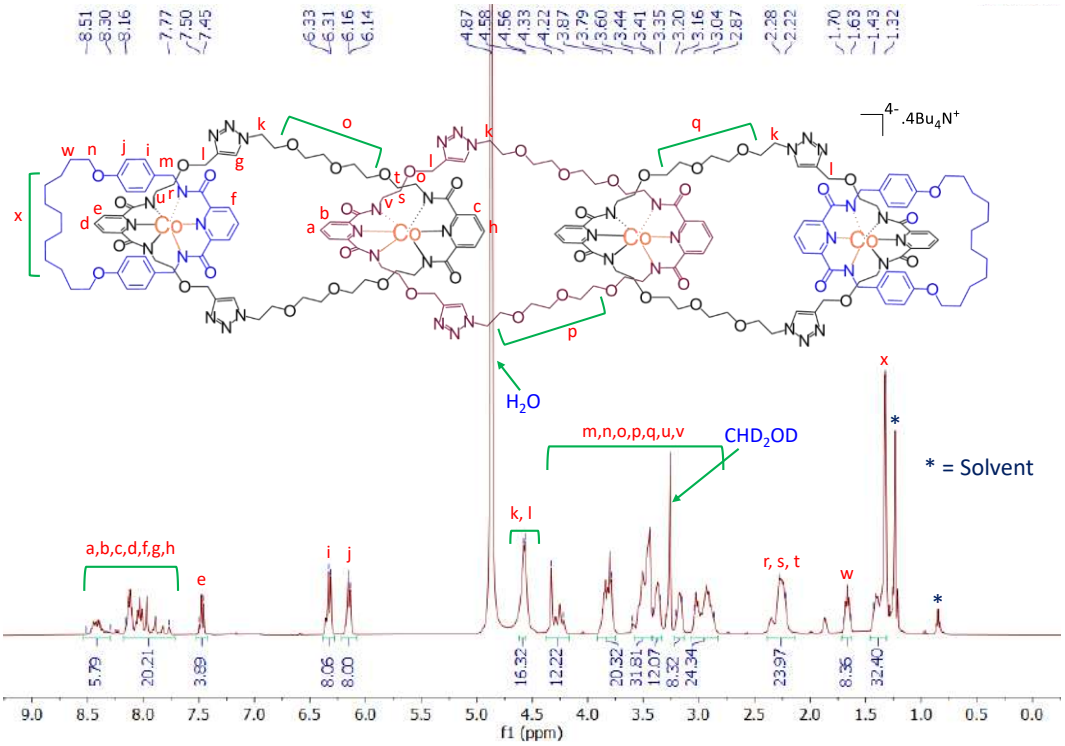

Figure 3.21. ^{1}H-NMR spectra of Co(III)-metalated linear [5]catenane, **L[5]Co** in MeOH-D$_4$ (400 MHz).

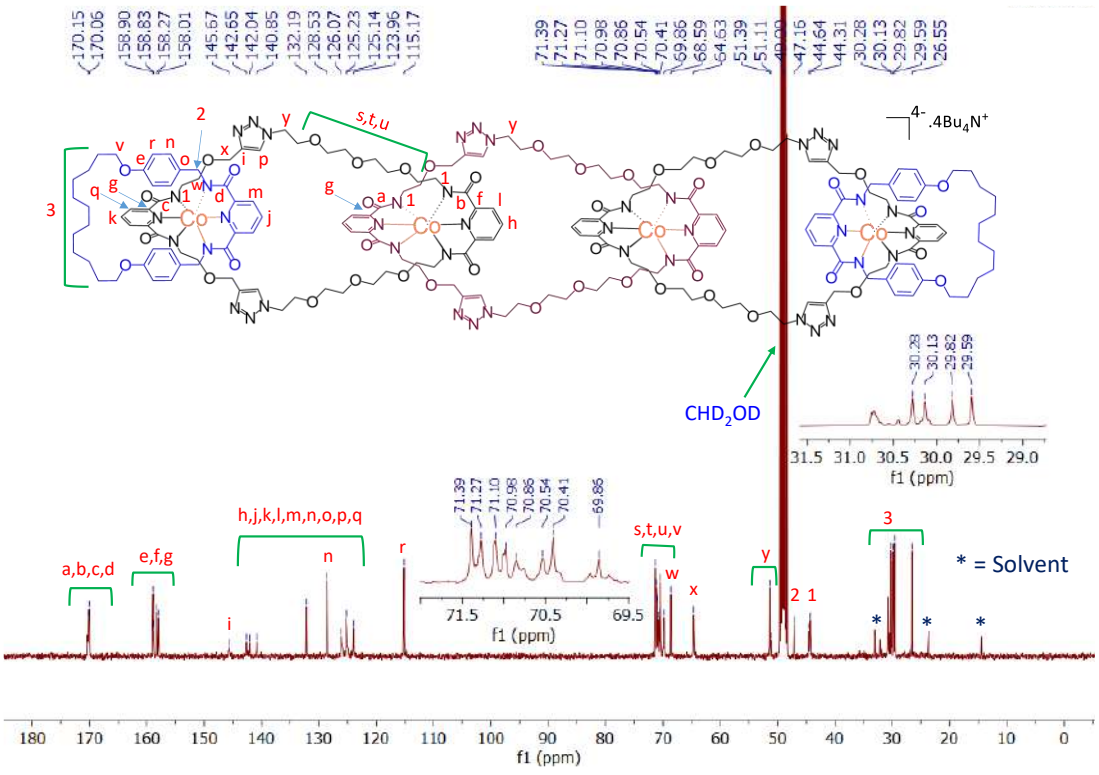

Figure 3.22. ^{13}C-NMR spectra of Co(III)-metalated linear [5]catenane, **L[5]Co** in MeOH-D$_4$ (100 MHz).

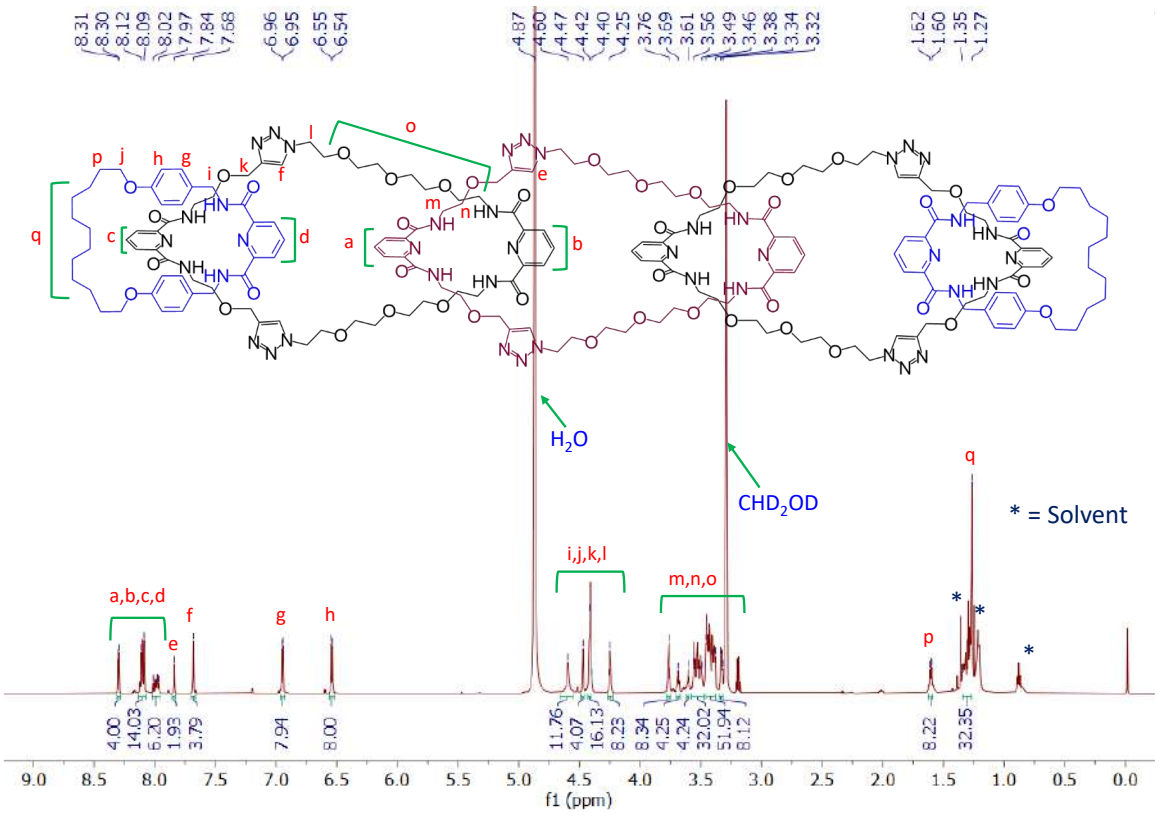

Figure 3.23. ^{1}H-NMR spectra of linear [5]catenane, **L[5]** in MeOH-D$_4$ (700 MHz).

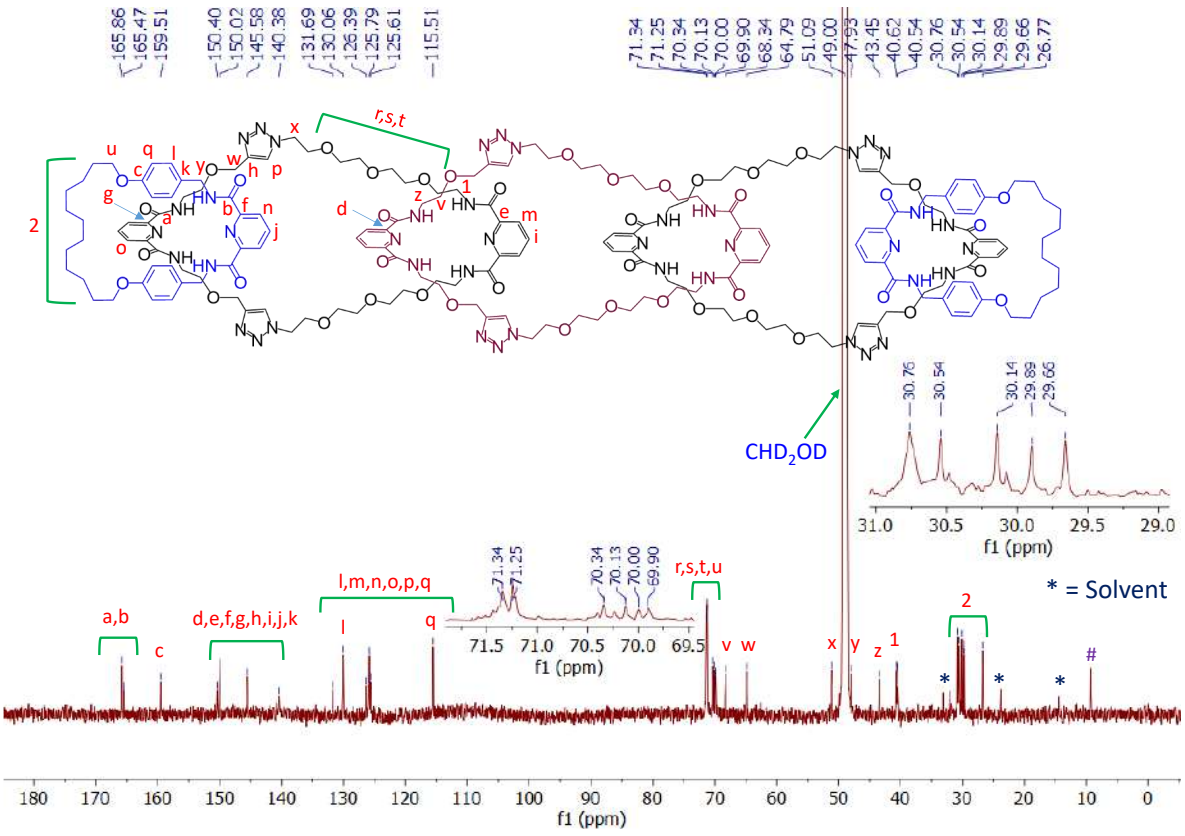

Figure 3.24. ^{13}C-NMR spectra of linear [5]catenane, **L[5]** in MeOH-D$_4$ (175 MHz).

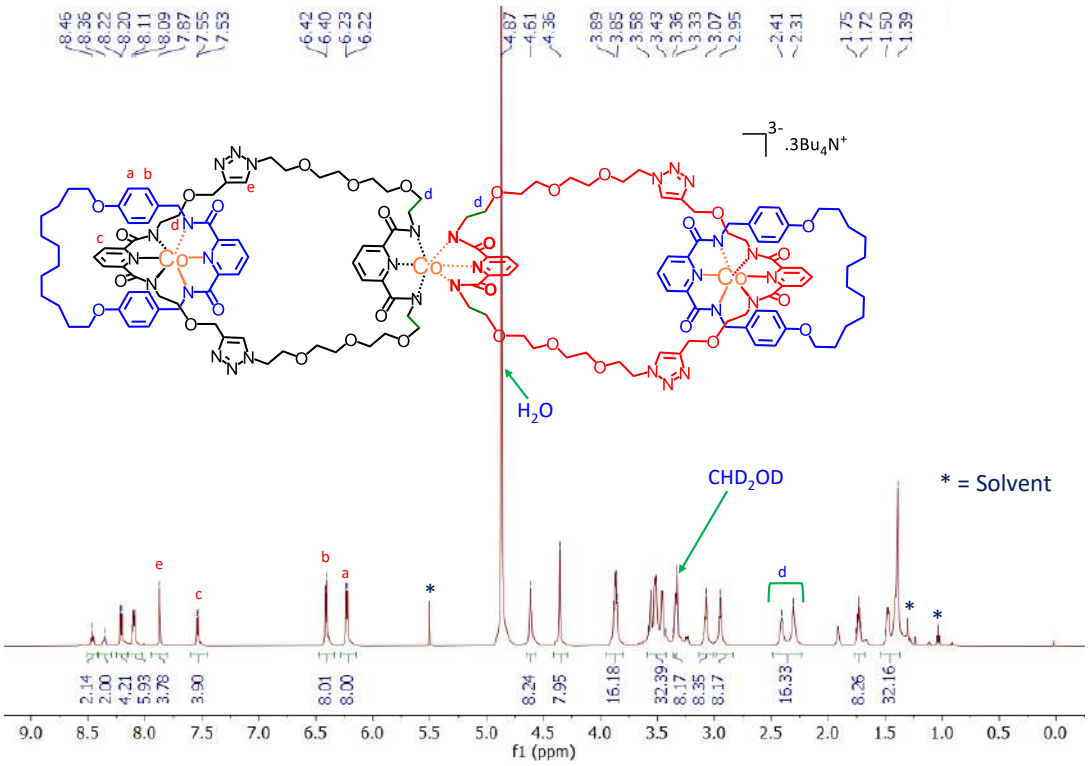

Figure 3.25. ^{1}H-NMR spectra of dimer of metalated [2]catenane, **[2]Co-D** in MeOH-D$_4$(700 MHz).

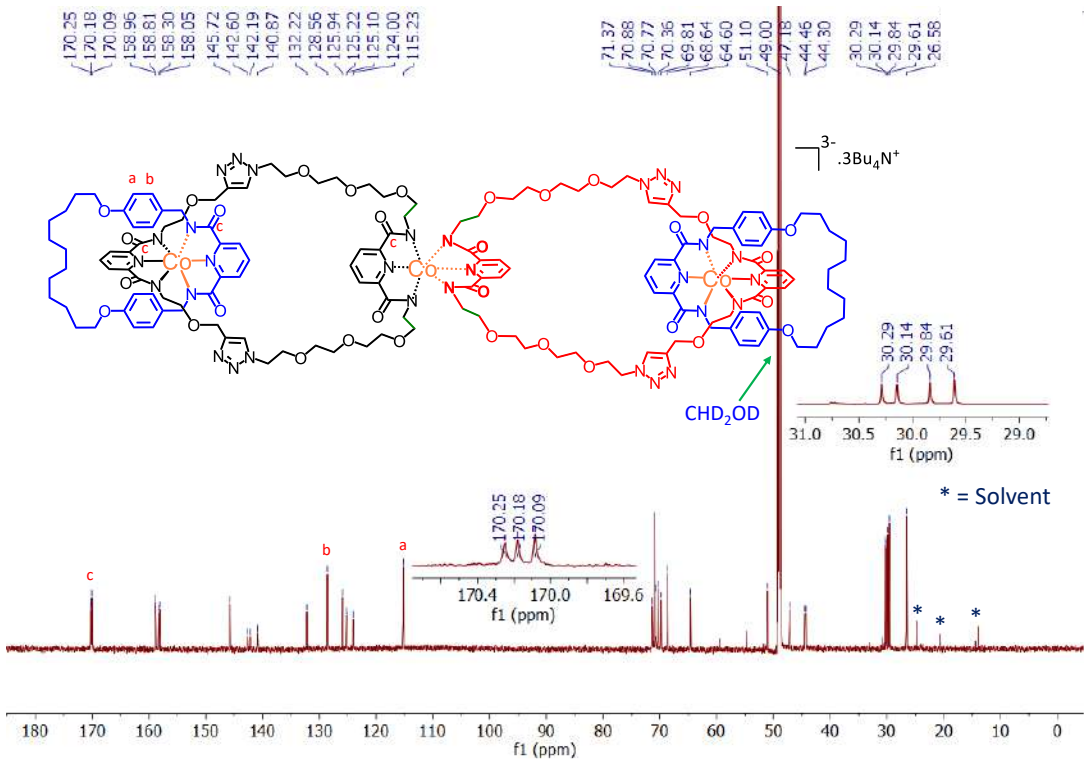

Figure 3.26. ^{13}C-NMR spectra of dimer of metalated [2]catenane, **[2]Co-D** in MeOH-D$_4$ (175 MHz).

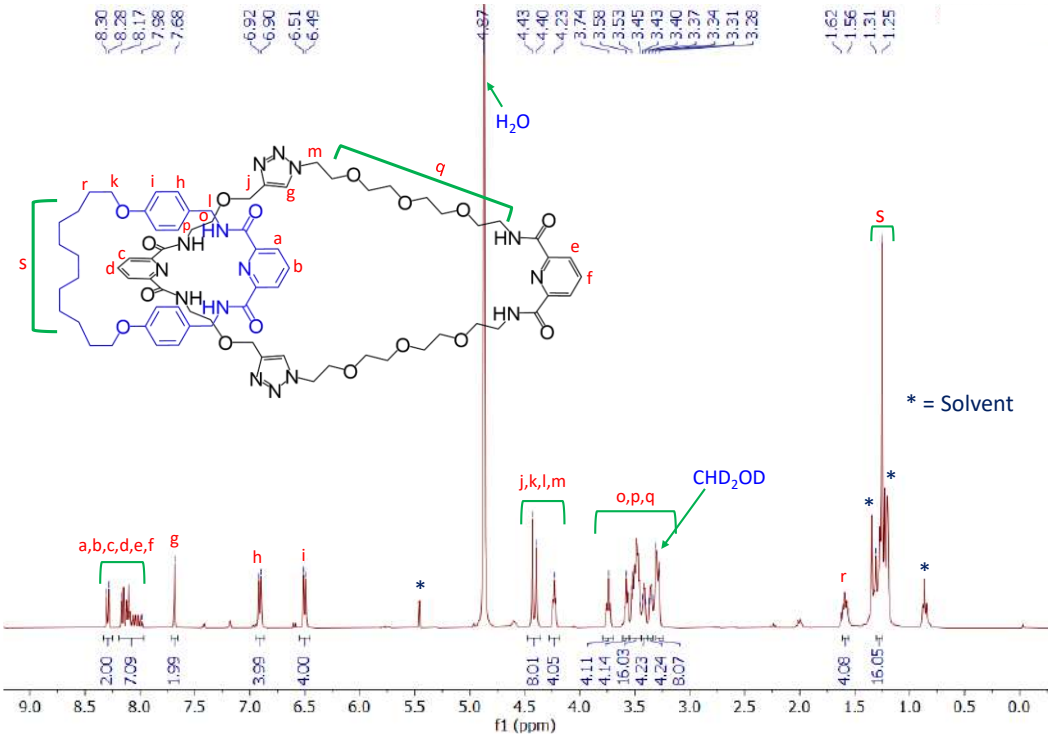

Figure 3.27. ^{1}H-NMR spectra of fully organic [2]catenane from **[2]Co-D** in MeOH-D4 (400 MHz).

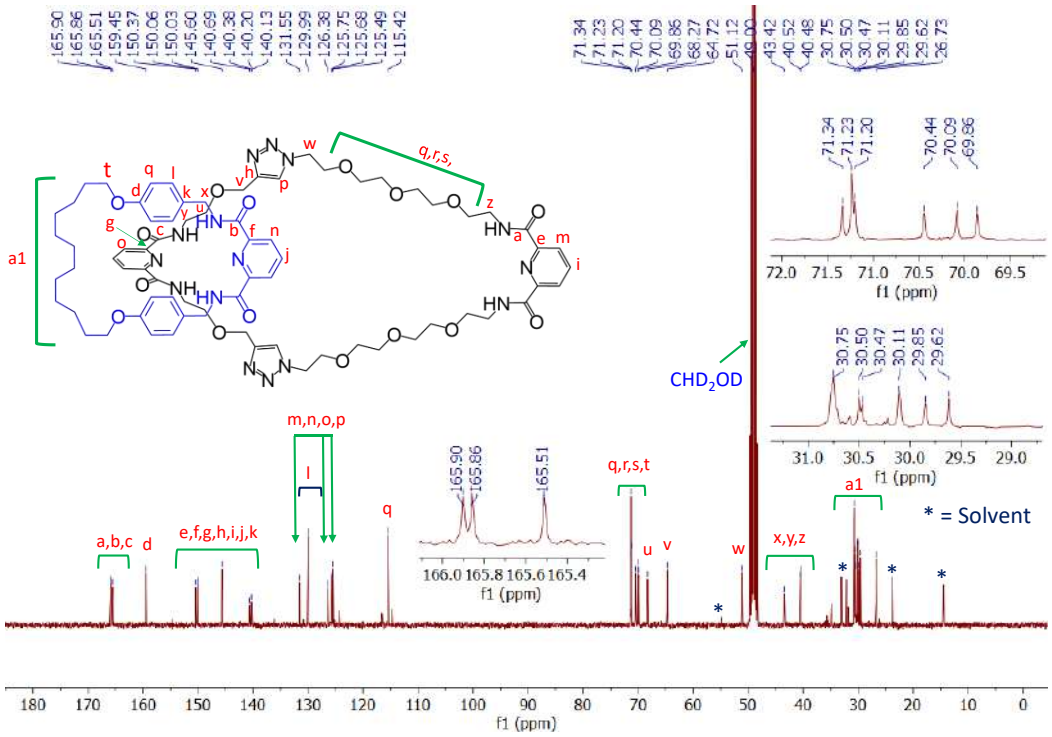

Figure 3.28. ^{13}C-NMR spectra of fully organic [2]catenane from **[2]Co-D** in MeOH-D4 (100 MHz).

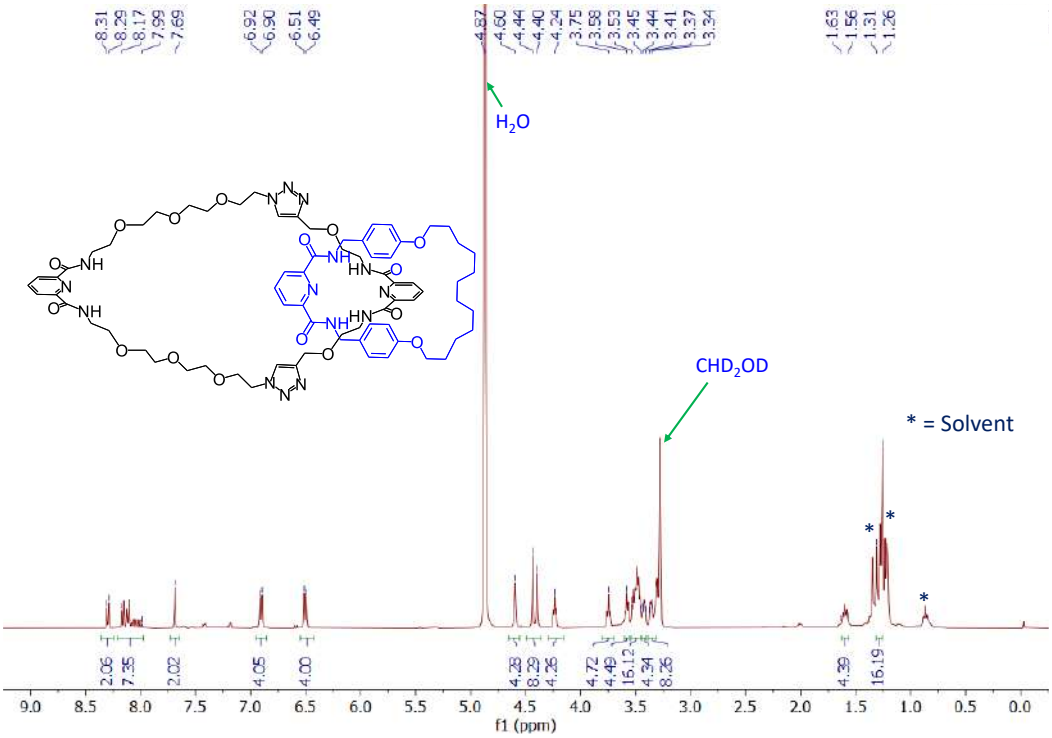

Figure 3.29. ^{1}H-NMR spectra of fully organic [2]catenane (in MeOH-D4, 400 MHz) formed during demetalation of **L[5]Co.**

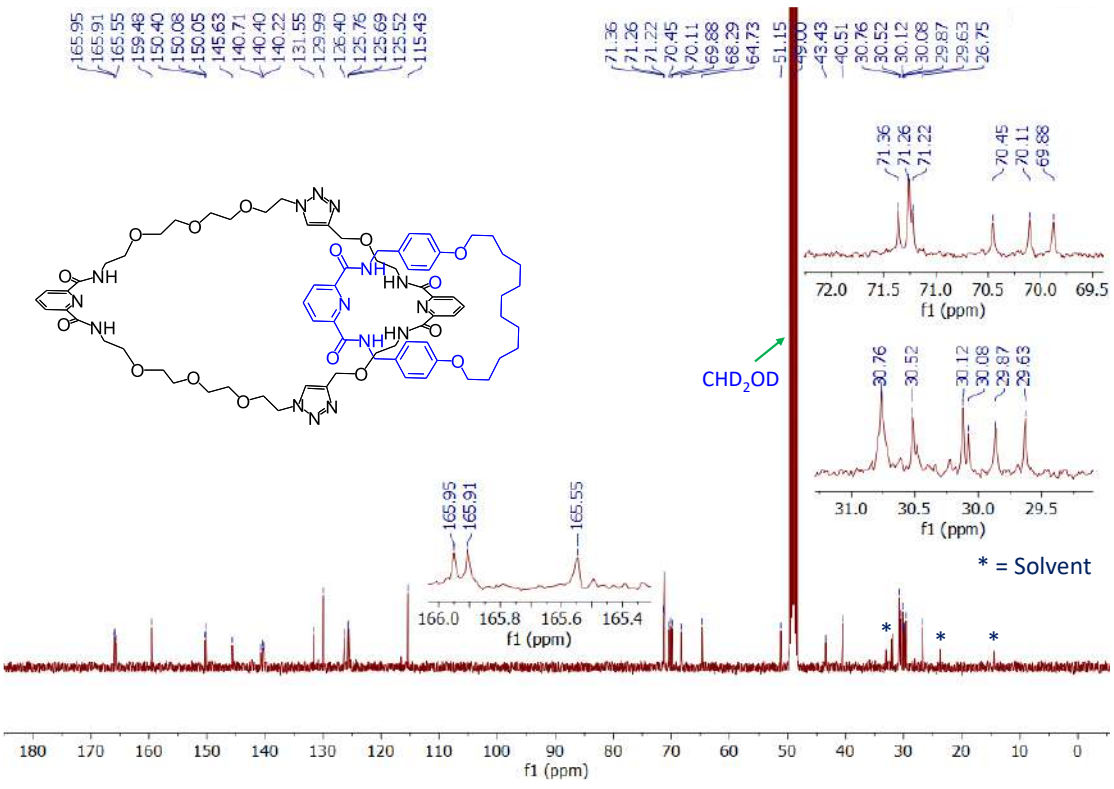

Figure 3.30. ^{13}C-NMR spectra of fully organic [2]catenane, (in MeOH-D4, 100 MHz) formed during demetalation of **L[5]Co.**

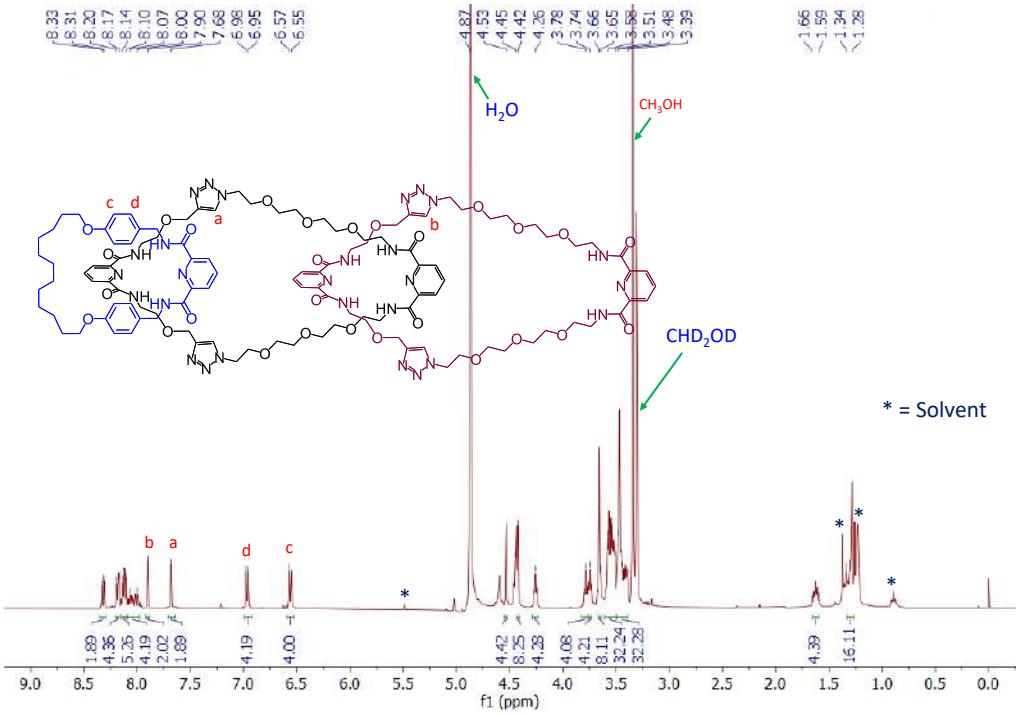

Figure 3.31. ^{1}H-NMR spectra of fully organic linear [3]catenane, **L[3]** (in MeOH-D_4, 400 MHz) formed during demetalation of **L[5]Co.**

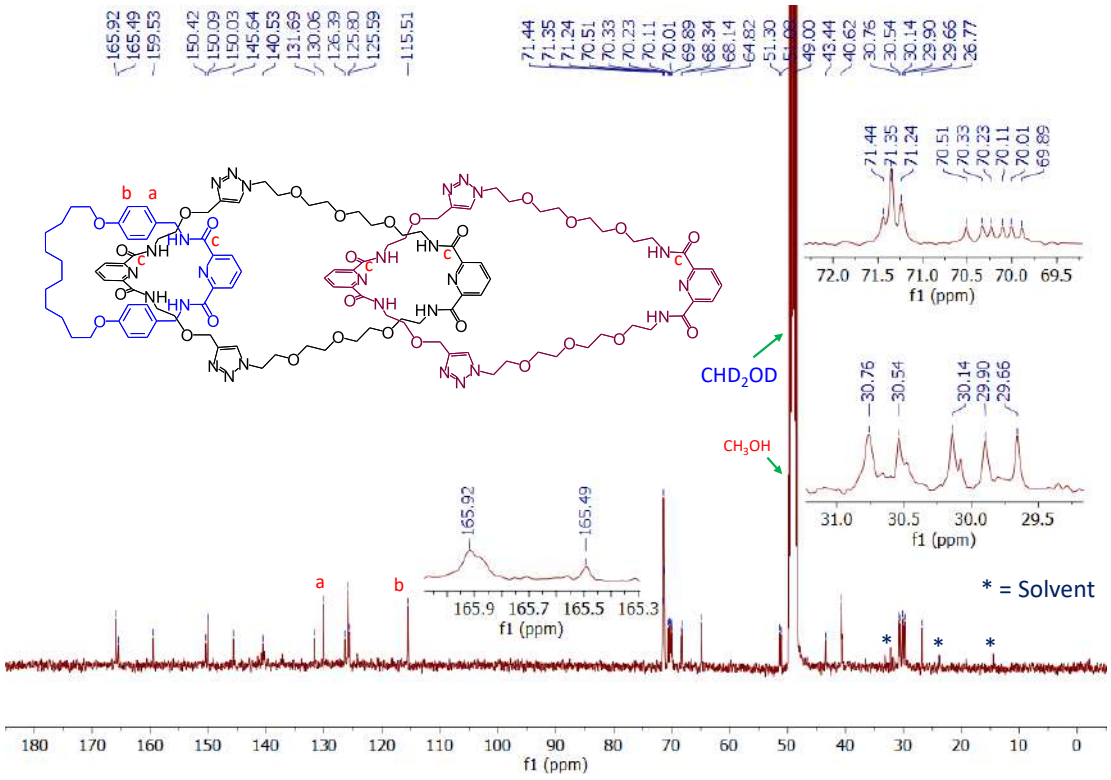

Figure 3.32. ^{13}C-NMR spectra of fully organic linear [3]catenane, **L[3]** (in MeOH-D_4, 100 MHz) formed during demetalation of **L[5]Co.**

3.6.2. Mass Spectra:

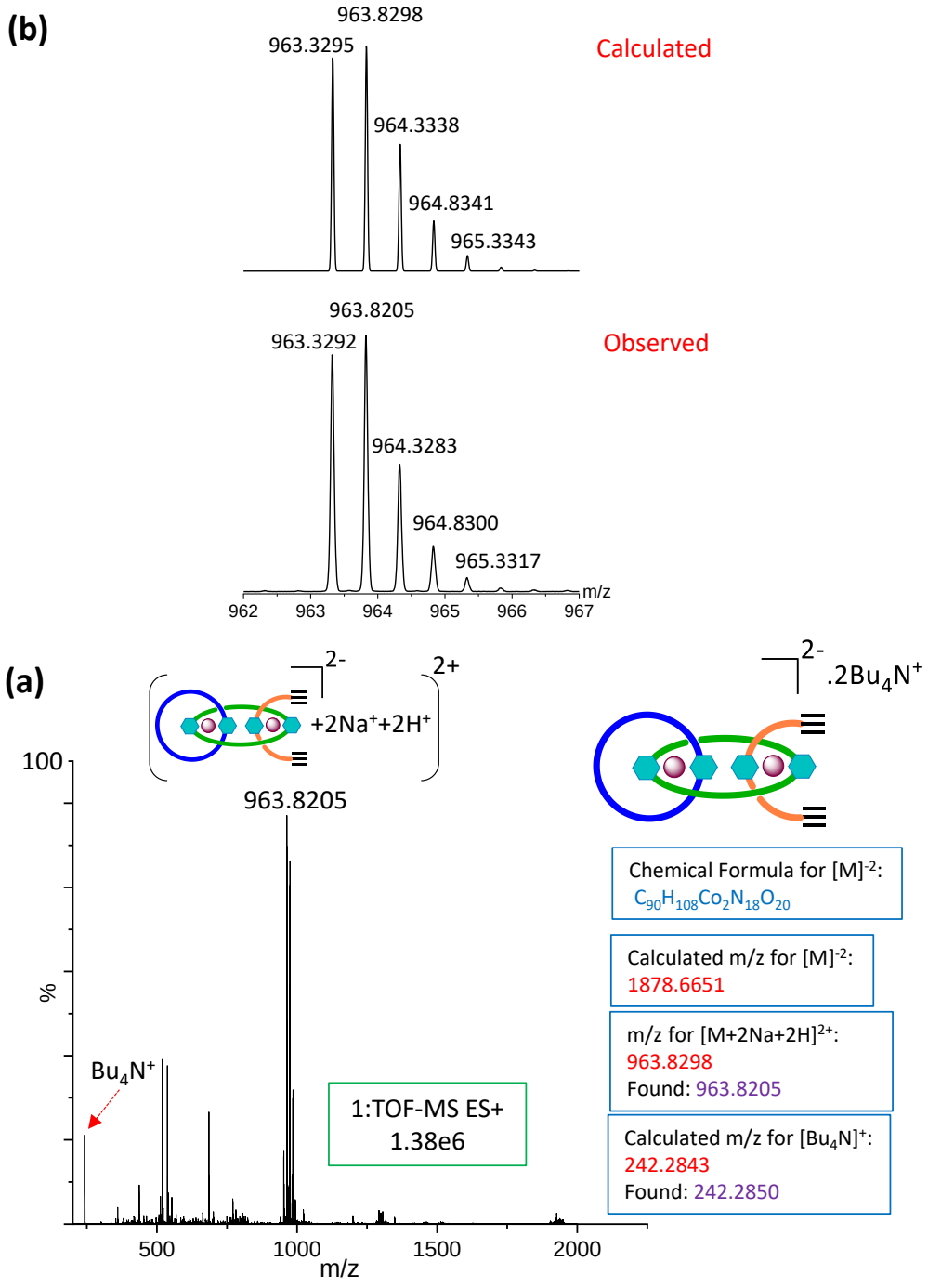

Figure 3.33. Mass spectra (ESI^+) analysis for synthesized di-alkyne terminus [3]pseudo-rotaxane **[3]PR-Y-Co** (a) full spectra (b) comparison between calculated and experimentally observed isotopic distribution peaks.

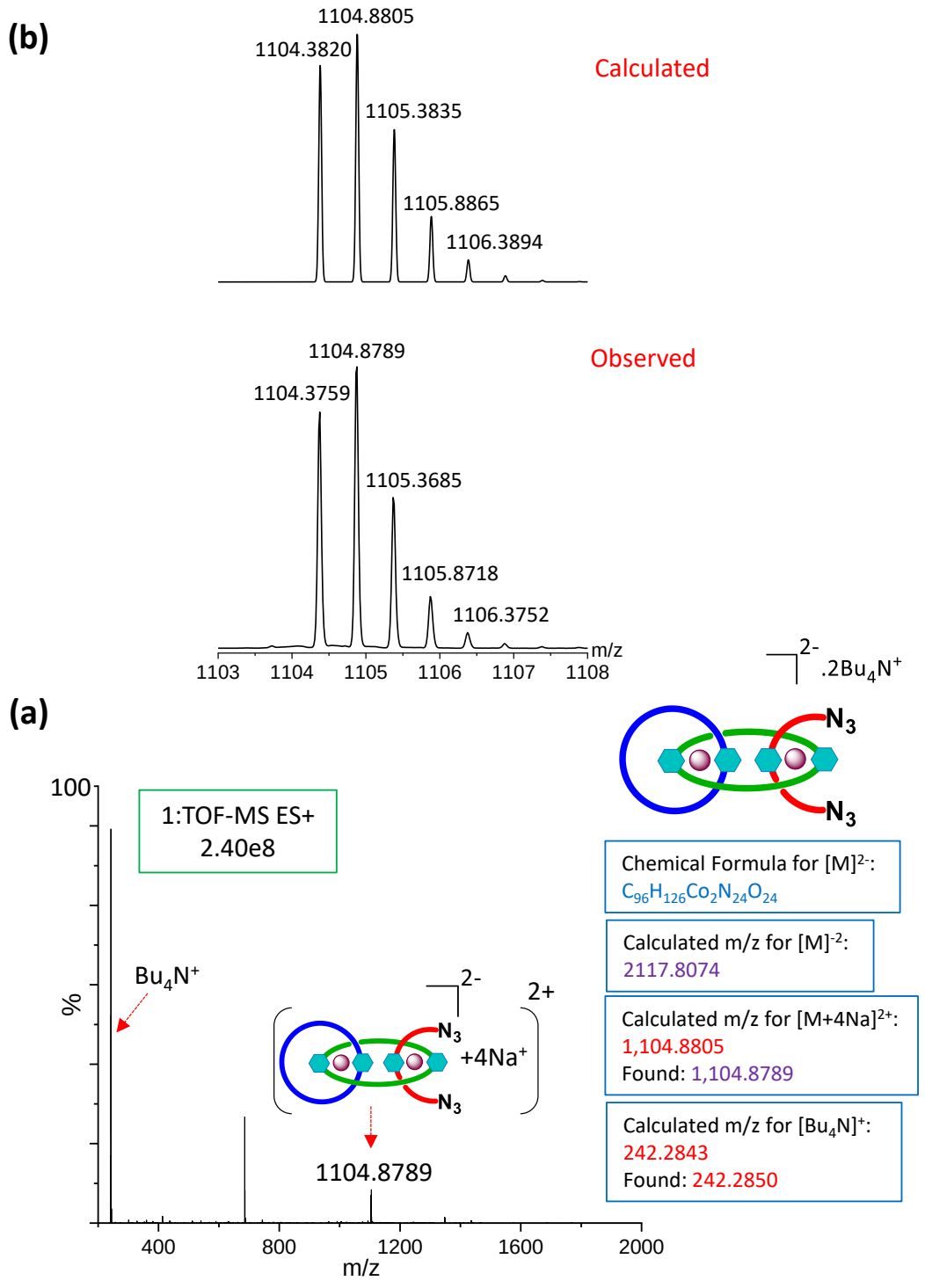

Figure 3.34. Mass spectra (ESI^+) analysis for synthesized di-azide terminus [3]pseudorotaxane **[3]PR-A-Co** (a) full spectra (b) comparison between calculated and experimentally observed isotopic distribution peaks.

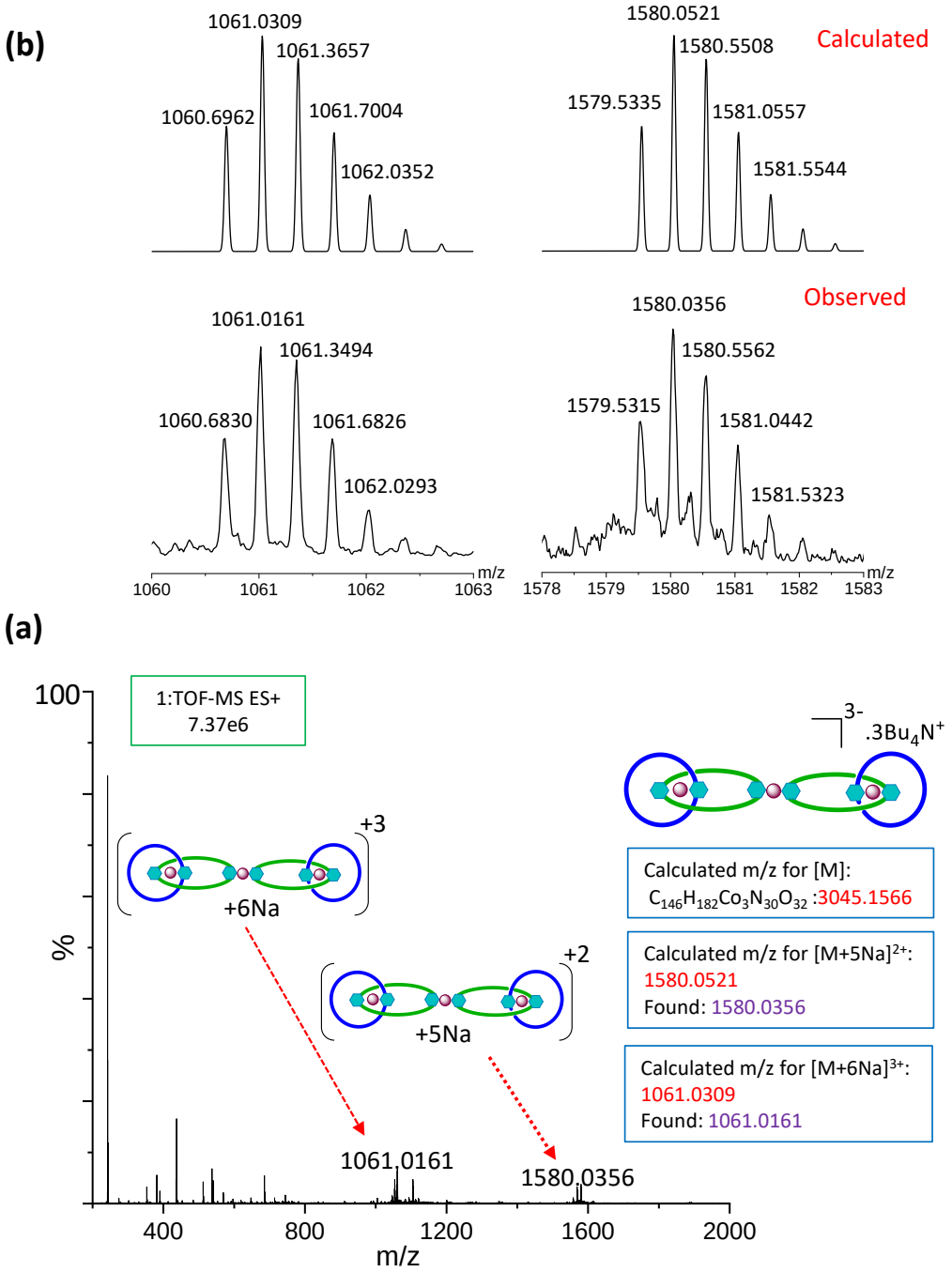

Figure 3.35. Mass spectra (ESI^+) analysis for synthesized metalated [2]catenane dimer, **[2]Co-D** (a) full spectra (b) comparison between calculated and experimentally observed isotopic distribution peaks.

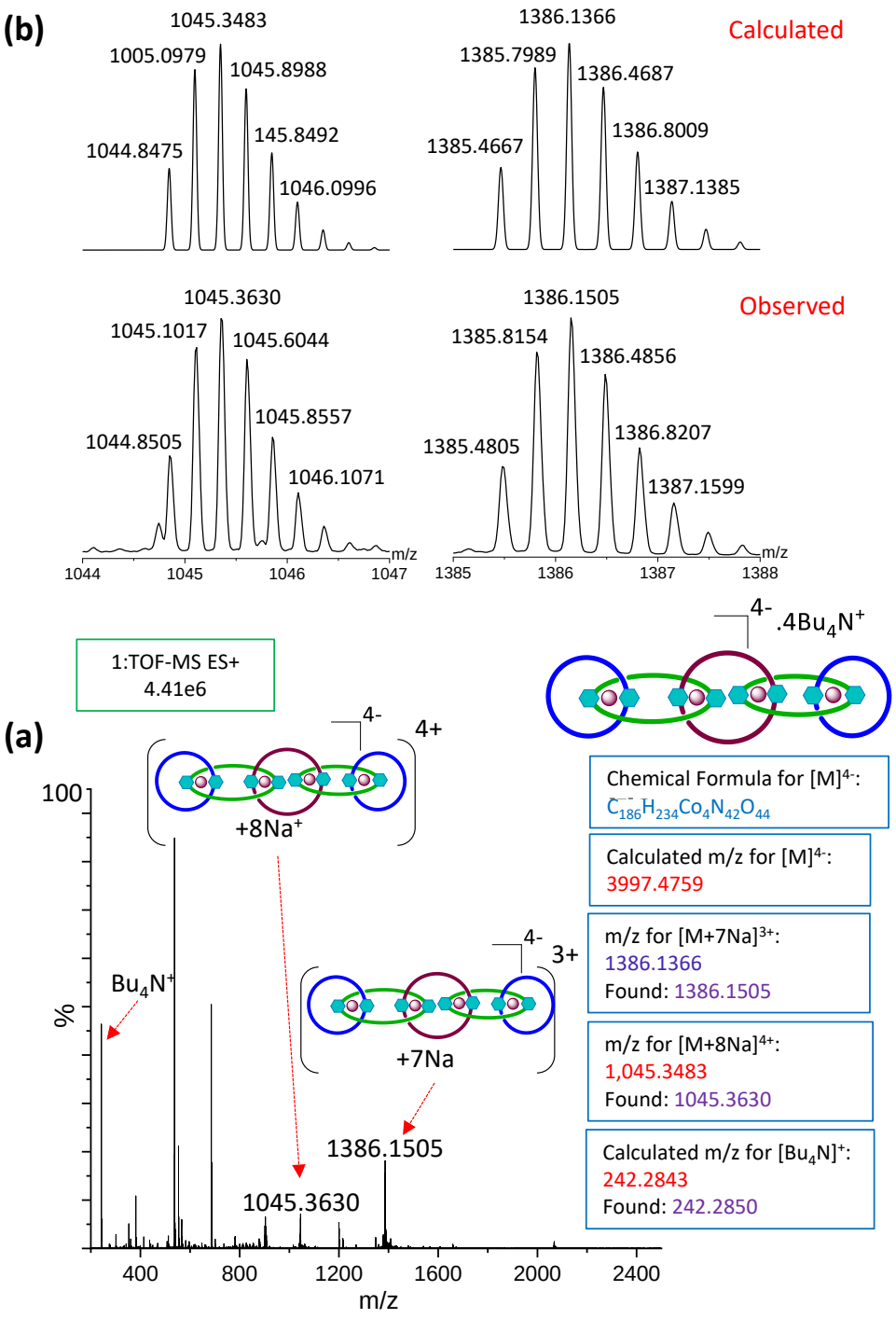

Figure 3.36. Mass spectra (ESI^+) analysis for synthesized **L[5]Co** (a) full spectra (b) comparison between calculated and experimentally observed isotopic distribution peaks.

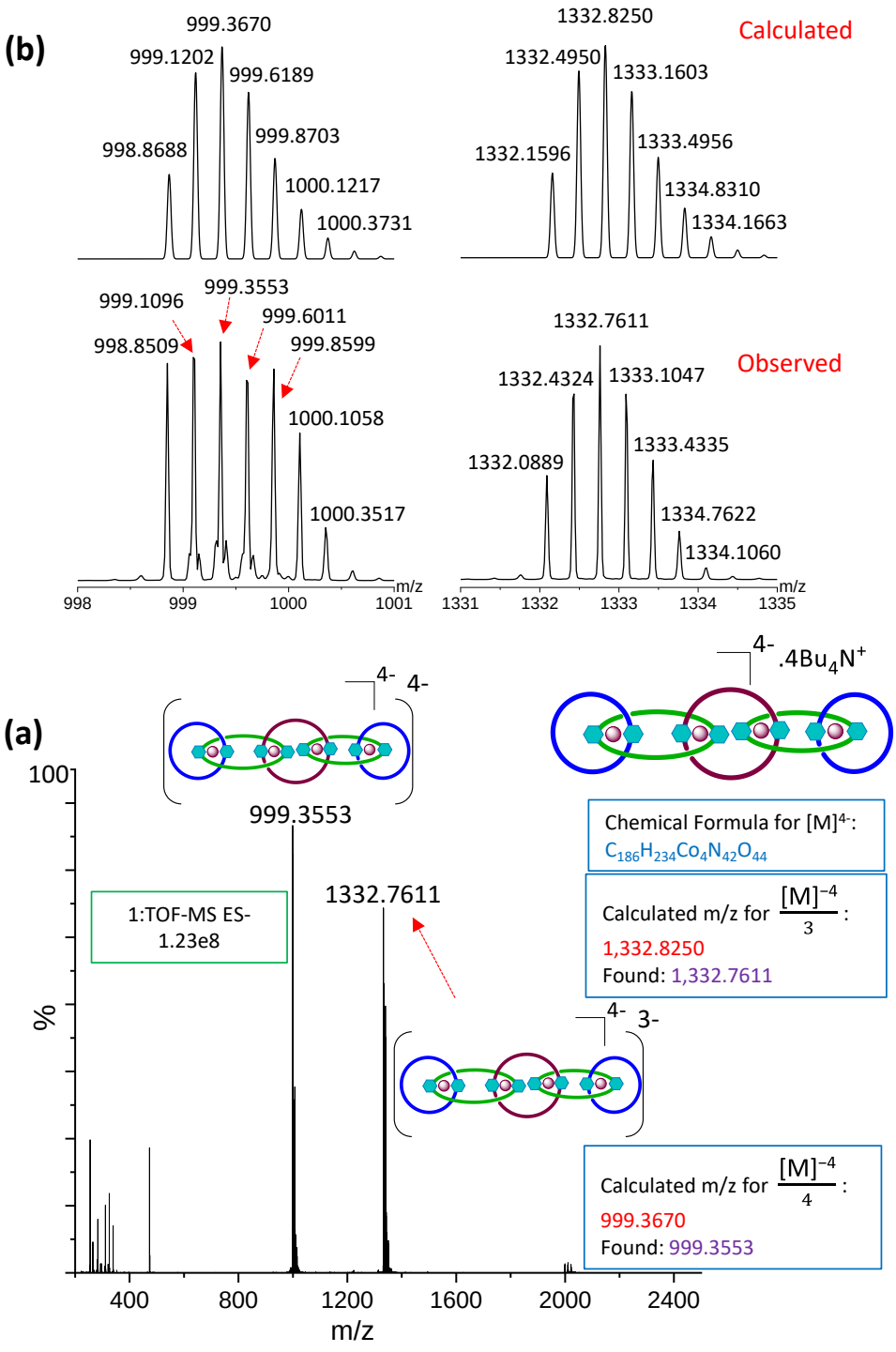

Figure 3.37. Mass spectra (ESI^-) analysis for synthesized **L[5]Co** (a) full spectra (b) comparison between calculated and experimentally observed isotopic distribution peaks.

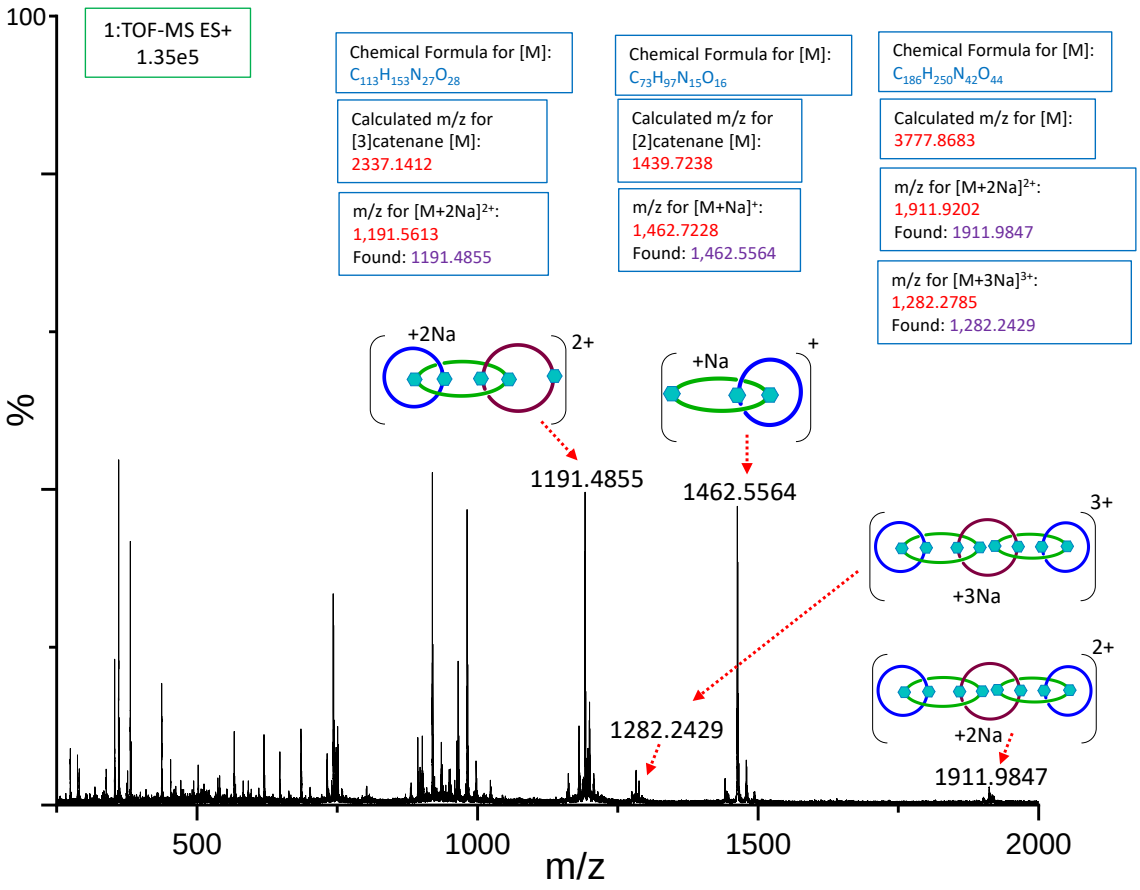

Figure 3.38. Mass spectra (ESI^+) analysis for reaction mixture after removal of cobalt(III)-metal ion from synthesized **L[5]Co**; shows peaks for solely organic [2], linear [3] and linear [5]catenane.

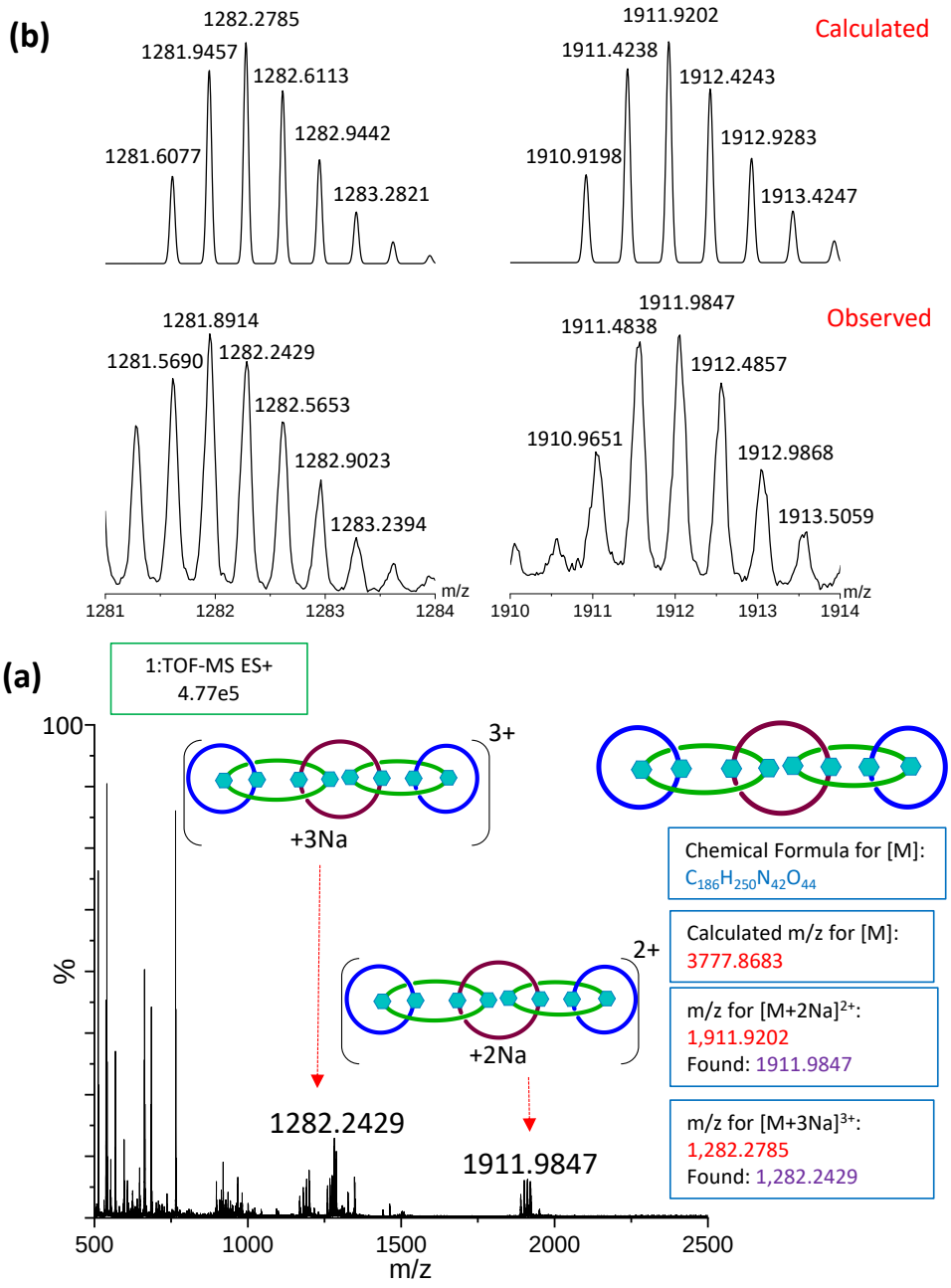

Figure 3.39. Mass spectra (ESI^+) analysis for synthesized **L[5]C** (a) full spectra (b) comparison between calculated and experimentally observed isotopic distribution peaks.

3.7. Reference:

1. Y. Xie, C. Y. Wang, N. Chen, Z. Cao, G. Wu, B. Yin, Y. Li, *Angew. Chem. Int. Ed.* **2023**, *62*, e202309605.
2. H. Min Tay, T. G. Johnson, A. Docker, M. J. Langton, P. D. Beer, *Angew. Chem. Int. Ed.* **2023**, *62*, e202312745.
3. L. Fang, C. Wang, A. C. Fahrenbach, A. Trabolsi, Y. Y. Botros, J. F. Stoddart, *Angew. Chem. Int. Ed.* **2011**, *50*, 1805–1809.
4. David A. Leigh, Jenny K. Y. Wong, Franc, ois Dehez, F. Zerbetto, *Nature* **2003**, *424*, 174–179.
5. a) L. Zhu, J. Li, J. Yang, H. Y. Au-Yeung, *Chem. Sci.* **2020**, *11*, 13008–13014; b) R. Mitra, H. Zhu, S. Grimme, J. Niemeyer, *Angew. Chem. Int. Ed.* **2017**, *56*, 11456–11459; c) X. Mo, Y. Deng, S. K. Lai, X. Gao, H. L. Yu, K. H. Low, Z. Guo, H. L. Wu, H. Y. Au-Yeung, E. C. M. Tse, *J. Am. Chem. Soc.* **2023**, *145*, 6087–6099; d) Y. Jiao, L. Dordevic, H. Mao, R. M. Young, T. Jaynes, H. Chen, Y. Qiu, K. Cai, L. Zhang, X. Y. Chen, Y. Feng, M. R. Wasielewski, S. I. Stupp, J. F. Stoddart, *J. Am. Chem. Soc.* **2021**, *143*, 8000–8010.
6. A. Bessaguet, Q. Blancart-Remaury, P. Poinot, I. Opalinski, S. Papot, *Angew. Chem. Int. Ed.* **2023**, *62*, e202216787.
7. M. Steudel, E. Ubasart, L. Leanza, M. Pujals, T. Parella, G. M. Pavan, X. Ribas, M. von Delius, *Angew. Chem. Int. Ed.* **2023**, *62*, 202309393.
8. K. M. Bak, B. Trzaskowski, M. J. Chmielewski, *Chem. Sci.* **2024**, *15*, 1796–1809.
9. a) Y. Wang, J. Gong, X. Wang, W. J. Li, X. Q. Wang, X. He, W. Wang, H. B. Yang, *Angew. Chem. Int. Ed.* **2022**, *61*, e202210542; b) Y. Yao, Y. C. Tse, S. K. Lai, Y. Shi, K. H. Low, H. Y. Au-Yeung, *Nat. Commun.* **2024**, *15*, 1952

10. a) M. A. Nosiglia, N. D. Colley, M. K. Danielson, M. S. Palmquist, A. O. Delawder, S. L. Tran, G. H. Harlan, J. C. Barnes, *J. Am. Chem. Soc.* **2022**, *144*, 9990–9996; b) R. Bai, Z. Zhang, W. Di, X. Yang, J. Zhao, H. Ouyang, G. Liu, X. Zhang, L. Cheng, Y. Cao, W. Yu, X. Yan, *J. Am. Chem. Soc.* **2023**, *145*, 9011–9020; c) L. Chen, W. You, J. Wang, X. Yang, D. Xiao, H. Zhu, Y. Zhang, G. Li, W. Yu, J. L. Sessler, F. Huang, *J. Am. Chem. Soc.* **2024**, *146*, 1109–1121; d) M. Ebe, A. Soga, K. Fujiwara, B. J. Ree, H. Marubayashi, K. Hagita, A. Imasaki, M. Baba, T. Yamamoto, K. Tajima, T. Deguchi, H. Jinnai, T. Isono, T. Satoh, *Angew. Chem. Int. Ed.* **2023,** *62*, e202304493; e) H. Marubayashi, M. Ebe, A. Imasaki, K. Fujiwara, N. Mashita, K. Hagita, T. Murashima, S. Mori, T. Isono, T. Satoh, H. Jinnai, *Polymer* **2024**, *292*, 126607.
11. H. Y. Au-Yeung, Y. Deng, *Chem. Sci.* **2022**, *13*, 3315–3334.
12. Mena-Hernando, E. M. Perez, *Chem. Soc. Rev.* **2019**, *48*, 5016–5032.
13. a) A. Bu, Y. Zhao, H. Xiao, C. H. Tung, L. Z. Wu, H. Cong, *Angew. Chem. Int. Ed.* **2022**, *61*, e202209449; b) A. Li, Z. Tan, Y. Hu, Z. Lu, J. Yuan, X. Li, J. Xie, J. Zhang, K. Zhu, *J. Am. Chem. Soc.* **2022**, *144*, 2085–2089; c) N. D. Colley, M. A. Nosiglia, S. L. Tran, G. H. Harlan, C. Chang, R. Li, A. O. Delawder, Y. Zhang, J. C. Barnes, *ACS Cent. Sci.* **2022**, *8*, 1672–1682.
14. a) L. Zhang, A. J. Stephens, A. L. Nussbaumer, J. F. Lemonnier, P. Jurcek, I. J. Vitorica-Yrezabal, D. A. Leigh, *Nat. Chem.* **2018**, *10*, 1083–1088; b) M. T. Nguyen, D. P. Ferris, C. Pezzato, Y. Wang, J. F. Stoddart, *Chem* **2018**, *4*, 2329–2344
15. D. P. August, R. A. W. Dryfe, S. J. Haigh, P. R. C. Kent, D. A. Leigh, J. F. Lemonnier, Z. Li, C. A. Muryn, L. I. Palmer, Y. Song, G. F. S. Whitehead, R. J. Young, *Nature* **2020**, *588*, 429–435.

16. a) D. A. Leigh, L. Pirvu, F. Schaufelberger, *J. Am. Chem. Soc.* **2019**, *141*, 6054–6059; b) D. A. Leigh, J. J. Danon, S. D. P. Fielden, J. F. Lemonnier, G. F. S. Whitehead, S. L. Woltering, *Nat. Chem.* **2021**, *13*, 117–122.
17. a) M. B. Podh, R. Ratha, C. S. Purohit, *Chem. Asian J.* **2024**, e202400031; b) M. Gauthier, K. Fournel-Marotte, C. Clavel, P. Waeles, P. Laurent, F. Coutrot, *Angew. Chem. Int. Ed.* **2023**, *62*, e202310643
18. a) T. A. Barendt, L. Ferreira, I. Marques, V. Felix, P. D. Beer, *J. Am. Chem. Soc.* **2017**, *139*, 9026–9037; b) N. Ponnuswamy, F. B. Cougnon, G. D. Pantos, J. K. Sanders, *J. Am. Chem. Soc.* **2014**, *136*, 8243–8251.
19. D. Megiatto, Jr., D. I. Schuster, *Chemistry* **2009**, *15*, 5444–5448.
20. D. B. Amabilino, P. R. Ashton, A. S. Reder, N. Spencer, J. F. Stoddart, *Angew. Chem. Int. Ed.* **1994**, *33*, 1286–1290.
21. H. Iwamoto, S. Tafuku, Y. Sato, W. Takizawa, W. Katagiri, E. Tayama, E. Hasegawa, Y. Fukazawa, T. Haino, *Chem. Commun.* **2016**, *52*, 319–322.
22. a) N. D. Colley, M. A. Nosiglia, L. Li, F. Amir, C. Chang, A. F. Greene, J. M. Fisher, R. Li, X. Li, J. C. Barnes, *Inorg. Chem.* **2020**, *59*, 10450–10460; b) G. H. Harlan, S. L. Tran, N. D. Colley, M. A. Nosiglia, Y. Zhang, J. C. Barnes, *Cell Rep. Phys Sci.* **2024**, *5*, 101767.
23. W. H. Ng, S. K. Lai, C. C. Yee, H. Y. Au-Yeung, *Angew. Chem. Int. Ed.* **2022**, *61*, e202110200.
24. Qiong Wu, Phillip M. Rauscher, Xiaolong Lang, Rudy J. Wojtecki, Juan J. de Pablo, Michael J. A. Hore, S. J. Rowan, *Science* **2017**, *358*, 1434–1439.
25. D. A. Leigh, F. Schaufelberger, L. Pirvu, J. H. Stenlid, D. P. August, J. Segard, *Nature* **2020**, *584*, 562–568.

26. David A. Leigh, Paul J. Lusby, Roy T. McBurney, Alessandra Morelli, Alexandra M. Z. Slawin, Andrew R. Thomson, D. B. Walker, *J. Am. Chem. Soc.* **2009**, *131*, 3762–3771.
27. H. Ishibashi, M. Rondelli, H. Shudo, T. Maekawa, H. Ito, K. Mizukami, N. Kimizuka, A. Yagi, K. Itami, *Angew. Chem. Int. Ed.* **2023**, *62*, e202310613.
28. M. B. Podh, R. Ratha, C. S. Purohit, *Chem. Asian J.* **2024**, *19*, e202400031.
29. D. A. Leigh, P. J. Lusby, R. T. McBurney, A. Morelli, A. M. Z. Slawin, A. R. Thomson, D. B. Walker, *J. Am. chem. Soc.* **2009**, *131*, 3762-3771

Chapter 4: Metal Ion-Responsive Dynamics in a Homo [2]Catenane: Circumrotation and Pirouetting

4.1. Abstract:

We describe a homo [2]catenane that is stable in two conformations and demonstrates a large-amplitude co-conformational change during the exchange between Cu(I) and Co(III)-metal ion. Each ring comprises a bi-dentate diphenyl-phenanthroline and a tri-dentate pyridine-diamide metal templating center.

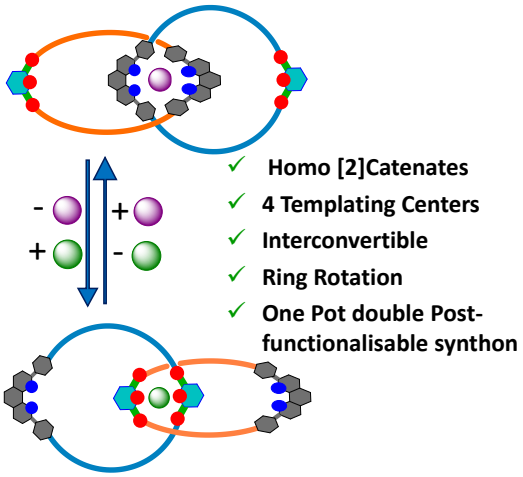

The Presence of multiple coordination centers results in orthogonal complexation behaviour with suitable metal ions, leading to a relative motion between the interlocked rings via pirouetting and circumrotation. Interconvertible catenates via homo [2]catenane has been characterized by ^{1}H-NMR, ^{13}C-NMR, mass, UV-visible spectroscopy and variable temperature NMR experiments.

4.2. Introduction:

Mechanically interlocked molecules (MIMs) such as catenanes can have many stable co-conformations among the interlocked components. [1,2] Interconversion among these conformations is often possible due to relative motion of interlocked rings, when triggered with stimulus such as electrical, [3] chemical, [4,5] electrochemical, [6] ionic guest, [7,8] etc. Sometimes, structural features such as π-π stacking [9] and ion-dipole interaction [10,11] help such motion. Such stimuli-triggered motion, when guided unidirectionally, results in synthetic molecular motors. [3-5,12,13] Moreover, ring rotation and switching imparts interesting properties to this class of molecules such as, circularly polarized luminescence (CPL),[14,15] chirality,[7,16] tuning light emitting properties[10,17,18] and memory device application.[19]

Out of various techniques designed to make relative motion in catenanes, metal triggered motion has unique advantages.[20] The stable nature of metal complexes and properties of the templating ion can generate controlled translocation of interlocked components.[21,22] Only a few reports are known for synthesis and co-conformational switching studies of catenanes having multiple metal bonding sites. One report relies on the important differences of stereochemical requirements for coordination of Cu(I) and Cu(II). When the catenane is complexed with Cu(I), the phenanthroline units from both the ring coordinate, but when it is oxidised, the terpyridine units coordinates changing one conformer to another.[23] Another report demonstrates a half rotation of one ring w.r.t. other by metalation and demetallation of Pd^{2+} ion.[21] They also designed a [2]catenane with three metal templating center functionalized (two in one ring and one in other) and demonstrated half-ring rotation using Pd(II) and Co(III)-metal ions.[22] A recent example displays a mechano-stereochemical switching of rings of a catenane having two bi-pyridine centers due to Cu(I) and SO_4^{2-} bonding. [8]

In our previous reports, we have demonstrated pyridine-diamide (pda) templating center for synthesis of higher order catenane. [24-26] In this chapter, we report a homo [2]catenane with each ring having a bi-dentate diphenyl-phenanthroline (dpp) and a tri-dentate pyridine-diamide (pda) metal-templating center. Due to orthogonal behaviour of these centers, this catenane shows switching behaviours in presence of Cu(I) and Co(III)-metal ion. This leads to inter-conversion between orthogonal catenates, where the interlocked rings undergo inevitable pirouetting and circumrotation.[27,28] Moreover, one pot double ring closing amide-bond formation strategy has been utilized in the catenation step.[29,30] It is worth mentioning that having two free templating centers after the first catenation, this metalated catenane may be threaded again, in one pot, to achieve step-economic synthesis[31] of higher order linear oligo[n]catenane similar to a recent report.[32]

4.3. Results and Discussion:

4.3.1. Design and synthesis of homo [2]catenane (H[2]C):

Synthesis of **H[2]Cu** is performed by self-complexing phenanthroline-diamine ligand **M6** (**Scheme 4.1**) and $Cu(CH_3CN)_4BF_4$ in a mixture of CH_3CN:DCM (1:1). This was followed by a double macrocyclization step[33] using 2,6-pyridinedicarbonyl dichloride resulting in 38% isolated yield of **H[2]Cu** (**Scheme 4.1**). De-metalation of **H[2]Cu** using ethylenediamine results in formation homo [2]catenane **H[2]C** (**Scheme 4.3**). In addition, the corresponding macro-cyclic monomer (**MC-1**), has been synthesized separately (**Scheme 4.2**) for comparison. **H[2]C** comprise of two **MC-1** containing dpp and pda templating center and tetraethylene ether as spacer between them (**Figure 4.1**). **H[2]Co** was synthesized from **H[2]C**.

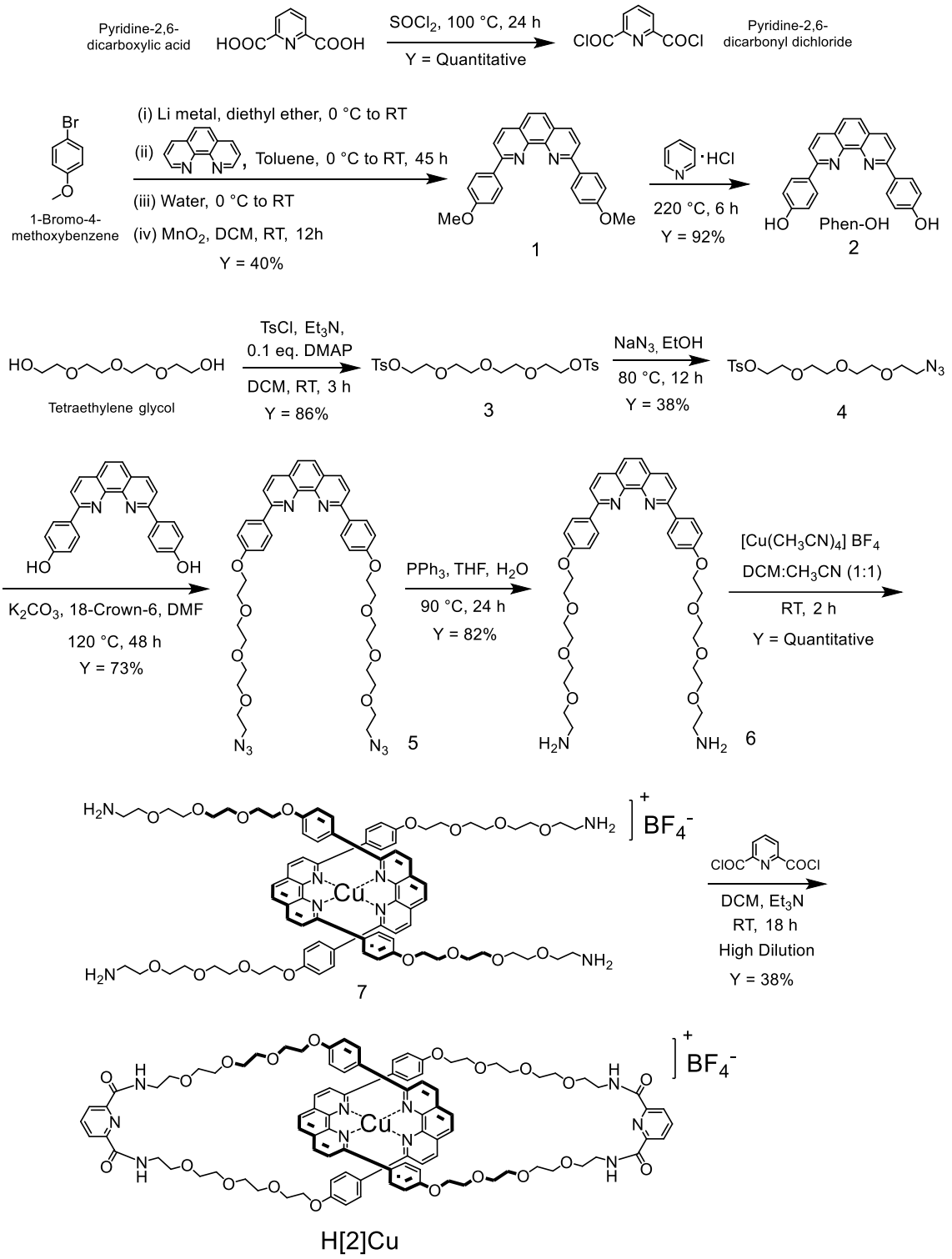

Scheme 4.1. Synthetic scheme for homo [2]Catenate copper complex **H[2]Cu** from commercial available starting materials: tetraethylene glycol, 2,2'-pyridine-dicarboxylic acid and p-bromo-anisole in 9 steps.

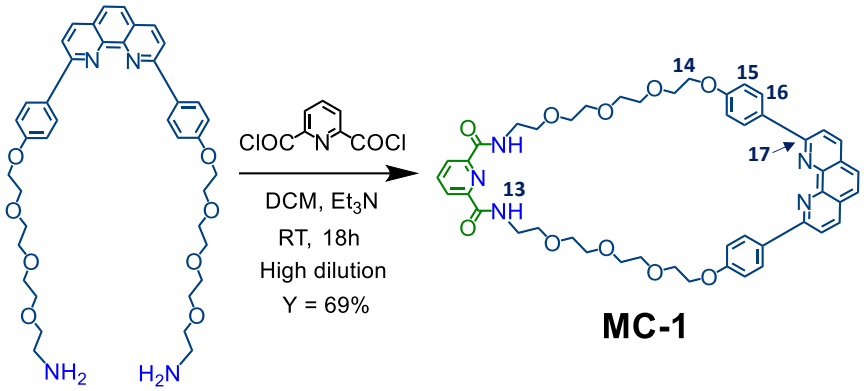

Scheme 4.2. Synthetic scheme for monomeric macrocyclic unit of homo [2]catenane **H[2]C** namely **MC-1:** synthesized separately for comparison and by ring closing amide bond formation between monomer **M6** and 2,6-pyridinedicarbonyl dichloride.

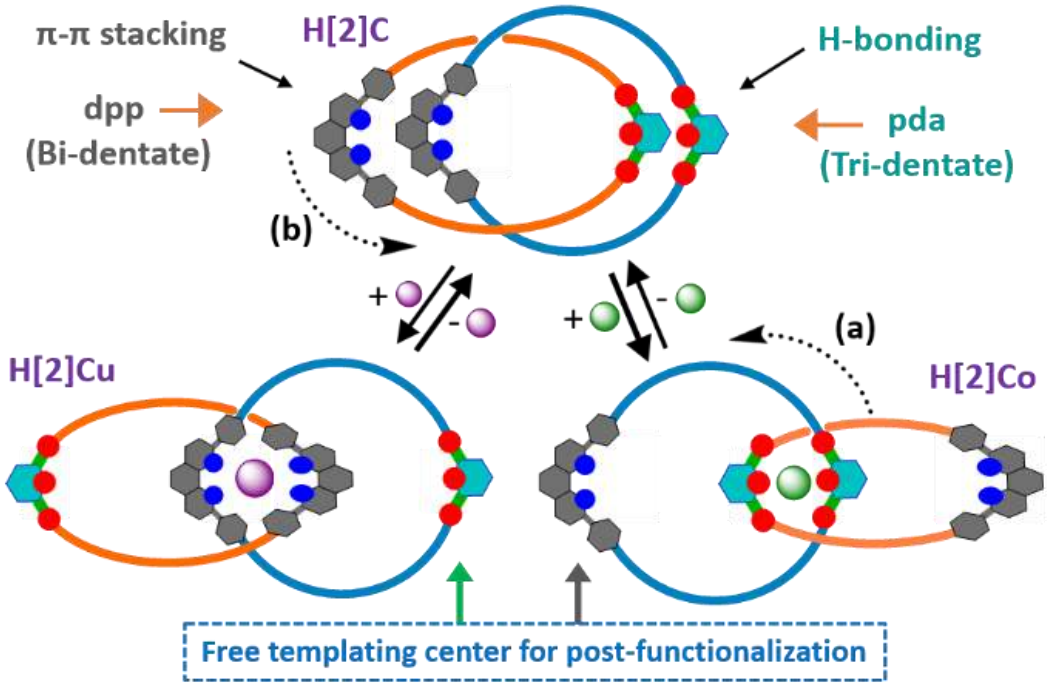

Figure 4.1. Schematic representation showing features of **H[2]C** having two dpp and pda templating centers and corresponding Co(III) and Cu(I)-catenates with free templating centers for post-functionalization. Blue dots represent tetrahedral binding site, and red dots represent octahedral binding site. Co(III) and Cu(I)-metal ion exchange mediated interconversion between **H[2]Co** to **H[2]Cu** leads to inevitably both (a) 180˚ pirouetting: revolving of one ring around other and (b) 180˚ circumrotation: rotation of macrocycle(s) around own axis. It is to be noted that for simplification, the blue ring is treated as static and orange ring is used as movable. The shown arrangement of rings in **H[2]C** is one of the various other possible conformations.

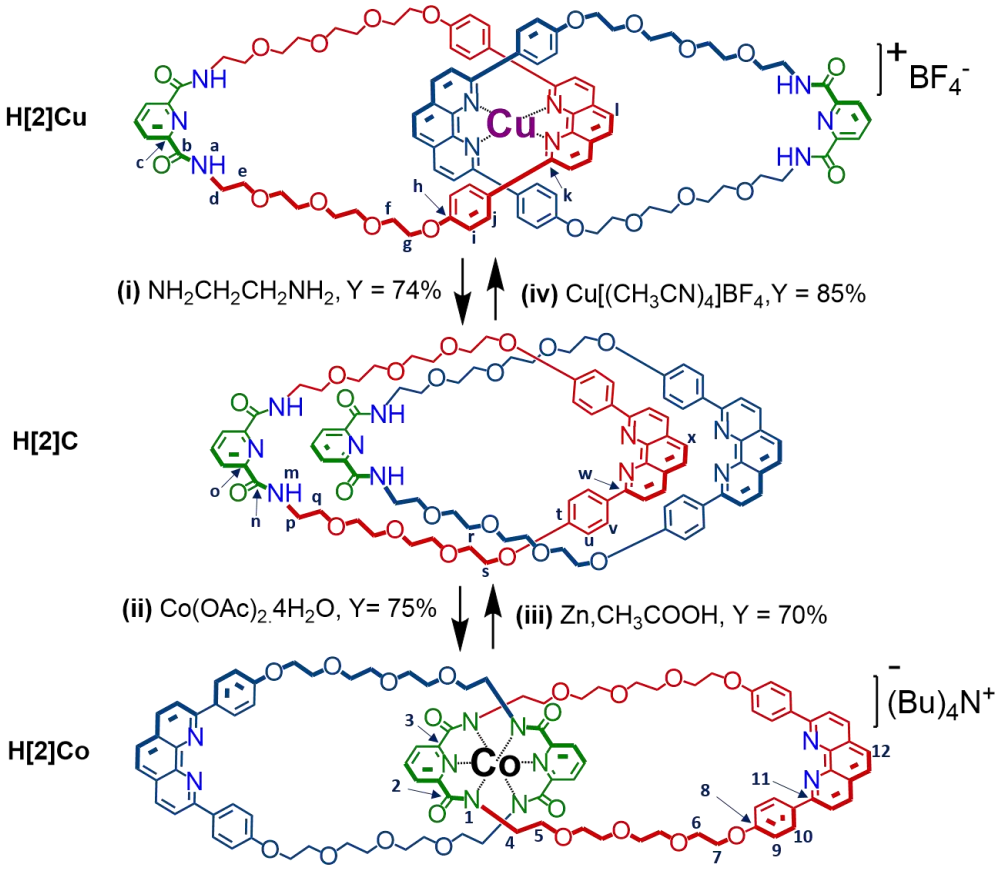

Scheme 4.3. Reaction scheme for synthesis of **H[2]Cu** and **H[2]Co** from homo [2]catenane **H[2]C** and interconversion between them (i) $NH_2CH_2CH_2NH_2$, DCM, RT, 5 min. (ii) $Co(OAc)_2.4H_2O$, NaH, MeOH, reflux, 24 h (iii) Zn dust, AcOH: MeOH(1:1), RT, 5 h. (iv) $Cu(CH_3CN)_4BF_4$, DCM:CH_3CN(1:1), RT, 2 h. Some bonds are elongated to show the molecules clearly.

4.3.2. ^{1}H-NMR signal change during synthesis of H[2]Cu, H[2]C and H[2]Co:

^{1}H-NMR provides evidence for the synthesis of catenates (**H[2]Cu** and **H[2]Co**) and homo [2]catenane (**H[2]C**). In $CDCl_3$, **H[2]Cu** shows signal of benzene protons of dpp units at 6.02 ppm (peak **i**) and 7.38 ppm (peak **j**). Peaks of amide protons of pda units appear at 8.84 ppm (peak **a**, **Figure 4.2a**) and signals for tetraethylene ether appears between 3.77 ppm to 3.61

ppm. Upon removal of Cu(I), de-shielding of amide protons and benzene protons was observed, suggesting removal of Cu(I) from **H[2]Cu** and the formation of fully organic homo catenane **H[2]C**. Peak **i** (6.02 ppm), **j** (7.38 ppm) and **a** (8.84 ppm) of **H[2]Cu** in **figure 4.2a** got de-shielded to peak **u** (6.67 ppm), **v** (7.84 ppm) and **m** (9.27 ppm) in **figure 4.2b** respectively.

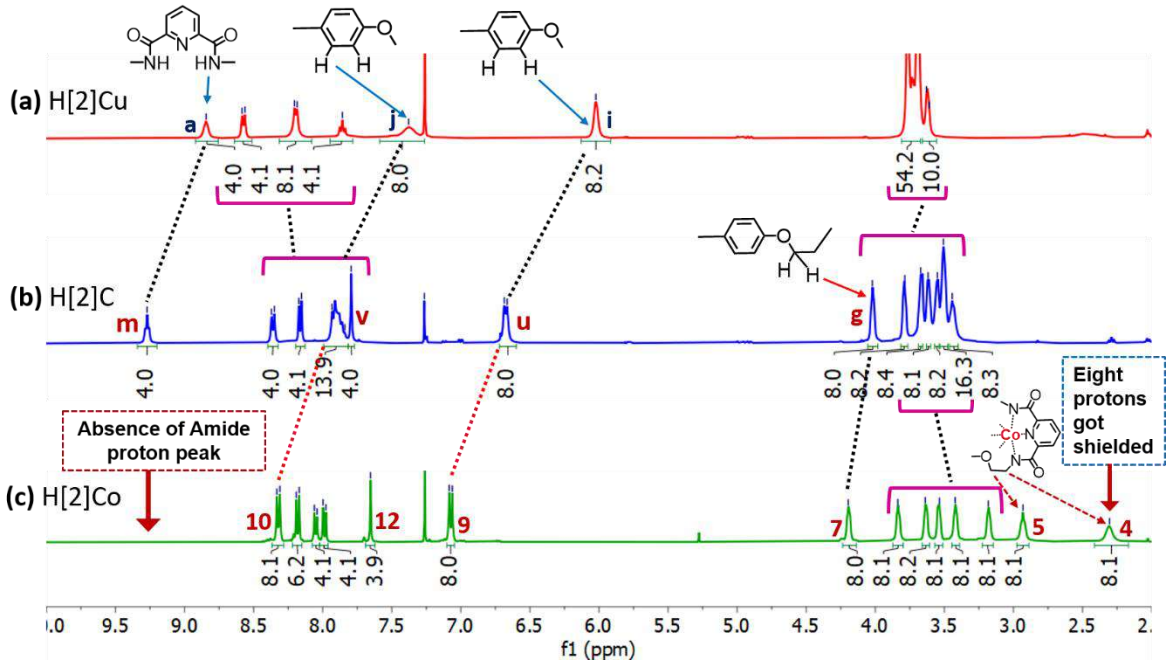

Figure 4.2. Partial ^{1}H-NMR (400 MHz, $CDCl_3$, at 298 K) comparison between (a) **H[2]Cu** (b) **H[2]C** (c) **H[2]Co**. The assigned numbers and letters are as shown in scheme-**4.3.**

De-shielding of NH-protons upon demetalation is attributed to increase hydrogen bonding between pda units. Similarly, de-shielding of dpp benzene protons can be attributed to diseng-agement of dpp units from Cu(I)-tetrahedral complex environment. Such de-shielding after demetalation of Cu(I) has also been observed in previous reports.[7] In addition, signals for the tetraethylene ether chains appears at a wider range from 4.02 to 3.44 ppm due to increased interaction between interlocked rings,[34] as rings are co-conformationally flexible in **H[2]C**. Similarly, formation of **H[2]Co** is evidenced by the absence of NH-protons (**Figure 4.2c**), due to base-mediated reaction between two pda centers. In parallel, due to complexation, eight

methylene protons (N^--**CH_2**-CH_2-O-) near the Co(III)-complex got shielded and appear at 2.3 ppm.

Moreover, -CH_2- peaks in ether chain are more shielded in **H[2]Co** compared to **H[2]C** and appears even wider ppm range from 4.20 to 2.93 (**Figure 4.2c**). This perturbation may be due to increased shielding of nearby carbons close to the anionic Co(III)-complex center. Benzene protons of dpp units are further de-shielded when complexed to form **H[2]Co**. This suggests, dpp rings are π-π stacked in **H[2]C** and upon complexation with Co(III), they separated out, disrupting the stacking effect, hence such deshielding is observed.[35]

4.3.3. ^{1}H-^{1}H 2D-COSY spectra of H[2]Cu, H[2]C, H[2]Co:

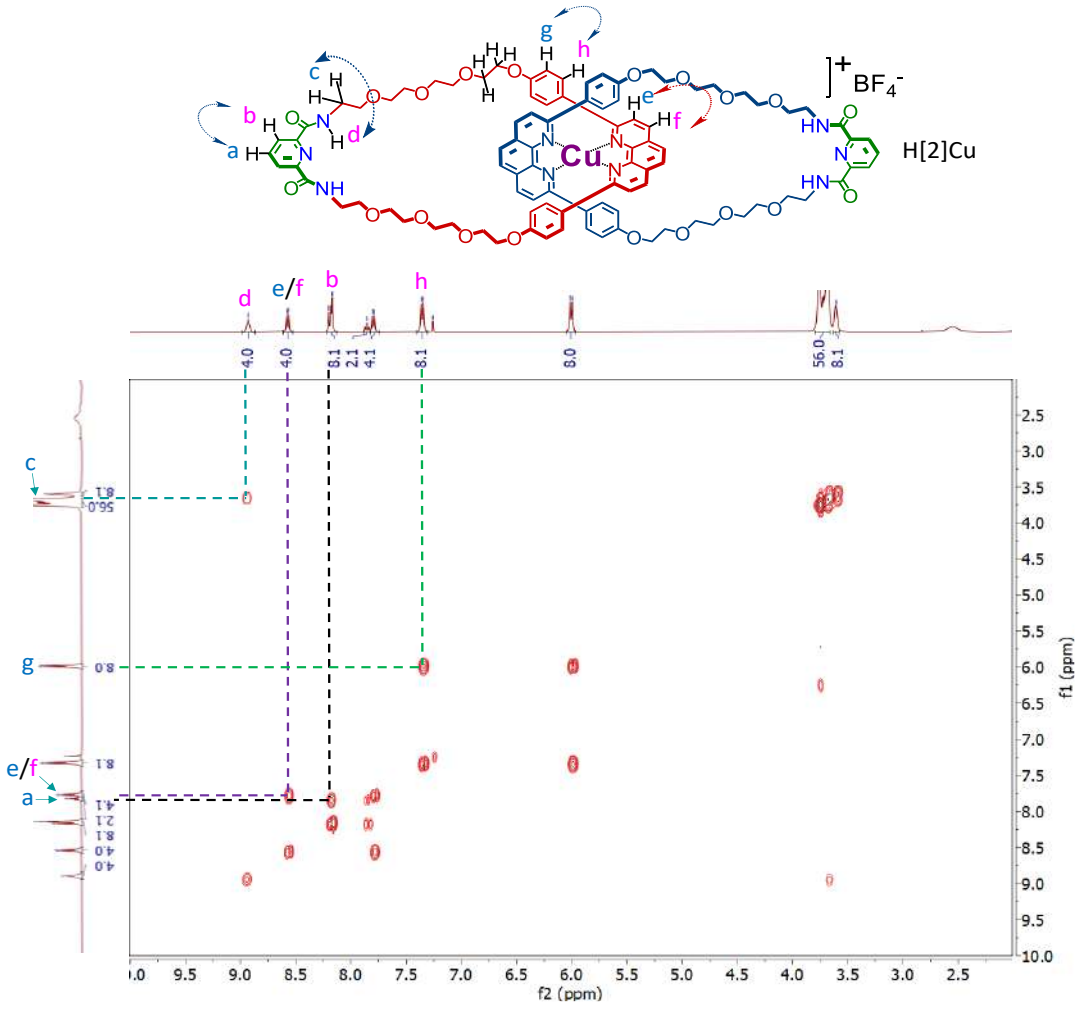

Figure 4.3. ^{1}H-^{1}H 2D-COSY spectra of H[2]Cu in $CDCl_3$ (400 MHz).

For attribution of NMR signals from pda and dpp units of interlocked structures, 2D-COSY NMR experiments were performed with $CDCl_3$. Corresponding spectral analysis are given in supporting information (**Figure 4.3, 4.4, 4.5**). For **H[2]C**, the coupled resonance peak from NH- protons with next methylene proton appears at a downfield position compared to **H[2]Cu**. This further suggests the presence of hydrogen bonding between NH-protons in **H[2]C**.

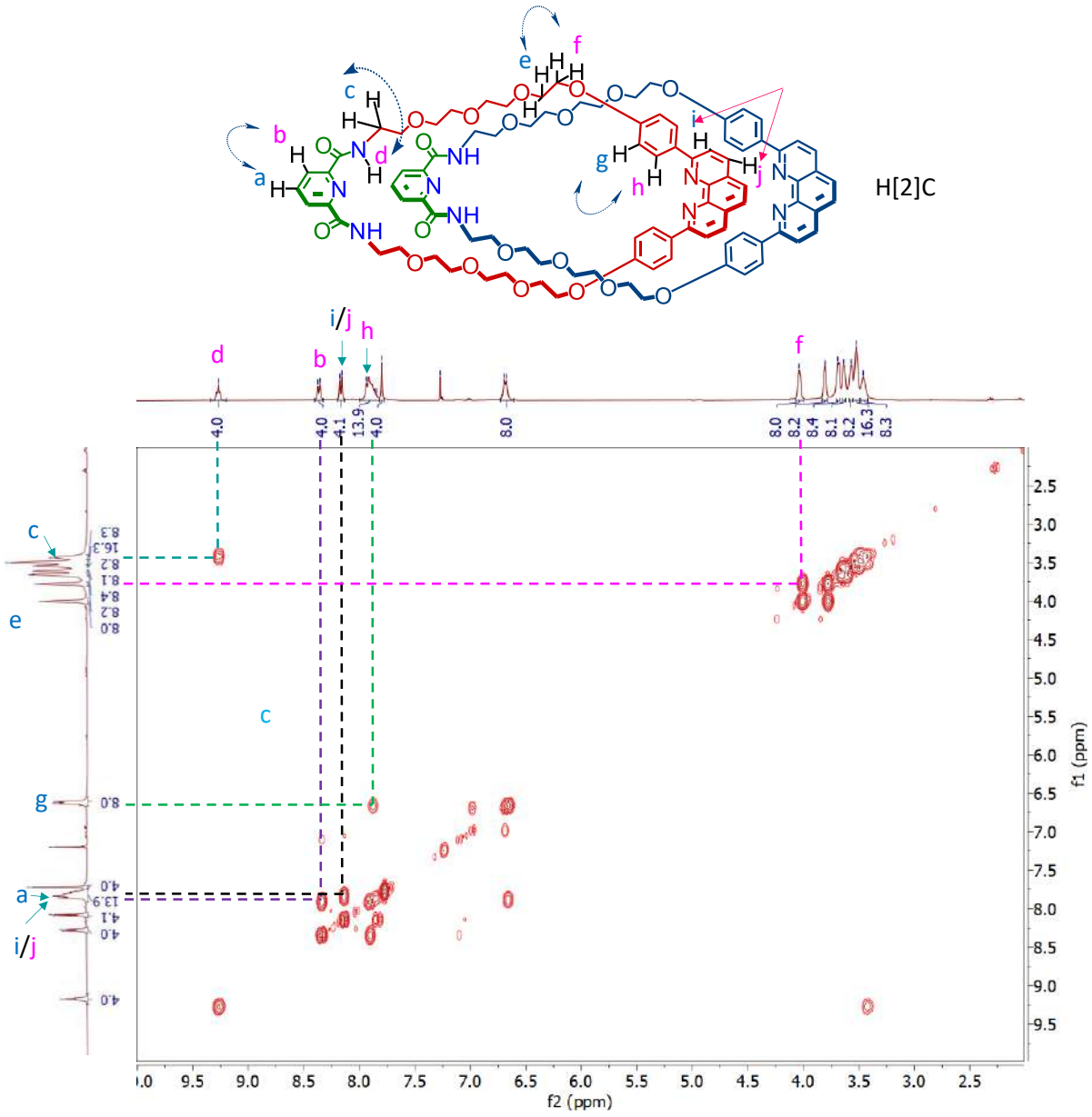

Figure 4.4. ^{1}H-^{1}H 2D-COSY spectra of H[2]C in $CDCl_3$ (400 MHz).

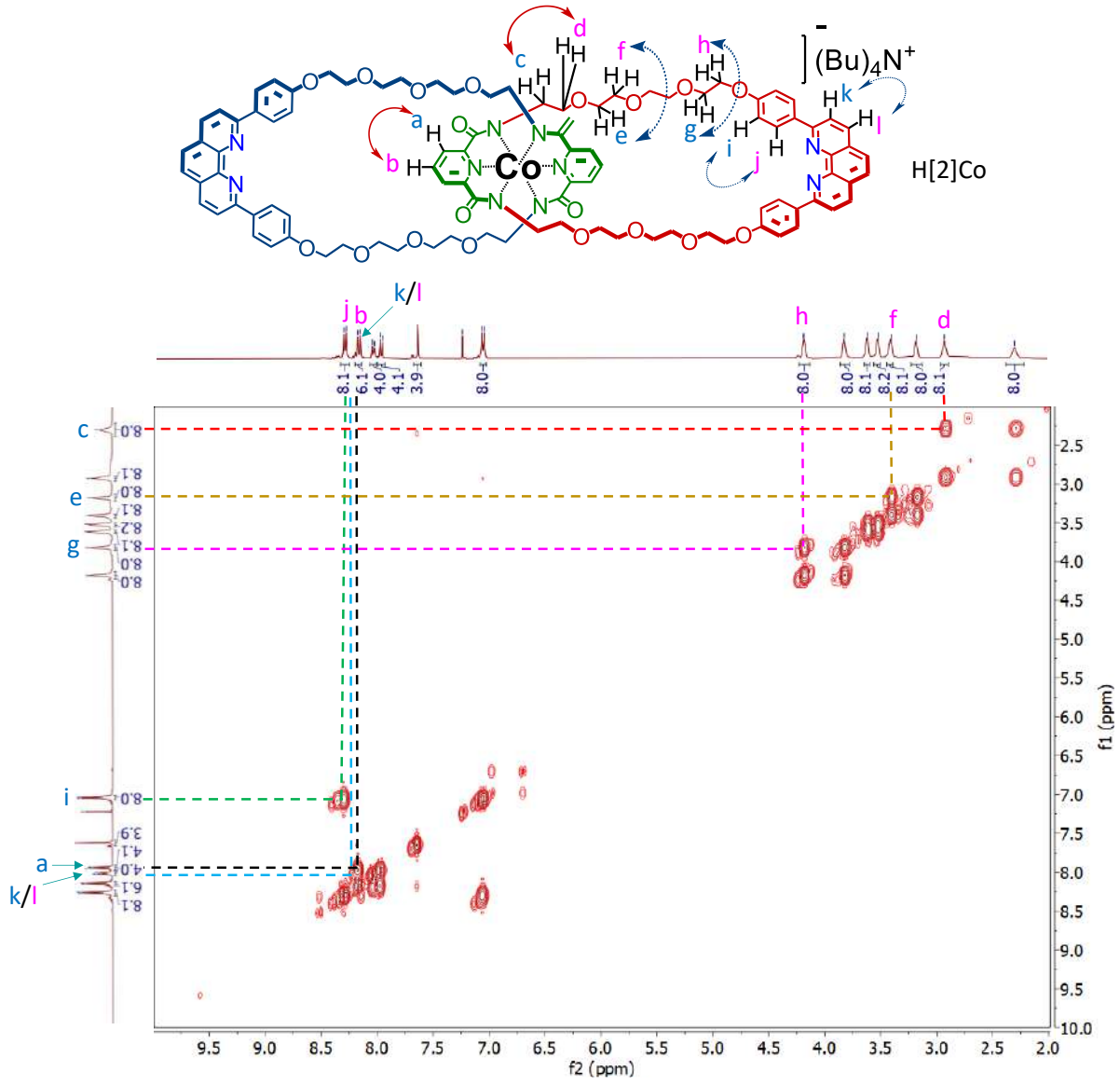

Figure 4.5. ^{1}H-^{1}H 2D-COSY spectra of H[2]Co in $CDCl_3$ (400 MHz).

4.3.4. ^{13}C-NMR signal change during synthesis of H[2]Cu, H[2]C and H[2]Co:

^{13}C-NMR further suggests completion of double ring closing amide bonds, and formation of **H[2]Cu**. It comprises signals of pda and dpp templating centers. Peak **b** (**Figure 4.6a**) at 163.98 ppm is attributed to carbonyl carbon, and the signal at 148.83 ppm (**peak c**) corresponds to

quaternary carbon of the free pyridine-diamide templating center. Signals for benzene rings of dpp unit can be distinctly seen at 112.77 and 129.15 ppm (peak **i** and **j** respectively). In addition, signals for methylene carbon attached next to Cu(I)-complexed dpp unit (Ph-O-**CH_2**-CH_2-O-) and methylene carbon next to free pda unit (NH-**CH_2**-CH_2-O-) in **H[2]Cu** appear at 67.27 ppm (peak **g**) and 39.07 ppm (peak **d**), respectively. Upon removal of Cu(I), shifting of phenanthroline ring carbons (**Figure 4.6a, 4.6b**) and minor de-shielding for benzene signals were observed (peak **i** and **j** of **Figure 4.6a** shifted to peak **u** and **v** in **Figure 4.6b** respectively). Moreover, no change in signals for pda unit, methylene carbon next to it (NH-**CH_2**-CH_2-O-) and methylene carbon next to dpp unit (Ph-O-**CH_2**-CH_2-O-) was observed (**Figure 4.6a, 4.6b**). Similarly, in **H[2]Co,** no change in signals for dpp unit, and the methylene carbon attached to it (Ph-O-**CH_2**-CH_2-O-) was observed (**Figure 4.6b, 4.6c**), suggesting complexation occurs between pda units only. However, due to complexation carbonyl carbon, quaternary carbon of pda unit and methylene carbon next to pda unit (NH-**CH_2**-CH_2-O-) got de-shielded by 4.5, 7.45 and 4.13 ppm, respectively (peak **n**, **o** and **p** of **Figure 4.6b** shifted to peak **2, 3** and **4** in **Figure 4.6c**).

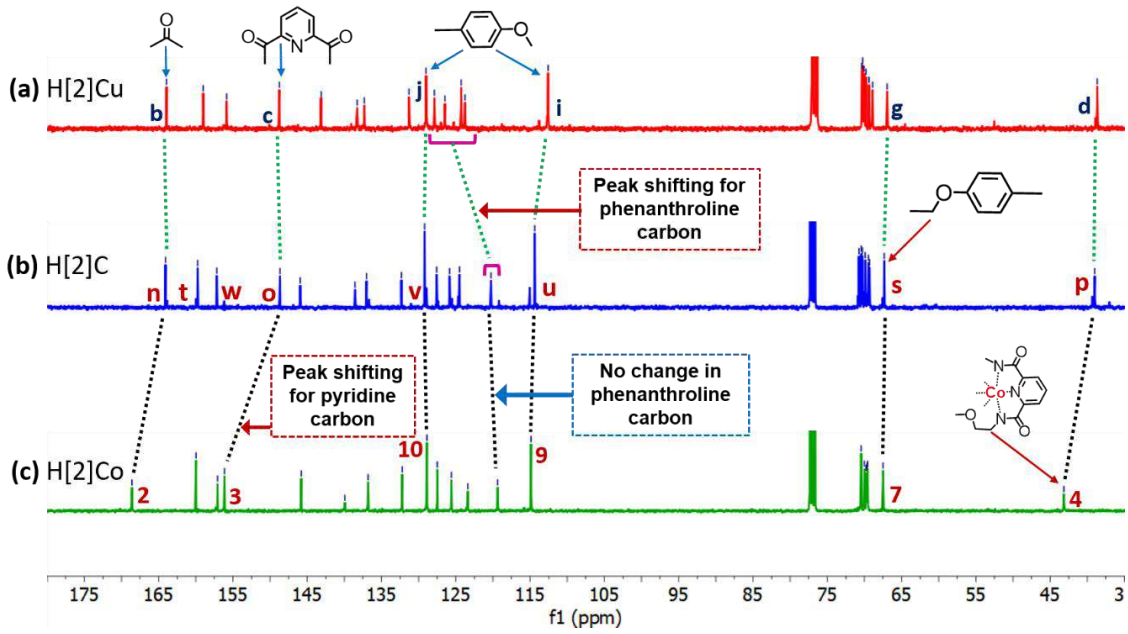

Figure 4.6. Partial ^{13}C-NMR (100 MHz, $CDCl_3$, at 298 K) comparison between (**a**) **H[2]Cu** (**b**) **H[2]C** (**c**) **H[2]Co**. The assigned numbers and letters can are as shown in scheme **4.3**

4.3.5. Comparison of ^{1}H-NMR spectra of H[2]C with MC-1:

Evidence of π-π stacking between dpp units and hydrogen bonding between pda templating centers was further drawn, by comparing ^{1}H-NMR spectra of **H[2]C** with corresponding macrocyclic monomer **MC-1(Figure 4.7)**. Signals for benzene protons of dpp unit of **H[2]C** (**Figure 4.7b**) appears at ≈0.45 ppm higher field (peak **u** at 6.67 ppm, peak **v** at 7.88 ppm) compared to corresponding signals of **MC-1** (peak **15** at 7.12 ppm and peak **16** at 8.41 ppm, **Figure 4.7a**).

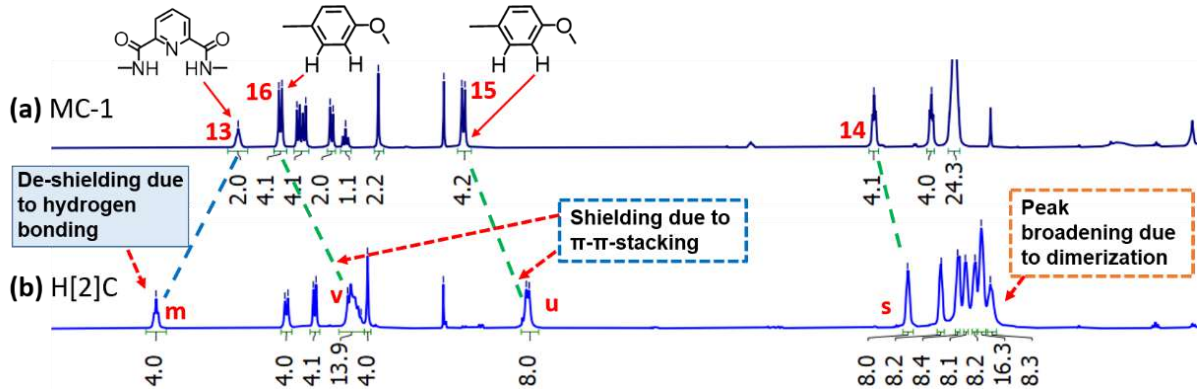

Figure 4.7. Partial ^{1}H-NMR (400 MHz, $CDCl_3$, at 298 K) comparison between (a) **MC-1** (b) **H[2]C** suggests presence of π-π stacking and hydrogen-bonding in **H[2]C**. The assigned numbers and letters are as shown in **scheme-4.3** for **H[2]C** and **scheme-4.2** for **MC-1**.

Up-field shift of proton signal suggests π-π stacking between dpp units in **H[2]C**. Similar change in NMR signals has also been observed due to π-π stacking in previously reported literature.[35] Moreover, NH-proton peaks of pda units in **H[2]C** are de-shielded by 0.58 ppm and appears at 9.27 ppm (peak **m**, **Figure 4.7b**) compared to **MC-1** (appears at 8.69 ppm, peak **13**, **Figure 4.7a**). De-shielding of NH-protons suggests H-bonding and has been observed in previous literature reports as well.[34,36, 37]

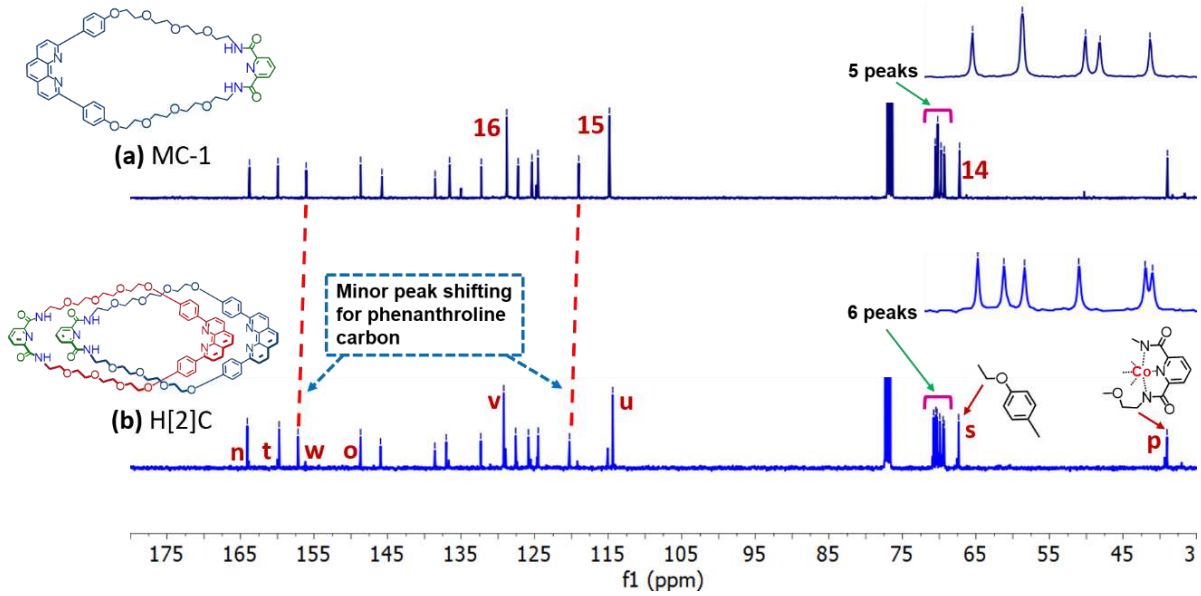

Figure 4.8. Partial ^{13}C-NMR (100 MHz, $CDCl_3$, at 298 K) comparison between homo [2]catenane and its corresponding monomeric macrocycle unit (a) **MC-1** (b) **H[2]C**. Detail spectral analysis are given in **section 4.6.1**. The assigned numbers and letters are as shown in scheme **4.2** for **MC-1** and scheme **4.3** for **H[2]C**.

4.3.6. Mass spectra change during synthesis of H[2]Cu, H[2]Co and H[2]C:

Positive mode ESI-MS further suggests formation of **H[2]Cu** ($[C_{94}H_{102}CuN_{10}O_{20}]^+$). A prominent di-cationic peak at m/z 877.8385 and mono-cationic peak at 1754.7827 was observed (**Figure 4.9a** and **Section 4.6.3**) and attributed to $[\mathbf{H[2]Cu}]^+ + H^+]^{2+}$ and $[\mathbf{H[2]Cu}]^+$. This is in good agreement with corresponding theoretical calculated m/z (calcd. for $(C_{94}H_{101}CoN_{10}O_{20})^{2+}$ is 877.8345 and for $[C_{94}H_{102}CuN_{10}O_{20}]^+$ is 1754.6599) and isotopic distribution pattern. When Cu(I)-metal ion template was removed from H[2]Cu, it shows a base peak having 2^+ charge at m/z 857.8529. This matches the theoretically calculated mass with the isotopic distribution pattern of $[\mathbf{H[2]C} + Na^+ + H^+]^{2+}$ (calcd. for $[C_{94}H_{103}N_{10}O_{20}Na]^{2+}$ is 857.8611 (**Figures 4.9b** and **Section 4.6.3**). This amounts to mass for two macrocyclic rings of **MC-1**.

When H[2]C was further complexed with Co(III), a diagnostic peak at m/z 874.8223 was observed and is di-cationic in nature. This peak is attributed to $[\mathbf{H[2]Co}]^{-}+3H^{+}]^{2+}$ and is in good agreement with the theoretically calculated mass for $(C_{94}H_{101}CoN_{10}O_{20})^{2+}$ 874.8268 (**Figures 4.9c** and **Section 4.6.3**).

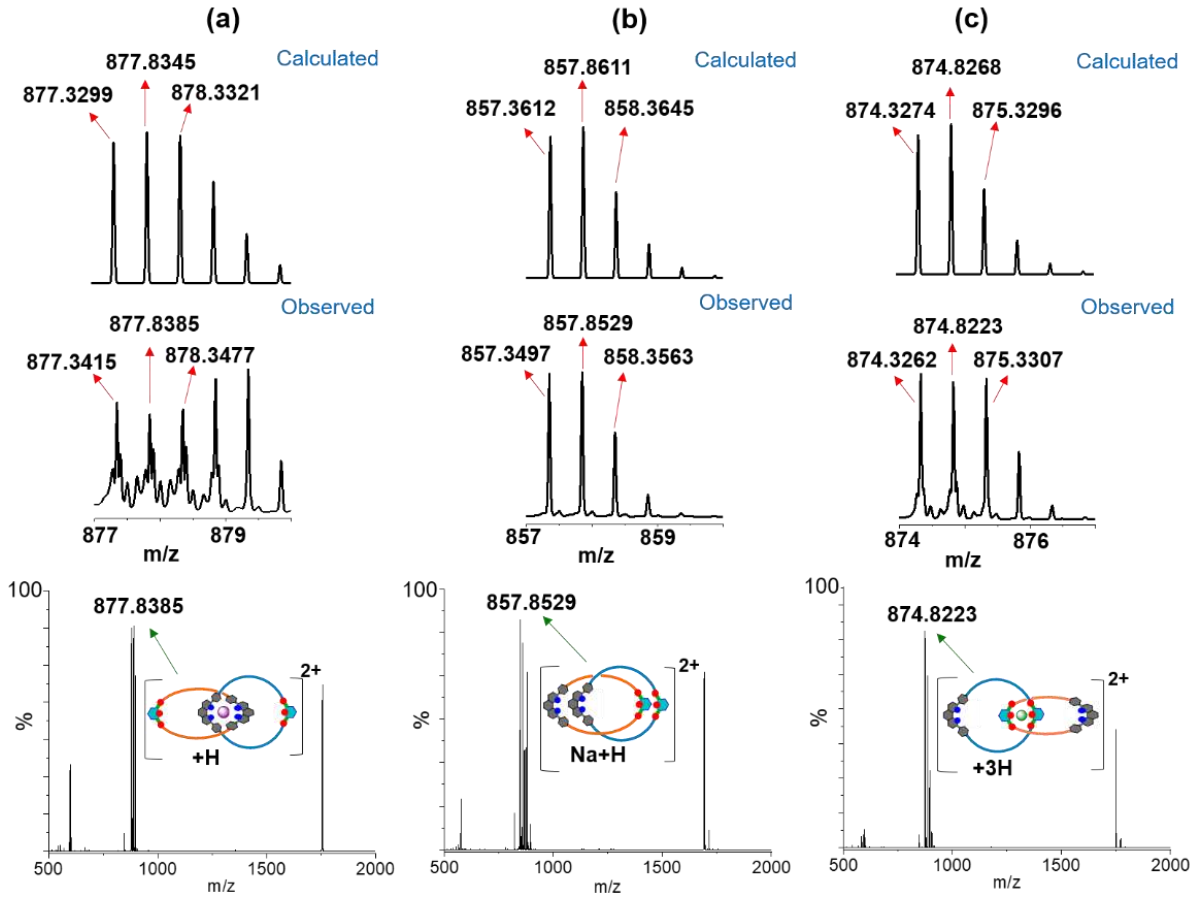

Figure 4.9. Comparisons of ESI^{+}-MS spectra of (a) **H[2]Cu** (b) **H[2]C** (c) **H[2]Co**. Full spectra (bottom), and its isotopic distribution peaks (top) with theoretically calculated spectra.

4.3.7. Interconversion between H[2]Cu, H[2]Co and H[2]C using chemical stimuli:

To study interconversion between catenates, demetalation of red-black colored **H[2]Cu** was performed by adding $NH_2CH_2CH_2NH_2$ in excess,[38] in DCM and stirring. Within 5 min, the disappearance of red-black color indicates removal of Cu(I) ion. **H[2]C** was isolated with 74%

yield (**scheme-4.3i**). In this process, conformationally locked **H[2]Cu** at dpp center converted to a catenane where the rings can freely move w.r.t. each other. Isolated **H[2]C** was further reacted with $Co(OAc)_2.4H_2O$ and $(Bu)_4N^+OAc^-$ using NaH in MeOH.[39] As **H[2]C** is co-conformationally flexible, rings can rotate under the influence of chemical stimuli. As Co(III) has octahedral preference, hence reaction occurs between two tri-dentate pda templating centers, forming yellow-green colored non-labile and negatively charged Co(III)-complex **H[2]Co** in 75% yield (**Scheme-4.3ii**). In the process of conversion of **H[2]Cu** to form **H[2]Co**, certainly interlocked rings have to go through 180˚ pirouetting and circumrotation (**Figure 4.1**). To further reverse the route i.e. conversion of **H[2]Co** to **H[2]Cu**, the synthesized **H[2]Co** was demetalated using Zn/CH_3COOH at RT for 5 h. Moderate disappearance of yellow-green color was observed resulting in formation of **H[2]C** in 70% yield (**Scheme-4.3iii**). **H[2]C** was again re-metalated with Cu(I) using $[Cu(CH_3CN)_4]BF_4$ in $DCM:CH_3CN$ at RT. Having tetrahedral preference, Cu(I)-complexed with two dpp units only, forming red-black colored **H[2]Cu** in 85% yield (**Scheme-4.3iv**). Again, in the conversion process of **H[2]Co** to **H[2]Cu**, interlocked rings have to undergo 180˚ pirouetting and circumrotation (**Figure 4.1**). As the interconversion process involves ring rotations caused by chemical stimuli, this is reminiscent of switching-like behaviour in supramolecular dynamic system.[40,41] This study further explores utilization dpp and pda as orthogonal templating centers as stations.[42,43]

4.3.8. Optical properties of H[2]Cu, H[2]Co and H[2]C:

Fluorescence spectra for **H[2]Cu**, **H[2]Co** and **H[2]C** were recorded from $CHCl_3$ solution, exciting at 282 nm (**figure 4.10**). Corresponding absorbance spectra are given in **figure 4.11a**. The λ_{max} appears at 400 nm in the emission spectrum of **H[2]C** with the full width at half maximum (FWHM) of 52 nm. Corresponding catenate **H[2]Co** and **H[2]Cu** are blue shifted with peak broadening and having increased FWHM. **H[2]Co** shows λ_{em} at 390 nm with FWHM of 59 nm and for **H[2]Cu** λ_{em} appears at 369 nm with FWHM of 65 nm.

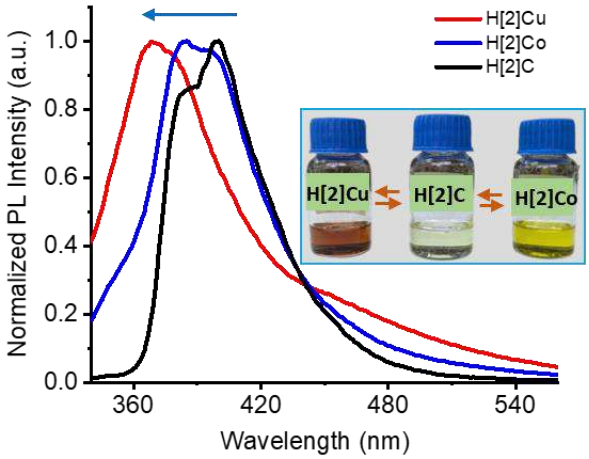

Figure 4.10. Fluorescence spectra of chloroform solution of **H[2]Cu**, **H[2]Co** and **H[2]C** (left) and their photographic images in chloroform solution under visible light (right) suggests interconversion from **H[2]Cu** to **H[2]Co** or vice versa is also witnessed by color change using naked eye.

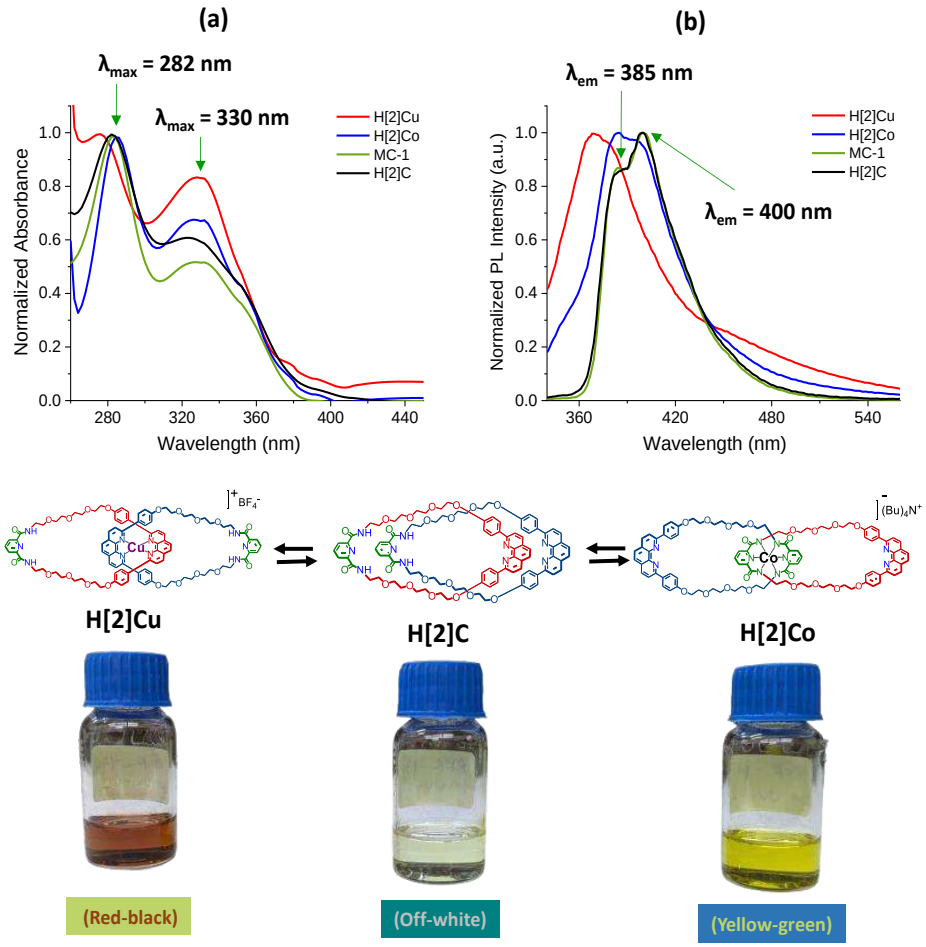

Figure 4.11. Optical properties of **H[2]Cu**, **H[2]Co**, **MC-1** and **H[2]C** (a) UV-visible spectra (b) Fluorescence Spectra by exciting at 282 nm. Photographic images of chloroform solution of corresponding samples are given at bottom.

Blue shift and peak broadening in homo [2]catenates may be attributed to change in π-π stacking interactions in solution[44] and formation of low energy MLCT transitions after complexation.[45] It is worth mentioning that emission spectra for synthesized structures are mainly generated from dpp unit, having extended conjugation compared to pda unit. The synthesized catenane and catenates have a distinguished color in $CHCl_3$ solution and hence interconversion can be monitored by naked eye. **H[2]Cu** is red-black in color whereas, **H[2]Co** is greenish-yellow in color and **H[2]C** appears light-green color (**Figure 4.10**).

4.3.9. VT-NMR study for homo [2]catenane H[2]C:

To gain better insight into the proposed co-conformation and co-conformation flexibility between interlocked **MC-1** rings of **H[2]C** (**Scheme 4.3**), a variable temperature NMR study were performed from -45 to +45 ˚C. Sharpening of peaks at higher temperature and broadening of peaks at lower temperature was observed (**Figure 4.12** and **Section 4.6.2**).

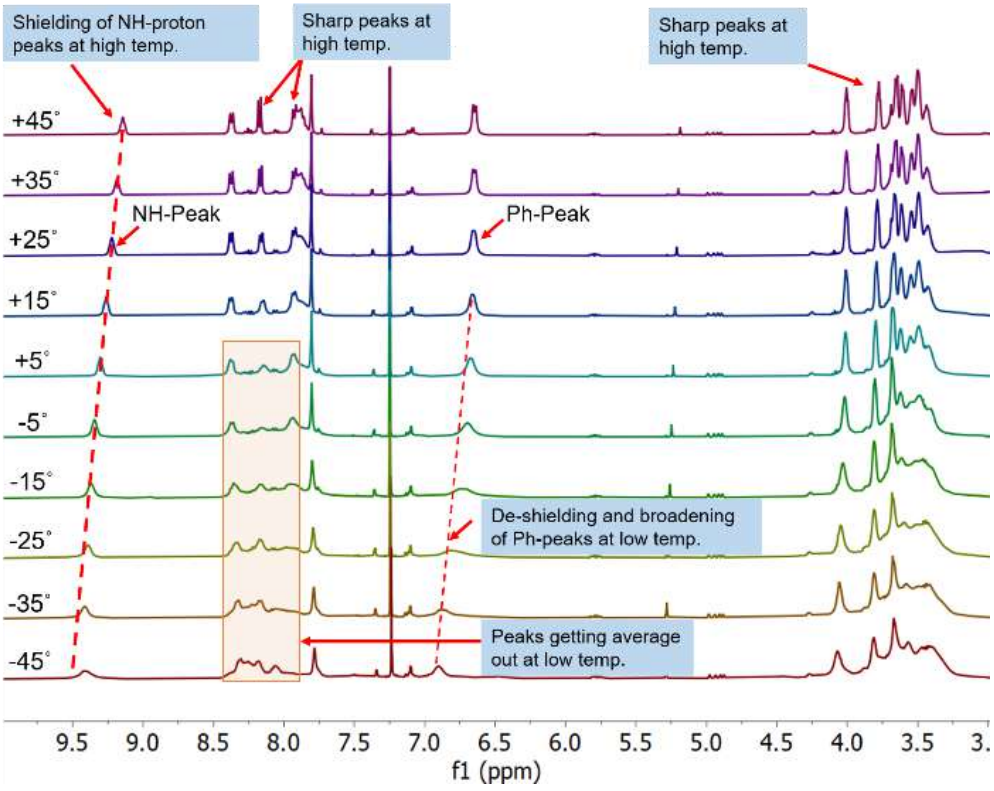

Figure 4.12. Variable temperature ^{1}H-NMR study for $CDCl_3$ solution of **H[2]C**. Data plotted with 10 ˚C variation, from -45 to +45 ˚C. Partial spectra are given for noticeable comparison.

This suggests that mechanical bonding via through-space interactions between interlocked rings in **H[2]C** can be varied with changing temperatures.[46] Also, when temperature is raised, NH-proton peak at 9.25 ppm gets shielded (**Figure 4.12, NH-peaks**), suggesting a decrease in strength of H-bonding present between pda units in solution.[34] Furthermore, when temperature is lowered from +25 to -45 ˚C, de-shielding for benzene proton peaks of dpp unit at 6.66 ppm was observed (**Figure 4.12, Ph-peaks**), suggesting co-conformational rigidity upon cooling. In addition, VT-NMR study of **MC-1** in $CDCl_3$ was performed for comparison (**Figure 4.13**). Negligible peak broadening was observed when temperature was lowered from +25 to –45 ˚C, unlike **H[2]C**.

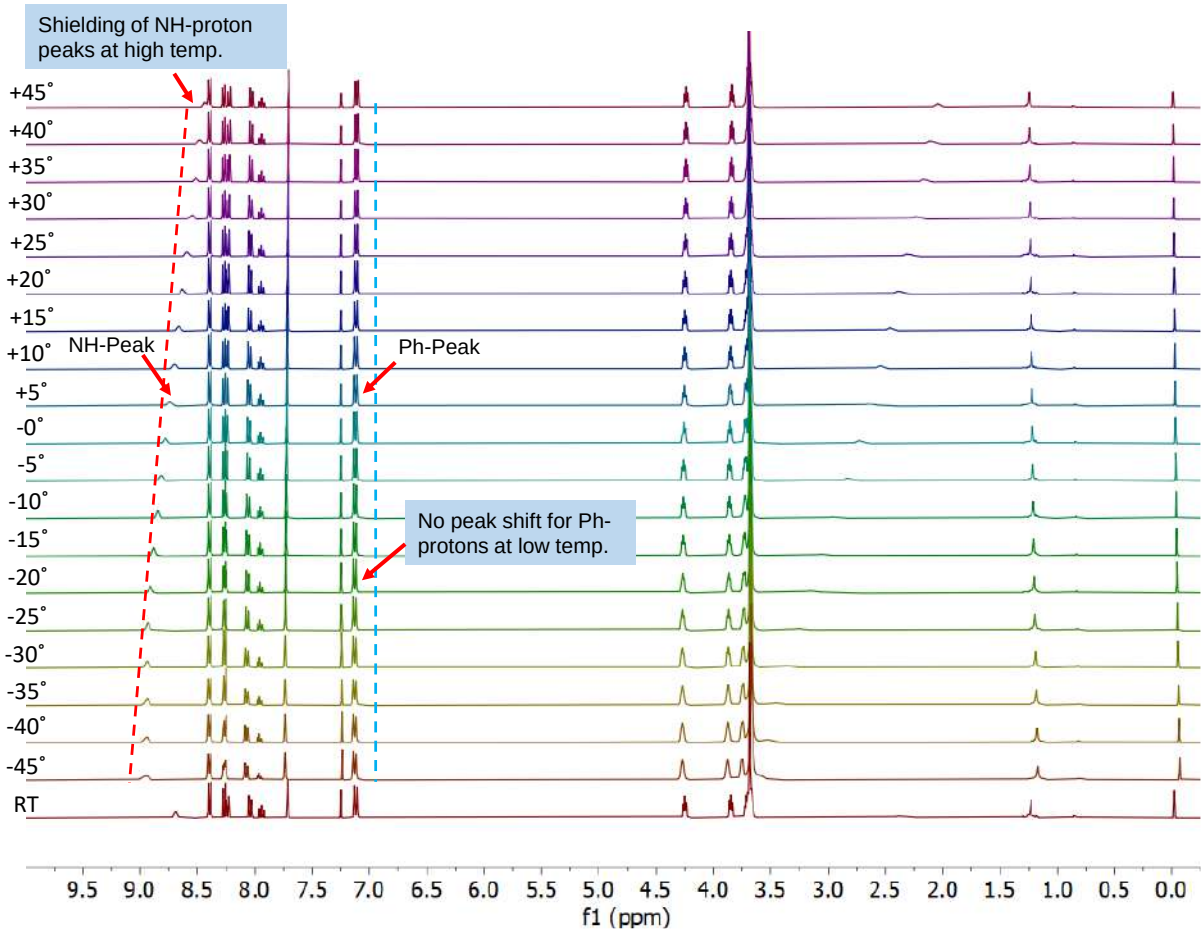

Figure 4.13. Variable temperature ^{1}H-NMR study for monomeric macrocycle **MC-1** ($CDCl_3$, 400 MHz). Data recorded from -45 ˚C to 45 ˚C with interval of 5 degrees. Minor peak broadening at lower temperature and at higher temperature minor sharpening of NMR signals was observed.

This suggests, the entangled molecules are freely moving at higher temperatures, but the motion gets restricted at lower temperatures. No peak shift for benzene protons for the dpp unit of **MC-1** at 7.15 ppm (**Figure 4.13**) was observed over the range of temperature, suggesting the absence of π-π stacking between dpp units in solution. However, when temperature is increased from –25 to +45 ˚C, shielding of NH-protons was observed. Possibly due to weakening of intermolecular H-bonding.

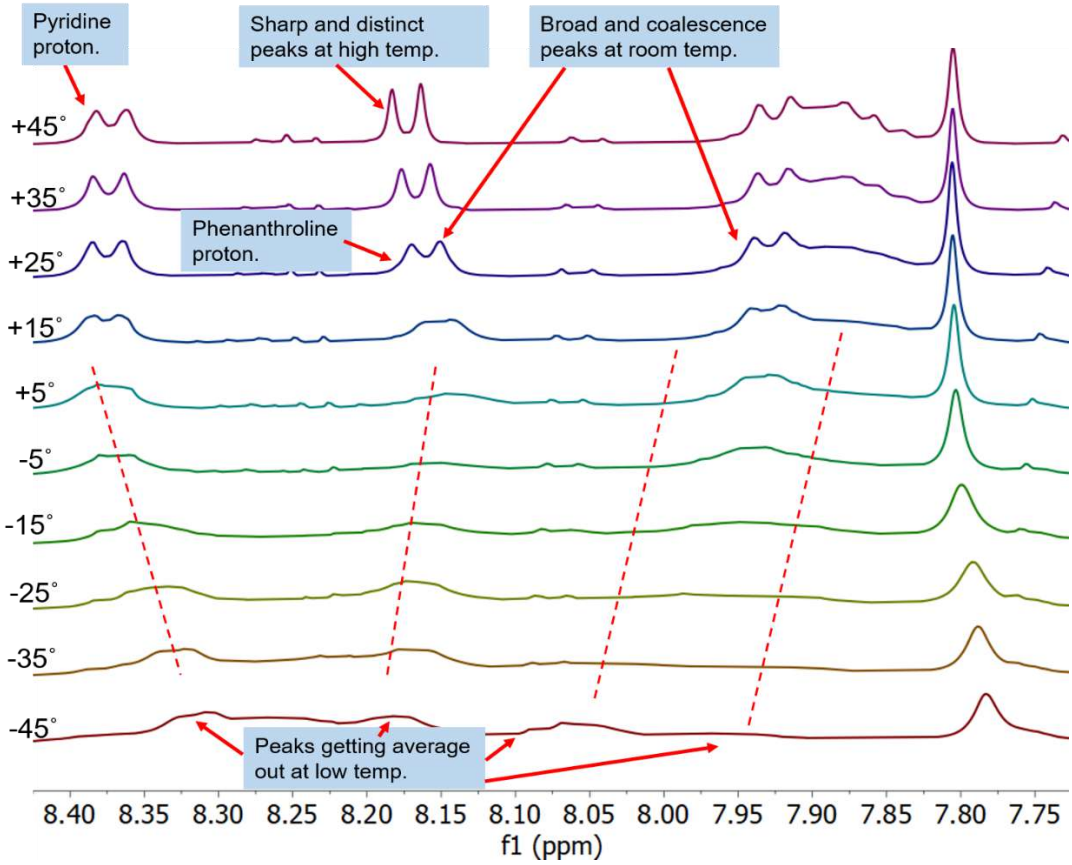

Figure 4.14. Variable temperature ^{1}H-NMR change for homo catenane **H[2]C** ($CDCl_3$, 400 MHz) from 8.4-7.75 ppm. Data recorded from -45 ˚C to 45 ˚C with interval of 5 degrees.

Moreover, at room temperature, broad and coalescence of NMR signals (from 7.75 to 8.2) were observed for dpp (8.15 ppm) and pyridine ring proton (**Figure 4.12**, **Figure 4.14**). This further suggests slow movement of interlocked rings w.r.t. each other at RT.[47,48] As temperature is raised up to 45 ˚C, NMR signals become distinct and sharp. This suggests, interlocked rings are gaining co-conformational flexibility by overcoming π-π stacking and hydrogen bonding.

Furthermore, with lowering of temperature from 25 to –45 ˚C, averaging out of NMR signals further indicates co-conformational rigidity.

4.3.10. MS-MS Experiment on Homo [2]Catenane H[2]C:

Homo [2]catenane is characterized by MS-MS analysis. Fragmentation of the molecular ion peak of **H[2]C** at 1692.5676 results in peaks at. 846.4591 with 1^+ charge. This suggests **MC-1** as a building block of **H[2]C** (**Figure 4.15**).

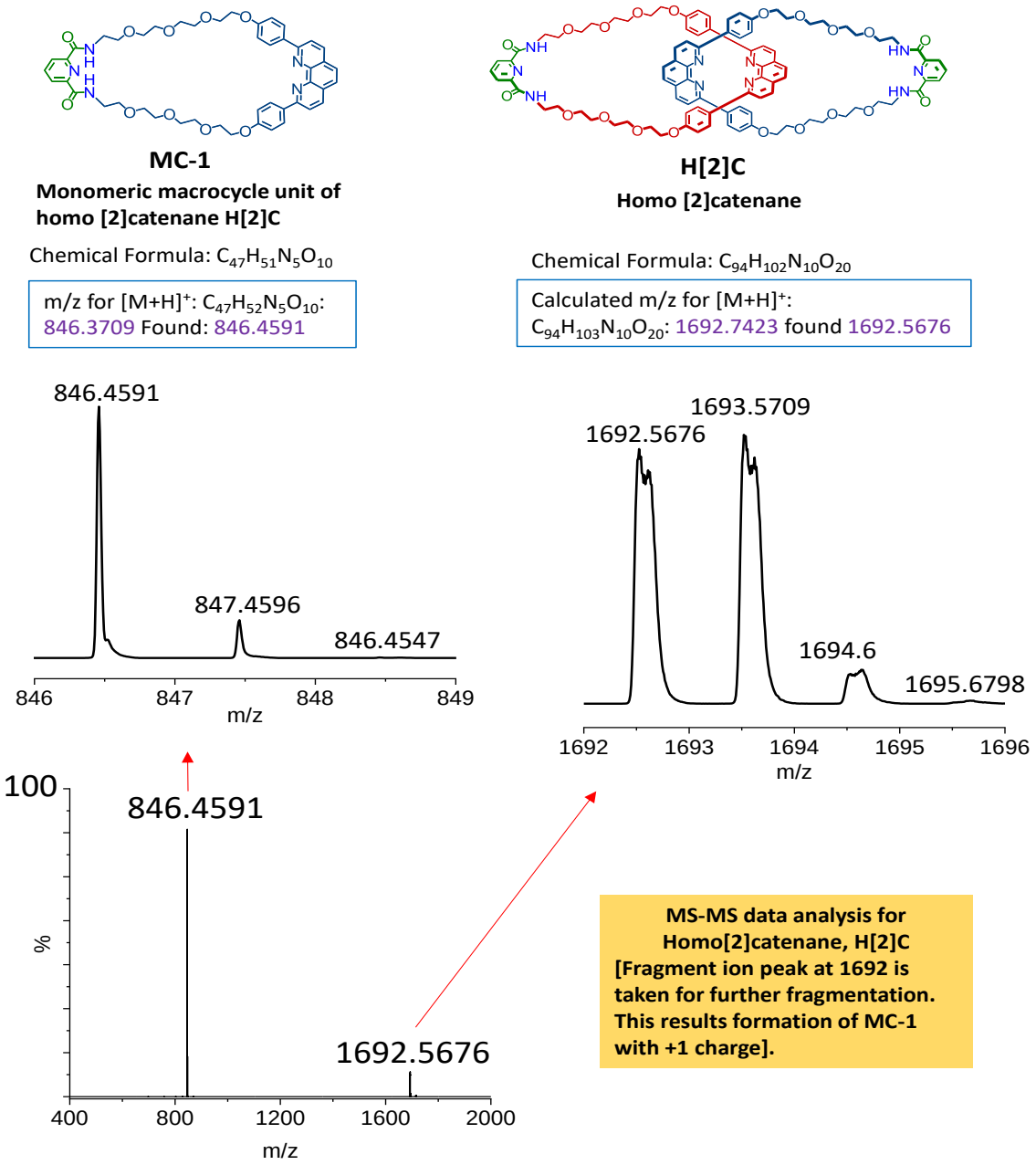

Figure 4.15. MS-MS analysis in positive mode mass spectrum suggests presence of **MC-1** in **H[2]C**.

4.4. Conclusion:

Interconversion between two homo [2]catenates bearing four templating centers is demonstrated via **H[2]C** using Metalation-demetalation-remetalation strategy with Co(III) and Cu(I)-metal ion exchange. Inevitably, this process involves relative pirouetting and circum-rotation motions between rings. The transformation is monitored by distinguished ^{1}H-NMR signals for all interlocked structures and a change in color of solution. Having two free dpp templating centers in **H[2]Co** and two pda in **H[2]Cu** makes these catenates suitable for synthesis of next higher ordered and even numbered homo catenanes in one pot. This study further establishes the use of one-pot double ring closing amide bond formation in the catenation step for the synthesis of interlocked structures.

4.5.Experimental Section:

4.5.1.Reagents and Instruments:

$SOCl_2$, Et_3N, ethylenediamine, 18-crown-6, pyridine hydrochloride, P-bromoanisole, 1,10-phenanthroline, Li-metal, $Co(OAc)_2.4H_2O$, anhydrous toluene and NaH has been purchased from Spectrochem India Pvt. Ltd. 2,6-pyridinedicarboxylic acid, MnO_2 is used from Himedia, India Pvt. Ltd. K_2CO_3, p-tolunesulfonyl choride, NaN_3, 4-dimethylaminopyridine, PPh_3, tetraethylene glycol brought from Sigma Aldrich. CH_3COOH taken from SRL Chemicals and tetrabutylammonium acetate is from Alfa Aeser. $Cu(CH_3CN)_4BF_4$ purchased from Acros Organics. Common organic solvents such as hexane, toluene, EtOAc, CH_3CN, DCM, DMF, THF, MeOH and EtOH purchased from Merck and used without further purification. Silica gel (100-200 mesh) has been used for column chromatography. Anhydrous MeOH, DCM, CH_3CN, THF, DMF has been prepared by common laboratory methods. $CDCl_3$ has been used from Sigma Aldrich. NMR spectra were recorded in a Bruker 400 MHz Spectrometer. Mass spectra

were recorded in Water ESI-MS and Bruker-ultraflextreme MALDI-TOF Spectrometer. UV-visible spectra were recorded in Jasco Spectrophotometer and fluorescence spectra were recorded in Agilent Cary Eclipse Fluorescence Spectrometer.

4.5.2. Synthesis of 2,6-Pyridinedicarbonyl dichloride:

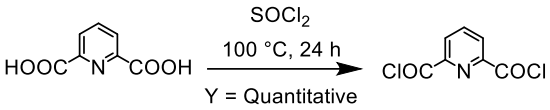

2,6-Pyridinedicarboxylic acid (5 g, 29.9186 mmol) was dissolved in 32 mL of $SOCl_2$ in a 100 mL round bottom flask. This reaction mixture was stirred and refluxed at 120 ˚C for 24 hours. Appearance of pink color solution indicates completion of reaction. After cooling to RT, excess $SOCl_2$ was evaporated under high vacuum to yield the desired product 2,6-pyridinedicarbonyl dichloride (white to pink solid) in quantitative yield. The product is moisture and air sensitive, and stored in a sealed and argon environment at 4 ˚C.

4.5.3. Synthesis of monomer M1:

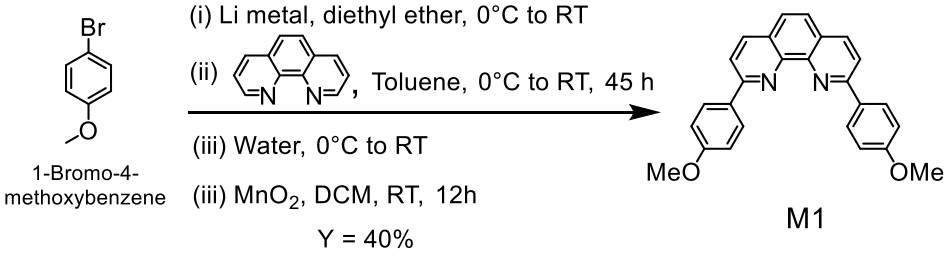

Monomer **M1** was synthesized by following reported literature procedure,[49-51] from p-bromoanisole and 1,10-phenanthroline. A three-neck 250 ml RB flask was taken, fitted with a 100 ml dropping funnel. 3.69 g of freshly and finely cut lithium metal was transferred into it under argon atmosphere. To it, 120 ml of anhydrous diethyl ether was transferred. Then, it was brought to 0 ˚C using ice bath and stirred well to form a suspension. In another 100 ml RB flask, 30 g of p-bromoanisole and 80 ml of anhydrous diethyl ether was transferred under argon atmosphere. This solution was poured into the dropping funnel fitted with the three-neck RB flask under argon atmosphere. Maintaining the temperature at 0 ˚C, 10 ml of p-bromoanisole

solution was added at once and stirred for 10 minutes. At this stage shining surface of lithium can be seen, indicates initiation of reaction. Now, rest of p-bromoanisole solution was added dropwise (1 drop per second) to the suspension of lithium metal in diethyl ether for 1 hour while maintaining the temperature at 0 ˚C. Then, it was slowly brought to RT and stirred for overnight. At this stage p-bromoanisole is converted to 4-methoxyphenyl lithium. In a another 500 ml RB flask, 5 g of anhydrous 1,10-phennanthroline was taken and kept at 125 ˚C inside oven for 30 minutes until it melts and all water gets removed. It was degassed and 200 ml of anhydrous toluene was transferred under argon atmosphere and sonicated to solubilize. This solution was brought to 0 ˚C using ice bath. To it, suspension of 4-methoxyphenyl lithium in diethyl ether was transfer using syringe under argon atmosphere. Initially, it was stirred for 1 h at 0 ˚C and slowly brought to RT and stirred for another 45 hours. This reaction mixture was quenched by slowly adding ice cold water into it while maintaining the outside temperature at 0 ˚C using ice bath. It was brought to RT and stirred for another 1 hour. Further, a work up was performed adding DCM into it. The organic layer was concentrated and 100 g of MnO_2 and 600 ml of fresh DCM was added to it and stirred for 12 hour at RT to re-aromatize. After this, anhydrous Na_2So_4 was added to it and filtered using filter paper at once. The filtrate was concentrated and purified by using silica column chromatography starting from 1:1 hexane: DCM up to 0.5:95.5 MeOH: DCM via 100% DCM. The collected product was washed twice with diethyl ether to get pure product **M1** as pale yellow solid (4.4 g) with yield of 40.41%.

^{1}H-NMR (400 MHz, $CDCl_3$) δ in ppm: 8.45-8.43 (d, 4H), 8.26-8.24 (d, 2H), 8.09-8.07 (d, 2H), 7.73 (s, 2H), 7.13-7.11 (d, 4H), 3.92 (s, 6H).

^{13}C-NMR (100 MHz, $CDCl_3$) δ in ppm: 160.86, 156.33, 145.97, 136.76, 132.12, 128.97, 127.50, 125.58, 119.33, 114.16, 55.36.

4.5.4. Synthesis of monomer M2 (Phen-OH):

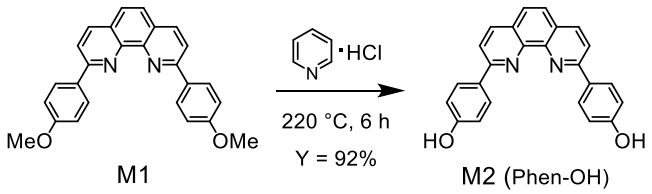

Monomer **M2** was synthesized following literature procedure.[51] To a 500 ml RB flask, 1.5 g (1 equiv., 3.82 mmol) monomer **M1** and pyridine hydrochloride 28.69 g (65 equiv., 248.43 mmol) was transferred**.** It was stirred and refluxed at 220 ˚C for 6 hours under argon atmosphere. Then, it was brought to 180 ˚C and 60 mL of hot water was added into it slowly. Effervescence will appear. Heating process was stopped to bring the reaction mixture to RT. To it, mixed solvent of EtOH and water in 40:60 ratio (50:75 mL) was added. It was stirred, for 1 hour at RT and left at 4 ˚C for overnight. This suspension was neutralized to pH 7.4 exactly, by adding 225 ml of 1M NaOH (prepared by taking 9 g NaOH and making volume up to 225 mL by adding DI water). A change in color from light red to orange was observed. The quenched suspension was left again at 4 ˚C for 2 hours and subsequently filtered to collect the precipitate. the precipitate was washed with a portion of mixed solvent of EtOH:H_2O (40:60, v/v) and dried using tissue paper at RT to get desired product **M2** brown colored solid in 92% yield.

^{1}H-NMR (400 MHz, DMSO-D_6) δ in ppm: 9.99 (br, 2H), 8.53-8.51 (d, 2H), 8.37-8.35 (d, 4H), 8.30-8.28 (d, 2H), 7.93 (s, 2H), 7.03-7.00 (d, 4H).

^{13}C-NMR (100 MHz, DMSO-D_6) δ in ppm: 159.38, 155.30, 137.64, 129.07, 127.25, 125.64, 119.55, 115.81.

4.5.5. Synthesis of monomer M3:

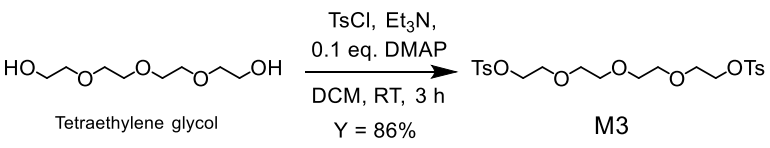

Tetraethylene glycol (20 g, 102.9 mmol), tosyl chloride (78.51 g, 411.8 mmol), triethylamine (172.4 mL, 1235.4 mmol) was dissolved in DCM under argon atmosphere at 0 ˚C and this reaction mixture was brought to RT and stirred for one hour. Again, it was brought to 0 ˚C using ice bath and DMAP (1.257 g, 0.1 equivalent, 10.29 mmol) was added into the mixture. This reaction mixture was stirred at RT for 2 hours. Immediately quenched by adding water at 0 ˚C and extracted with DCM. The combined DCM layer were dried over anhydrous Na_2SO_4, concentrated and purified by column chromatography (with hexane: EtOAc, 50:50 v/v as eluent) to produce pale yellow liquid product **M3** (34 g, 65.7%).

^{1}H-NMR (400 MHz, $CDCl_3$) δ in ppm: 7.79-7.77 (d, 4H), 7.34-7.32 (d, 4H), 4.16-4.13 (m, 4H), 3.68-3.67 (dd, 4H), 3.55 (s, 8H), 2.43 (s, 6H).

^{13}C-NMR (100 MHz, $CDCl_3$) δ in ppm: 144.79, 132.94, 129.80, 127.93, 70.68, 70.50, 69.22, 68.64, 21.60.

HR-MS (ESI$^+$): Calcd. m/z for $C_{22}H_{30}O_9S_2Na$ $[M+Na]^+$ 525.1398, found 525.1376.

4.5.6. Synthesis of monomer M4:

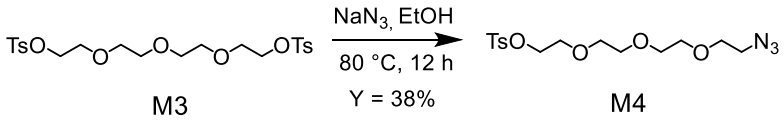

M3 M4

Monomer **M4** was synthesized according to reported literature procedure.[52] Monomer **M3** (4 g, 7.96 mmol) and NaN_3 (0.556 g, 8.56 mmol) were mixed in a 250 mL RB flask and 150 ml absolute ethanol was added into it. The reaction mixture was heated at 80 ˚C for not more than 12 hours. EtOH was evaporate to dryness under reduced pressure followed by column chromatography using 75:25 hexane: EtOAc as eluent to get desired product (colorless liquid) **M4** in 38% yield (1.13 g). The product formed can be visualize over thin layer chromatography using UV-lamp.

^{1}H-NMR (400 MHz, $CDCl_3$) δ in ppm: 7.79-7.77 (d, 2H), 7.34-7.32 (d, 2H), 4.14 (t, 2H), 3.68-3.58 (m, 12H), 3.36 (t, 2H), 2.43 (s, 3H).

^{13}C-NMR (100 MHz, $CDCl_3$) δ in ppm: 144.75, 132.90, 129.75, 127.89, 70.66, 70.56, 70.50, 69.94, 69.18, 68.58, 50.59, 21.55.

HR-MS (ESI$^+$): Calcd. m/z for $C_{15}H_{23}N_3O_7SNa$ $[M+Na]^+$ 412.1149, found 412.0855.

4.5.7. Synthesis of monomer M5:

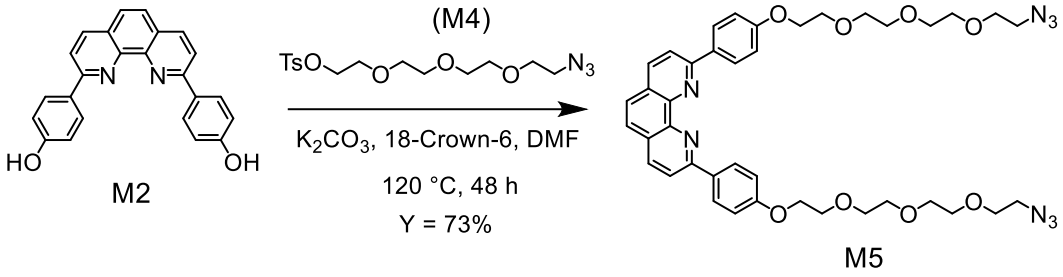

Monomer **M4** (5 g, 13.389 mmol), **M2** (2.244 g, 6.159 mmol), anhydrous K_2Co_3 (18.5 g, 133.897 mmol), 18-crown-6 (0.264 g) and 80 mL of anhydrous DMF were mixed in a 250 mL RB flask. It was refluxed at 120 ˚C for 48 hours. Then, DMF was evaporated completely and the crude mixture was subjected to silica gel column chromatography with 98:2 DCM: MeOH as eluent. Desired product **M5** was collected and washed with hexane to purify further to isolate in 73% yield (3.44 g).

^{1}H-NMR (400 MHz, $CDCl_3$) δ in ppm: 8.42-8.40 (d, 4H), 8.26-8.24 (d, 2H), 8.08-8.06 (d, 2H), 7.73 (s, 2H), 7.13-7.11 (d, 4H), 4.26 (t, 4H), 3.92 (t, 4H), 3.78 (t, 4H), 3.76 (t, 4H), 3.73-3.66 (m, 12H), 3.38 (t, 4H).

^{13}C-NMR (100 MHz, $CDCl_3$) δ in ppm: 160.07, 156.31, 145.98, 136.76, 132.29, 128.95, 127.52, 125.61, 119.35, 114.83, 70.87, 70.71, 70.66, 70.00, 69.72, 67.49, 50.65.

HR-MS (ESI$^+$): Calcd. m/z for $C_{40}H_{47}N_8O_8[M+H]^+$ 767.3511, found 767.418.

4.5.8. Synthesis of macrocycle M6:

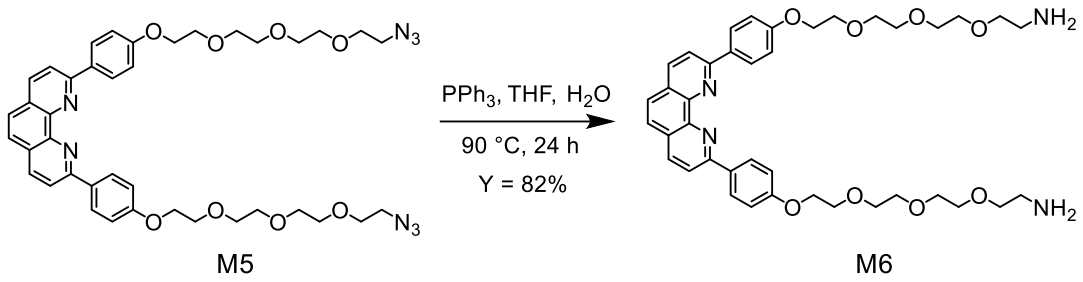

Monomer **M5** (3 g, 3.912 mmol), PPh_3 (5.13 g, 19.56 mmol) and H_2O (0.422 mL, 23.475 mmol) were mixed with 100 mL anhydrous THF under argon atmosphere in a RB flask. The reaction mixture was refluxed at 90 ˚C for 24 hours. It was evaporated to dryness under reduced pressure and purified by silica gel column chromatography using DCM: MeOH: Et_3N (90:10:3) as eluent to isolate desired di-amine product, off-white thick liquid **M6** (2.3 g, yield 82%). TLC visualization of di-amine product was carried out under UV-lamp as well as ninhydrin test. Isolated **M6** was immediately used for next reaction without further characterization. It is to be note that **M6** is moisture and air sensitive.

4.5.9. Synthesis of monomer M7:

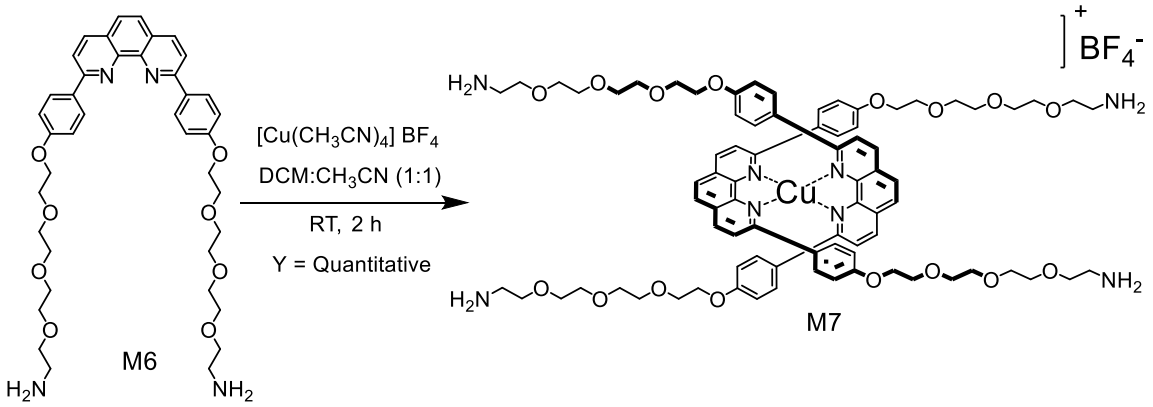

In a 1 Liter RB flask, **M6** (1.14 g, 1.594 mmol) was transferred and 100 mL anhydrous DCM was added under argon atmosphere to solubilize it. To it, solution of $Cu(CH_3CN)_4BF_4$ (0.26 g, 0.829 mmol) in 20 mL CH_3CN was added under argon atmosphere. Instant change in color to red-black was observed. This reaction mixture was stirred at RT for 2 hours. Then, concentrated

in rotatory evaporator and proceed further for ring closing reaction without any purification. Quantitative formation of the product **M7** was assumed in this step.

4.5.10. Synthesis of catenate H[2]Cu:

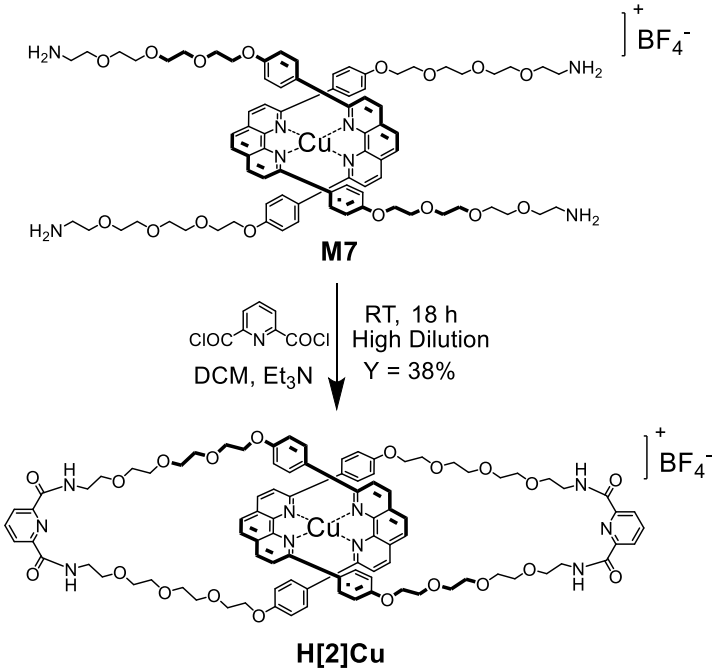

Double macrocyclization in one pot, was performed under high dilution conditions. To 1 Liter RB flask having monomer **M7** (1.19 g, 0.796 mmol), was added 714 mL of anhydrous DCM under argon atmosphere. This solution was then brought to 0 ˚C and Et_3N (0.5 mL, 3.586 mmol) was injected and stirred. To it, 2,6-pyridinedicarbonyl dichloride (0.325 g, 1.593 mmol) dissolved in 30 mL of anhydrous DCM was added dropwise over a 10 minutes at 0 ˚C. It was stirred for 18 hours at RT. Solvent was removed under reduced pressure and the crude was purified by silica gel column chromatography using DCM: MeOH (96:4 to 90:10) as eluent to get the desired product **H[2]Cu**. Then, work up was performed with **H[2]Cu** with DCM and water to remove any possible Et_3NHCl salt present. The DCM layer was dried with anhydrous Na_2SO_4, concentrated and washed with hexane twice to get pure product **H[2]Cu** as red-black colored semi solid in 38% yield, 0.54 g.

^{1}H-NMR (400 MHz, $CDCl_3$) δ in ppm: 8.84 (br, 4H), 8.58-8.56 (d, 4H), 8.20-8.18 (d, 8H), 7.86 (m, 4H), 7.38 (m, 8H), 6.02 (br, 8H), 3.77-3.69 (m, 54H), 3.63-3.61 (m, 10H).

^{13}C-NMR (100 MHz, $CDCl_3$) δ in ppm: 163.98, 159.05, 155.91, 148.83, 143.22, 138.39, 137.43, 131.43, 129.15, 128.03, 126.61, 124.43, 123.92, 112.77, 70.66, 70.55, 70.36, 70.10, 69.70, 69.21, 67.27, 39.07.

HR-MS (ESI^{+}): Calcd. m/z for $C_{94}H_{102}CuN_{10}O_{20}$ $[M]^{+}$ is 1754.6599, found 1754.5001 and for $C_{94}H_{102}NaN_{10}O_{20}$ $[M^{+}+Na^{+}]^{2+}$ 888.8230, found 888.8469.

4.5.11. Demetalation of H[2]Cu to form H[2]C:

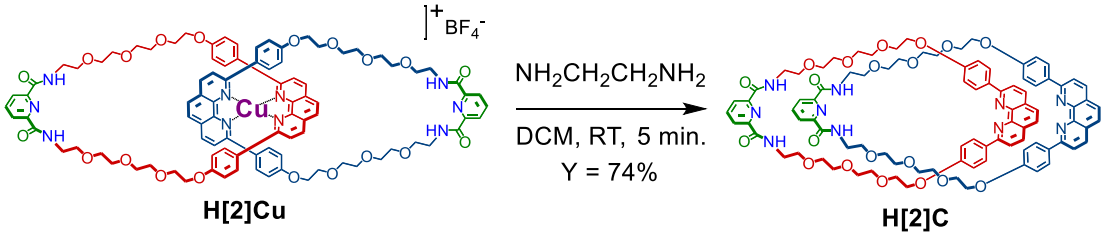

H[2]Cu (0.14 g, 0.0797 mmol) was dissolved in 40 ml of DCM and ethylene diamine was added into it in excess and stirred for 5 minutes. Immediate disappearance of red-black color was observed and a colorless solution was formed, indicates demetalation of Cu(I) from **H[2]Cu**. This reaction mixture was subjected to work up with water and DCM. DCM layer was collected, dried with anhydrous Na_2SO_4, concentrated and subjected to silica gel column chromatography with 96:4 DCM: MeOH to isolate **H[2]C**. It was washed with hexane 2 times to purify further and collect pure **H[2]C** product with 74% yield (0.1 g).

^{1}H-NMR (400 MHz, $CDCl_3$) δ in ppm: 9.27 (br, 4H), 8.37-8.35 (d, 4H), 8.17-8.15 (d, 4H), 7.93-7.84 (br, 14H), 7.79 (br, 4H), 6.68-6.66 (d, 8H), 4.02 (t, 8H), 3.78 (t, 8H), 3.67 (br, 8H), 3.62 (br, 8H), 3.55 (br, 8H), 3.50 (br, 16H), 3.44 (t, 8H) .

^{13}C-NMR (100 MHz, $CDCl_3$) δ in ppm: 164.09, 159.77, 157.19, 148.68, 145.96, 138.59, 137.03, 132.34, 129.22, 127.60, 125.86, 124.52, 120.28, 114.40, 70.75, 70.45, 70.30, 69.92, 69.48, 69.33, 67.36, 39.02.

HR-MS (ESI$^+$): Calcd. m/z for $C_{94}H_{104}N_{10}O_{20}$ $[M+2H]^{2+}$ is 846.8712, found 846.8930.

4.5.12. Synthesis of catenate H[2]Co from fully organic catenane H[2]C:

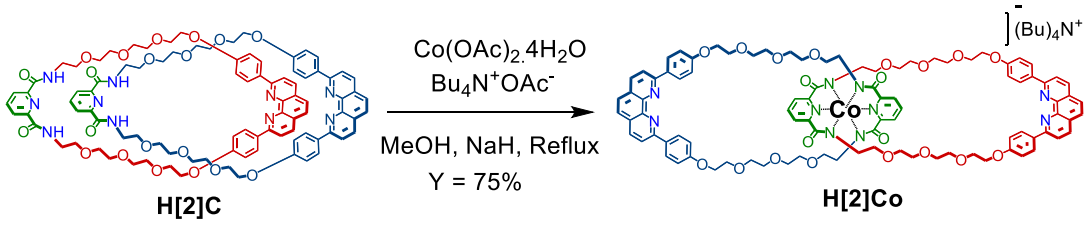

Cobalt metal complexation was performed according to reported literature procedure.[53] To a 100 mL two-neck round bottom flask **H[2]C** (0.143 g, 0.0845 mmol), $Co(OAc)_2.(H_2O)_4$ (0.021 g, 0.0845 mmol) and Bu_4NOAc (0.025 mL, 0.0845 mmol) was transferred and it was purged with anhydrous methanol (25 mL) under inert atmosphere. Then, this two neck RB was fitted with a condenser and two rubber septum and brought under argon atmosphere. This mixture was refluxed at 80 ˚C for 1 hour under inert atmosphere to obtain a clear pale pink solution. In another RB flask, sodium methoxide was prepared (by the slow addition of 25 mL anhydrous methanol into 1 g NaH at 0 ˚C). Prepared NaOMe was injected into the reaction mixture at reflux conditions. This results a color change to deep-red. At this conditions, it was stirred for 1 hour. Then, the rubber septum attached to the condenser was removed to let the reaction mixture oxidize. At this stage, the solution start to turn light-green and it was further refluxed for 24 hours. Solvent was evaporated to dryness and the residue was subjected to SiO_2 column chromatography using DCM: MeOH (92:8 to 85:15 v/v) as eluent to collect green colored product **H[2]Co**. It was further purified by washing with Hexane and EtOAc (two times each) to result **H[2]Co** in 75% yield (0.11 g) with improved purity.

^{1}H-NMR (400 MHz, $CDCl_3$) δ in ppm: 8.33-8.31 (d, 8H), 8.19-8.17 (d, 6H), 8.06-8.04 (d, 4H), 8.00-7.98 (d, 4H), 7.65 (s, 4H), 7.08-7.06 (d, 8H), 4.20 (t, 8H), 3.84 (t, 8H), 3.64 (t, 8H), 3.54 (t, 8H), 3.42 (t, 8H), 3.18 (t, 8H), 2.93 (t, 8H), 2.30 (t, 8H).

^{13}C-NMR (100 MHz, $CDCl_3$) δ in ppm: 168.59, 159.96, 157.07, 156.13, 145.80, 139.93, 136.80, 132.21, 128.88, 127.49, 125.59, 123.38, 119.38, 114.87, 77.00, 70.44, 70.01, 69.76, 69.63, 69.57, 67.50, 43.15.

HR-MS (ESI$^+$): Calcd. m/z for $C_{94}H_{101}CoN_{10}O_{20}$ $[M^-+3H^+]^{2+}$ is 874.8268, found 874.8223 and for $C_{94}H_{102}CoN_{10}O_{20}$ $[M^-+4H^+]^{3+}$ is 583.5531, found 583.5580. For $(Bu)_4N^+$ calculated m/z is 242.2850, found m/z 242.2858.

4.5.13. Demetalation of H[2]Co to form H[2]C:

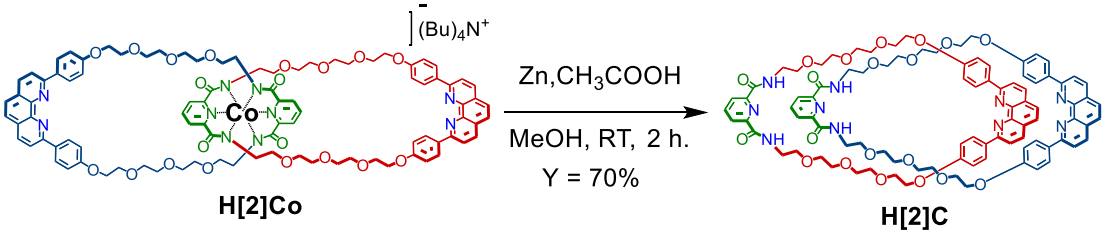

H[2]Co H[2]C

Removal of cobalt metal from **H[2]Co** was done according to reported literature procedure.[54] 0.069 g of **H[2]Co** was transferred to a 100 RB flask, and anhydrous MeOH and 20 ml CH_3COOH each was added, followed by addition of activated zinc 0.2 g. This reaction mixture was stirred for 5 hours in open air. Partial disappearance of green color from the reaction mixture can be used as an indication for completion of reaction. Solvent was removed to dryness using rotatory evaporator and 30 mL of $CHCl_3$ was added. To it 1:1 mixture of 12.5 mL of 17.5% ammonia solution and 12.5 mL of saturated Na_4EDTA was added. The mixture was stirred for 30 minutes and work up was performed with $CHCl_3$ three times. Organic layer was collected and again work up was performed using brine solution once. The final organic layer was collected, dried with anhydrous Na_2SO_4, evaporated to dryness, and purified by

column chromatography using DCM: MeOH in 96:4 as eluent to isolate **H[2]C** in 70% yield (0.047 g). Formation of **H[2]C** is confirmed by ^{1}H-NMR, ^{13}C-NMR and ESI-MS analysis.

12.5 mL of saturated Na_4EDTA was prepared by mixing 5 g of EDTA with 2.73 g of NaOH and making the volume up to 12.5 mL with water and stirring it well. Activated Zinc was prepared by taking 10 g of Zinc powder in a RB flask and washing it with 2N HCl three times followed by washing with DI water, ethanol, acetone, diethyl ether two times each and drying in hot air oven at 100 ˚C for 15 minutes.

4.5.14. Synthesis of catenate H[2]Cu from fully organic catenane H[2]C:

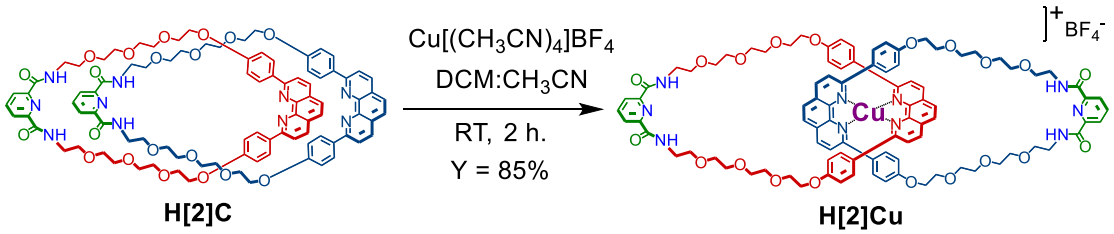

In a 100 ml RB flask, **H[2]C** (0.136 g, 0.0803 mmol) was transferred, and 20 mL anhydrous DCM was added under argon atmosphere. To it, solution of $Cu(CH_3CN)_4BF_4$ (0.0252 g, 0.0803 mmol) dissolved in 20 mL CH_3CN was added under argon atmosphere. Instant change in color to red-black was observed. This solution was stirred at RT for 2 hours. It was concentrated in rotatory evaporator and subjected to silica gel column chromatography using 95:5 to 90:10 DCM: MeOH as eluent to isolate red-black colored **H[2]Cu**. It was washed 2 times with hexane to remove oily impurity to get **H[2]Cu** in 85% yield (0.12 g). Formation of **H[2]Cu** is confirmed by ^{1}H-NMR, ^{13}C-NMR and ESI-MS analysis.

4.5.15. Synthesis of macrocyclic monomer MC-1:

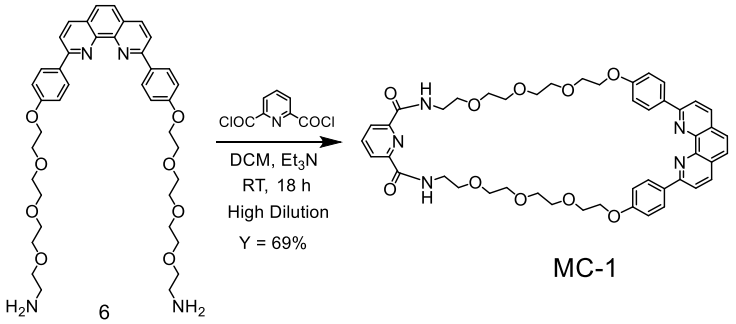

Macrocyclization was performed under high dilution conditions. To 500 mL RB flask having di-amine monomer **M6** (0.341 g, 0.477 mmol), 204.6 mL of anhydrous DCM was added under argon atmosphere. This solution was then brought to 0 ˚C, and Et_3N (0.148 mL, 1.063 mmol) was injected into it, and stirred. To it, 2,6-pyridinedicarbonyl dichloride (0.0973 g, 0.477 mmol) dissolved in 20 mL of anhydrous DCM was added dropwise over a 10 minutes at 0 ˚C. It was stirred for 18 hours at RT. Solvent was removed under reduced pressure, and the crude was purified by silica gel column chromatography using DCM: MeOH (97:3) as eluent to get the desired product **MC-1**. It was washed with hexane to get pure product as light green colored solid in 69% yield 0.278 g.

^{1}H-NMR (400 MHz, $CDCl_3$) δ in ppm: 8.70 (br, 2H) , 8.41-8.39 (d, 4H), 8.29-8.22 (m, 4H), 8.05-8.03 (d, 2H), 7.95 (t, 1H), 7.72 (s, 2H), 7.13-7.11 (d, 4H), 4.26 (t, 4H), 3.85 (t, 4H), 3.73-3.66 (m, 24H).

^{13}C-NMR (100 MHz, $CDCl_3$) δ in ppm: 163.82, 159.96, 156.14, 148.76, 145.86, 138.65, 136.69, 132.39, 128.94, 127.40, 125.53, 124.71, 119.18, 115.02, 70.85, 70.51, 70.07, 69.97, 69.62, 67.55, 39.36.

HR-MS (ESI$^+$): Calcd. m/z for $C_{47}H_{52}N_5O_{10}$ $[M+H]^+$ is 846.3709, found 846.3807 and for $C_{47}H_{53}N_5O_{10}$ $[M+H]^{2+}$ is 423.6892, found 423.6970.

4.6. Spectral data:

4.6.1. ^{1}H and ^{13}C NMR Spectra:

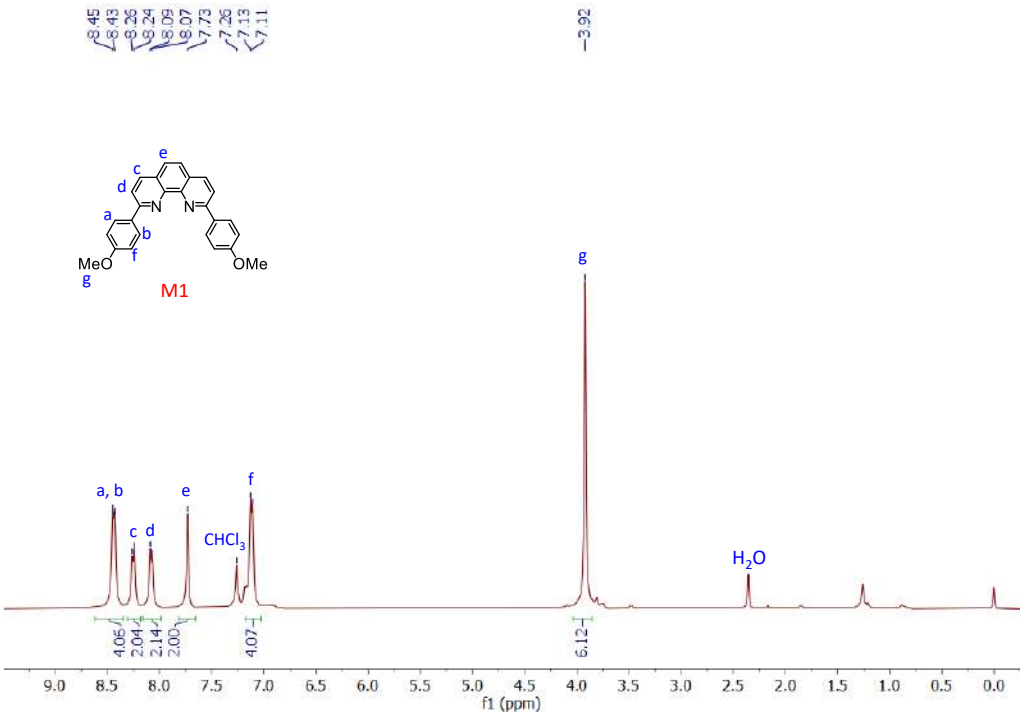

Figure 4.16. ^{1}H-NMR spectra of monomer M1 in $CDCl_3$ (400 MHz).

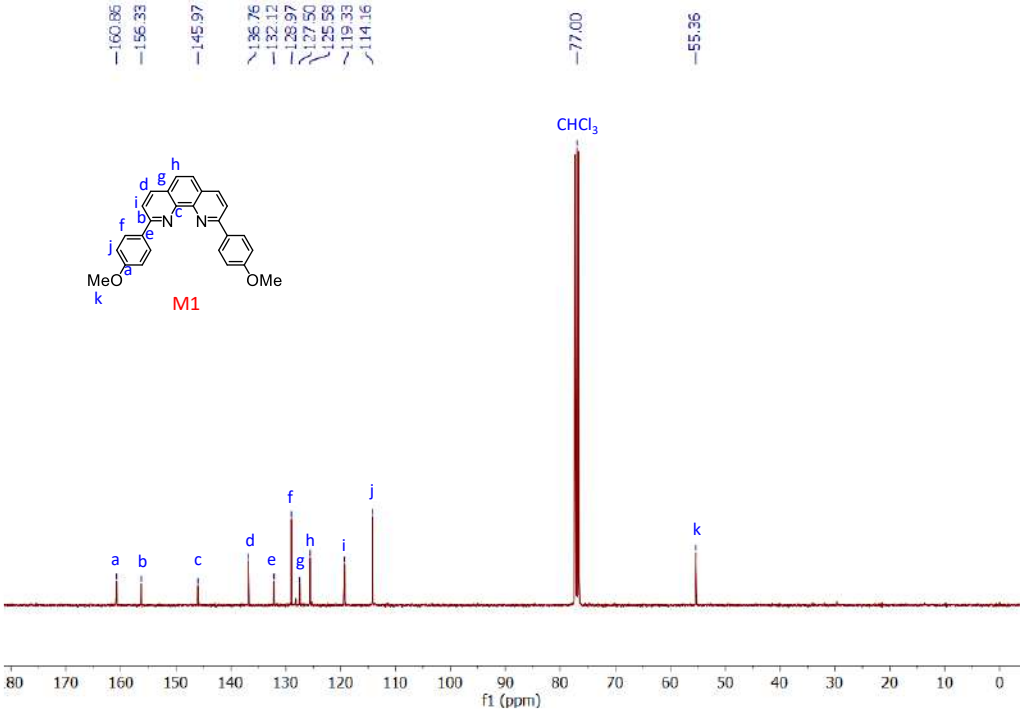

Figure 4.17. ^{13}C-NMR spectra of monomer M1 in $CDCl_3$ (100 MHz).

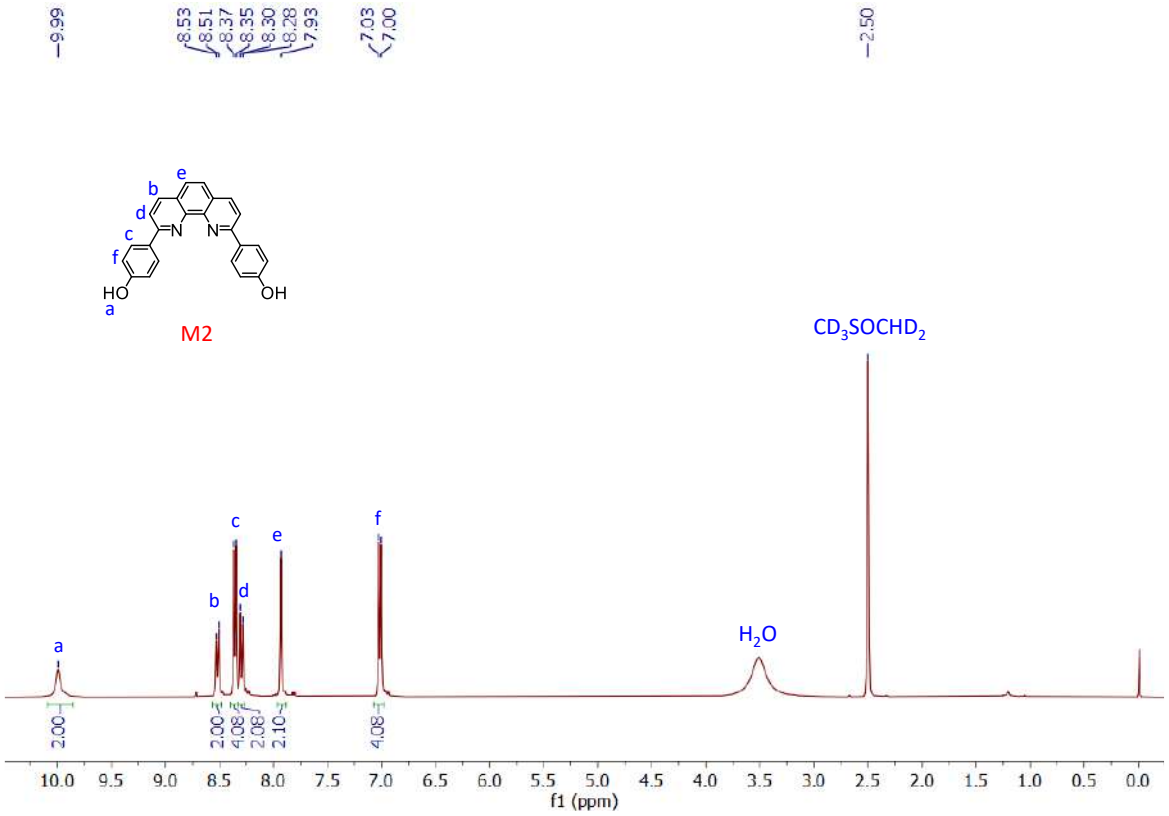

Figure 4.18. ^{1}H-NMR spectra of monomer M2 (Phen-OH) in DMSO-D_6 (400 MHz).

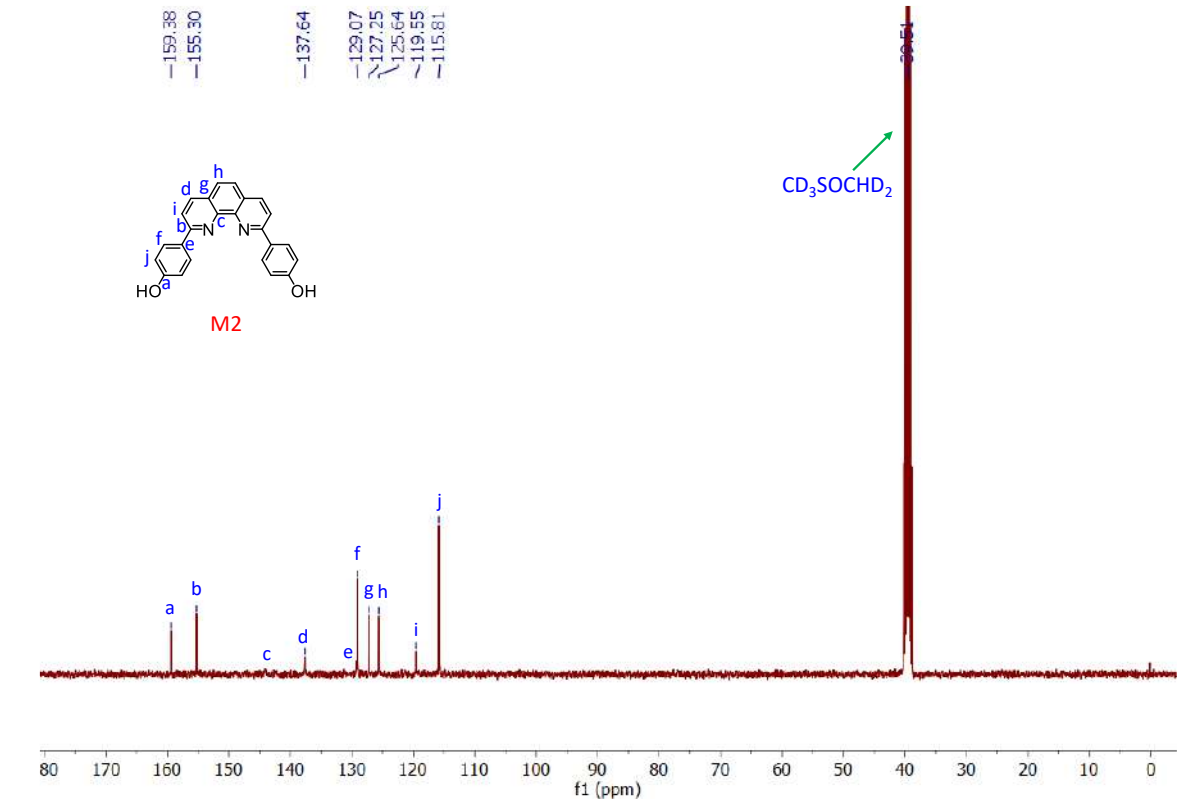

Figure 4.19. ^{13}C-NMR spectra of monomer M2 (Phen-OH) in DMSO-D_6 (100 MHz).

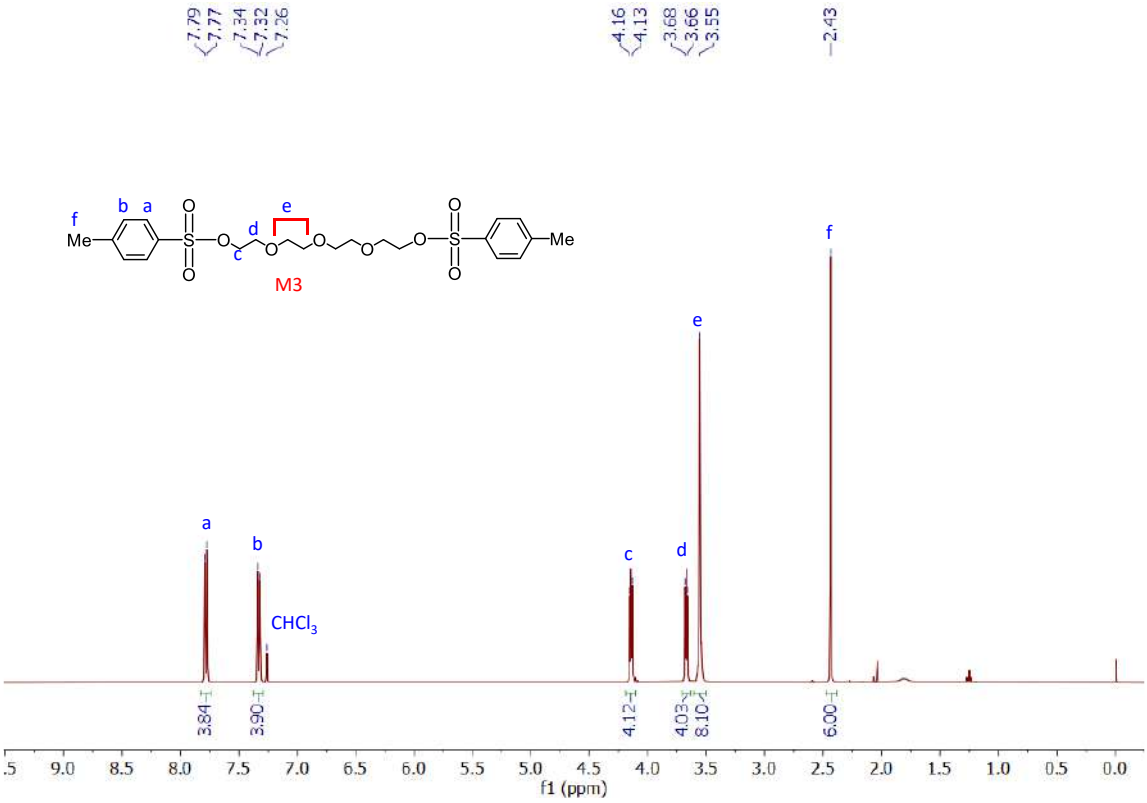

Figure 4.20. ^{1}H-NMR spectra of monomer M3 in $CDCl_3$ (400 MHz).

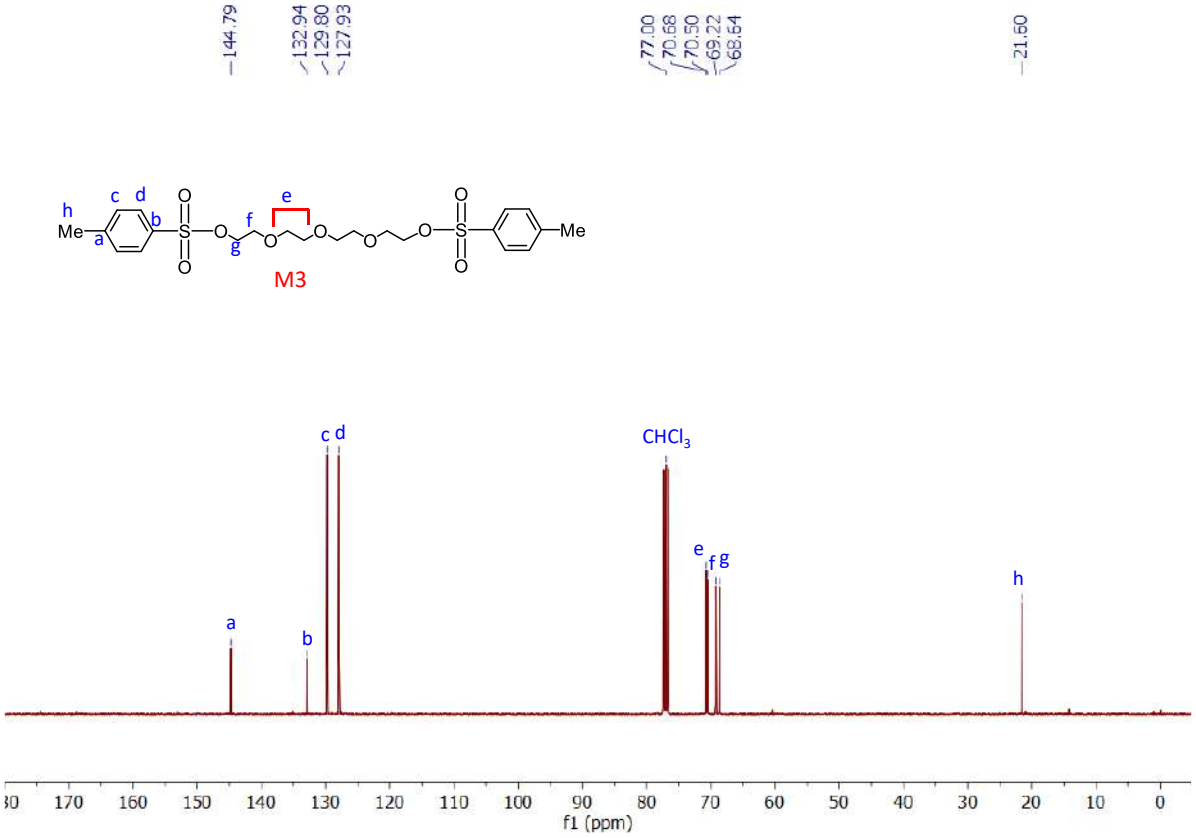

Figure 4.21. ^{13}C-NMR spectra of monomer M3 in $CDCl_3$ (100 MHz).

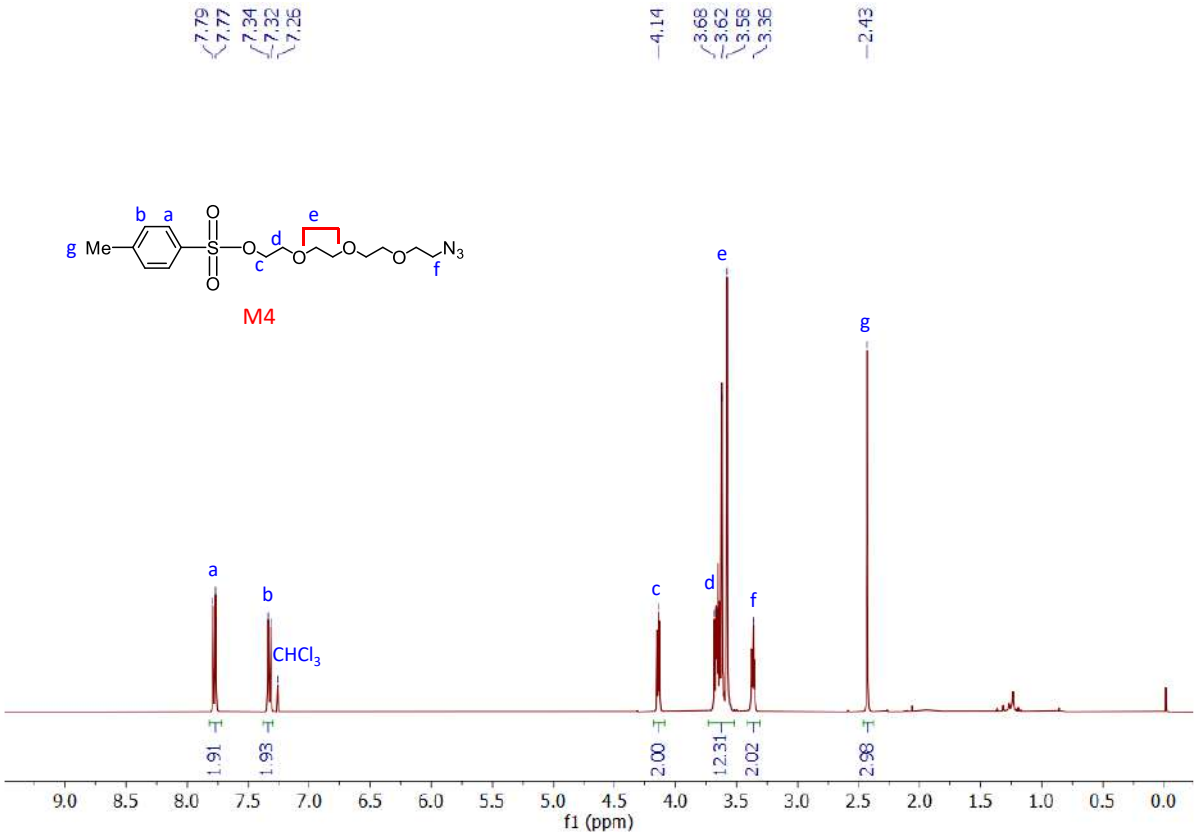

Figure 4.22. ^{1}H-NMR spectra of monomer M4 in $CDCl_3$ (400 MHz).

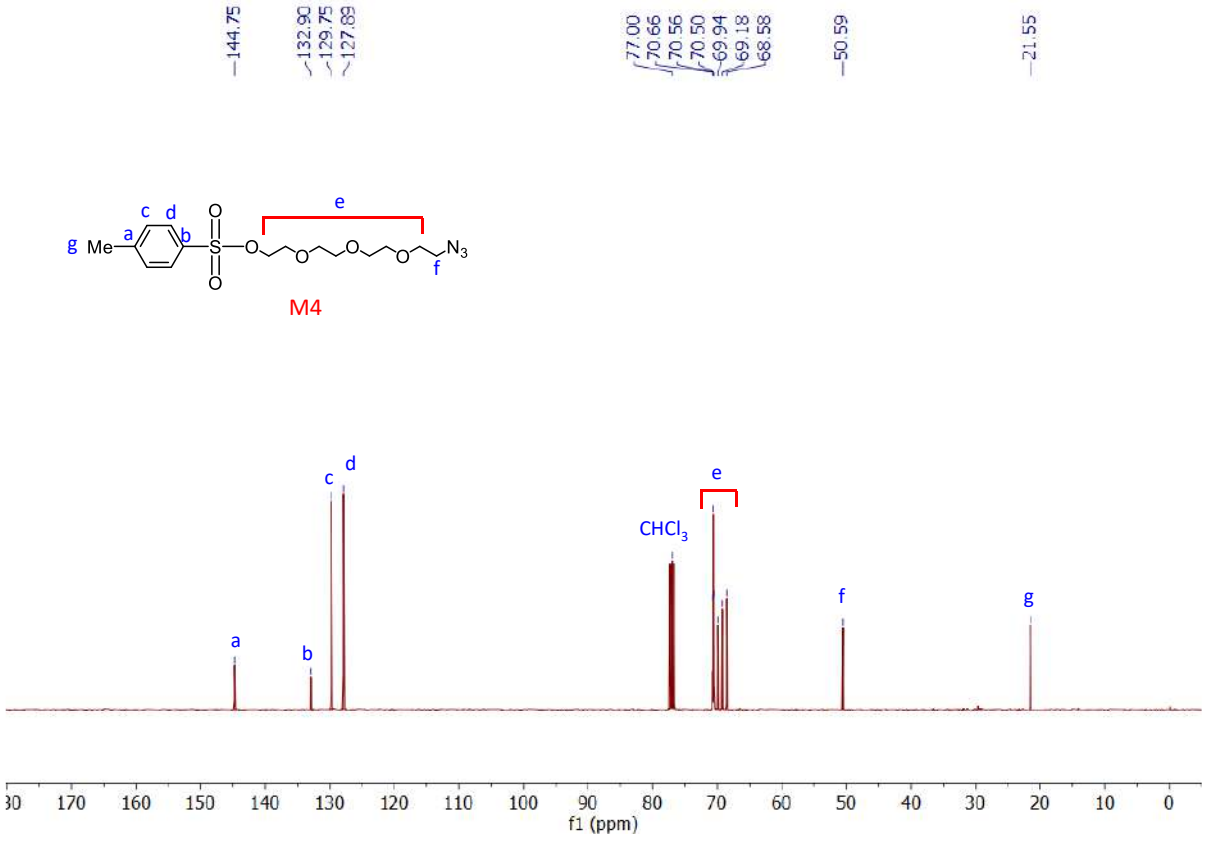

Figure 4.23. ^{13}C-NMR spectra of monomer M4 $CDCl_3$ (100 MHz).

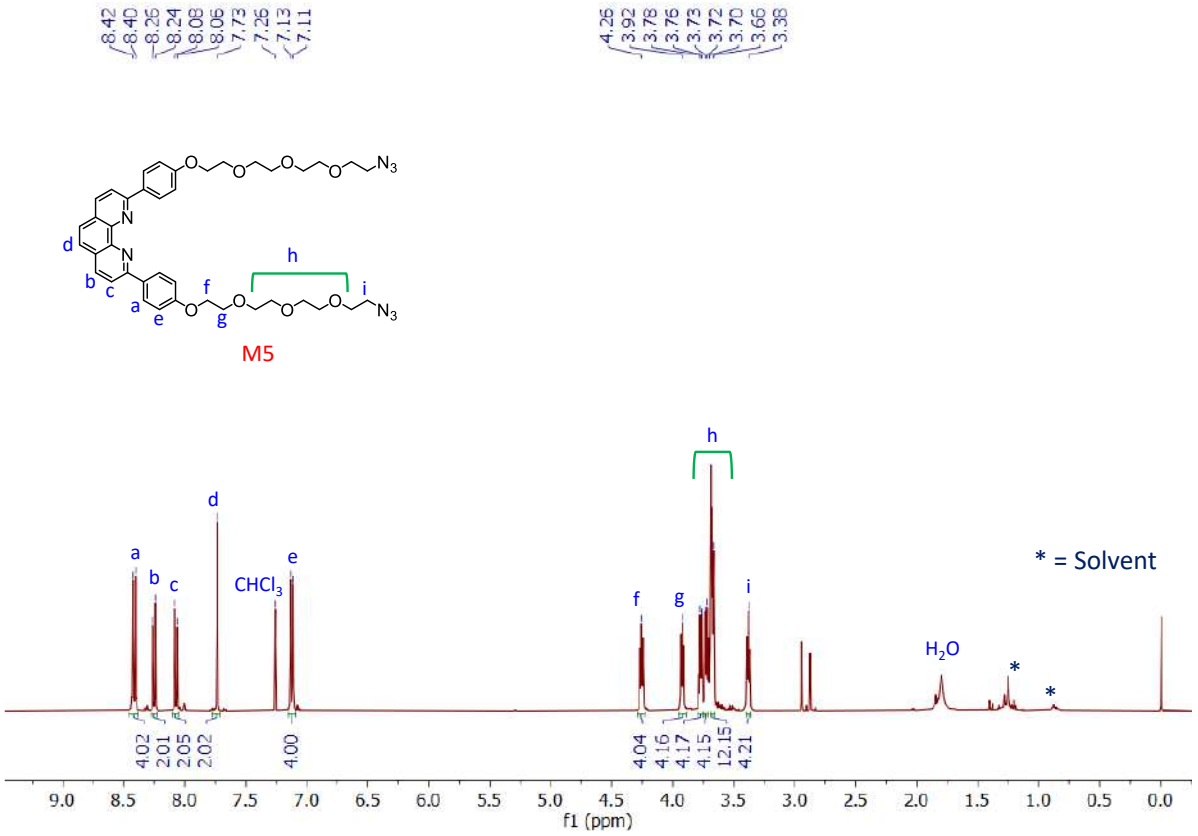

Figure 4.24. ^{1}H-NMR spectra of monomer M5 in $CDCl_3$ (400 MHz).

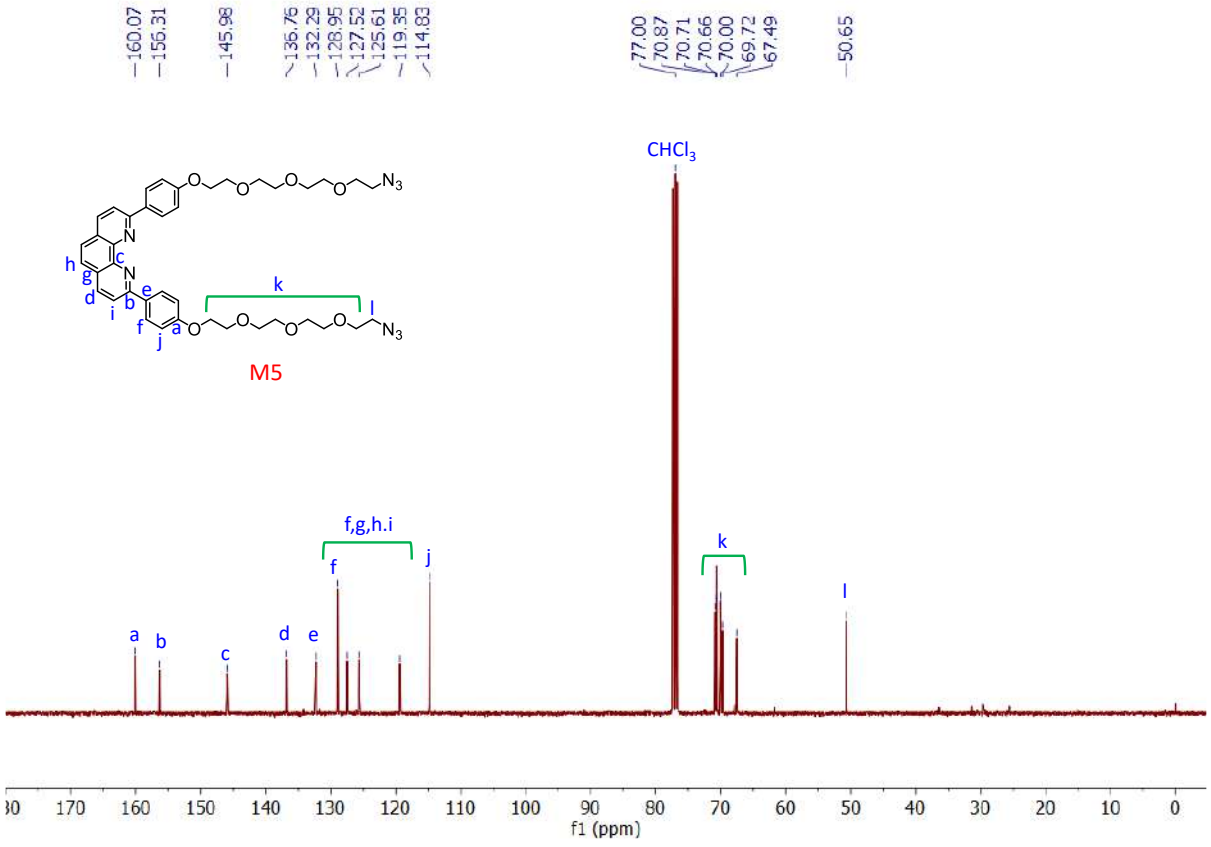

Figure 4.25. ^{13}C-NMR spectra of monomer M5 in $CDCl_3$ (100 MHz).

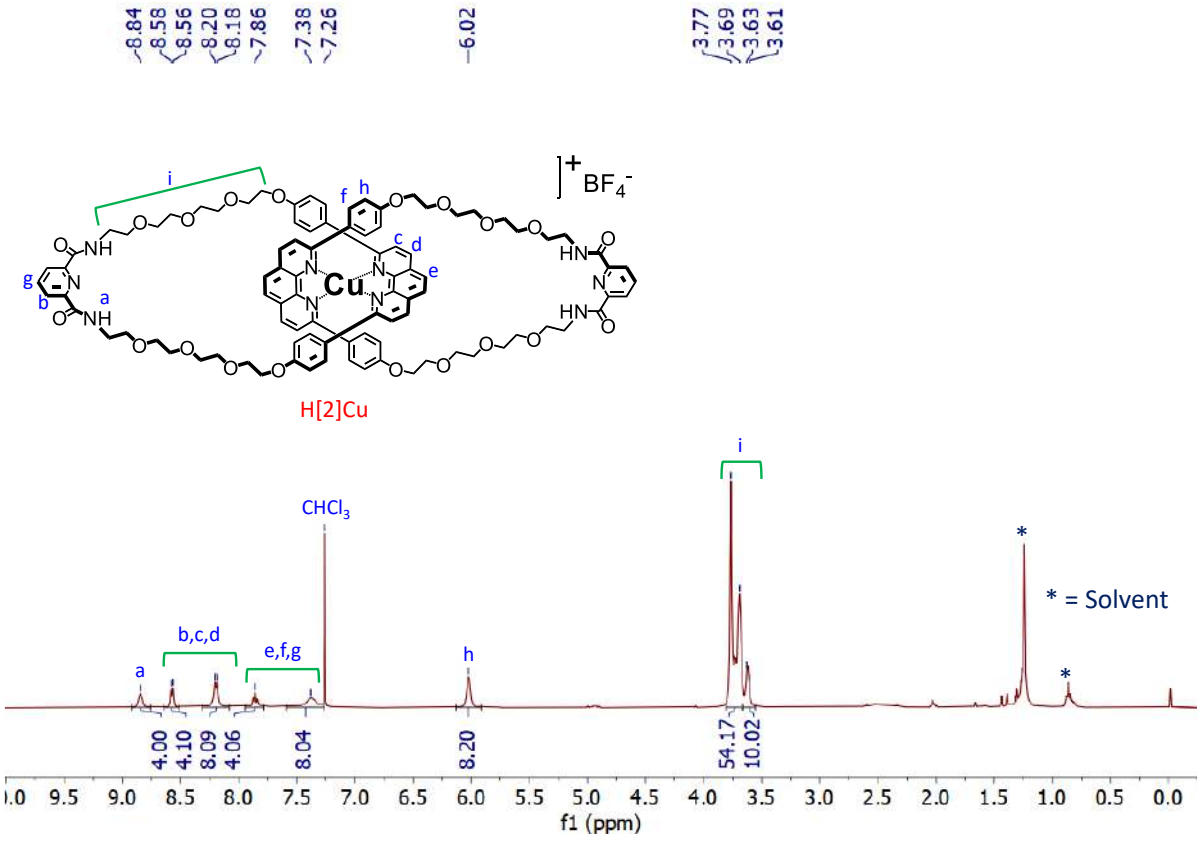

Figure 4.26. ^{1}H-NMR spectra of H[2]Cu in $CDCl_3$ (400 MHz).

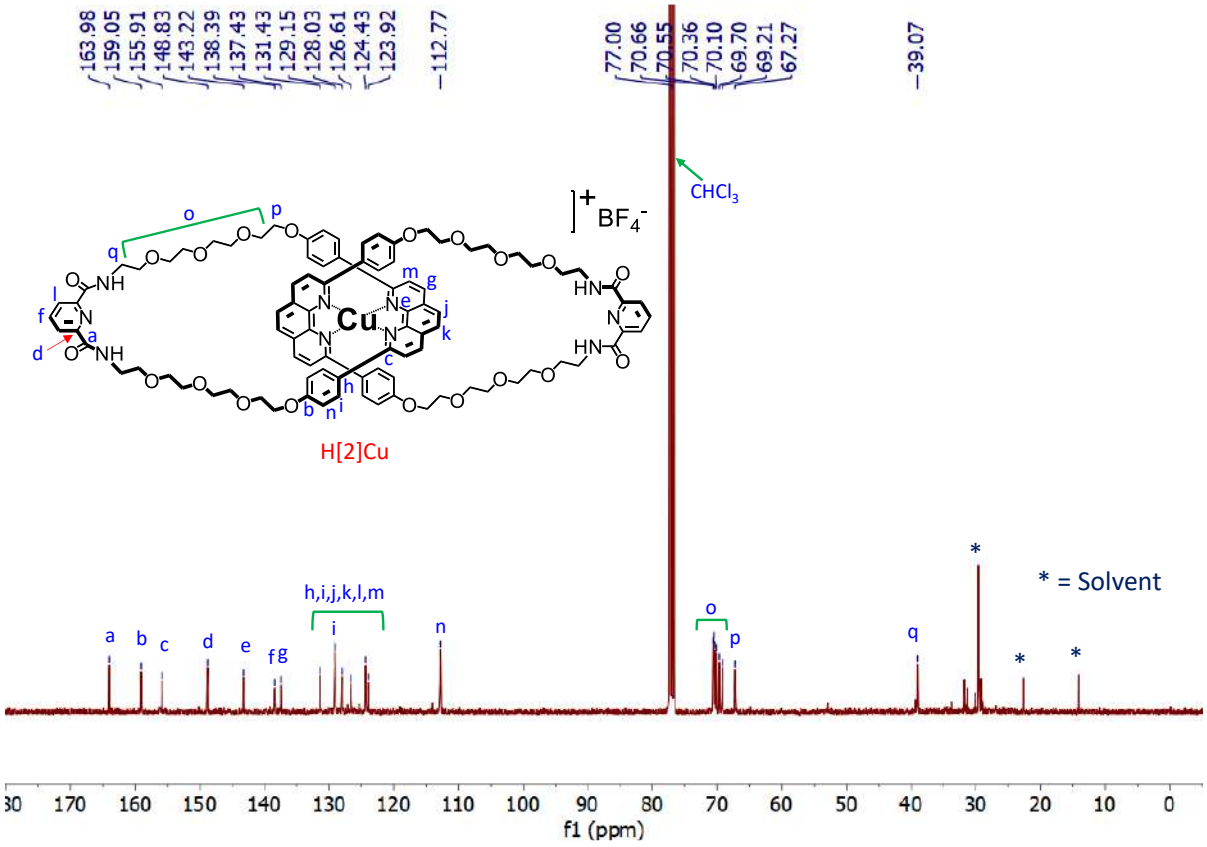

Figure 4.27. ^{13}C-NMR spectra of H[2]Cu in $CDCl_3$ (100 MHz).

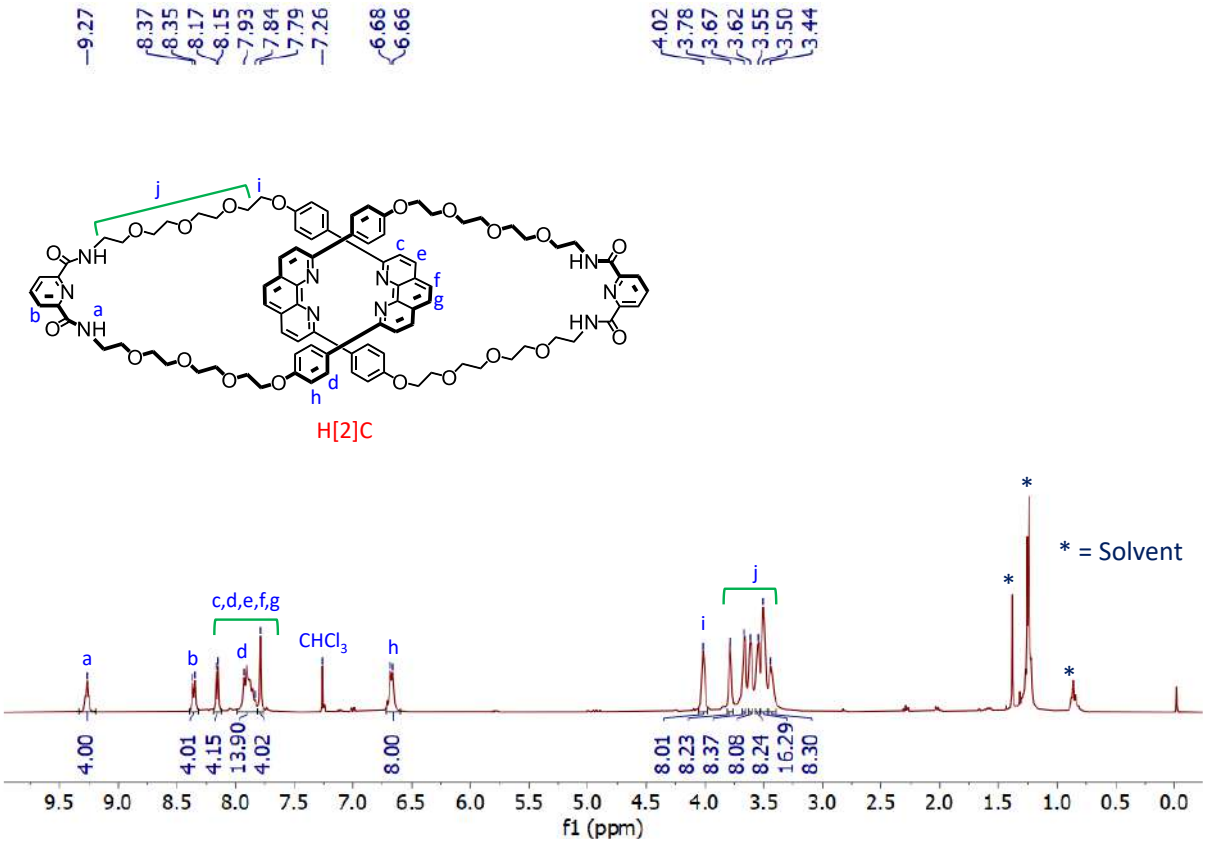

Figure 4.28. ^{1}H-NMR spectra of homo [2]catenane H[2]C in $CDCl_3$ (400 MHz)

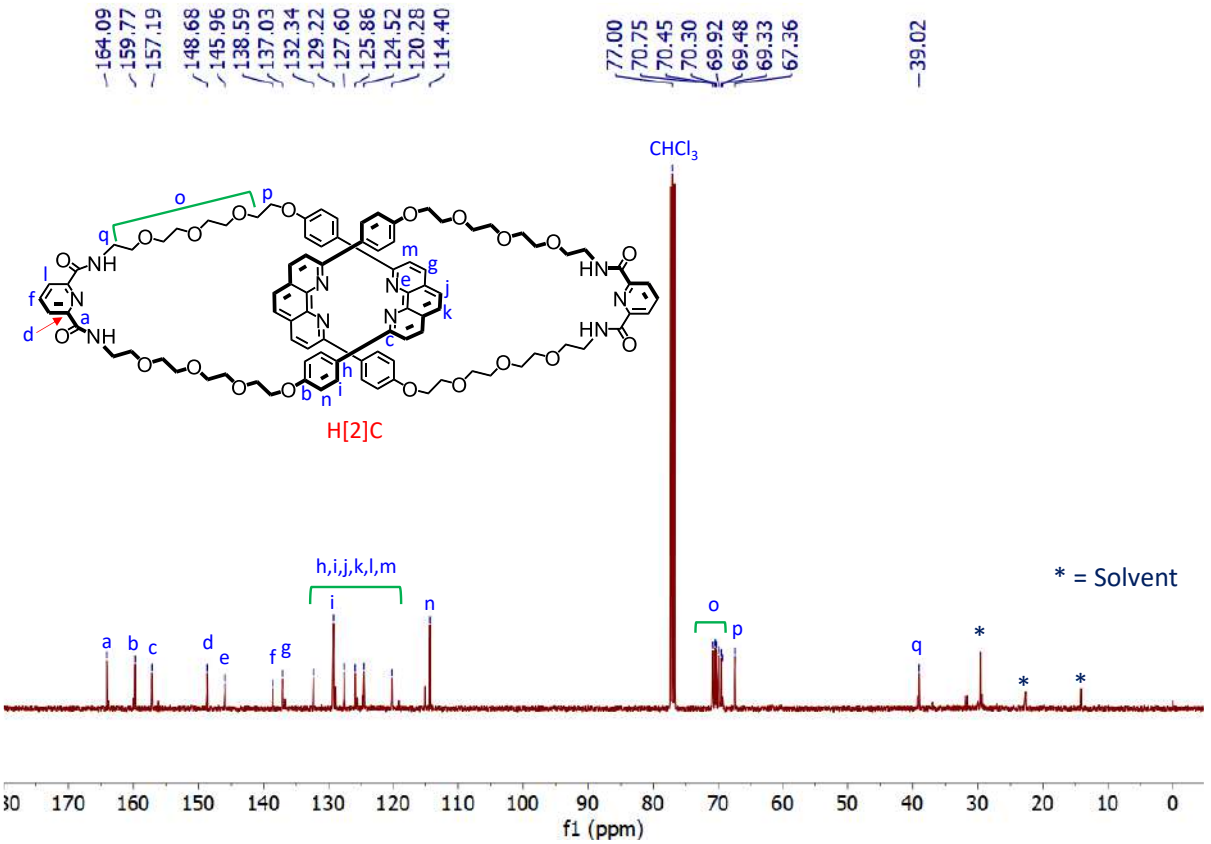

Figure 4.29. ^{13}C-NMR spectra of homo [2]catenane H[2]C in $CDCl_3$ (100 MHz).

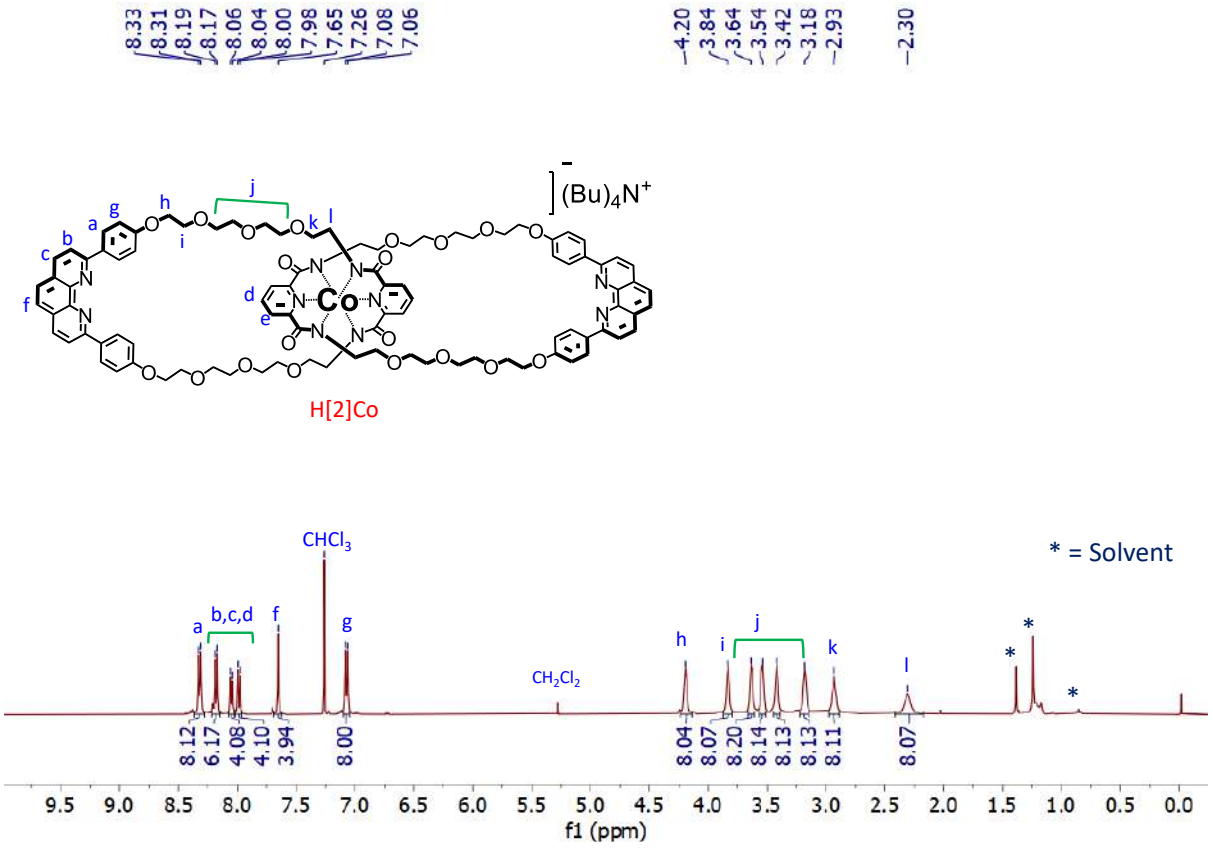

Figure 4.30. ^{1}H-NMR spectra of H[2]Co in $CDCl_3$ (400 MHz).

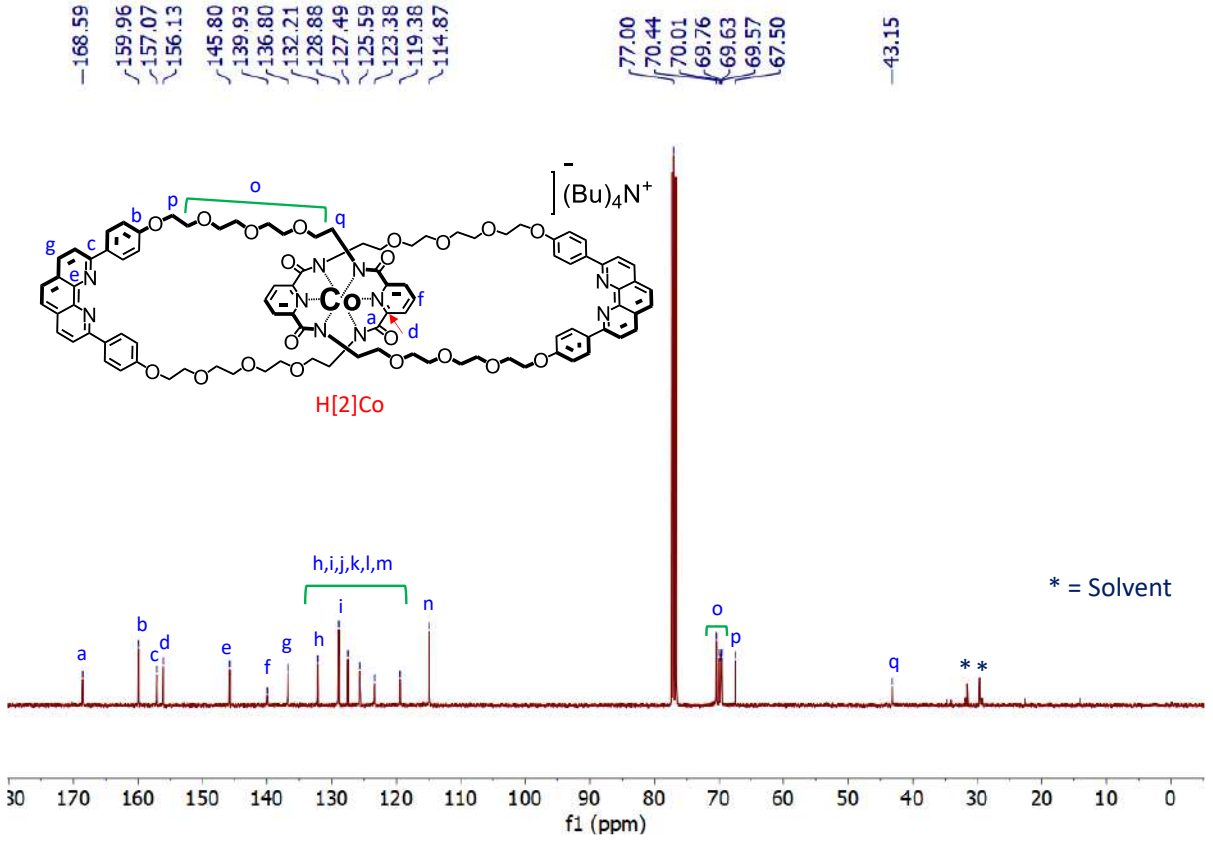

Figure 4.31. ^{13}C-NMR spectra of H[2]Co in $CDCl_3$ (100 MHz).

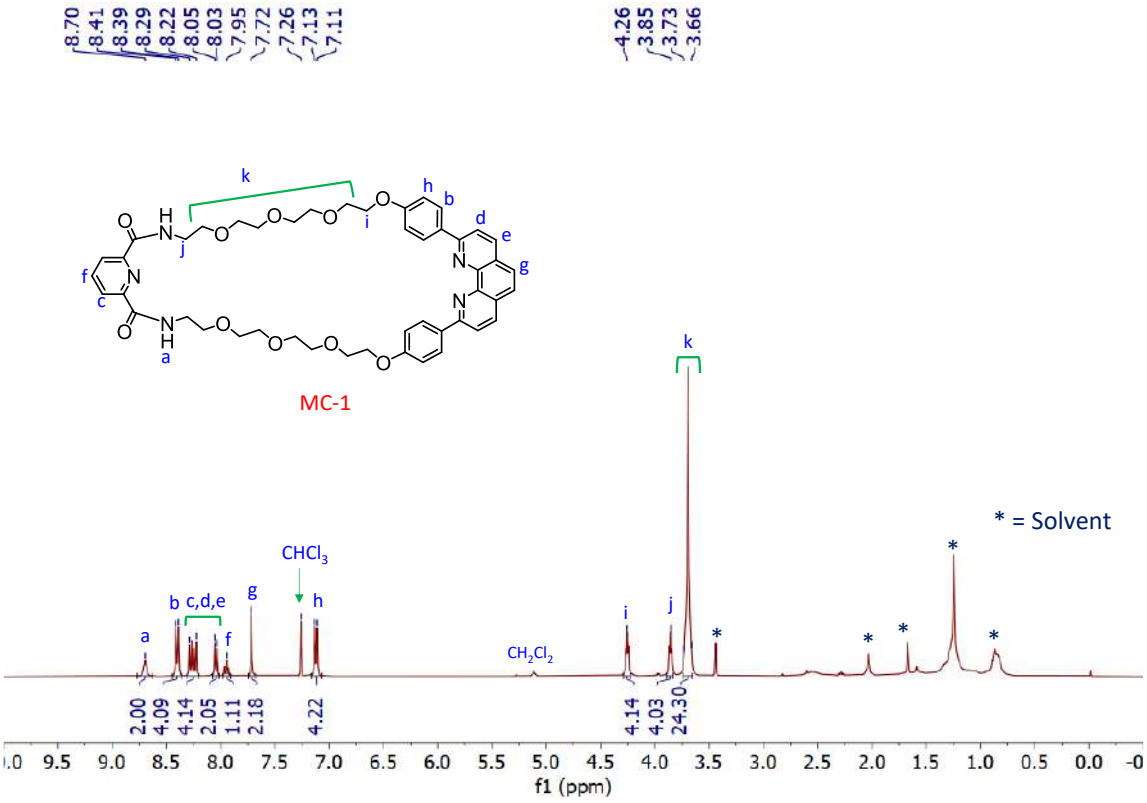

Figure 4.32. ^{1}H-NMR spectra of MC-1 in $CDCl_3$ (400 MHz).

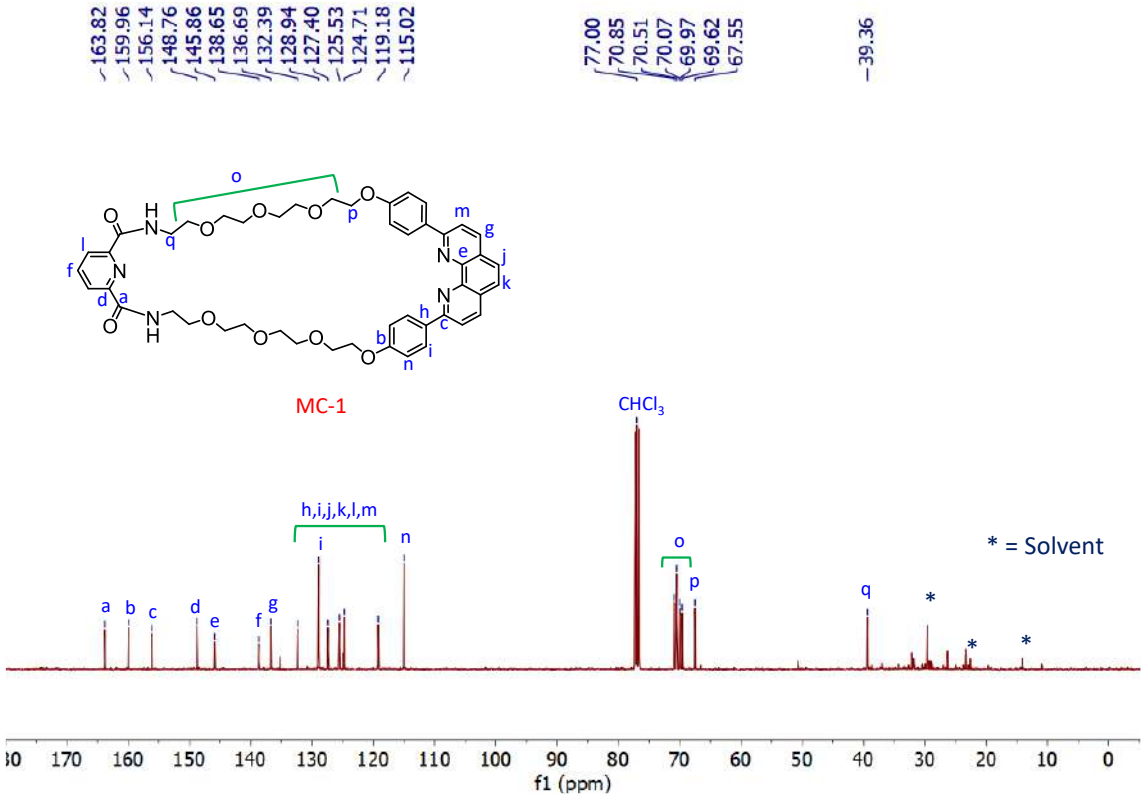

Figure 4.33. ^{13}C-NMR spectra of MC-1 in $CDCl_3$ (100 MHz).

4.6.2. VT-NMR spectra:

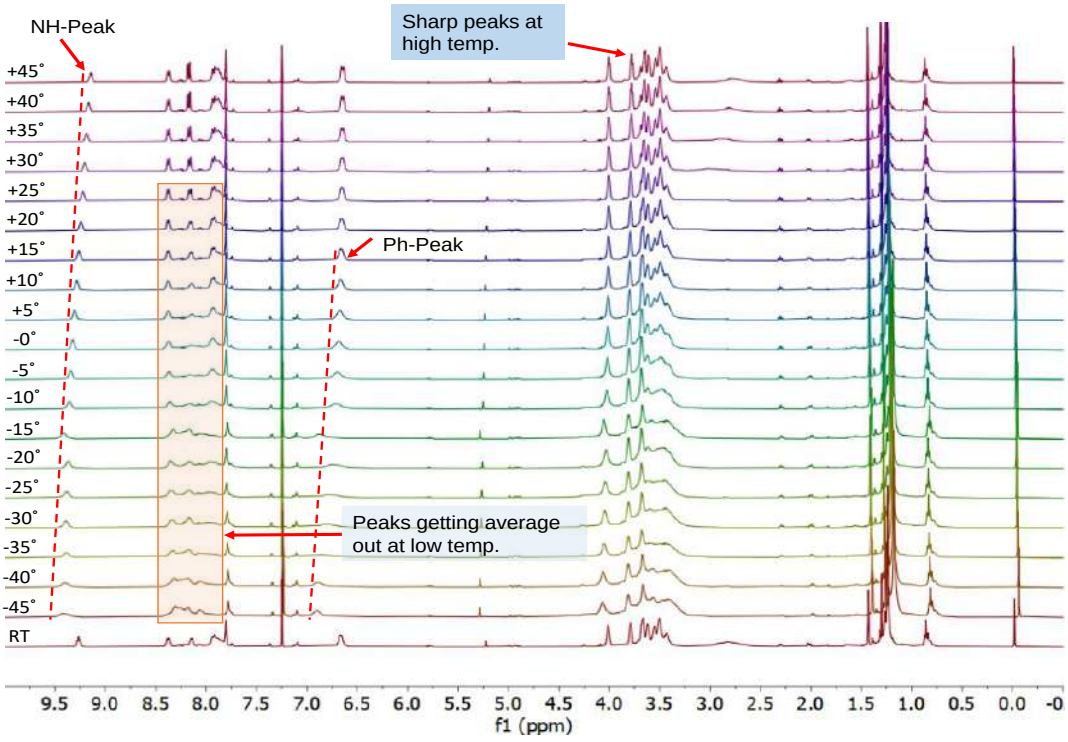

Figure 4.34. Variable temperature ^{1}H-NMR study for homo catenane **H[2]C** ($CDCl_3$, 400 MHz). Data recorded from -45 ˚C to 45 ˚C with interval of 5 degrees. Noticeable peak broadening at lower temperature and at higher temperature sharpening of NMR signals was observed. This suggest both interlocked **MC-1** rings in **H[2]C** are co-conformationally flexible compared to its monomeric macrocycle **MC-1.**

4.6.3. Mass Spectra:

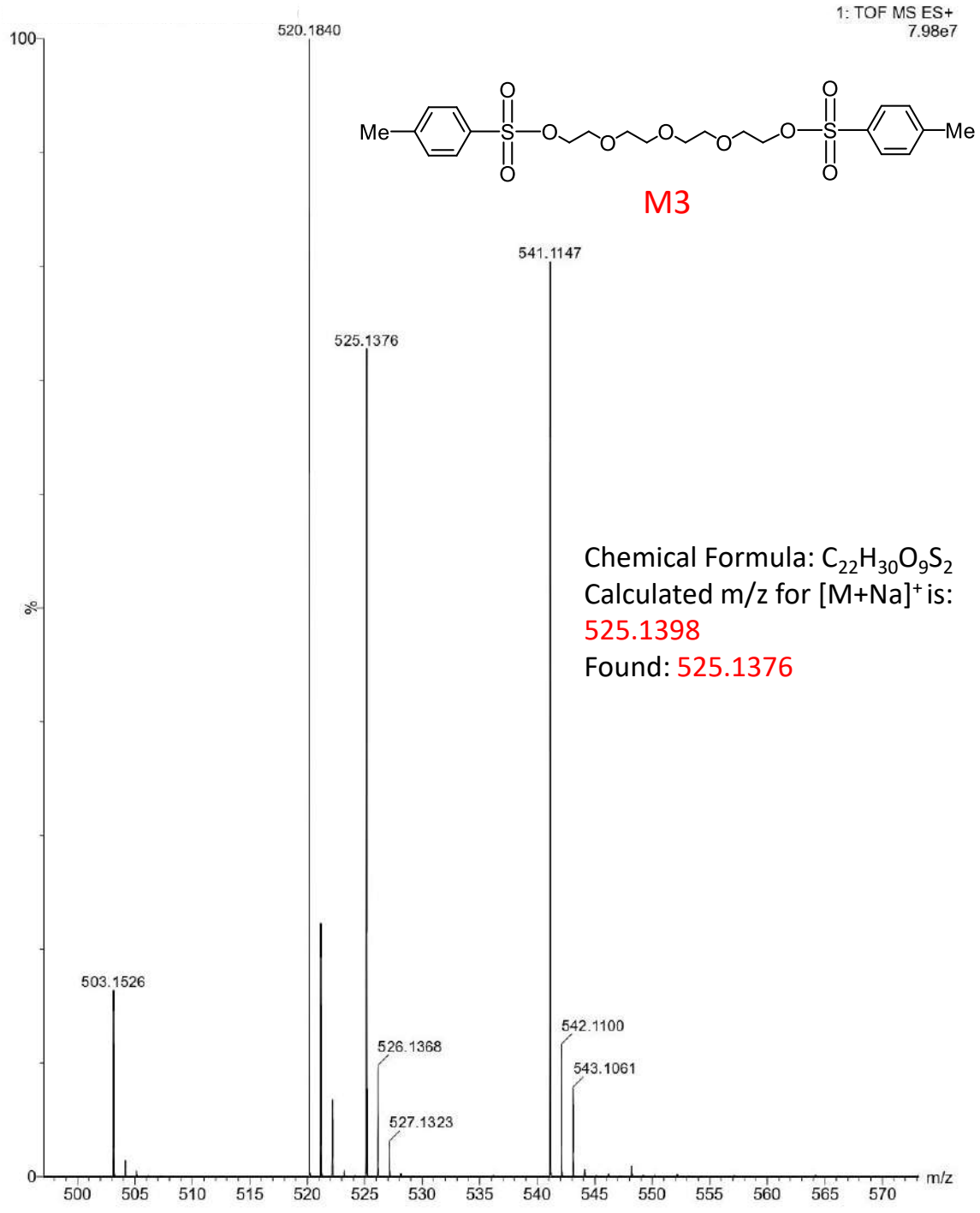

Figure 4.35. Mass spectrum (ESI^+) analysis for monomer M3.

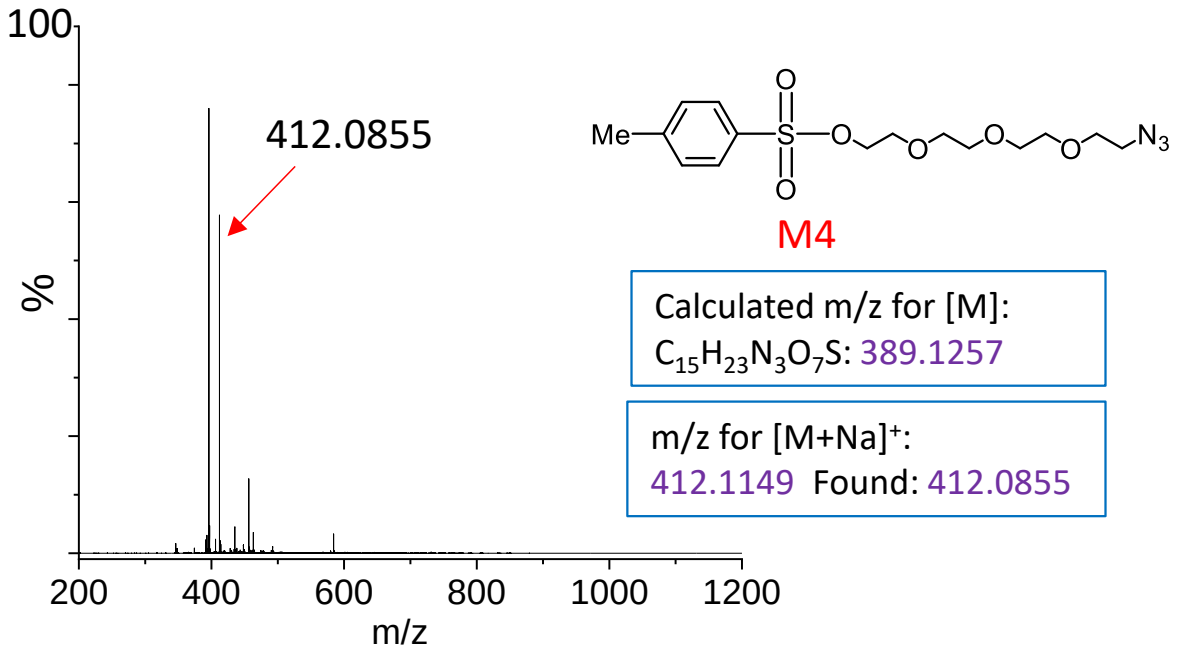

Figure 4.36. Mass spectrum (ESI^+) analysis for monomer M4.

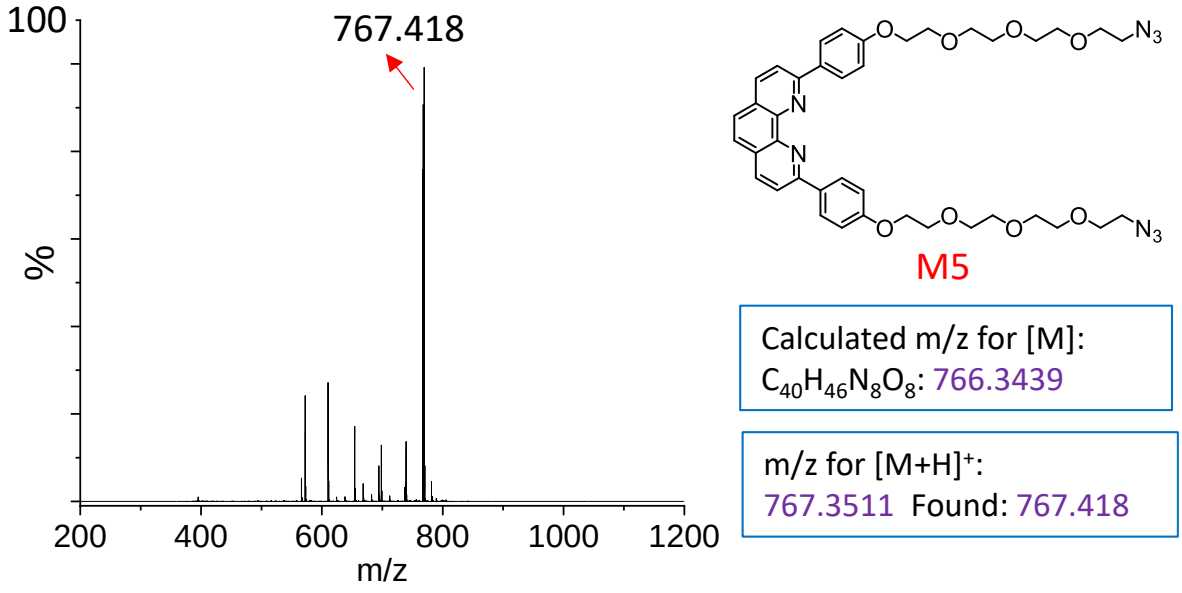

Figure 4.37. Mass spectrum (ESI^+) analysis for di-azide monomer M5.

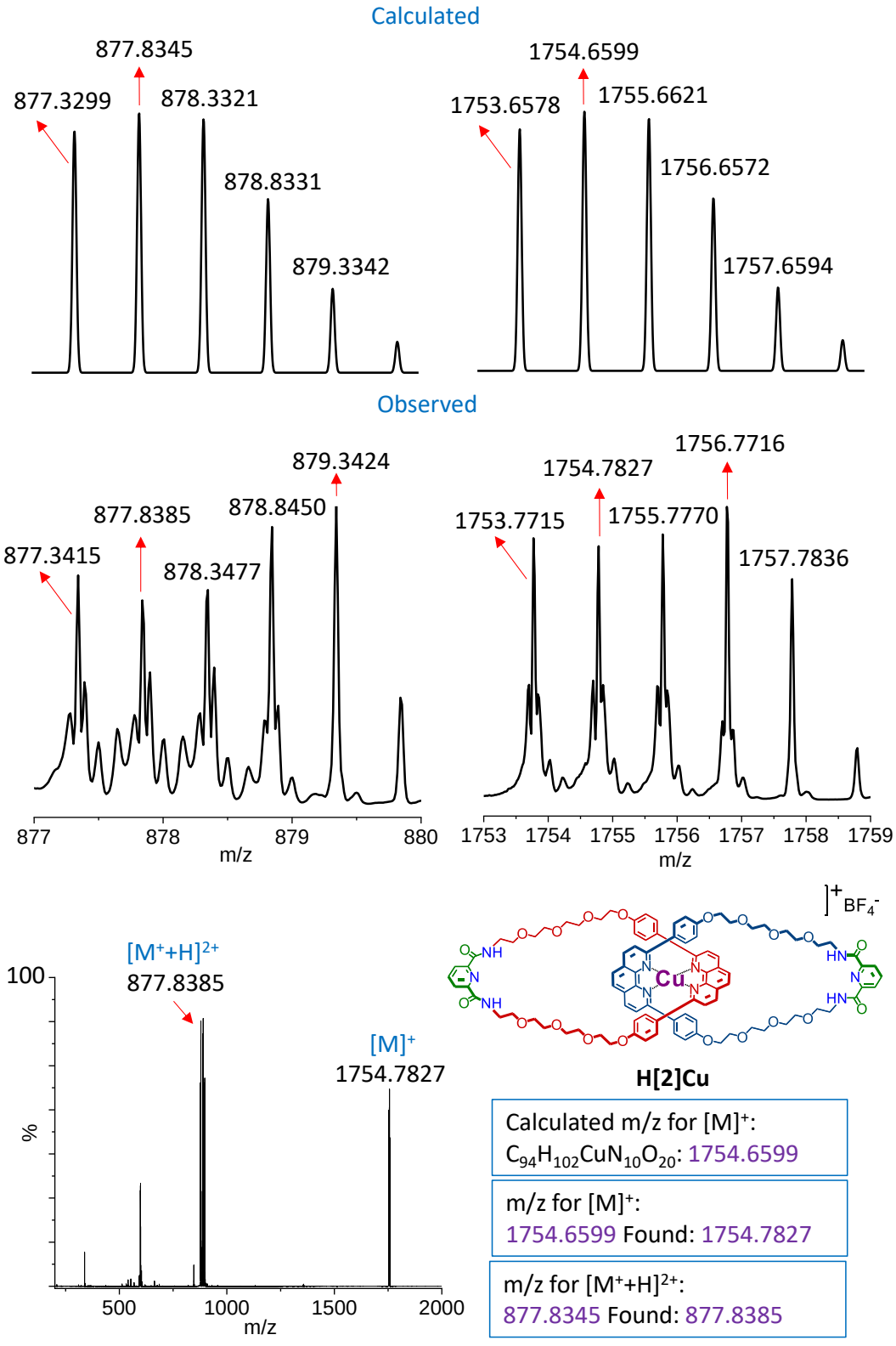

Figure 4.38. Mass spectrum (ESI⁺) analysis for H[2]Cu complex.

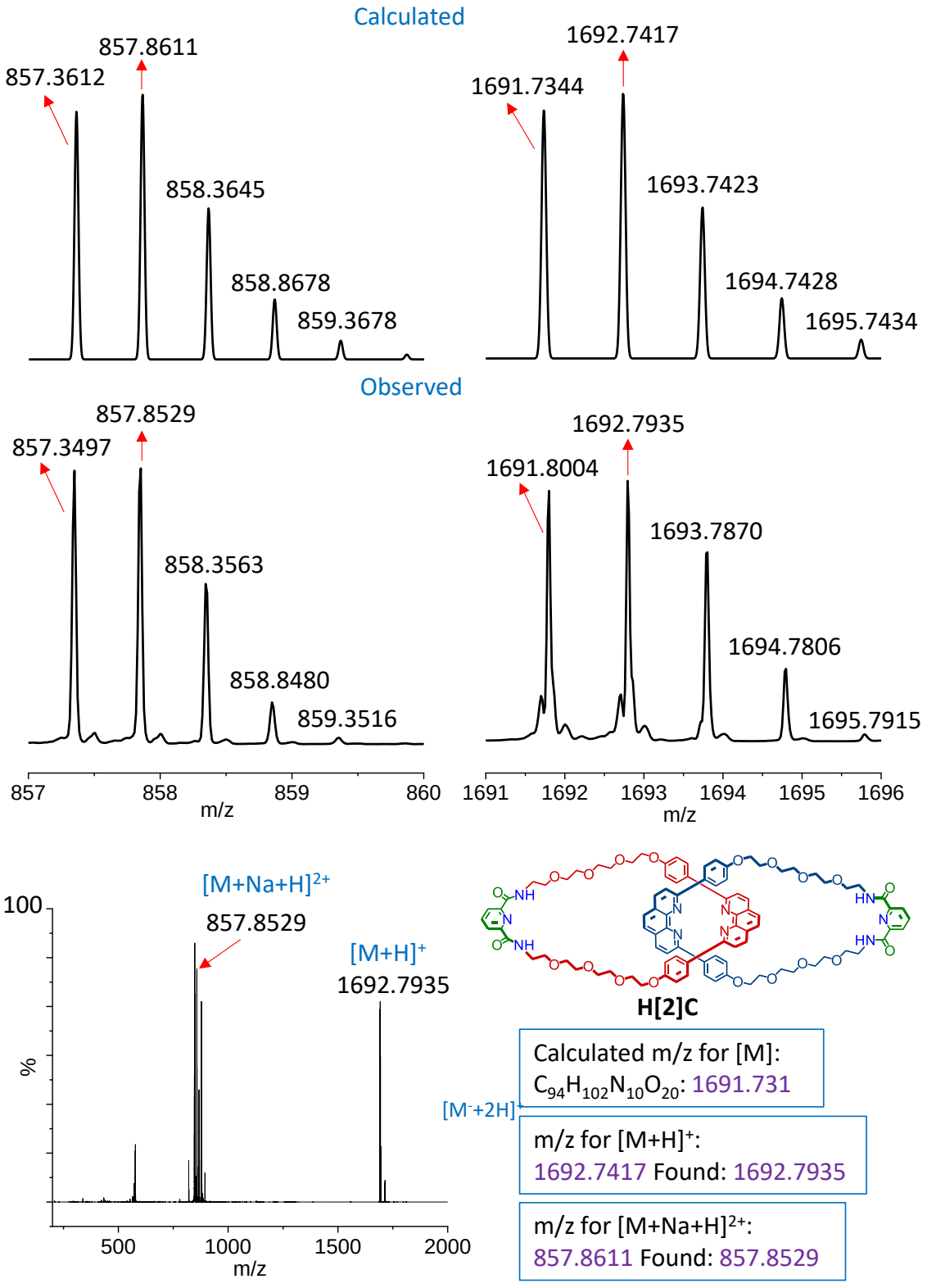

Figure 4.39. Mass spectrum (ESI$^+$) analysis for homo [2]catenane H[2]C.

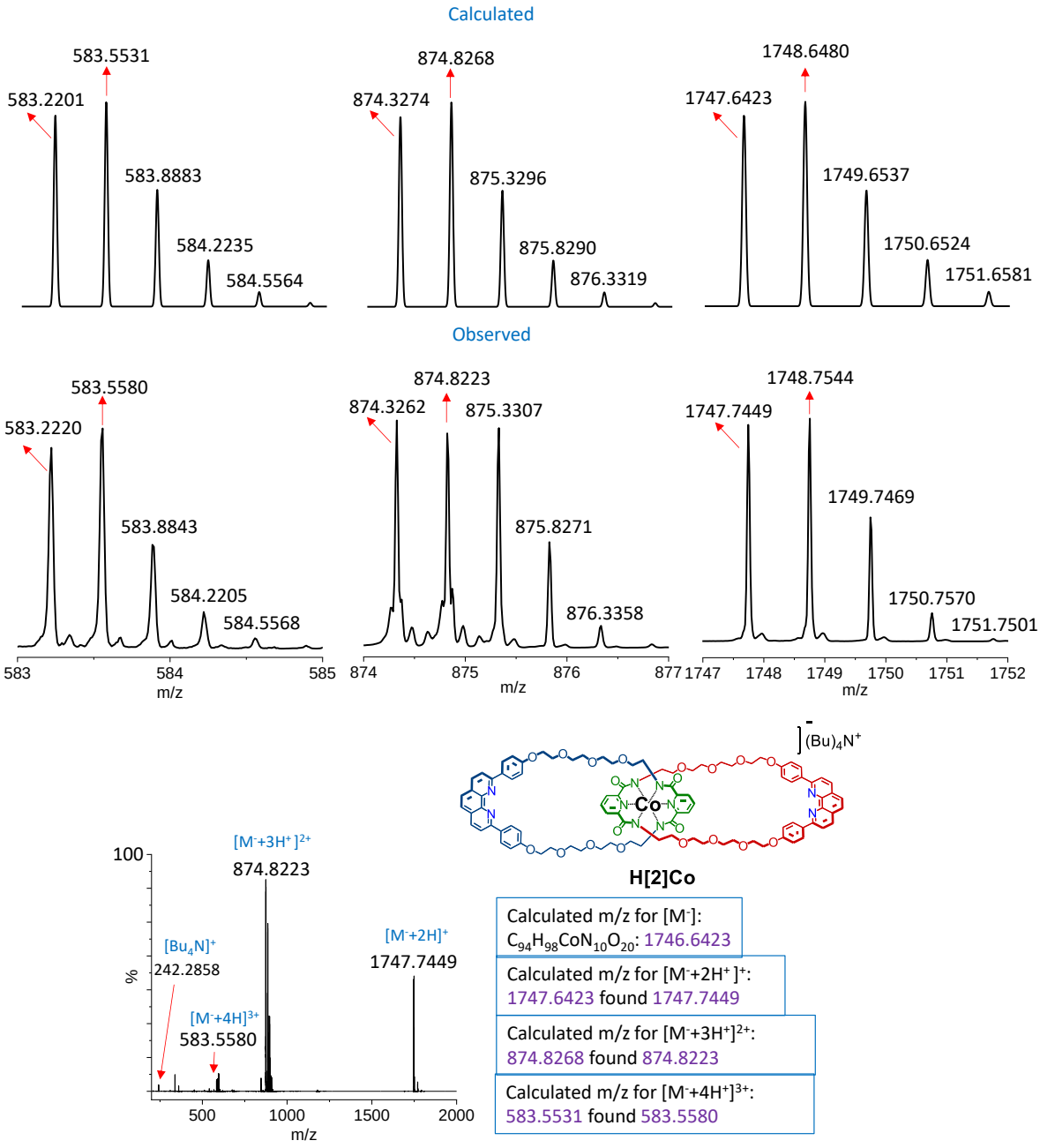

Figure 4.40. Mass spectrum (ESI$^+$) analysis for H[2]Co complex.

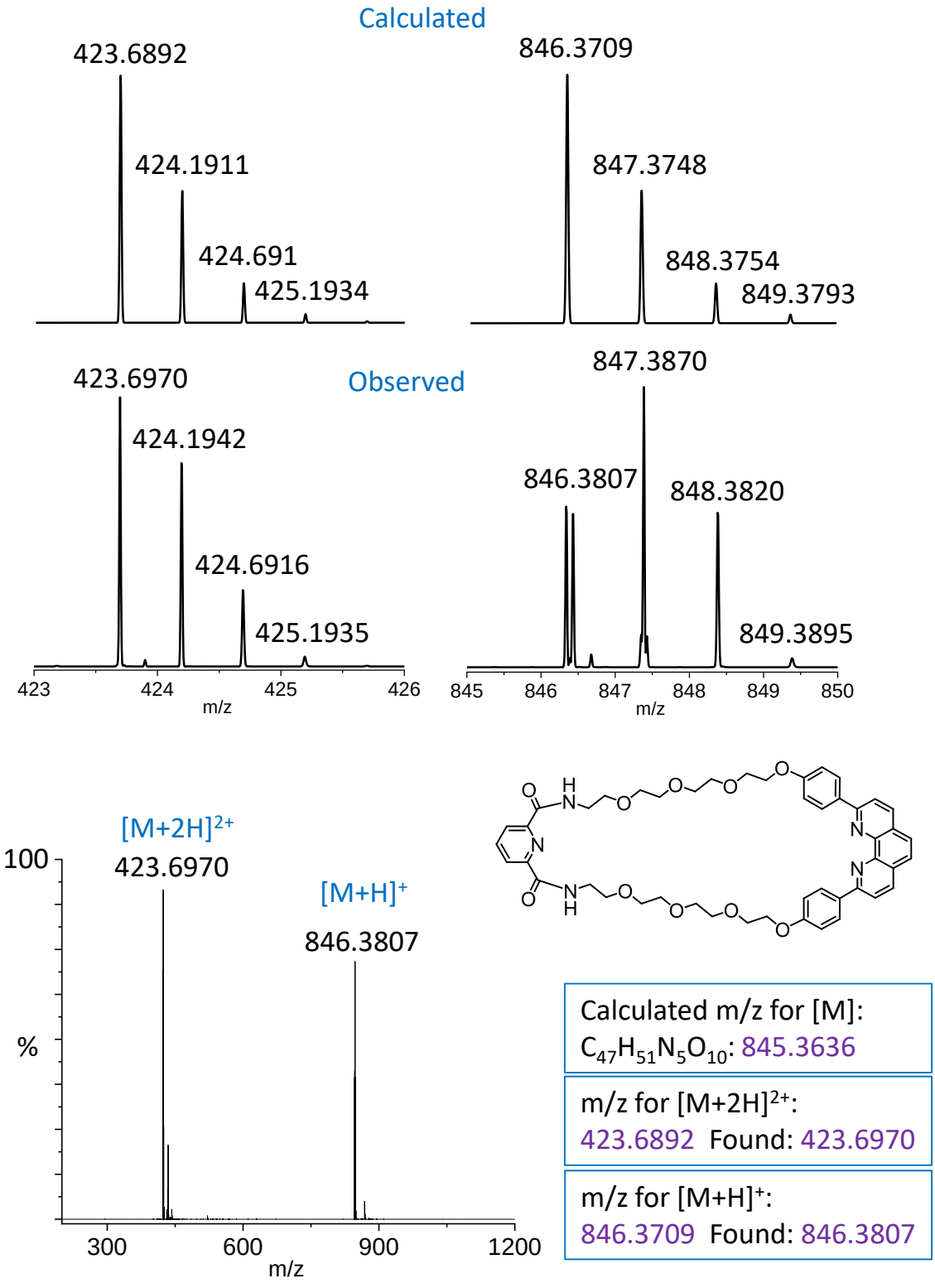

Figure 4.41. ESI-MS positive mode mass spectrum analysis for MC-1.

4.7. Reference:

1. Q. Chen, K. Zhu, *Chem. Soc. Rev.* **2024**, *53*, 5677–5703.
2. J. de Jong, M. A. Siegler, S. J. Wezenberg, *Chem. Commun.* **2025**, *61*, 2548–2551.
3. L. Zhang, Y. Qiu, W. G. Liu, H. Chen, D. Shen, B. Song, K. Cai, H. Wu, Y. Jiao, Y. Feng, J. S. W. Seale, C. Pezzato, J. Tian, Y. Tan, X. Y. Chen, Q. H. Guo, C. L. Stern, D. Philp, R. D. Astumian, W. A. Goddard, J. F. Stoddart, *Nature* **2023**, 613, 280–286.
4. S. E. Cakmak, S. D. P. Fielden, U. Karaca, D. A. Leigh, C. T. McTernan, D. J. Tetlow, M. R. Wilson, *Science* **2017**, *358*, 340–343.
5. M. R. Wilson, J. Solà, A. Carlone, S. M. Goldup, N. Lebrasseur, D. A. Leigh, *Nature* **2016**, *534*, 235–240.
6. Y. Zhang, Q. Chen, Y. Wang, X. Zheng, H. Wang, F. Cao, A. C. Sue, H. Li, *Chem. Commun.* **2020**, *56*, 11887–11890
7. Y. Yao, Y. C. Tse, S. K. Lai, Y. Shi, K. H. Low, H. Y. A. Yeung, *Nat. Commun.* **2024**, *15*, 1952
8. K. M. Bak, B. Trzaskowski, M. J. Chmielewski, *Chem. Sci.* **2024**, *15*, 1796–1809.
9. T. A. Barendt, L. Ferreira, I. Marques, V. Felix, P. D. Beer, *J. Am. Chem. Soc.* **2017**, *139*, 9026–9037.
10. S. Yang, C. X. Zhao, S. Crespi, X. Li, Q. Zhang, Z. Y. Zhang, J. Mei, H. Tian, D. H. Qu, *Chem* **2021**, *7*, 1544–1556.
11. Z. Meng, Y. Han, L. N. Wang, J. F. Xiang, S. G. He, C. F. Chen, *J. Am. Chem. Soc.* **2015**, *137*, 9739–9745
12. A. Li, Z. Du, S. Zhang, J. Xie, X. Li, Q. Chen, Y. Tang, J. Chen, K. Zhu, *Chem. Sci.* **2024**, *15*, 14721–14725
13. D. A. Leigh, J. K. Y. Wong, F. Dehez, F. Zerbetto, *Nature* **2003**, *424*, 174–179

14. Y. Wang, W. L. Zhao, Z. Gao, C. Qu, X. Li, Y. Jiang, L. Hu, X. Q. Wang, M. Li, W. Wang, C. F. Chen, H. B. Yang, *Angew. Chem., Int. Ed.* **2024**, *64*, e202417458
15. Y. Wang, J. Gong, X. Wang, W. J. Li, X. Q. Wang, X. He, W. Wang, H. B. Yang, *Angew. Chem., Int. Ed.* **2022**, *61*, e202210542.
16. N. Pairault, F. Rizzi, D. Lozano, E. M. G. Jamieson, G. J. Tizzard, S. M. Goldup, *Nat. Chem.* **2023**, *15*, 781–786
17. Y. Deng, S. K. Lai, L. Kong, H. Y. A. Yeung, *Chem. Commun.* **2021**, 57, 2931–2934.
18. A. Garci, A. H. G. David, L. Le Bras, M. Ovalle, S. Abid, R. M. Young, W. Liu, C. S. Azad, P. J. Brown, M. R. Wasielewski, J. F. Stoddart, *J. Am. Chem. Soc.* **2022**, *144*, 23551–23559.
19. Y. Xie, C. Y. Wang, N. Chen, Z. Cao, G. Wu, B. Yin, Y. Li, *Angew. Chem., Int. Ed.* **2023**, *62*, e202309605
20. J. D. Crowley, K. D. Hanni, D. A. Leigh, A. M. Z. Slawin, *J. Am. Chem. Soc.* **2010**, *132*, 5309–5314.
21. D. A. Leigh, P. J. Lusby, A. M. Z. Slawin, D. B. Walker, *Chem. Comm.* **2012**, *48*, 5826
22. D. A. Leigh, P. J. Lusby, A. M. Z. Slawin, D. B. Walker, *Chem. Commun.* **2005**, 4919–4921\
23. D. J. Cárdenas, A. Livoreil, J. P. Sauvage, *J. Am. Chem. Soc.* **1996**, *118*, 11980–11981
24. M. B. Podh, R. Ratha, C. S. Purohit, *Chem. Asian J.* **2024**, *19*, e202400031.
25. P. Ghosh, R. Ratha, C. S. Purohit, *Chem. Asian J.* **2024**, *19*, e202400668.
26. M. B. Podh, R. Ratha, C. S. Purohit, *Chem. Asian J.* **2024**, *19*, e202400351

27. K. Y. Ng, V. Felix, S. M. Santos, N. H. Rees, P. D. Beer, *Chem. Commun.* **2008**, 1281–1283.
28. F. B. L. Cougnon, N. Ponnuswamy, G. D. Panto¸s, J. K. M. Sanders, *Org. Biomol. Chem.* **2015**, *13*, 2927–2930.
29. J. D. Megiatto Jr., D. I. Schuster, *J. Am. Chem. Soc.* **2008**, *130*, 12872–12873.
30. P. F. Cao, A. Bunha, J. Mangadlao, M. J. Felipe, K. I. Mongcopa, R. Advincula, *Chem. Commun.* **2012**, *48*, 12094–12096.
31. J. Liu, M. Wu, L. Wu, Y. Liang, Z. B. Tang, L. Jiang, L. Bian, K. Liang, X. Zheng, Z. Liu, *Angew. Chem., Int. Ed.* **2023**, *62*, e202314481.
32. N. D. Colley, M. A. Nosiglia, S. L. Tran, G. H. Harlan, C. Chang, R. Li, A. O. Delawder, Y. Zhang, J. C. Barnes, *ACS Cent. Sci.* **2022**, *8*, 1672–1682.
33. A. Bessaguet, Q. B. Remaury, P. Poinot, I. Opalinski, S. Papot, *Angew. Chem., Int. Ed.* **2023**, *62*, e202216787.
34. M. V. R. Raju, H. C. Lin, *Org. Lett.* **2014**, *16*, 5564–5567.
35. D. A. Leigh, P. J. Lusby, R. T. McBurney, A. Morelli, A. M. Z. Slawin, A. R. Thomson, D. B. Walker, *J. Am. Chem. Soc.* **2009**, *131*, 3762–3771.
36. L. Chen, W. You, J. Wang, X. Yang, D. Xiao, H. Zhu, Y. Zhang, G. Li, W. Yu, J. L. Sessler, F. Huang, *J. Am. Chem. Soc.* **2024**, *146*, 1109–1121.
37. S. R. Barlow, G. R. Akien, N. H. Evans, *Org. Biomol. Chem.* **2023**, *21*, 402–414.
38. Y. Yao, Y. Deng, L. Kong, H. Y. A. Yeung, *Eur. J. Inorg. Chem.* **2022**, e202200271.
39. Reaction occurs with Co(II) metal ion which later oxidized to Co(III) upon exposure to air.
40. C. Y. Tsai, C. C. Lai, Y. H. Liu, S. M. Peng, R. P. Cheng, S. H. Chiu, *J. Org. Chem.* **2018**, *83*, 5619–5628.

41. H. Tang, H. N. Zhang, X. Gao, Y. Zou, G. X. Jin, *J. Am. Chem. Soc.* **2024**, *146*, 16020–16027.
42. Y. C. You, M. C. Tzeng, C. C. Lai, S. H. Chiu, *Org. Lett.* **2012**, *14*, 1046–1049.
43. S. K. Moharana, R. Ratha, C. S. Purohit, *ChemistryOpen* **2025**, e202500081.
44. M. M. Montoya, R. A. J. Janssen, *Adv. Funct. Mater.* **2017**, *27*, 1605779.
45. J. L. Appleton, L. Ballerini, S. Choua, C. Gourlaouen, R. Ruppert, M. Mauro, *Eur. J. Inorg. Chem.* **2024**, *27*, e202400278.
46. K. Shi, G. Jia, Y. Wu, S. Zhang, J. Chen, *ChemistryOpen* **2024**, *13*, e202300304.
47. D. A. Leigh, F. Schaufelberger, L. Pirvu, J. H. Stenlid, D. P. August, J. Segard, *Nature* **2020**, *584*, 562–568
48. C. Tang, R. Zhang, S. Almunif, P. J. Das, P. J. Brown, R. M. Young, G. Wu, H. Han, X. Zhao, A. H. G. David, H. Wu, B. Song, A. Abhervé, Y. Wu, Y. M. Ye, Y. Feng, A. X. Y. Chen, C. L. Stern, Z. Li, E. A. Scott, M. R. Wasielewski, J. F. Stoddart, *Nat. Synth.* **2025**, http://doi.org/10.1038/s44160-025-00781-z.
49. C. D. Buchecker, J. P. Sauvage, *Tetrahedron* **1990**, *46*, 503-512.
50. J. Chen, J. W. Lim, D. Y. Ong, S. Chiba, *Chem. Sci.* **2022**, *13*, 99-104.
51. N. D. Colley, M. A. Nosiglia, S. L. Tran, G. H. Harlan, C. Chang, R. Li, A. O. Delawder, Y. Zhang, J. C. Barnes, *ACS Cent. Sci.* **2022**, *8*, 1672-1682.
52. K. L. Dao, R. R. Sawant, J. A. Hendricks, V. Ronga, V. P. Torchilin, R. N. Hanson, Bioconjug. *Chem.* **2012**, *23*, 785-795.
53. M. B. Podh, R. Ratha, C. S. Purohit, *Chem. Asian. J.* **2024**, *19*, e202400031.
54. Y. Yao, Y. Deng, L. Kong, H. Y. A. Yeung, *Eur. J. Inorg. Chem.* 2022, e202200271.

Thesis at a glance

Chapter-1: Classification and different strategies to catenane synthesis, and its functional aspect

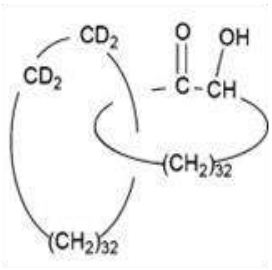

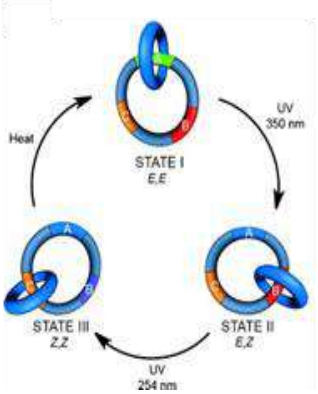

Chapter 2: Template Assisted One-Pot Synthesis of [2], Linear [3], and Radial [4]Catenane via Click Reaction

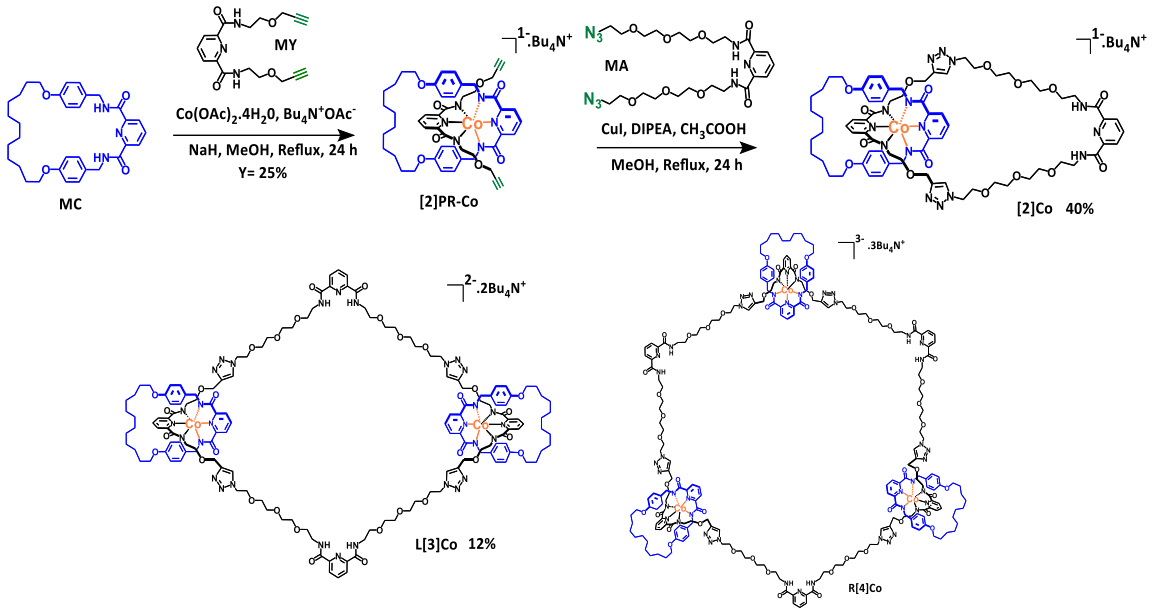

Chapter 3: Template Assisted Synthesis of Linear [5]Catenane by Post-Functionalization of Templated [2]Catenane and Using Click Reaction

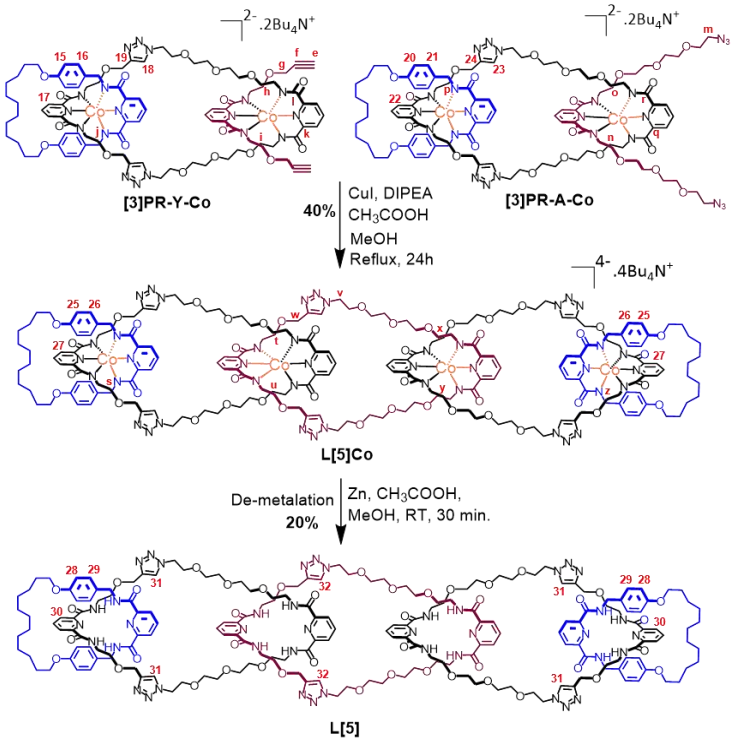

Chapter 4: Metal Ion-Responsive Dynamics in a Homo [2]Catenane: Circumrotation and Pirouetting

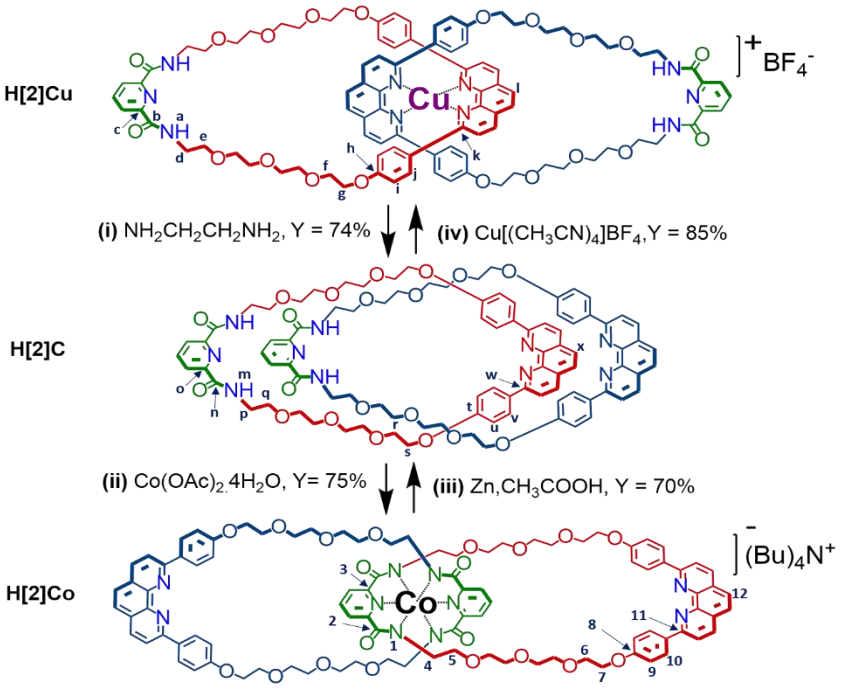

Summary and Future Scope

Catenanes, a unique class of mechanically interlocked molecules formed by interwoven macrocycles, have progressed remarkably since their early days, with various methods developed for their synthesis. The advent of molecular recognition started with the use of the template method, and self-assembly principles have enabled the template-directed construction of a wide variety of structurally sophisticated catenanes. This rapid advancement has driven the creation of artificial molecular switches and machines, paving the way for more integrated functional systems and materials. Development of computational models to predict behaviour and guide rational design. Even with this development, the synthesis of higher-order catenane is still a challenge. The work in this thesis mainly uses templated methods to synthesise higher linear and radial catenane and carried out a study on the functional aspect of catenane. However, this new material faces various challenges that need to be overcome for further development and use of this material. The following are a few challenges and the scope of going ahead with the progress of the work in various fields:

A. Advanced Synthetic Strategies

- Development of greener, more efficient, and scalable methods for producing higher-order catenanes.
- Exploration of one-pot and automated synthesis for complex interlocked architectures.
- Expanding beyond traditional metal–ligand or hydrogen-bond templation to include novel noncovalent interactions (e.g., halogen bonding, chalcogen bonding, π–π stacking).

B. Functional Materials

- Incorporating catenanes into stimuli-responsive polymers, gels, and frameworks for adaptive materials.
- Using catenanes as dynamic crosslinkers to enhance toughness, elasticity, or self-healing properties.
- Integration into metal–organic frameworks (MOFs) and covalent organic frameworks (COFs) for tunable porosity and responsiveness.

C. Molecular Machines & Devices

- Designing catenane-based molecular switches, shuttles, and rotors with higher precision and controllability.

- Application in molecular electronics, spintronics, and data storage.
- Creating energy conversion systems by coupling mechanical motion with chemical or photonic energy.

D. Biological & Medicinal Applications

- Engineering biocompatible catenanes for drug delivery, controlled release, and biosensing.
- Studying enzyme-like catalytic activity in catenanes for biomimetic chemistry.
- Investigating catenane–protein interactions for potential therapeutic or diagnostic tools.

E. Fundamental Understanding

- Probing mechanical bond effects on molecular dynamics, reactivity, and stability.
- Understanding topology–property relationships, e.g., how the number and arrangement of rings impact function.

ACES Asian Chemical Editorial Society

doi.org/10.1002/asia.202400031

CHEMISTRY AN ASIAN JOURNAL Research Article

www.chemasianj.org

Template Assisted One-Pot Synthesis of [2], Linear [3], and Radial [4]Catenane via Click Reaction

Mana Bhanjan Podh[+],[a, b] Radhakrishna Ratha[+],[a, b] and Chandra Shekhar Purohit*[a, b]

Design and synthesis of higher order catenane are unexpectedly complex and involve precise cooperation among the precursors overcoming competing and opposing interactions. We achieved synthesis of [2], linear [3], radial [4] in a one-pot reaction by consecutive ring closing through click reactions. This synthesis gave three isolable products due to two, four, and six-click reactions between suitable coupling partners. Yields of the isolate templated-catenane decrease from lower to higher-ordered catenane (40%, 12%, and 4%), probably due to the bite angle as well as the flexibility of the reacting partners. Removal of templating cobalt(III) ion leads to the formation of fully organic [2], linear [3], and radial [4]catenane. These synthesized catenanes were purified by column chromatography and characterized by ^{1}H-NMR, ^{13}C-NMR, and ESI-MS spectroscopy. The synthesized catenanes have free binding sites suitable for post-functionalization and may be used for the synthesis of higher-ordered catenane.

Introduction

In recent years, synthesis of supramolecular topologies/architectures comprising mechanically interlocked molecules (MIMs) and investigations into their properties have gained significant attention.[1] Study of MIMs are essential to understand biologically important knotted structures those are found in DNA, proteins, and polymers, playing a vital role in their functions.[2] These structures also have a wide range of applications as molecular machines such as a molecular motor,[3] molecular pump,[4] ion transport system,[5] and photoswitch.[6] Among MIMs, catenanes are a class of interlocked molecules and are fascinating due to their molecular topologies. In recent times, many applications, such as in catalysis,[7] photo-catalysis,[8] as electro catalyst,[9] a catalyst for click reaction,[10] memory device,[11] and guest molecule encapsulation,[12] etc. have surfaced for this class of molecules. Also, structurally modified catenanes show optical activity and chirality.[13] Common strategies for catenane synthesis include self-assembly, π-π stacking, hydrogen bond, halogen bond, metal templated, and covalent bonding.[14] Among these methods, use of a template is the most common one. The template brings the precursor units to suitable orientation for effective ring closing; therefore, higher yields can be realized.[15] Despite development of various synthetic methods, higher ($\geq$4) catenanes are still difficult to achieve, and only two reports of poly[n]catenane synthesis exists in literature so far; one solely organic poly[n]catenane using Zn^{2+} template with double bond metathesis for ring closing,[16] and other one is a recent report of infinite twisted metalla-poly[n]catenane linked due to Ag^{+}.[17] The major difficulty is the lower yield in the ring-closing step(s).[18] Thus, click chemistry is conceived as one of the methods for the ring-closing step[19] and subsequently employed for the synthesis of [2], radial [4], and branched [8]catenanes.[20] Another reaction for ring closing is the Grubbs ring closing metathesis.[21] In the synthesis of complex molecular architectures such as square knot, and granny knot, both these reactions have been used.[22] Although the use of click reaction for the synthesis of catenanes and rotaxanes is well explored,[20d] only a few reports exist for the synthesis of higher (n > 3) catenanes.[20a–c] These reports are restricted to a limited number of topological structures and need to be explored further in terms of a wide range of available templates and other useful tectons.[19e,20b,c]

Among higher-ordered catenanes, radial [n]-catenane, also known as molecular necklace (when n > 3), are catenanes with a cyclic backbone containing (n-1) catenated peripheral rings.[23] Different strategies are adapted for the construction of these peripherally interlocked structures that include: head to tail cyclization of a pseudo-polyrotaxane[24]/polyrotaxane,[25] using macrocycles having multiple recognition sites as the template,[26] utilizing metal coordination for macro-cylisation of [2]pseudorotaxane monomer[27] and covalent bonding.[28]

Sauvage group reported the synthesis of [n]catenane and radial-[n]catenane using Cu(I) as a template and Glaser coupling as a ring-closing step.[15a,23] Similar to this report, the click reaction with suitable substrate can combine in various ratios to give many products that may include linear or radial catenane(s) but have never been investigated.

Thus, we designed suitable pre-organized coupling partners for click reaction(s) that would either cyclize to [2], [3] linear, or higher radial catenanes and study the possible outcome of this one-pot reaction. Although there are few reports, we choose Co(III) as our template due to its non-labile nature in the amide complexes. Thus, the templated assembly, once synthesized, is

[a] M. B. Podh,[+] R. Ratha,[+] C. S. Purohit
School of Chemical Sciences, National Institute of Science Education and Research (NISER), Jatni Bhubaneswar, Odisha India – 752050
E-mail: purohit@niser.ac.in

[b] M. B. Podh,[+] R. Ratha,[+] C. S. Purohit
Homi Bhabha National Institute (HBNI) Mumbai, India – 400094

[+] Authors contributed equally

Supporting information for this article is available on the WWW under https://doi.org/10.1002/asia.202400031

ACES Asian Chemical Editorial Society

doi.org/10.1002/asia.202400351

CHEMISTRY AN ASIAN JOURNAL Research Article

www.chemasianj.org

Template Assisted Synthesis of Linear [5]Catenane by Post-Functionalization of Templated [2]Catenane and Using Click Reaction

Mana Bhanjan Podh[+],[a, b] Radhakrishna Ratha[+],[a, b] and Chandra Shekhar Purohit*[a, b]

Polymers with all mechanically interlocked rings, such as linear [n]catenanes, have great potential as functional materials due to possible higher degrees of freedom that may contribute to their flexibility but remain elusive. All the synthetic methods used to prepare such a polymer yield mixtures of products. In the absence of higher molecular weight linear [n]catenanes, emphasis on synthesizing low molecular weight oligomers is being pursued. Here, we have described the synthesis of a linear [5]catenane by post-functionalizing a Co(III) templated [2]catenane having a pyridine-diamide unit free for further metal ion coordination. Two molecules were synthesized with suitable threading groups: one, two terminal azide groups, and two, with two terminal alkyne groups to form two [3]pseudorotaxane utilizing Co(III) coordination. These units were then joined, forming a macrocycle, using click reaction, giving the desired metalated linear [5]catenane in 40% yield. Removal of metal ions leads to linear [5]catenane. In addition, the formation of linear [3] and [2]catenane are also observed. All synthesized structures have been isolated by column chromatographic technique and characterized by ^{1}H-NMR, ^{13}C-NMR, and mass spectroscopy.

Introduction

Mechanically interlocked molecules (MIMs), such as catenanes, are emerging as new materials as they show applications such as in memory devices,[1] ion transport,[2] molecular switch,[3] molecular motor,[4] catalysis,[5] including their use as catalyst in click reaction,[6] guest molecule encapsulation,[7] and sensors,[8] to name a few. In addition, the mechanical bond in catenane imparts stereochemistry[9] and improves mechanical properties.[10] Although various methods exist for simple catenane synthesis,[11] higher-ordered catenanes, particularly linear polycatenane, pose an intriguing synthetic challenge to chemists. One of the challenges is that the ring-closing reactions utilized to make the mechanical bond generate non-interlocked by-products, thereby reducing yield.[12] A few other challenges are isolation of the intermediate catenated structures in pure form and the formation of by-products such as topological isomeric products. Nevertheless, formation of multiple mechanical bonds is achieved due to newer synthetic strategies.[13] Thus, construction of previously unknown structures was possible,[14] and novel functions of these materials due to entanglement were discovered.[15]

Synthesis of such topological architectures is achieved by designing and exploring novel templating centers,[16] utilizing different tectons,[17] implementing novel synthetic strategy,[18] and utilizing different reactions for the ring-closing step.[16a,18b,19] Yet, only a few higher-ordered ($n > 4$) catenane have been synthesized. [5]catenane, named olympiadane, was the first high-ordered catenane synthesized by Stoddart's group utilizing strong π-π interaction between electron-deficient viologens and electron-rich aromatic rings for threading, followed by covalent capture to close the ring.[20] Iwamoto's group synthesized linear [5]catenane using hydrogen bonding between ether and ammonium ion for threading and Grubb's method for ring-closing.[21] Recently, Jonathan and co-workers used zip-tie strategy along with orthogonal templating, utilizing phenanthroline and terpyridine groups for one-pot synthesis of linear [4], [5], [6], [7] and [8]catenane.[13c,22] The branched [8]catenane geometry is another significant topology.[23] The highest linear catenane achieved so far is a 26-mer by Rowan and co-workers.[24] Although most of these syntheses rely on a metal template followed by ring-closing, the choice of templating unit is limited to phenanthroline, terpyridine, and bipyridine. Only a few reports utilized non-ionic pyridine-diamide,[16a,25] anionic pyridine-diamide,[17a,26] di-benzimidazole pyridine[24] and thiazolothiazole pyridine[15,16b] unit as coordination site.

Pyridine-diamide based anionic template with suitable metal ion provides a non-labile site ideal for synthesizing catenane that can be used further for higher-ordered catenanes, but only a few reports exist.[25b] Recently, our group reported the synthesis of [2], linear [3], and radial [4]catenane by using a pyridine-diamide based anionic templation center and utilizing

[a] M. B. Podh,[+] R. Ratha,[+] C. S. Purohit
School of Chemical Sciences, National Institute of Science Education and Research (NISER), Jatni, Bhubaneswar, Odisha India-752050
E-mail: purohit@niser.ac.in

[b] M. B. Podh,[+] R. Ratha,[+] C. S. Purohit
Mana Bhanjan Podh, Radhakrishna Ratha, Chandra Shekhar Purohit
Homi Bhabha National Institute (HBNI) Mumbai,Mumbai, India-400094

[+] Authors contributed equally

Supporting information for this article is available on the WWW under https://doi.org/10.1002/asia.202400351

ChemistrySelect

Research Article
doi.org/10.1002/slct.202504348

Chemistry Europe
European Chemical Societies Publishing

www.chemistryselect.org

Metal Ion-Responsive Dynamics in a Homo [2]Catenane: Circumrotation and Pirouetting

Radhakrishna Ratha[+],[a, b] Mana Bhanjan Podh[+],[a, b] Priyanka Ghosh,[a, b] Tanmaya Kumar Majhi,[a, b] and Chandra Shekhar Purohit*[a, b]

We describe a homo [2]catenane that is stable in two conformations and demonstrates a large-amplitude co-conformational change during the exchange between Cu(I) and Co(III) metal ions. Each ring comprises a bi-dentate diphenyl-phenanthroline and a tri-dentate pyridine-diamide metal templating center. The presence of multiple coordination centers results in orthogonal complexation behavior with suitable metal ions, leading to a relative motion between the interlocked rings via pirouetting and circumrotation. Interconvertible catenates via homo [2]catenane have been characterized by 1H-NMR, 13C-NMR, mass, UV–visible spectroscopy, and variable temperature NMR experiments.

1. Introduction

Mechanically interlocked molecules (MIMs) such as catenanes can have many stable co-conformations among the interlocked components.[1,2] Interconversion among these conformations is often possible due to relative motion of interlocked rings, when triggered with a stimulus such as electrical,[3] chemical,[4,5] electrochemical,[6] ionic guest,[7,8] etc. Sometimes, structural features such as $\pi-\pi$ stacking[9] and ion–dipole interaction[10,11] help such motion. Such stimuli-triggered motion, when guided unidirectionally, results in synthetic molecular motors.[3–5,12,13] Moreover, ring rotation and switching imparts interesting properties to this class of molecules such as circularly polarized luminescence (CPL),[14,15] chirality,[7,16] tuning light emitting properties,[10,17,18] and memory device application.[19]

Out of various techniques designed to make relative motion in catenanes, metal-triggered motion has unique advantages.[20] The stable nature of metal complexes and properties of the templating ion can generate controlled translocation of interlocked components.[21,22] Only a few reports are known for synthesis and co-conformational switching studies of catenanes having multiple metal bonding sites. One report relies on the important differences in stereochemical requirements for the coordination of Cu(I) and Cu(II). When the catenane is complexed with Cu(I), the phenanthroline units from both rings coordinate, but when it is oxidized, the terpyridine units coordinate, changing one conformer to another.[23] Another report demonstrates a half rotation of one ring w.r.t. other by metalation and demetallation of the Pd^{2+} ion.[21] They also designed a [2]catenane with three metal templating center functionalized (two in one ring and one in the other) and demonstrated half-ring rotation using Pd(II) and Co(III) metal ions.[22] A recent example displays a mechano-stereochemical switching of rings of a catenane having two bi-pyridine centers due to Cu(I) and SO_4^{2-} bonding.[8]

In our previous reports, we have demonstrated a pyridine-diamide (pda) templating center for the synthesis of higher-order catenane.[24–26] Herein, we report a homo [2]catenane with each ring having a bi-dentate diphenyl-phenanthroline (dpp) and a tri-dentate pyridine-diamide (pda) metal-templating center. Due to the orthogonal behavior of these centers, this catenane shows switching behaviors in the presence of Cu(I) and Co(III) metal ions. This leads to interconversion between orthogonal catenates, where the interlocked rings undergo inevitable pirouetting and circumrotation.[27,28] Moreover, one pot double ring closing amide-bond formation strategy has been utilized in the catenation step.[29,30] It is worth mentioning that, having two free templating centers after the first catenation, this metalated catenane may be threaded again, in one pot, to achieve step-economic synthesis[31] of higher order linear oligo[n]catenane similar to a recent report.[32]

Reaction Scheme (Scheme 1)

2. Results and Discussion

2.1. Design and Synthesis of Homo [2]Catenane H[2]C

Synthesis of **H[2]Cu** is performed by self-complexing phenanthroline-diamine ligand **M6** (Scheme S1) and $Cu(CH_3CN)_4BF_4$ in a mixture of CH_3CN:DCM (1:1). This was followed by a double macrocyclization step[33] using 2,6-

[a] R. Ratha[+], M. B. Podh[+], P. Ghosh, T. K. Majhi, C. S. Purohit
School of Chemical Sciences, National Institute of Science Education and Research (NISER), Jatni, Bhubaneswar, Odisha 752050, India
E-mail: purohit@niser.ac.in

[b] R. Ratha[+], M. B. Podh[+], P. Ghosh, T. K. Majhi, C. S. Purohit
Homi Bhabha National Institute (HBNI), Mumbai, Maharashtra 400094, India

[+] Both authors contributed equally to this work.

Supporting information for this article is available on the WWW under https://doi.org/10.1002/slct.202504348

CHEMISTRY
AN ASIAN JOURNAL

www.chemasianj.org

19/13
2024

A Journal of

ACES
Asian Chemical Editorial Society

Front Cover:
Chandra Shekhar Purohit, and co-workers
Template Assisted Synthesis of Linear [5]Catenane by Post-Functionalization of Templated [2]Catenane and Using Click Reaction

WILEY VCH